ELECTROCHEMICAL OXIDATION OF PHENOL IN SIMULATED PETROCHEMICAL WASTEWATERS USING BORON-DOPED DIAMOND ELECTRODES: INVESTIGATION OF EFFECT OF NH_4^+, CN^- AND S^{2-} PRESENCE

BY

MU'AZU NUHU DALHAT

A Dissertation Presented to the

DEANSHIP OF GRADUATE STUDIES

KING FAHD UNIVERSITY OF PETROLEUM & MINERALS

DHAHRAN, SAUDI ARABIA

In Partial Fulfillment of the

Requirements for the Degree of

DOCTOR OF PHILOSOPHY

In

CIVIL ENGINEERING

January 2010

KING FAHD UNIVERSITY OF PETROLEUM & MINERALS
DHAHRAN 31261, SAUDI ARABIA

DEANSHIP OF GRADUATE STUDIES

This dissertation, written by **MU'AZU NUHU DALHAT** *under the direction of his dissertation advisor and approved by his dissertation committee, has been presented to and accepted by Dean of Graduate Studies, in partial fulfillment of the requirements for the degree of:* **DOCTOR OF PHILISOPHY IN CIVIL ENGINEERING**

Dissertation Committee

Prof. Muhammad H. Al-Malack (Advisor)

Dr. Nabil Abuzaid (Co-Advisor)

Dr. Alaadin A. Bukhari (Member)

Dr. Saleem U. Rahman (Member)

Dr. Mazen Khaled (Member)

Dr. Husain Jubran Al-Gahtani
(Department Chairman)

Dr. Salam A. Zummo
(Dean of Graduate Studies)

Date 10/4/10

DEDICATION

Dedicated to my Beloved Daddy and Mummy

ACKNOWLEDGEMENT

Most excellent thanks and praises are always for Al-mighty Allah (S.W.T) alone who made everything possible toward achieving this unique milestone. May peace and blessings be upon His most beloved servant, the last messenger and seal of the Prophet-hood, Prophet Muhammad (May Peace and Blessings of Allah be Upon him), his noble family, companions and those that follow their distinctive and most guided foot-steps till the day of resurrection.

I wish to acknowledge with gratitude another round of rare scholarship opportunity awarded to me by KFUPM to pursue my doctorate degree and also to King Abdul-Aziz City of Science and Technology (KACST) for the partial financial support provided for this research. My special gratitude and appreciations are due for my dissertation supervisor Dr. Muhammad H. Al-Malack whose guidance, immense supports and caring significantly contributed to the successful completion of this research. I also wish to express similar gratitude and appreciations to my committee members, particularly to Dr. Alaadin A. Bukhari for the invaluable support provided for this research by the Center for Water & Environment at RI-KFUPM, my co-advisor Dr. Nabil Abuzaid for his additional guidance and positive criticisms, Dr. Saleem Ur Rahman and Dr. Mazen Khaled for their helpful contributions that collectively ensured the overall success of this work.

I am highly indebted to express my special profound appreciations and thanks - I am short of apt words to express- that I preserve at all times for my much-loved parents for their caring, guidance, relentless prayers for my success in my life endeavors and the moral upbringing they put me through right from childhood. My deserving thanks are to my darling wife for her love, compassion and concern for my success and also to my brothers, sisters and friends for their prayers, supports and concerns. I pray that the Almighty Creator provide us all with the best in this life and grant us together His endless bliss in the hereafter.

The attention and assistance provided by Dr. M.H Essa of KFUPM Civil Engineering department both during the course of the experimental and reporting stages of this research is highly commended and appreciated. I am also thankful to the Nigerian community at KFUPM and environs for making my stay at KFUPM during my graduate studies enjoyable and memorable one. In that regard, special appreciations are for my Brother Dr. Sa'idu Waziri, Engr. Awwal Suleiman and Engr. Bello Mukthar for the cordial relationships and good times we had together. I wish you and your families all the best in your various lives endeavors and eternal pleasure in the life to come after present one.

Table of Contents

List of Figures

List of Tables

ABSTRACT (ENGLISH)

Name: Mu'azu Nuhu Dalhat
Title: Electrochemical Oxidation of Phenol in Simulated Petrochemical Wastewaters Using Boron-Doped Diamond Electrodes: Investigating Effect of NH_4^+, CN^- and S^{2-} Presence
Major Field: Civil Engineering
Date of Degree: January 2010

Presence of high concentrations of inorganic pollutants in phenolic wastewater effluents from refinery and petrochemical industries renders improper discharge of such wastewaters liable to leading to detrimental environmental consequences and also posing greater challenge for effective phenol oxidation and overall decontamination process. This dissertation thoroughly addressed such issues considering electrochemical oxidation of phenol in simulated petrochemical wastewaters containing NH_4^+, CN^- and S^{2-} in different single, binary, ternary and quaternary mix matrixes using Boron Doped Diamond (BDD) anodes.

Statistical experimental design was employed to model and optimize the experimental operating conditions through Response Surface Methodology (RSM) modeling technique. Phenol, TOC and COD decay profiles excellently fitted experimentally verified second order quadratic models having all investigated influencing parameters statistically significant. The overall decontamination process was mainly kinetically controlled process dominated by heterogeneous and irreversible direct oxidation reactions on the BDD anode surface mainly mediated by electro-generated $OH^\bullet$ with mass transfer effects as the rate limiting step. At pH < pKa of phenol, oxidation of phenol was effectively achieved regardless of phenol initial concentration, while at pH > the pKa and low phenol concentration, accumulation of intermediary byproducts and polymerization hindered phenol oxidation.

Erroneous predictions of phenol oxidation kinetics from existing COD evolution based models due to presence of the inorganic species were corrected with modified models based on TOC decay data. With the exception of NH_4^+ ions, the degradation kinetics for phenol as well as the inorganic species in the different mix matrixes were consistently pseudo-first order kinetics with the kinetic and hydrodynamic constants for phenol, TOC and COD been reduced mainly as result of decline in the BDD anodes' activities. Comprehensive analyses of oxidation byproducts suggested that the mechanism for phenol oxidation was primarily initiated by speciation of the phenol molecules that led to the generation of aromatic intermediates via hydroxylation which were further oxidized and converted to short chain aliphatic acids before finally converting to CO_2. Presence of the inorganic species didn't hamper the phenol oxidation ability of the BDD anode, though reaching steady state of complete decontamination was significantly delayed according to the inorganic species presence in solution.

DOCTOR OF PHILOSOPHY
KING FAHD UNIVERSITY OF PETROLEUM AND MINERALS
Dhahran, Saudi Arabia
January 2010

الملخص (بالعربية)

اسم الباحث: معاذ نوح طلحة.

عنوان الرسالة: محاكاة الأكسدة الكهروكيميائية للفينول في مياه الصرف الصحي المعالجة بتروكيماوياً بواسطة الأقطاب شبه الموصلة الموجبة للبورون الماسيِّ للتحقق من تأثير وجود كل من الـكبريتيد S^{2-} و الـسيانيد CN^- والأمونيوم NH_4^+.

مجال التخصص: الهندسة المدنية التطبيقية.

تاريخ الدرجة العلمية: شهر صفر 1431هـ الموافق لشهر يناير 2010م.

إن وجود التّركيزات العالية للملوّثات الغير عضويّة في فينول (أحماضِ الكربوليك) مياه الصرف المتدفقة كمخلّفات من المصانع البتروكيماويّة ومن محطّة التّكرير يشكل تحدياً ومسؤولية في خروجها مع مياه الصّرف الصحي ويعرّض البيئية لعواقب ضّارّة وكما يطرح أيضاً التّحدّي الأكبر لأكاسيد الفينول المؤثّرة في عمليّة التّطهير الكلّيّة والشاملة. ولقد تطرَّقتْ هذه الرّسالة العلمية لمثل هذه القضايا بدقة والّتي تعتبر معالجة ومحاكاة للأكسدة الكهروكيميائيّة للفينول في مياه الصرف التي تحتوي على البتروكيماويات الآتية: الـكبريتيد S^{2-} والـسيانيد CN^- والأمونيوم NH_4^+ بنسب مختلفة في هذا الخليط كمزيج مترابط في أشكاله الرّباعيّة والثّلاثيّة والثنائيّة والأحادية باستخدام الأقطاب شبه الموصلة الموجبة للبورون الماسيِّ(بي دي دي).

التّصميم التّجريبيّ الإحصائيّ اُسْتُخْدِمَ هنا لعرض وزيادة فاعليّة ظروف التّشغيل التّجريبيّة من خلال قياس مدى الاستجابة السطحية لهذه المواد وفق منهج علمي بتقنية النمذجة لاستجابة السطوح:(آر إس إم). ولقياس مدى انحلال مادة الفينول، والمقدارالكلي للكربون العضوي (سي أو دي) ومقدار الأكسجين الكيميائي المطلوب(تي أو سي) التي تُلْمح بشكل ممتاز لمدى ملائمتهم تجريبيًّا للتحقّق من نتائج النّماذج الرياضية من الدرجة الثانية التي يتوافر فيها كل معالم التأثير ذات الدلالة إحصائية. كانت عمليّة التطهير وإزالة التلوث الكلّيّة عمليّةً محدّدةً حركيًّا بشكل رئيسيّ مسيطر عليها بتفاعلات الأكسدة المباشرة الغير قابلة للتّغيير والمختلفة الأثر على سطح القطب شبه الموصل (بي دي دي) المتوسّط بشكل رئيسيّ بالهدروكسيل المولد كهربائياً للحد من آثار انتقال محتوى المادة. إن أكسدة الفينول حُقِّقَتْ بفاعليّة بصرف النّظر عن تركيز الفينول الأوَّلي على درجة الحموضة pH أقل من تركيز درجة الـ pK_a في الفينول، وعندما كان الرقم الهيدروجيني pH أكبر من درجة حمضيَّة الـ pK_a وتركيز الفينول منخفض أدى ذلك إلى تراكم المشتقات الناتجة مصاحِبَةً وإلى تكوين المبلمرات التي تعوق وتمنع من تأكسد الفينول.

إن التّنبّوات الخاطئة لسلوك تحرك أكسدة الفينول كان بسبب وجود زيادة في نماذج الـ (سي أو دي) وترجع لوجود بعض الأنواع غيرالعضوية والتي تم تصحيحها بالنماذج المُعَدَّلةِ مستندة على بياناتِ انحلال الـ (تي أو سي). بإستثناء آيونات الأمونيوم NH_4^+ ، ولوَهَنْ قوَى حركة الفينول لحامضِ الكربوليك بالإضافة إلى تواجد المواد غير العضوية في أخلاط ذات خصائص نشأة مختلفة كَانتْ متوائمة مع شبيه النوع الحركي من الدرَجة الأولى بالثوابتِ الحركيّةِ والهايدروديناميكيةِ لكل من: الفينول والـ (تي أو سي) والـ (سي أو دي) قد تناقصت بشكل رئيسي كنتيجة لهبوطِ في أنشطة الأقطاب شبه الموصلة الموجبة بي دي دي. إن التّحليلات الشّاملة لمشتقات الأكسدة للفينول تجعل قولنا سائغاً بأن آليّة الأكسدة في المقام الأول التي بدأتها أصناف من عينات جزيئات الفينول والتي أدّت إلى توليد مواد مصاحبة عطريّة وسيطة بواسطة الهيدروكسيل الذي تَأَكْسَدَ أكثر وتحول إلى سلسلة من الأحماض الأليفاتأية الدُّهنيّة القصيرة قبل تحوّلها في نهاية المطاف إلى ثاني أكسيد الكربون CO_2 . ووجود هذه العينات من الجزيئات غيرالعضوية لم يكن عائقاً لقدرة كسدة الفينول لأقطاب البورون شبه الموصلة الموجبة بي دي دي، رغم أن الوصول إلى حالة ثابتة مستقرّة من درجة التطهير وإزالة التلوّث بالكامل تأخر بشكل ملحوظ وذلك لوجود هذا النوع من الجزيئات الغيرعضويّة في المحلول السائل المراد دراسته هنا.

درجة العالِميَّة في علوم الهندسة التطبيقية
جامعة الملك فهد للبترول والمعادن
مدينة الظهران ، المملكة العربية السعودية
شهر صفر1431هـ الموافق لشهر يناير 2010م.

Chapter 1

Introduction

Immense demands for industrial water conservation and compliance with stricter environmental regulations have led to a dramatic rise in research in industrial wastewater treatment over the last few decades. Researchers dissipate valuable effort in trying mainly to assist various categories of industries by providing valuable information for the best available technologies to adopt via trading between meeting environmental regulations and effective wastewater treatment schemes for economically viable operations. However, industries are usually baffled regarding the most appropriate treatment choice to adopt from options available to ensure their sustainability in an environmentally friendly manner. For petroleum refining and petrochemical industries, the grim situation cannot be overemphasized due to the fact that such industrial categories are among the major sources of phenolic wastewater (Awad and Abuzaid, 1997; Berne. and Cordonnier, 1995). Improper discharges of phenolic wastewater from such industries are likely to lead to detrimental environmental consequences since phenol is a toxic substance that poses great risk to aquatic life, micro-organisms and mammal (Busca et al., 2008). This necessitated many national and international environmental regulatory bodies such as the US Environmental Protection Agency (USEPA), European Environmental Commission (EEC), Saudi Arabia's Presidency of Metrology and Environment (PME) to set stricter discharge limits for phenols to below 0.1 mg/l (PME, 2001; USEPA, 2006). Moreover, the issue becomes more complicated owing to the fact that phenolic wastewater discharges from refineries and petrochemical industries are characterized by high chemical oxygen demand (COD) and may contain many other pollutants such as cyanide (CN^-), sulfide (S^{2-}), ammonium (NH_4^+), oil and grease and suspended solids

(Alessandra et al., 2006; Berne. and Cordonnier, 1995; Galil et al., 1988; Hamoda and Al-Haddad, 1987; Thiem and Alkhatib, 1988; Tyagi et al., 1993) that also have negative repercussions on the environment if not reduced below their regulated threshold concentrations prior to discharge. Hence, these render effective treatment of phenolic wastewater from refineries and petrochemical industries prior to discharge a crucial and integral attribute of sustainable development. Table 1.1 shows the USEPA maximum discharge limits (regulated thresholds) for some of the petroleum refining and petrochemical industry's wastewaters environmental parameters (USEPA, 2006). Table 1.2 shows typical wastewater characteristic from some petroleum refineries which are usually comparative to those from petrochemical industries(Berne. and Cordonnier, 1995).

Under suitable circumstances and in concentrations above 2000-4000 mg/L, phenol can be economically recovered from wastewaters. Below this concentration range, phenol destruction is always the best method for treating phenol contaminated wastewaters (Canizares et al., 1999; Lanonette, 1977). Numerous treatment technologies have been investigated for destruction of phenol in aqueous matrixes which were comprehensively reviewed by Busca et al (2008). Cheap and attractive conventional biological treatment technologies are very ineffective due to the bio-recalcitrant nature of phenolic compounds. Eventhough, many other physical and chemical treatment technologies have been proposed for effectiveness, however, electrochemical oxidation methods for treatment have received greater attention in recent years (Awad and Abuzaid, 1999; Comninellis and Nerini, 1995; Comninellis and Pulgarin, 1991, 1993; Koparal and Ogutveren, 2002; Koparal et al., 2002; Stucki et al., 1991). This can be attributed to many distinctive advantages they offer over other conventional technologies that include environmental compatibility, versatility, energy efficiency, safety, selectivity, amenability to automation, and

Table 1.1: USEPA Maximum Discharge Standards for Land and Surface Water (USEPA, 2006)

Parameter	**Permissible Limit (ppm)**
Phenolic Compounds (as C_6H_5OH)	0.5
Cyanide (as CN^-)	0.1
Ammonical Nitrogen	1
Total Kjeldahl Nitrogen (TKN)	25
Sulphide	0.002
Biochemical Oxygen Demand (BOD_5)	40
Chemical Oxygen Demand (COD)	120
Oil & Grease	10

Table 1.2: Typical Concentrations in milligram per liter for Parameters in Wastewater from Different Refineries

Parameter	Elf Grandpuits Refinery[a]	Esso-SAF Port-Jerome Refinery[a]	Shell Complex in Berre Refinery[a]	Unknown Refinery in Kuwait[b]	Ashland Refinery New York[c]	Unkown Refinery[d]	Unknown Refinery[e]	Reported by Alessandra Coelho *et al*[f]
S^{2-}	500-3500	750	-	3-35	-	-	-	15-23
NH^{+}_{4}	300-600	45	49	-	35-390	3-51	4.7	5.1-21.1
Phenols	50-60	60	2.8	-	5-15	6-88	22	98-128
CN^{-}	100-120	100-120	-	-	0.1-5	-	-	-
COD	350-400	1000-1600	460-1580	475	125-400	234-925	625	850-1020
Cl^{-}	-	-	350	213	150-300	-	-	-
SS	-	-	45-385	261	15-50	63-110	46	-
Oil	-	-	-	36.1	8-57	26-124	-	12.7
TDS	-	-	-	533	-			

a (Berne. and Cordonnier, 1995)
b (Hamoda and Al-Haddad, 1987)
c (Thiem and Alkhatib, 1988)
d (Tyagi et al., 1993)
e(Galil et al., 1988)
f (Alessandra et al., 2006)

cost effectiveness (Juttner et al., 2000; Rajeshwar and Ibanez, 1997) and require no additional oxidative reagents (Al-Maznai and Conway, 2001).

Apparently, despite the numerous advantages, the practical application of electrochemical techniques to phenolic wastewater treatment has been limited by a variety of factors which include:

- The difficulty in finding electrode materials -especially the anode- with appropriate characteristics to make the process economically competitive (Canizares et al., 2002a; Polcaro et al., 2003). An ideal electrode material for the degradation of organic pollutants should be completely stable in an electrolysis medium; cheap or should possess low cost to life ratio; and should exhibit high activity toward organic oxidation and low activity toward secondary reactions (e.g., oxygen evolution).

- Other toxic compounds contained in the wastewater which can have different degrees of oxidizability whose presence may have negative impacts on the process efficiency for phenol destruction.
- Possibility of polymerization and accumulation of phenol oxidation intermediate byproducts such as the quinone compounds which were proven to be more toxic than phenol (Xiao-yan et al., 2005) and could significantly hinder effective phenol oxidation.
- Experimental conditions such as applied current density, electrolyte choice and its concentration, temperate, pH, flowrate etc and the overall cell design which govern the efficiency of the electrochemical treatment process (Canizares et al., 2002a).

Comninellis and co-workers (Comninellis and Nerini, 1995; Comninellis and Pulgarin, 1991, 1993) reported that one of the curial factors that immensely influence the performance of electrochemical oxidation of organic compound is the anode material as it controls the process selectivity, final oxidation products and the current efficiency. Hence, the oxidation of phenol and substituted phenols has been investigated intensively on a variety of metal anodes (Bruno et al., 1977), with special attention given to Pt (Al-Maznai and Conway, 2001; Bruno et al., 1977; Glarum and Marshall, 1985; Glarum et al., 1987; Jedral et al., 1999; Lapuente et al., 1998; Lotov and Kalcheva, 1998; Ureta-Zanatu et al., 2001) and Au (Lotov and Kalcheva, 1998; Ureta-Zanatu et al., 2001), but also to Ag (Conway et al., 2001) and Ni–Nb–Pt–Sn alloy (Sistiaga et al., 1998) were also investigated. Owing to the good activity for total organic carbon (TOC) removal, the anodes based on conductive metal oxides, such as PbO_2, SnO_2, IrO_2 and RuO_2 appeared to be promising materials for use in effective treatment of wastewaters containing organic impurities (Comninellis, 1994; Comninellis and Nerini, 1995; Comninellis and Pulgarin, 1993; Feng and Li, 2003; Foti et al., 1999; Iniesta et al., 2002; Stucki et al., 1991). Several other materials consisting of titanium-supported coatings of noble-metal oxides, known as dimensionally stable anodes (DSA) such as Ti/TiO_2, Ti/PbO_2(Polcaro et al., 2002), Ti/SnO_2 (Comninellis and Pulgarin, 1993; Yao et al., 2008), Ti/RuO_2 and Ti/SnO_2-Sb(Xiao-yan et al., 2005), Ti/IrO_2 (Polcaro et al., 2000), RuO_2-TiO_2/Ti(Panic et al., 2005) and Ti/$Ru_{0.3}Pb_{(0.7-x)}Ti_xO_y$ (Cestarollia and Andrade, 2007) have also been tested in anodic oxidation of phenol with great successes. DSA-type anodes proved to be better anode materials compared to their based conductive metal oxides as they have large electrochemical active surface areas and hence higher electrochemical activity. Moreover, investigations of the activity of non-metal materials have been undertaken by many authors (Al-Maznai and Conway, 2001; Awad and Abuzaid, 1997; Awad and Abuzaid, 1999; Boudenne et

al., 1996; Bruno et al., 1977). Particularly, attractive ones are glassy carbon (Ureta-Zanatu et al., 2002) and the quasi-3D materials, such as carbon black slurry electrodes (Boudenne et al., 1996) and carbon felt (Al-Maznai and Conway, 2001; Bruno et al., 1977), as they are highly-porous materials with large surface areas and relatively low cost (Panic et al., 2005).

However, the practical applications of most of these anodes materials are mired by a number of problems. Some of these problems are loss of activity due to surface fouling of glassy carbon (Gattrell and Kirk., 1990), limited service life of Ti/SnO_2 (Correa-Lozano et al., 1997) and SnO_2 (Correa-Lozano et al., 1997)), release of toxic ions by PbO_2 (Panizza and Cerisola, 2005)), selective oxidation of IrO_2 (Comninellis, 1994)), polarity irreversibility and low current efficiency. Moreover, analysis of reaction intermediates and the measurement of current efficiencies have shown that many traditional anode materials (Pt, Ti/IrO_2, Ti/RuO_2) are prone to favoring electrochemical conversion leading to production of undesirable by-products (carboxylic acids are the final oxidation products) rather than electrochemical destruction and/or very low achievable current efficiencies (Gattrell and W, 1993; Lotov and Kalcheva, 1998; Vercesi et al., 1991)

Boron Doped Diamond (BDD) electrodes, newer anode materials, have recently attracted the attention of researchers because of their very distinctive characteristics that contrast with that of other anodic materials (Alexander, 2007; Beck et al., 1998; Fisher et al., 1998; Panizza and Cerisola, 2005; Panizza et al., 2001; Troster et al., 2002a). They consist of support materials such as titanium, tantalum, niobium, silicon and glassy carbon coated by a layer of synthetic diamond, heavily doped with boron to obtain acceptable electrical conductivity. The characteristics of these

materials, such as hardness, resistance to fouling, longer operating life span, polarity reversibility, stability up to high anodic potentials and wide potential window for water discharge and electro-generation of powerful oxidants make it an excellent candidate anodic material for oxidation of organic compounds (Alexander, 2007; Cui et al., 2009; Güven et al., 2009; Liu et al., 2009a; Nasr et al., 2009; Panizza and Cerisola, 2005; Panizza et al., 2001; Troster et al., 2002a). BDD electrode once employed as anode material allows high efficiencies to be achieved in the use of electric energy and, as a consequence decreases considerably the operating cost of this technology, thereby rendering it economically competitive with other anode materials.

Considering surveyed literature revealed that electrochemical oxidation of phenol in aqueous solution cohabited by other oxidizable inorganic species found in refinery and petrochemical industries using boron doped diamond electrode has not been addressed, this dissertation's main aim was to conduct a thorough and in-depth experimental study at bench-scale to address such a deficiency in the existing literature. For this given wastewater decontamination system, a pragmatic and holistic approach needs to be brought into play to comprehend the complex interplay of parameters that need to be optimized in order to obtain an effective, environmentally sound and economical incineration of pollutants to reaffirm its competitiveness with other treatment alternatives. Moreover, bringing this important issue into the realm of literature would pave way for understanding feasibility of practical applicability of electrochemical oxidation using BDD anode approach for solving and mitigating wastewater pollution problems associated with refinery and petrochemical industries.

Chapter 2

Literature Review

2.1 Electrochemical Advanced Oxidation Process (EAOP)

Numerous treatment technologies are proposed for decontamination of phenols and related compounds. One of the most suitable alternative method in aqueous systems is chemical oxidation processes (Alexander et al., 2003) . This processes aim at the total mineralization or production of harmless or biodegradable compounds. Commonly used chemicals are oxygen, hydrogen peroxide (H_2O_2), ozone (O_3), hydroxyl radical ($OH^{\bullet}$), permanganate and persulfate. Among these oxidants, $OH^{\bullet}$ is the most powerful oxidant in water because it possess the highest oxidation potential, with a redox potential of about 2.8 V against normal hydrogen electrode (NHE) as shown in Table 2.1. Advanced oxidation processes (AOP) are characterized by the production and use of these $OH^{\bullet}$ for the oxidation of chemical substances (Andreozzi et al., 1999; Katsuki et al., 1998; Lanonette, 1977; Zwiener and Frimmel, 2004).

The most common AOPs for the production of $OH^{\bullet}$ radicals are the Fenton process which involves addition of H_2O_2 to Fe^{2+} salts (Neyens and J. Baeyens 2003), the photo-assisted fenton process, photocatalysis using TiO_2 and UV radiation (Herrmann, 1999), the O_3/ H_2O_2 and the H_2O_2 photolysis using UV light. Some of the drawbacks of the conventional AOPs include the relatively high costs, the necessity of adding chemicals and the complications of using UV light such as the high absorption coefficients of water to be treated or the relatively short lifetime of UV light sources (Alexander et al., 2003). Electrochemical Advanced Oxidation Process (EAOP)

Table 2.1: Formation Potential of Typical Chemical Oxidants (Guohua, 2004)

Oxidants	Formation Potential E vs NHE
$H_2O/ OH^{\bullet}$ (Hydroxyl radical)	2.8
$O_{2//}O_3$ (Ozone)	2.07
$SO_4^{2-}/S_2O_8^{2-}$ (Peroxodisulfate)	2.01
MnO_2/MnO_4^{2-} (Permanganate ion)	1.77
H_2O/H_2O_2 (Hydrogen Peroxide)	1.77
Cl^-/ClO_2^- (Chlorine Dioxide)	1.57
Ag^+/Ag^{2+} (Silver (II) ion)	1.5
Cl^-/Cl_2 (Chlorine)	1.36
$Cr^{3+}/Cr_2O_7^{2-}$ (Dichromate)	1.23
H_2O/O_2	1.23

offers solutions to problems associated with the conventional AOPs (Troster et al., 2002a). In this process, the $OH^{\bullet}$ radicals are produced electrochemically in an anodic reaction directly from water which has to be treated according to Equations 2.1 and 2.2 (Canizares et al., 2002b; Foti et al., 1999; Marselli et al., 2003)

$$H_2O \rightarrow OH^{\bullet} + e^{-} + H^{+} \qquad 2.1$$

$$OH^{-} \rightarrow OH^{\bullet} + e^{-} \qquad 2.2$$

However, with the electrode materials available, this could not be effectively accomplished or only with very low current efficiencies and very short electrode lifetime until recently, with the discovery of boron-doped thin-film diamond (BDD) electrodes. This is due to the fact that for the electrochemical production of $OH^{\bullet}$ radicals, electrode materials with a very high oxygen overvoltage are necessary (Marselli et al., 2003). Additionally, the electrode material has to be stable in the presence of large amounts of hydroxyl radicals (Alexander et al., 2003). Otherwise, large amount of the supplied current will be wasted in decomposing water towards oxygen evolution producing O_2, leading to a very low current efficiency. Moreover, polymerization reactions may take place, thus inactivating the electrode (Iniesta et al., 2001a; Pacheco et al., 2007). Consequently, as common electrodes such as graphite, platinum, and DSA, which do not have a sufficient O_2 evolution overpotential, they are not very good for use for electro-degradation of organic compounds because current efficiency for $OH^{\bullet}$ production is extremely low. Similarly, other stable anode materials with relatively high overvoltage for oxygen production such as TiO_2 , PbO_2 (Bonfatti et al., 1999; Sharifian and Kirk, 1986a) and SnO_2 (Kotz

et al., 1991; Stucki et al., 1991) are characterized by excessively low current efficiency for OH• production. They also show low stability and are prone to releasing undesired precipitates (Hegea et al., 2004). Moreover, Alexander and colleagues (Alexander et al., 2003) reported that theses electrode materials are not stable during polarity reversal or else some (SnO_2 or PbO_2) are reduced when working as cathode and that they possess low chemical and mechanical stability. In the practical application of electrochemical wastewater treatment, current reversal is often necessary to remove calcareous deposits from cathode surfaces (Alaxender. et al., 1999).

However, the boron-doped diamond (BDD) thin films deposited on self-passivating metals such as niobium show the largest overvoltage for oxygen production from water ever found for an electrode material (Marselli et al., 2003; Perret et al., 1999; Troster et al., 2002a; Troster et al., 2002b). They also exhibit high chemical and mechanical stability and operate at very high current efficiency. Because of their unique properties, BDD electrodes are much more suited for EAOP than any other known electrode materials (Alexander et al., 2003).

2.2 Synthetic Boron-Doped Diamond Thin Film Electrodes

Over the past decade, the use of diamond electrodes gained overwhelming acceptance in electro-synthesis of chemicals (Marco et al., 2006; Panizza and Cerisola, 2005), electro-analysis and sensor technology (Marco et al., 2006; Panizza and Cerisola, 2005; Yu et al., 2009) and in wastewater treatment (Alexander, 2007; Marco et al., 2006; Panizza and Cerisola, 2005; Scialdone et al., 2009; Troster et al., 2002a; Troster et al., 2002b). In fact, a number of published articles showed the BDD electrodes are the most effective anode material in the destruction of wide range of bio-recalcitrant organic substances, inorganic compounds such as cyanide,

ammonia, sulfide and other nitrogenous compounds with the highest current efficiency (Adelaida et al., 2007; Canizares et al., 2005a; Fryda et al., ; Guohua, 2004; Hegea et al., 2004; Katie et al., 2007; Marco et al., 2006; Pacheco et al., 2007; Perret et al., 1999; Troster et al., 2002a; Troster et al., 2002b).

BDD electrodes consist mainly of a thin-film of diamond (few microns) grown by energy-assisted (plasma or hot-filament) chemical vapor deposition on a substrate support material which could be silicon, titanium, niobium, tantalum, molybdenum or glassy carbon. Diamond, a well known good electrical insulator, has films that are rendered conducting usually by doping them with different concentrations of boron atoms. The most important factors that influence the electrochemical behavior of boron-doped diamond electrodes include the crystallographic structure (Duo et al., 2003; Kondo et al., 2002; Martin et al., 1999), the surface functional groups (Duo et al., 2003; Hayashi et al., 1996), the boron doping level (Duo et al., 2003; Zhang et al., 1996), and the presence of non-diamond amorphous carbon species (sp2) (Duo et al., 2003; Martin et al., 1999). For moderate doping of 10^8 boron atoms per cm^3 the resistivity is 10^4 Ωcm and the electrode has semiconductor behavior. At the same time, for high doping of 10^{20} to 10^{21} boron atoms per cm^3, the resistivity decreases to 10^{-3} Ωcm and, consequently, takes on semimetal behavior (Pleskov, 1999; Pleskov, 2002).

The characteristics that render BDD electrodes to be unique anodic material compared to other anode materials could be enumerated as:

- Electrically conductive (Typically 0.4~1.0 x 10^{-3} Ω.cm)
- Extremely high working potential window for hydrolysis of water to produce O_3 and $OH^{\bullet}$

- Hydroxyl radicals are produced with higher current efficiency
- Chemically inert up to 600 ^{0}C , mechanically robust and very high stability to corrosion in aggressive environment
- Non-Porous with negligible adsorption phenomena and high fouling resistance
- Stable as anode and cathode, hence polarity reversibility is rendered possible
- Complete mineralization of organic and inorganic impurities in water and wastewater

Formation potentials of typical oxidants are listed in Table 2.2. It can be seen that BDD film on titanium substrate (Chen et al., 2003b) or other value metals as in DiaChem electrodes (Troster et al., 2002a; Troster et al., 2002b) give the highest value of oxygen evolution overpotential. Thus, anodic oxidation can take place on its surface at significantly high current density with minimal amount of oxygen evolution side reaction, thereby leading to an effective and efficient process (Guohua, 2004).

Interestingly, Iniesta *et al* (Iniesta et al., 2001b) experimentally reported that at high anodic potentials (close to the potential of water decomposition) the activity of BDD electrodes was considerably enhanced, and there was no evidence of a loss of electrode activity. In the case of aromatic compounds, such as phenol and related compounds, they found that the polymeric film formed in the region of water stability could be destroyed by subjecting the electrode to high anodic potentials (E > 2.3 V vs. SHE) in the region of O_2 evolution, thereby restoring the electrode's activity. In fact, applied potential located in the region of water discharge at BDD electrode involves the production of reactive intermediates (hydroxyl radicals, $OH^{\bullet}$) which oxidizes the polymeric film on the anode surface. This unique behavior has also been reported by

Table 2.2: Potential of Oxygen Evolution for Different Anodes (V vs NHE)

Anode Material	Value and its Reference(s)	Electrolyte
Pt	1.3 (Troster et al., 2002b)	0.5 M H_2SO_4
Pt	1.6 (Swain et al., 1998)	0.5 M H_2SO_4
IrO_2	1.6 (Mraz and Krysa, 1994; Troster et al., 2002b)	0.5 M H_2SO_4
Graphite	1.7 (Swain et al., 1998)	0.5 M H_2SO_4
PbO_2	1.9 (Feng and Johnson, 1991)	1 M $HClO_4$
SnO_2	1.9 (Correa-Lozano et al., 1996)	0.5 M H_2SO_4
Pb-Sn	2.5 (Troster et al., 2002b)	0.5 M H_2SO_4
Ebonex (Titanium Oxides)	2.2 (Smith and Walsh, 1998)	0.5 M H_2SO_4
Si/BDD	2.3 (Fryda et al., 1999; Martin et al., 1996)	0.5 M H_2SO_4
Ti/BDD	2.7 (Chen et al., 2003a)	0.5 M H_2SO_4
DiaChem	2.8 (Troster et al., 2002a; Troster et al., 2002b)	0.5 M H_2SO_4

many other authors (Gandini et al., 2000; Gherardini et al., 2001; Iniesta et al., 2001a; Rodrigo et al., 2001).

2.3 Mechanisms of Anodic Oxidation of Organic Pollutants on Boron-Doped Diamond Electrode

Electrochemical oxidation treatment of wastewater at BDD anode is achievable via two major mechanisms; direct oxidation at the anode surface (Guohua, 2004; Marco et al., 2006; Panizza and Cerisola, 2005) and indirect oxidation in the bulk aqueous system by the anodically formed oxidants, such as hydrogen peroxide (Marselli and Comninellis, 2004; Marselli et al., 2003), persulfate (Canizares et al., 2005b), peroxocarbonatev(Bergmann and Rollin, 2007; Nishiki et al., 2004), Cl_2, hypochlorite, peroxide, ozone (Juttner et al., 2000)and fenton's reagent (Juttner et al., 2000), peroxodisulphate (Bergmann and Rollin, 2007; Juttner et al., 2000) and peroxodisulphuric (Panizza and Cerisola, 2005), generated via decomposition of appropriate respective supporting electrolyte(s).

For the direct oxidation mechanism, the process involves the electro-oxidation of pollutants which occurs directly on the BDD by generating physically adsorbed "active oxygen" (adsorbed hydroxyl radicals, $OH^{\bullet}$) which causes the complete combustion of organic compounds. The electrochemical activity (overpotential for oxygen evolution) and the chemical reactivity of adsorbed hydroxyl radicals (rate of oxidation of the organic substances by electrogenerated hydroxyl radicals) are strongly related to the strength of interaction between the BDD and $OH^{\bullet}$ (Marco et al., 2006; Marselli et al., 2003). The weaker the BDD-OH• interaction is, the lower will

be the anode's activity toward oxygen evolution (high overvoltage anodes), and the higher its reactivity for the oxidation of organics (Marselli et al., 2003).

Depending on the interactions between hydroxyl radicals and the electrode surface, anodes can be distinguished as either active or non-active materials (Comninellis, 1994; Foti et al., 1997; Simond et al., 1997). Among the particular characteristics of BDD electrode is its well recognized chemical inertness and as such, BDD material is considered an ideal non-active electrode i.e., it doesn't provide any catalytically active site for the adsorption of reactants and/or products in aqueous media (Comninellis, 1994; Foti et al., 1999; Marco et al., 2006; Marselli et al., 2003).

Based on several experimental results corroborating one another, a generalized mechanism, as shown in Figure 2.1, has been proposed by Comninellis and co-workers (Comninellis, 1994; Foti et al., 1999; Marselli et al., 2003; Panizza et al., 2001) to describe the combustion of organic compound (designated as R) on BDD anodes in acidic media. The model assumes that both the oxidation of organics and the oxygen evolution reaction take place exclusively through mediation by hydroxyl radicals, i.e., the electrode itself does not exhibit any active character.

Considering the reaction pathways *a-e* and *a-b* in Figure 1 for non-active electrodes, and M replaced with BDD, the first reaction is the electrochemical discharge of water leading to hydroxyl radical formation as given in Equations 2.1 and 2.2. The hydroxyl radicals physically interact with the BDD according to Equation 2.3:

$$BDD + H_2O \rightarrow BDD(^{\bullet}OH) + H^+ + e^- \qquad 2.3$$

These hydroxyl radicals are then consumed by two competing reactions. First combustion of organics according to Equation 2.4:

$$BDD(^{\bullet}OH) + R \rightarrow BDD + mCO_2 + H_2O + H^+ + e^- \qquad 2.4$$

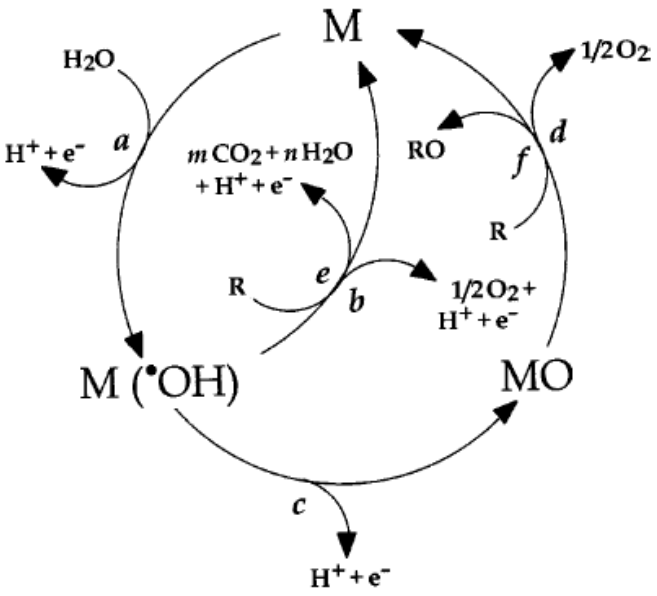

Figure 2.1: Model for Electrochemical Combustion of Organic Compounds on Non-active and Active Electrodes (Canizares et al., 2005c)

And second is the oxygen evolution reaction according to Equation 2.5:

$$BDD(^{\bullet}OH) \rightarrow BDD + \frac{1}{2}O_2 + H^+ + e \qquad 2.5$$

The second oxidation mechanism suggests that molecular oxygen also participates in the combustion of organics according to the following two-step reaction scheme:

1) Formation of organic radicals, $R^{\bullet}$, by a dehydrogenation mechanism (Equation 2.6):

$$RH + BDD(^{\bullet}OH) \rightarrow R^{\bullet} + H_2O + BDD \qquad 2.6$$

2) Reaction of the organic radical with dioxygen (Equation 2.7):

$$R^{\bullet} + O_2 \rightarrow ROO^{\bullet} \qquad 2.7$$

Further abstraction of a hydrogen atom with the formation of an organic hydroperoxide (ROOH) according to Equation 2.8:

$$ROO^{\bullet} + R^{'}H \rightarrow ROOH + R^{'\bullet} \qquad 2.8$$

The relatively unstable organic hydro-peroxide intermediates decompose leading to molecular breakdown and formation of subsequent intermediates with lower carbon numbers. These scission reactions continue rapidly until the organic substance is completely transformed to CO_2 and H_2O. However, because oxygen evolution (given in Equation 2.5), can also take place at the anode, high over-potentials for O_2 evolution is required in order for Equations 2.4 and 2.6 to proceed with high current efficiency. Otherwise, most of the current supplied will be wasted in splitting water.

Depending on the experimental conditions and regardless of anodic material used (Canizares et al., 2004), several investigations (Canizares et al., 2003; Canizares et al., 2002a; Canizares et al., 2002b; Canizares et al., 2007; Chen et al., 2003a; Comninellis and Pulgarin, 1991, 1993; Diniz et al., 2003; Iniesta et al., 2001b; Panic et al., 2005; Perret et al., 1999; Polcaro et al., 2003; Sharifian and Kirk, 1986a, b; Tahar and Savall, 1999; Xiao-yan et al., 2005; Yusuf and Koparal,

2006) have corroborated the mechanism of phenol oxidation in non-chlorinated electrolyte. They showed that the electrochemical oxidation of phenolic wastes lead to the sequential formation of more toxic aromatic intermediates, the quinonic compounds (hydroquinone, benzoquinone and catechol), followed by carboxylic acids intermediates, and then carbon dioxide as the sole final product in case of complete mineralization. However, for particular case of BDD anode, Iniesta et al (2001b) reported that at low current density, high phenol concentration and low conversion, phenol is mainly oxidized, particularly in acidic media, to the aromatic intermediaries, due to a low local concentration on the anode surface of electro-generated hydroxyl radicals relative to phenol. However, they found that at high current density and low phenol concentration phenol is directly combusted to CO_2 due to a high local concentration on the anode surface of electro-generated hydroxyl radicals relative to phenol.

2.4 Anodic Oxidation of Phenol on Boron-Doped Diamond Electrodes

Anodic degradation of phenol on BDD anode has been the focus of numerous authors in the last few decades (Canizare et al., 2006; Canizares et al., 2005c; Canizares et al., 2002a; Canizares et al., 2002b; Hagans et al., 2001; Pacheco et al., 2007; Polcaro et al., 2003; Tian et al., 2006; Zhao et al., 2008; Zhu et al., 2008). Under different operating conditions with active electrodes such as stainless steel which has been the major counter electrode used, investigators dissipated tremendous efforts in attempting to study the effects of influencing parameters- mainly current intensity, pH, supporting electrolyte, electrolysis and temperature- on pollutants removal kinetics and process efficiency using variety of electrochemical reactors.

Canizares *et al.*(Canizares et al., 2005c; Canizares et al., 2002a; Canizares et al., 2002b) have intensively studied the degradation of phenol on BDD anodes. They reported that different phenolic compounds were completely mineralized on BDD anodes regardless of the characteristics of the wastewater (initial concentration, pH and supporting media) and operating conditions (temperature and current density) used. They found that under the range of current density 15 - 30 $mAcm^{-2}$ and temperature range of 15 - 60 ^{o}C, mineralization rate decreases with increasing current density and with decreasing initial phenol concentration. Also an increase and decrease in temperature lead to an increase in the mineralization rate for basic (Canizares et al., 2005c; Canizares et al., 2002a) and acidic medium (Canizares et al., 2005c; Canizares et al., 2002b) respectively, although its effect is less significant (not visible) than those of current density and initial phenol concentration.

Tian et al. (2006) investigated the degradation of phenols on BDD anode using recycling batch reactor with platinum as counter electrode for operating conditions of current density 10 - 80 $mAcm^{-2}$ and pH values of 1.1, 6.1 and 12.1. They reported that the removal efficiency increases with increase in current density and pH with optimum current density of 400 $mAcm^{-2}$. At higher current density than the optimum current density, no improvement in the electro-oxidation rate was found when more current was applied, indicating that the mass-transfer effect became the dominant mechanism. The COD removal efficiency was over 90% at neutral or basic pH values after passing through a charge loading of 6.5 Ah/L, with the efficiency increasing with the charge loading. They noted that for the condition of 91% COD removal, the current efficiency is slightly over 50% and higher charge loading further decreases the current efficiency.

Work reported by Pacheco and other authors (Pacheco et al., 2007) introduced the concept of quantifying the extent of combustion in anodic oxidation of several phenolic compounds from the classical theory of instantaneous current efficiency. Experimental values of combustion efficiencies (ICE_C) in tests performed at different current densities show that generally, ICE_C increases with increasing current densities. Under their experimental condition applied of current density of 10 - 30 $mAcm^{-2}$ and phenol concentration of 50 - 300 mg/l, the effect of the solute concentration on ICE_C shows that under conditions of diffusive control, ICE_C is independent of the concentration, pointing out that combustion and current efficiencies are independent quantities. Within the range of their experimental parameters, they concluded that complete combustion of phenol requires the application of higher current density.

Hagans and co-investigators (Hagans et al., 2001) used BDD anode and platinum cathode to treat 10 mM phenol in 0.1 M H_2SO_4 electrolyte circulated through two compartment flow cell with the electrodes separated by nafion 423 Membrane. They reported that TOC in solution was reduced from 1% to 0.1% with no observable decrease in decomposition rate and the effect of current was found to be insignificant

Using impinging cell equipped with BDD anode and stainless steel counter electrode, electrolysis of phenol conducted by Polcaro in collaboration with other investigators (Polcaro et al., 2003) showed that removal of phenol was not significantly affected by current density but rather was controlled by mass transfer due to the enhanced hydrodynamic conditions of the cell. In contrast, they found the current density to have more effect on COD and TOC removal. They verified that during oxidation of organic compounds, such as phenol, the crucial point to obtain high current

efficiency is the rate of mass transfer of the reactant towards the electrode surface. They obtained high mass transfer coefficients (e.g. 9.98 x 10^5 ms^{-1}) at the current density of 15 $mAcm^{-2}$, achieving a faradic yield of 100% and almost complete disappearance of their initial organic loading. Moreover, they established that the first order rate of oxidation of phenol is higher than that of its intermediations (aromatic compounds; hydroquinone and benzoquinone, and carboxylic acids; maleic & oxalic acids) during the oxidation of phenol.

2.5 Kinetic Modeling of Electrochemical Oxidation on Boron-Doped Diamond Electrode

Beside the pollutant removal efficiency, the ratio of the current effectively used in the electro-oxidation of organics (I_{eff}) at a given time (t) to the applied current (I_{app}) defined as the instantaneous current efficiency (ICE), measures the performance of the electro-oxidation process, thus;

$$ICE = \frac{I_{eff}}{I_{app}} \qquad 2.9$$

Gherardini in collaboration with other researchers (Gherardini et al., 2001) observed that, at sufficiently high organic species concentration, high values of ICE can be achieved which indicates that the anode material used promotes the electro-oxidation and reduces the side reaction of oxygen evolution. However, when the concentration of the organic species in the electrolyte is low and the hydrodynamic conditions are not favorable, usually low values of ICE are obtained. They attributed the latter case to the mass-transfer effects that limit the ability of the organic species reaching the anode surface rather than to the low activity of their anodic material.

At any given time, t , the limiting current ($I_{\lim}$) in the electro-oxidation of organics defined in Equation 2.10, is directly a function of both hydrodynamic conditions and organic compound concentration, C.

$$I_{\lim} = nAFk_d C \qquad 2.10$$

Where F the Faraday constant, COD is given in mg/L, n is the number of transferred electrons and C is the organic concentration in mg/l.

For electro-combustion of organic compound, the global parameter, COD, is more appropriate in representing the oxidation process in lieu of the organic compound concentration, thus, Equation 2.10 becomes:

$$I_{\lim} = nAFk_d COD \qquad 2.11$$

Henceforth, depending on the applied current density, I_{app} ,with respect to the $I_{\lim}$,which decreases during the treatment, two different operating regimes were identified based on the equations describing temporal evolution of COD and ICE during oxidation of organic compounds on BDD anode (Boye et al., 2002; Comninellis and Pulgarin, 1991; Gherardini et al., 2001; Panizza et al., 2001; Rodrigo et al., 2001).

$I_{app} \leq I_{\lim}$; for low current density, sufficiently high concentration of the organic, electrolysis was under current-limit control, the current efficiency was 100% and the COD decreased linearly over time as given in Equation 2.12 indicating kinetically controlled process.

$$COD_t = COD_0\left(1-\frac{\alpha A k_d}{V_r}t\right) \qquad 2.12$$

$I_{app} > I_{\lim}$; for high current densities and low organic concentrations, the electrolysis was under mass-transport control, secondary reactions (such as oxygen evolution) commenced, resulting in a decrease in the current efficiency according to Equation 2.13. In this regime, the COD removal followed an exponential trend (Equation 2.14) due to the mass-transport limitation and the effects of oxygen evolution reactions.

$$ICE = \exp\left(-\frac{Ak_d}{V_r}t+\frac{1-\alpha}{\alpha}\right) \qquad 2.13$$

$$COD_t = \alpha COD_0 \exp\left(-\frac{\alpha A k_d}{V_r}t+\frac{1-\alpha}{\alpha}\right) \qquad 2.14$$

Where COD_0 and COD_t represent chemical oxygen demand at time zero and t in mol O_2 m^{-3} respectively, V_r is reservoir volume in m^3, k_d is mass transfer coefficient in ms^{-1}, A is electrode area in m^2 and $\alpha = i_{appl}/ i^0_{lim}$ where i^0_{lim} is initial limiting current density.

Alternatively, the ICE could be estimated according to the rate of COD removal in Equation 2.15 (Boye et al., 2002; Comninellis and Plattner., 1988; Comninellis and Pulgarin, 1991; Gandini et al., 2000; Morao et al., 2004; Panizza et al., 2001).

$$ICE = \frac{\left(COD_t - COD_{t+\Delta t}\right)}{8 I_{app} \Delta t} FV_r \qquad 2.15$$

Pacheco and co-investigators (Pacheco et al., 2007) argued that Equations 2.14 and 2.15 are not suitable for the estimation of effective rates of combustion, unless complete mineralization is assumed in the oxidation process. Therefore, they introduced the concept of combustion efficiency, ICE_C , for measuring the performance of the electro-oxidation process for a generic organic compounds of the type $C_x H_y O_z$. They identified the ICE_C as the efficiency of the mineralization of the whole compound in accordance to fundamental Equation 2.16 and they derived the semi-empirical function given in Equation 2.17.

$$C_x H_y O_z + (2x - z) H_2O \rightarrow x CO_2 + (4x + y - 2z) H^+ + (4x + y - 2z) e^- \qquad 2.16$$

$$ICE_C = \frac{32}{12}\left(\frac{n}{4x}\right)\frac{dTOC}{dCOD} \qquad 2.17$$

Inferably, the ICE_C can be calculated from the slope of a TOC vs COD plot, if n and x are known. Where n is the number of moles of electrons transferred to the electrode in the combustion reaction.

2.6 Oxidation of Phenol in Presence of Cyanide, Sulfide and Ammonia

As enumerated earlier regarding the complexity of industrial wastewater effluents from refinery and petrochemical industries, in addition to presence of the phenolic compounds, these category of wastewaters are prone to containing other environmental pollutants which may include CN^-,

S^{2-} and NH^{+}_{4} . The toxicities and/or general environmental impacts of these inorganic species have been well documented (Adelaida et al., 2007; Bagarinao, 1992; Dasha et al., 2009). Once released above their regulated thresholds, they are prone to negatively altering the natural settings of the ecosystem. Cyanide as a singly-charged anion containing unimolar amounts of carbon and nitrogen atoms triply-bonded together CN^{-} is a strong ligand capable of complexing even at low concentrations with virtually any heavy metal thereby possessing strong ability to mobilize and leach toxic metals (Dasha et al., 2009; Ogtveren et al., 1999). Therefore, the consequence of its release is the fact that the health and survival of most of the victim plants and animals are dependent on the transport of these heavy metals through their tissues. Sulfide has been mostly studied as an industrial health hazard for people working in oil wells and refineries, kraft paper mills, tanneries, sewers, manure pits, fishing fleets and hot-spring reservoirs (Bagarinao, 1992). At the physiological level, sulfide is known to have two major effects on mammals: (i) local inflammatory and irritative effects on moist membranes including the eye and respiratory tract, and (ii) cessation of respiratory function, specifically cardiac arrest due to paralysis of the respiratory centers of the brainstem (Bagarinao, 1992). While natural oxidation of released NH_4^{+} into the ecosystem produces nitrite and nitrate which are among the major precursors of excessive increase in nutrients in the ecosystem balance thereby causing undesirable eutrophication. Consequently, mitigating pollution associated with industrial wastewater from refineries and petrochemical industries would unavoidably require simultaneous removal of phenol and the cohabiting inorganic species for meeting discharge regulatory requirements. However, literature surveyed suggested that simultaneous oxidation of phenol and cohabiting inorganic species such as cyanide, sulfide and ammonia using electrochemical oxidation using BDD anodes has not been reported. Pearl and other authors (Pearl et al., 1988) have investigated the competitive oxidation

of phenol in presence of sulfide and cyanide ion in binary mix matrixes using photocatalysis with ZnO catalyst. At higher initial concentration of S^{2-} , they found the presence S^{2-} lowers the yield of phenol oxidation. Similarly, they reported that in phenol-cyanide solutions a strong competition occurs that decreased the bio-oxidation yield of phenol. A number of other studies on this subject matter focused on employing biological processes in degradation of phenol in mainly binary and ternary mix matrixes. One of such studies was a research credited to Vazquez and his colleagues (Vazquez et al., 2006) where simultaneous removal of phenol, ammonium and thiocyanate from industrial coke wastewater by aerobic biodegradation at bench scale was reported. Eventhough, maximum removal efficiencies of 75%, 98% and 90% were obtained for COD, phenols and thiocyanates, respectively, however, the retention time runs into tens of hours (up to 90 hours). In addition, Ricardo and other researchers (Ricardo et al., 2009) claimed to be the first authors to have reported the simultaneous oxidation of sulfide and phenol in a denitrifying biofilm reactor. They found the consumption efficiencies of phenol and sulfide by microbial consortium they used to be as high as 100%. However, a critical look into all these studies which mainly employed biodegradation processes revealed that large reactors necessitating very longer retention time were used and the bacterial consortiums utilized cannot always be reliable or harnessed whenever the need arose. Moreover, the issues of total mineralization were not often taken into account by most of the authors as the parent compounds might have been transformed into other harmful byproducts which were not taken into cognizance in process efficiency evaluation.

Chapter 3

Research Objectives

The intensive literature survey conducted clearly showed enormous studies have been conducted pertaining to electrochemical oxidation of phenol on BDD anodes. Reports corroborating one another from such studies well established that under varying experimental conditions, complete oxidation of phenol is achievable with highest current efficiency ever found with any other electrode material. Moreover, they established the superiority of the BDD electrodes over other electrodes in terms of attractive attributes in environmental pollution mitigation. However, the current situation apparently appeals for addressing areas deficient in the literature to advance the understanding of the mechanism and reaction pathways during application BDD electrodes in phenol oxidation. One key area found to be more appealing was the oxidation of phenol in wastewater matrixes containing other cohabiting oxidizable inorganic species where unavoidable competitive oxidation may adversely affect phenol oxidation process. Thereby, under such scenarios, the vast reputations, superiority and competitiveness of the BDD electrodes over other conventional electrodes in pollution control may be jeopardized. Despite the fact that some of the scanty studies available currently on degradation of phenol in presence of these inorganic species revealed that the cohabiting inorganic species strongly influenced phenol oxidation, the literature surveyed suggested that no single documented article has so far specifically addressed the electrochemical oxidation of phenol using BDD anodes in this regard.

Besides, the foregoing findings from the literature surveyed regarding hindrances of electrochemical oxidation of phenol on BDD anode due to polymerization from different authors

were observed not to be very consistent. A report credited to Comninellis and Pulgarin (1991) suggested the experimental conditions that favors formation of polymeric film on BDD anode during electrochemical oxidation phenol as; alkaline media (pH > 9), low current density (< 30 $mAcm^{-2}$), high temperatures (> 50^0 C) and high phenol concentration (> 50 mM). However, contrary to that, Canizares et al (2002a) reported complete mineralization at pH 12 regardless of other experimental conditions while operating at a temperature range 15-60 ^{0}C, initial phenol concentration of 10 - 40.2 mM and current density range of 15 - 60 $mAcm^{-2}$. While, at initial COD of 1170 ppm (12.45 mM phenol), Tian et al. (2006) effectively degraded phenol on Ti/BDD anode irrespective of initial pH value (1.1, 6.1 and 12.1) with applied CD of 20 $mAcm^{-2}$ and operating temperature of 30 ^{0}C. A different research finding reported by other authors (Gattrell and Kirk., 1990) reaffirmed Comninellis and Pulgarin (1991) assertion that polymer formation due to phenol oxidation could be combated by operating at low pH and high potential (though with reduced activity) and also selection of electrode materials that favor other reaction pathways over polymerization. For that, there was also need to investigate electrochemical oxidation of phenol using BDD anode considering different experimental set-up from those used by the previous authors. By doing so, the most likely operating regime that is more susceptible to leading to phenol oxidation hindrance or polymerization will be comprehended from different perspective.

Therefore, the main objective of this dissertation was to address vital issues related to electrochemical oxidation of phenol using BDD anode with graphite as the counter electrode taking into cognizance the effect of presence of some inorganic species in simulated petrochemical wastewaters. The specific target objectives of the current research are:

- To experimentally investigate the electrochemical oxidation of phenol in simulated wastewaters using BDD anode in presence of some inorganic pollutants found in refinery and petrochemical industries. The presence of cyanide (CN^-), ammonium (NH_4^+) and sulfide (S^{2-}) will be considered for treatment in different single, binary, ternary and quaternary mix matrixes.
- To investigate the effect of current density, initial phenol concentration, initial pH and supporting electrolyte concentration on the phenol oxidation mechanisms and efficiencies of removal of phenol, Total Organic Carbon (TOC) and Chemical Oxygen Demand (COD).
- To study the removal kinetics of phenol, TOC, COD and the inorganic pollutants in the different mix matrixes and also to assess the effects of the presence of the inorganic species on kinetics of phenol oxidation.
- To investigate the mechanisms and the most likely pathways for phenol oxidation in the presence of the inorganic species via comprehensive analysis of the phenol oxidation intermediary by-products.
- To model the electrochemical oxidation of phenol using Response Surface Methodology (RSM) technique in order to optimize the process and also to comprehend the interactive effects of the influencing parameters on effective oxidation of phenol.

Chapter 4

Experimental Design, Materials and Methods

4.1 Experimental Design

Experiments were designed and conducted in accordance to statistical design of experiments (DOE) technique. The design employed was second order statistical model using 2^4 full factorial design supplemented with other necessary runs to form a complete Face-Centered Central Composite Design (FC-CDD). The factors varied during the experiments were current density, electrolyte concentration, initial pH and electrolysis time at three levels each strictly according to the FC-CDD statistical experimental design as detailed in Chapter Seven. In addition to central point that was replicated six times, other data points that were also replicated as result of increase in electrolysis times accounted for data reproducibility for guaranteeing its data credibility.

Experimental runs for the simulated wastewater matrixes containing phenol cohabited by the inorganic species i.e., NH_4^+, CN^- and S^{2-} ions in different binary, ternary and quaternary mix matrixes were undertaken at two levels of the inorganic ions concentration (100 ppm and 200 ppm) at the optimum conditions obtained from the single phase optimization results. Most of the runs were duplicated (also for ensuring data reproducibility and credibility). A total of about twenty five (25) experiments were conducted.

4.2 Materials and Methods

4.2.1 Chemical Reagents

Several AnalaR@ high grade chemical reagents were used for both the experiments and several analytical techniques employed in this study. They include phenol (C_6H_6O), benzoquinone, hydroquinone, catechol, sodium sulfide ($Na_2S.3H_2O$), sulfuric Acid (H_2SO_4), sodium sulfate (Na_2SO_4), sodium cyanide (NaCN) and ammonium sulfate $(NH_4)_2SO_4$, iron Sulfate $FeSO_4.7H_2O$, potassium dichromate ($K_2Cr_2O_7$), silver sulfate (Ag_2SO_4), mercury sulfate ($HgSO_4$), sodium hydroxide (NaOH), hydrochloric acid (HCl) among many others.

4.2.2 Electrochemical Reactor and Experimental Procedure

All the electrolytic experiments were undertaken in a two (2) liters batch mode using an undivided reactor made of up 2000 cm^3 capacity internal glass compartment and external Plexiglas@ material with a water jacket system. Figure 4.1 provides details of the reactor set-up. The water jacket of the reactor was connected to a HAAKE GE model temperature control water-bath that recycled water continuously through the jacket during the experiments to maintain constant temperature (room temperature). The temperature variation with time during experiments was recorded with the aid of a digital thermometer (Cole Parmer, USA). Synthetic Boron-Doped Diamond electrodes with niobium substrate (Nb/BDD) (CONDIAS, Germany) and graphite electrodes (CONDIAS, Germany) both 10 cm in diameter connected to a DC power supply and multi-meter data acquisition system served as the working and counter electrode respectively. Sodium sulphate (Na_2SO_4) was used as the aqueous phase supporting electrolyte. The electrolysis were carried out at galvanostatic state with constant current supplied by a

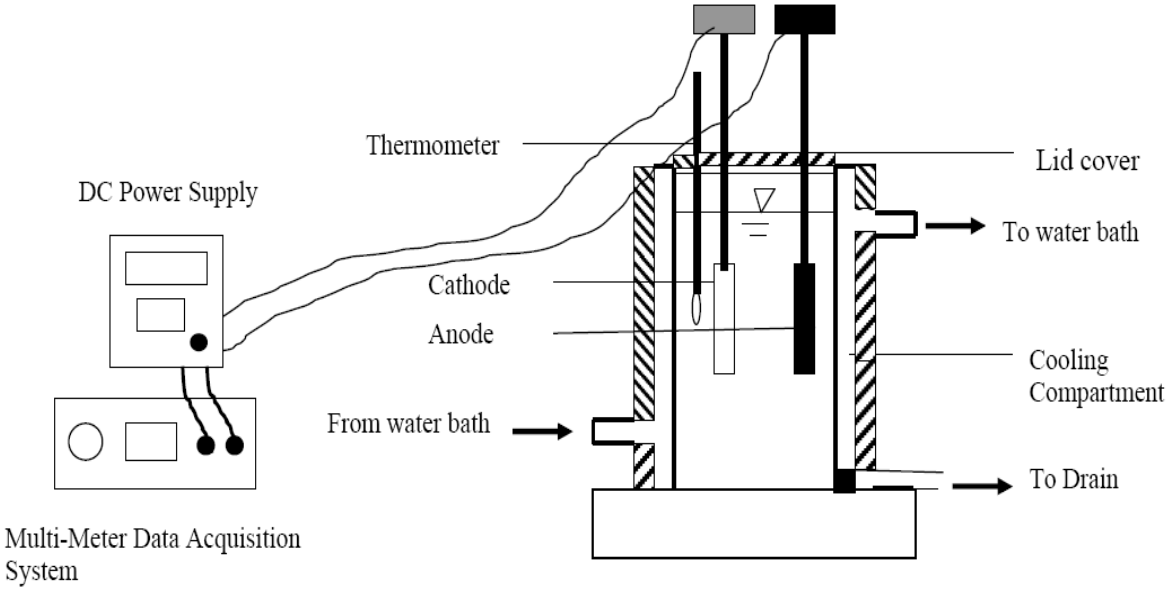

Figure 4.1: Electrochemical Reactor Set-up Used for the Experiments

Kenwood regulated DC power supply PD110-5AD model while voltage fluctuation during electrolysis was automatically recorded using an integrated series Keithley 2700 digital millimeter data acquisition system.

The characteristics of the different simulated wastewaters used for the different mix matrixes experiments are provided in Table 4.1. The concentration ranges of the various species in the simulated wastewaters were chosen so as to have a representatives of wastewaters' characteristics provided in Table 1.2. It was assumed that the simulated wastewaters represented pretreated wastewater effluents that were mainly still laden with high concentrations of the phenol and the inorganic species. The concentrations of other parameters added were comparatively negligible. For any experiment, the simulated wastewater was produced by spiking and mixing predetermined volume of prepared stock solutions of respective species of interest into deionized water in order to get respective targeted initial concentrations of species in solution. Fresh stock solutions were prepared by dissolving high purity reagent chemicals and allowing proper mixing to ensure homogeneity. The desired initial pH of the wastewater was set by adjusting the original pH of the mixed chemicals in solution using H_2SO_4 and/or NaOH. The initial pH of solution and its subsequent changes with time during electrolysis was monitored and recorded using Thermo Scientific Orion 4-Star pH/ISE meter and electrode. During the electrolysis, adequate and homogenous mixing of supplied current and species in solution was maintained by using Eurostar digital IKA@ Werke model mechanical stirrer equipped with polymer shaft and blade operating at constant speed of 1200 rpm. Samples were drawn at specified time intervals (according to the preliminary studies and experimental design), capped and kept in pre-cleaned 20 or 40 ml glass

4.1: Characteristics of the Synthetic Wastewaters used for the Different Mix Matrixes Experiments

Nature of Mix Matrix	Experiment no.	pH	Concentration, mg/l				
			Na_2SO_4	Phenol	NH_4^+	CN^-	S^{2-}
Single	1	5	1000	100	-	-	-
Binary	2	5	1000	100	100		-
	3	5	1000	100	-	100	-
	4	5	1000	100	-	-	100
	5	5	1000	100	200	-	-
	6	5	1000	100	-	200	-
	7	5	1000	100	-	-	200
	8	12	1000	500	200	-	-
	9	12	1000	500	-	200	-
	10	12	1000	500	-	-	200
Ternary	11	5	1000	100	100	100	-
	12	5	1000	100	100	-	100
	13	5	1000	100	-	100	100
	14	5	1000	100	200	200	-
	15	5	1000	100	200	-	200
	16	5	1000	100	-	200	200
Quaternary	17	5	1000	100	100	100	100
	18	5	1000	100	200	200	200

vials and samples were analyzed immediately for the various parameters of interest. Due to the toxicity high risk of exposure to phenol, the cohabiting inorganics and some byproducts expected to be generated during electrolysis, all experiments and some of the analytical procedures were strictly conducted inside well ventilated fumehood.

4.2.3 HPLC and GS-MS Analysis for Phenol and its Oxidation Byproducts

A WATERS 1525 High Performance Liquid Chromatography (HPLC) model, equipped with a binary pump, WATERS 2996 Photodiode Array Detector (PDA), WATERS 717 plus Autosampler and Spergel C18 reversed-phase column, was calibrated and used to quantify phenol and the aromatic intermediate compounds of phenol degradation, mainly benzoquinone, hydroquinone and catechol from the drawn samples at various time intervals of the electrolysis. The most suitable mobile phase used was analytical grade methanol and dionized water 1/4 (volume/volume) at a flow rate of 1 mL/min and injection volume of 10 µl. The column temperature was kept at 25 ^{o}C, while the column pressure was 195–2000 atmospheres and the analytical wavelength of the PDA was set at 270 nm. In addition, analysis for oxidation byproducts was further supplemented with analysis employing a set of Agilent Technologies instruments' series that comprised of 6890N gas chromatogram (GC) equipped with 5973 mass selective detector (MSD) and 7683 auto injector. The column used was a Fused silica capillary column 30 m x 2.55 µm while extraction solvent was HPLC grade dichloromethane. More details for the analysis for the GC-MS are provided in Chapter Six. Pictures of the complete HPLC and GC-MS set-ups are provided in Figures 4.2 and 4.3, respectively

Figure 4.2: HPLC Set-up for Phenol and its Aromatic Intermediates Quantifications

Figure 4.3: GC-MS Assembly for Phenol and Its Oxidation Byproducts Qualifications

4.2.4 Chemical Oxygen Demand and Total Organic Carbon Analysis

Chemical Oxygen Demand (COD) was determined using widely known closed-refluxed titrametric method according to standard procedure described by (Jirka and Carter, 1975) with the aid of ECO25 Thermoreactor and 10µl precision digital burette (BRAND, Germany). TOC was analyzed using TOC-V_{CSN} Analyzer model (Shidmazu, Japan) equipped with Autosampler ASI-V model (Shidmazu, Japan) whose picture is displayed in Figure 4.4.

4.2.5 Inorganic Ions Analysis

The inorganic species (i.e., ammonium, cyanide and sulfide ions) were analyzed using their respective Ion Selective Electrode (ISE) (Cole Parmer, USA) in conjunction with Thermo Scientific Orion 4-star bench-top pH/ISE meter according to standard methods and their respective procedures as provided by their manufacture. Appropriate procedures were taken to ensure interferences were eliminated for each sample before analysis started for all the entire samples.

Figure 4.4: TOC-Analyzer Set-Up for TOC Analysis

Chapter 5

Phenol, TOC and COD Removal and Mechanism of Phenol Oxidation

5.1 Introduction

The various levels of the experimental operating parameters that defined the experimental design's region of interest of the central composite design (CCD) adopted for this study were selected based on preliminary studies and literature surveyed. Similarly, based on the preliminary studies, the maximum electrolysis time of 3.5 hours was observed to be sufficient for complete detoxification of the wastewater optimally, and as such, 3.5 hours retention time was fixed for all the experiments to enable basis for results comparative analysis. To optimize the utilization of the boron doped diamond (BDD) anode, the minimum operating cell potential required was selected according to limitations of the DC power supply used, thus, the range of current density was chosen and studied at three levels (30, 45 and 60 $mAcm^{-2}$). The Initial pH was set at three levels; acidic, neutral and basic pH of 2, 7 and 12, respectively, to cover wide range of possible initial pH values of wastewaters effluent from refinery and petrochemical industries. At the beginning of each experiment, the pH of the simulated wastewater was adjusted to the desired initial pH and it was neither buffered nor kept constant by adding acid or base while running the experiment. This was opted for in the view that by allowing the pH to freely vary with time, vital inferences regarding the nature of byproducts produced would be made retrievable which would be completely lost if it were done otherwise. As the nature and concentration of supporting electrolyte significantly influence byproducts to be generated and hence the oxidation pathways

during electro-oxidation of phenol (Canizares et al., 2009), sodium sulphate (Na_2SO_4) electrolyte was selected for the present study due to three reasons. First, the possibility of in-situ generation of powerful oxidants such as peroxodisulphate (the third in hierarchy of powerful oxidants; see Table 2.1) due to decomposition of Na_2SO_4 when used as supporting electrolyte. The availability of peroxodisulphate in the bulk solution could supplement the direct electro-oxidation (purely electron transfer reactions on the anode surface) via promoting the indirect oxidation process thereby increasing the process efficiency. Second, the avoidance of generation of chlorinated byproducts from commonly used chlorine based electrolytes. The last reason was the fact that both Na^+ and SO_4^+ are not of great concern once released into the environment as their allowable threshold concentrations are high. The electrolyte was also varied at three levels (1000, 3000 and 5000 ppm) so as to assess the influence of an increase in the SO_4^+ species concentration on the process efficiency.

Typical variations of cell voltage and pH with time during electrolysis are illustrated in Figures 5.1A and 5.1B, respectively. It can be deduced from the cell voltage-time variation that the anode had neither deteriorated nor passivated (a common phenomenon associated with many electrode material during electrolysis of phenols); and it also indicated that there was neither formation of non-conductive layers on the surface of the electrodes nor electrode corrosion during the treatment (Canizares et al., 2009). Belaid and his research colleagues (Belaid et al., 2006) attributed this observation of voltage variation with time to the superb performance and robust nature of the BDD electrode when used as an anode during aqueous electrolysis. While the variation of pH with time shows that for both initial pH 7 and 12, there existed pH decay with time; in most cases, the pH moving downward to the acidic region. However, for initial pH 2, no

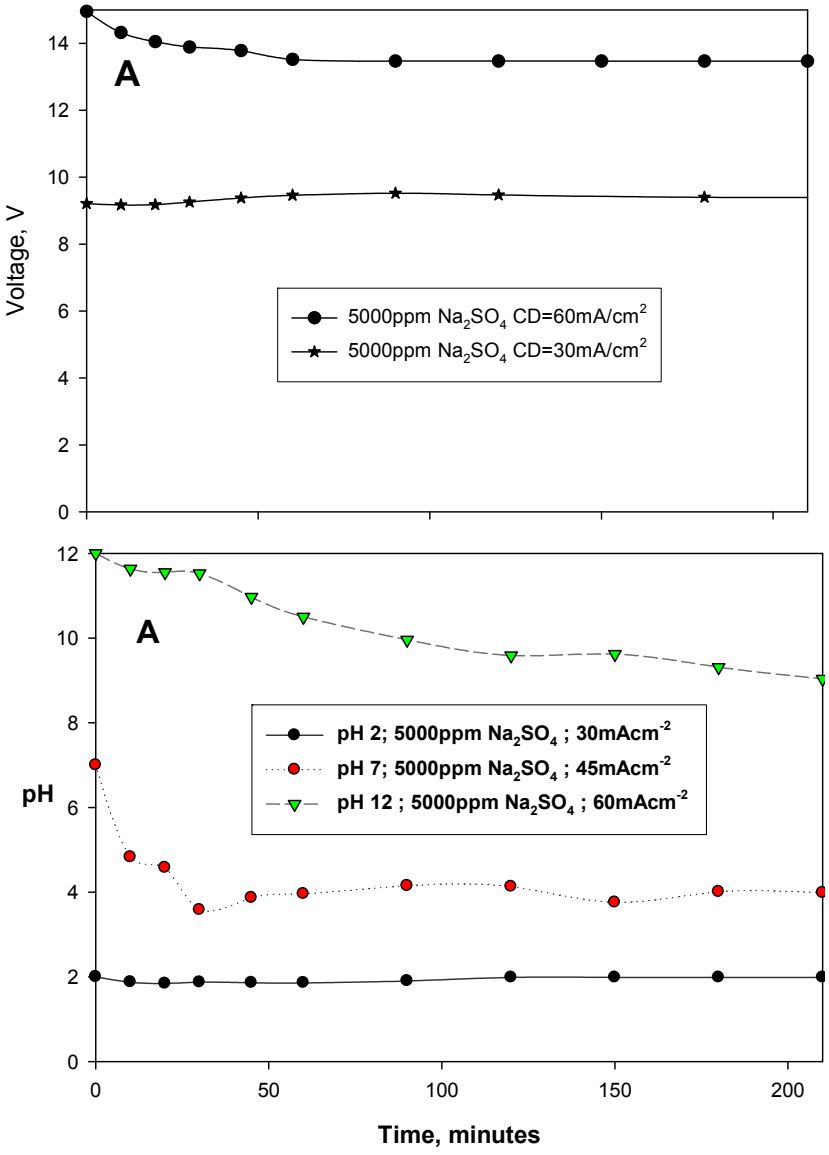

Figure 5.1: Typical Variations of (A) Cell Voltage and (B) pH with Electrolysis Time

considerable change in the pH was encountered. Under all the three initial pH values, these observations suggest that some of the compounds generated during the phenol oxidation were acidic in nature. The buffering that appeared to have occurred while operating at initial pH 2 may indicate that the generated compounds acidities were not high enough to alter the pH of the existing strong acidic environment.

5.2 Effect of Operating Parameters on Removal of Phenol, TOC and COD

5.2.1 Effect of Current Density on Removal of Phenol

Figures 5.2A and 5.2B show the influence of current density on the removal of phenol at initial pH 2 and 12, respectively. At the initial pH 2, elimination of phenol increases with time at different removal rates with more than 80 % removal at the end of the 210 minutes electrolysis time under all operating conditions. Regardless of the level of the electrolyte concentration, the removal efficiency was found to slightly improve by doubling the current density from 30 $mAcm^{-2}$ to 60 $mAcm^{-2}$. The highest removals at the two current densities were recorded as 99.73 % and 97.69 %, respectively. Although characterized with slight improvements, phenol removal trends at initial pH 12 presented in Figure 5.2B show no marked deviation from the removal at initial pH 2. Moreover, at the design central point operating conditions (i.e., initial pH 7 and 3000 ppm Na_2SO_4), the removal rate initially increases with current density, but eventually complete phenol removal was approximately observed under all applied current density (Figure 5.3).

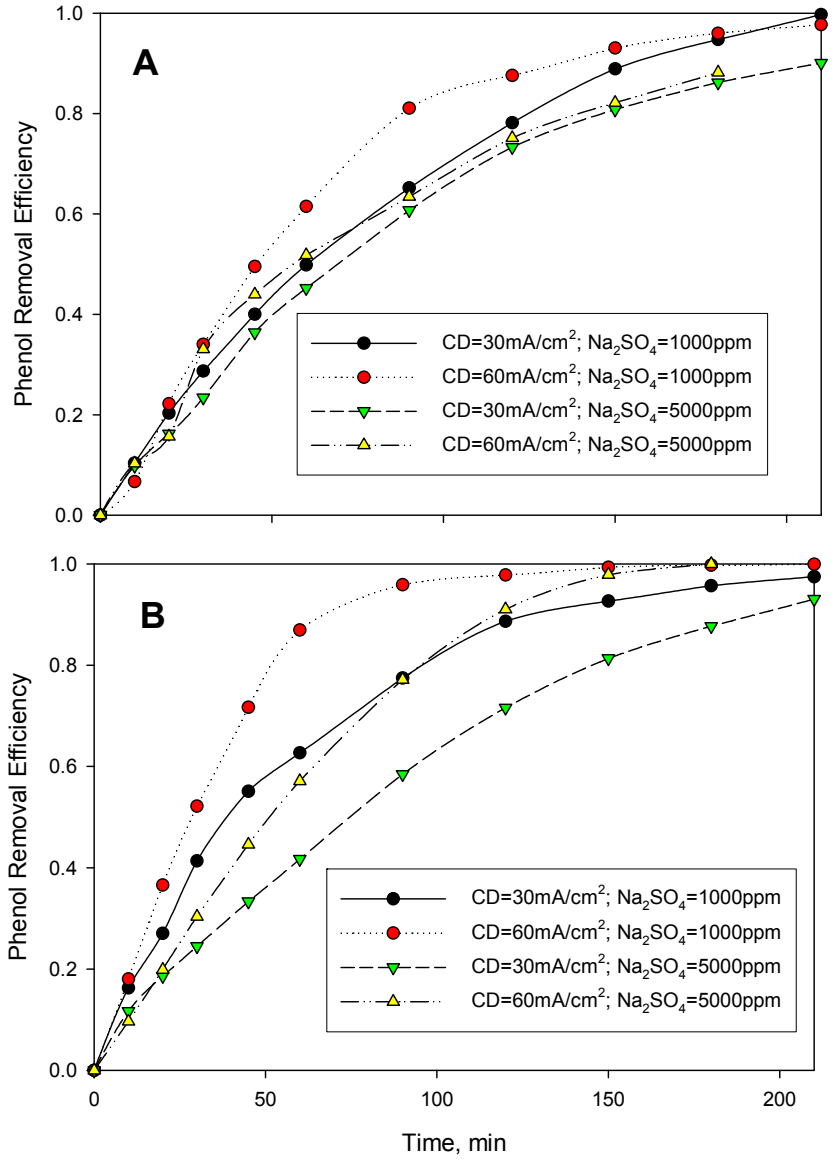

Figure 5.2: Effect of Current Density on Phenol Removal at (A) pH 2 and (B) pH 12

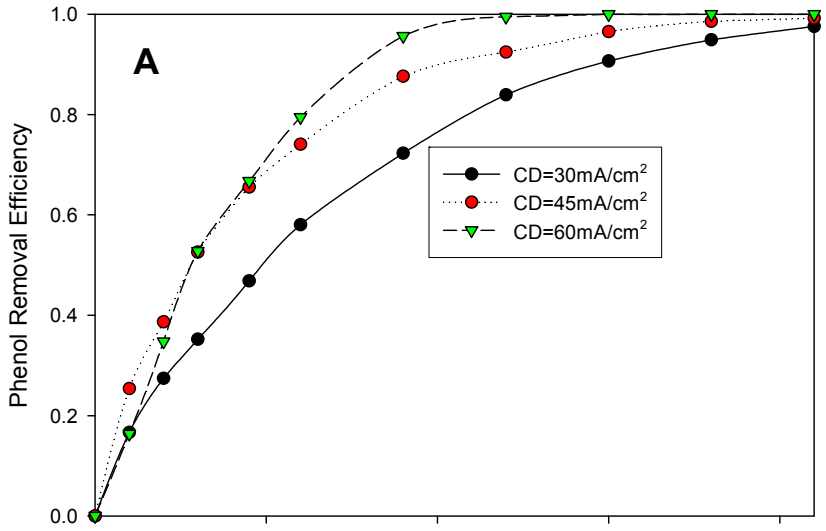

Figure 5.3: Effect of Current Density on Phenol Removal at pH 7 and 3000 ppm Na_2SO_4

These observations reveal that under the present experimental conditions, increasing current density doesn't always lead to better results as anticipated. This goes in accord with data presented by other researchers (Tian et al., 2006) which indicated that increase in current density may not improve the phenol oxidation efficiency when mass transfer effect dominates and controls the process during electrochemical oxidation of phenol. Hence, in the present case, the influence of mass transfer might be the reason that rendered the effect of change in current density to be mild in most of the cases. Moreover, improvements of removal as results of change in current density apparently show that the process was kinetically controlled and that attainment of steady state or equilibrium (necessitating longer electrolysis time in some cases) would ensure total phenol removal regardless of the operating condition. It is noteworthy to mention that the ability to remove phenol effectively within the defined region of interest within the range of parameters investigated couldn't justify complete decontamination of the original wastewater (i.e., effectively oxidizing phenol to harmless byproducts (i.e., H_2O and CO_2). Consequently, the effect of the parameters on corresponding TOC and COD are presented in the following sections in order to comprehend the efficiency of overall oxidation of phenol rather than its mere disappearance.

5.2.2 Effect of Current Density on Removal of TOC

The dependency of TOC removal on current density at initial pH 2 and 12 are shown, respectively, in Figures 5.4A and 5.4B. This figures show many similarities to observations made regarding phenol removal. At the initial pH 2, with treatment at 30 $mAcm^{-2}$ exhibiting lower TOC removal compared to 60 $mAcm^{-2}$, the general removal tendency suggests that the process was also a kinetic controlled process and hence, at longer electrolysis time (beyond the design

retention time of 3.5 hour), complete removal of TOC was achievable at different removal rates. While the removal efficiency at the lower current density shows smooth and continuous trends throughout the treatment time, however, regardless of the electrolyte concentration, at 60 $mAcm^{-2}$, higher removal efficiencies were first observed for the first 2 hours of electrolyses before slowing down slightly thereafter. Also, in support of observations made in case of phenol, at initial pH 2 , increasing the electrolyte concentration from 1000 ppm to 5000 ppm also reduces the TOC removal efficiency in both cases. TOC removal of up to 98% was achieved at 60 $mAcm^{-2}$ and 1000 ppm Na_2SO_4, while the highest for removal at 30 $mAcm^{-2}$ was far below (about 75%). In complete contradiction to such positive removal trends, at initial basic pH of 12, results presented in Figure 5.4B imply that TOC removal was completely not forthcoming at both 30 $mAcm^{-2}$ and 60 $mAcm^{-2}$. However, at the central point of the defined region of interest (3000 ppm Na_2SO_4 and initial pH 7) TOC removal slightly increased with increase in current density (Figure 5.5). Although there was good phenol removal under all experimental conditions which appeared to be kinetically controlled process; the foregoing analyses suggest that removal of TOC always goes proportionally in agreement with that of phenol at any other initial pH beside pH 12. Apparently, there are clear indications that at initial pH 12, the original organic carbon content at time zero (around 77 ppm) were almost the same with the effluent carbon content even after treatment with no sign that it was kinetically controlled (within the retention time of 3.5 hours) process. For this reason, it was speculated that phenol conversion to other organic compounds might be the most predominant phenomenon at initial pH 12 which contrasted oxidation that occurred at initial pH values of 2 and 7.

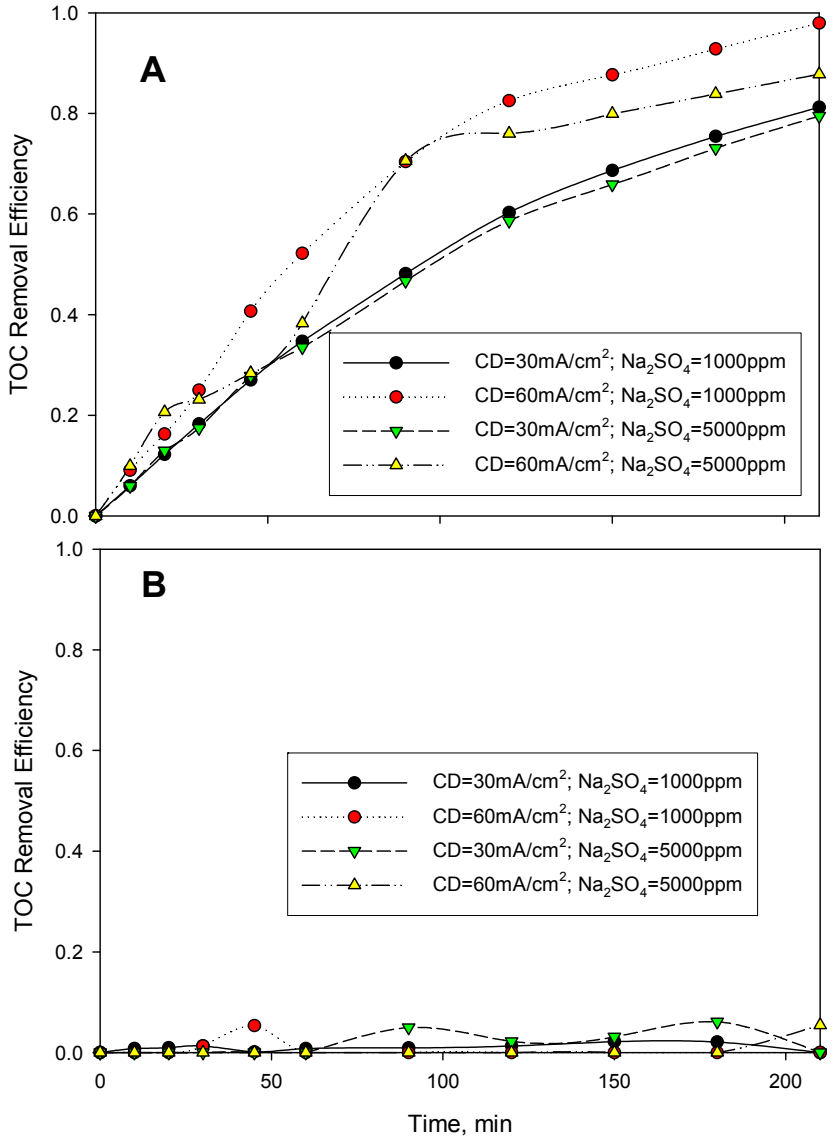

Figure 5.4: Effect of Current Density on TOC Removal at (A) pH 2 and (B) pH 12

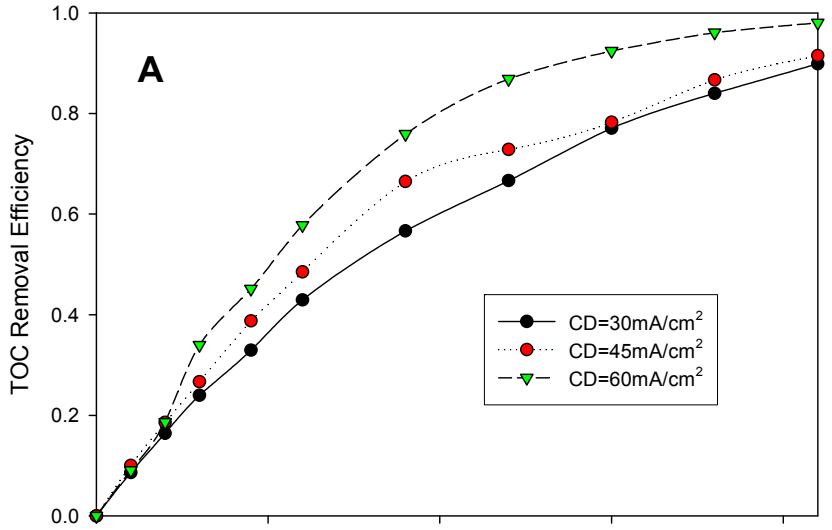

Figure 5.5: Effect of Current Density on TOC Removal at pH 7 and 3000 ppm Na_2SO_4

5.2.3 Effect of Current Density on Removal of COD

The results for dependence of COD removal on current density as shown in Figures 5.6 and 5.7 reaffirm the fact that current density has also significant effects on the COD removal during electrolysis with BDD anode. Moreover, the outcomes are in good agreement with most of the trends previously presented regarding TOC removal under varying experimental conditions studied. This could be understood considering the trends at initial acidic pH 2 (Figure 5.6A) which revealed that COD removal rate could be increased by raising the applied current density from 30 $mAcm^{-2}$ to 60 $mAcm^{-2}$. At these operating conditions, removal efficiency of COD in the effluent was measured as 70% and 85%, respectively. Similarly, at initial basic pH 12, most of the COD experimental results corroborate the trends found in the case of the TOC counterparts, though the removal efficiencies are somewhat better in this case as shown in Figure 5.6B. Electrolysis at this basic pH value led to poor removal with the best removal realized at combination of 60 $mAcm^{-2}$ and 1000 ppm Na_2SO_4. In deviation from the trend found in TOC removal at the central design point (i.e., pH 7 and 3000 ppm Na_2SO_4), Figure 5.7A suggests that both COD removal efficiencies at 60 $mAcm^{-2}$ and 30 $mAcm^{-2}$ superseded removal at 45 $mAcm^{-2}$. However, results for treatment at the star deign point on the CCD design matrix (i.e., initial pH of 2 and 5000 ppm Na_2SO_4) provided in Figure 5.7B shows better removal at 45 $mAcm^{-2}$ over 60 $mAcm^{-2}$, reiterating the fact that the highest current density was not the optimum current density for phenol destruction within the ranges of the various experimental parameters investigated. The COD removal results also buttress the fact that under certain experimental conditions, increasing current density wouldn't always yield better results due to the speculated mass transfer effect that limits the process efficiency; also, additional substantive reaffirmation of results presented elsewhere (Tian et al., 2006).

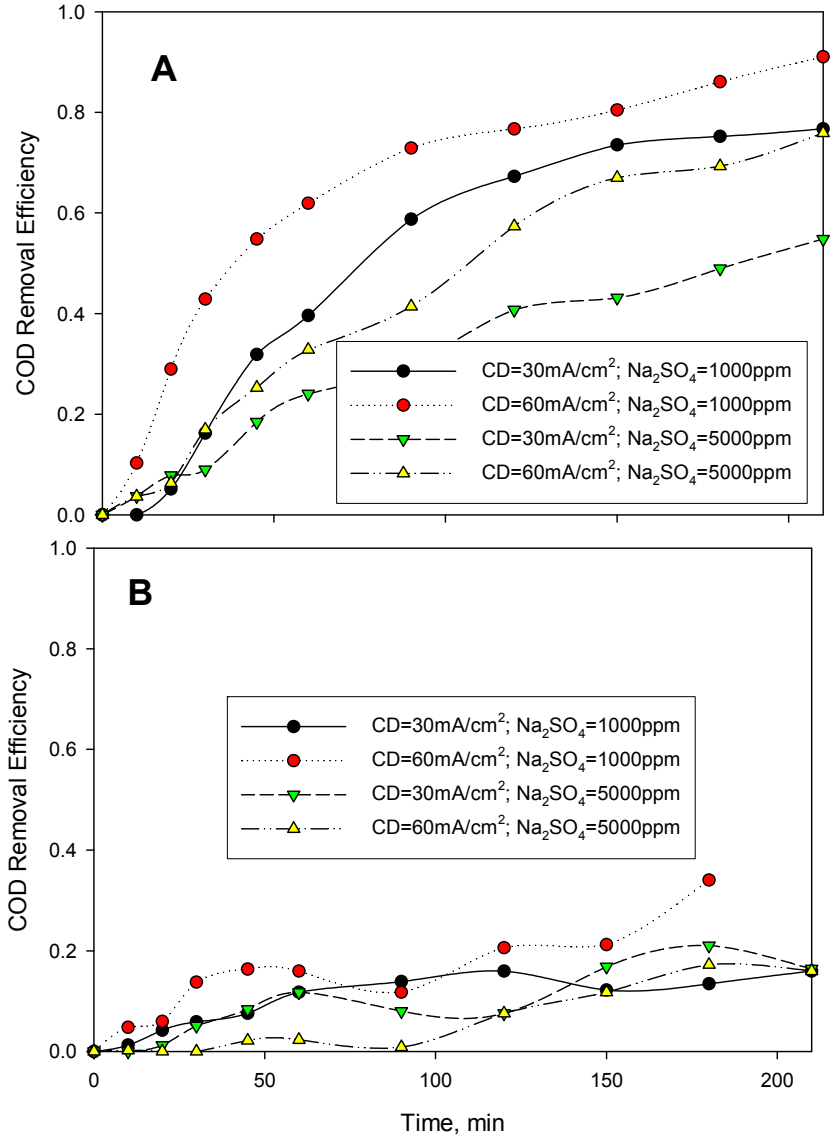

Figure 5.6: Effect of Current Density on COD Removal at pH of (A) pH 2 and (B) pH 12

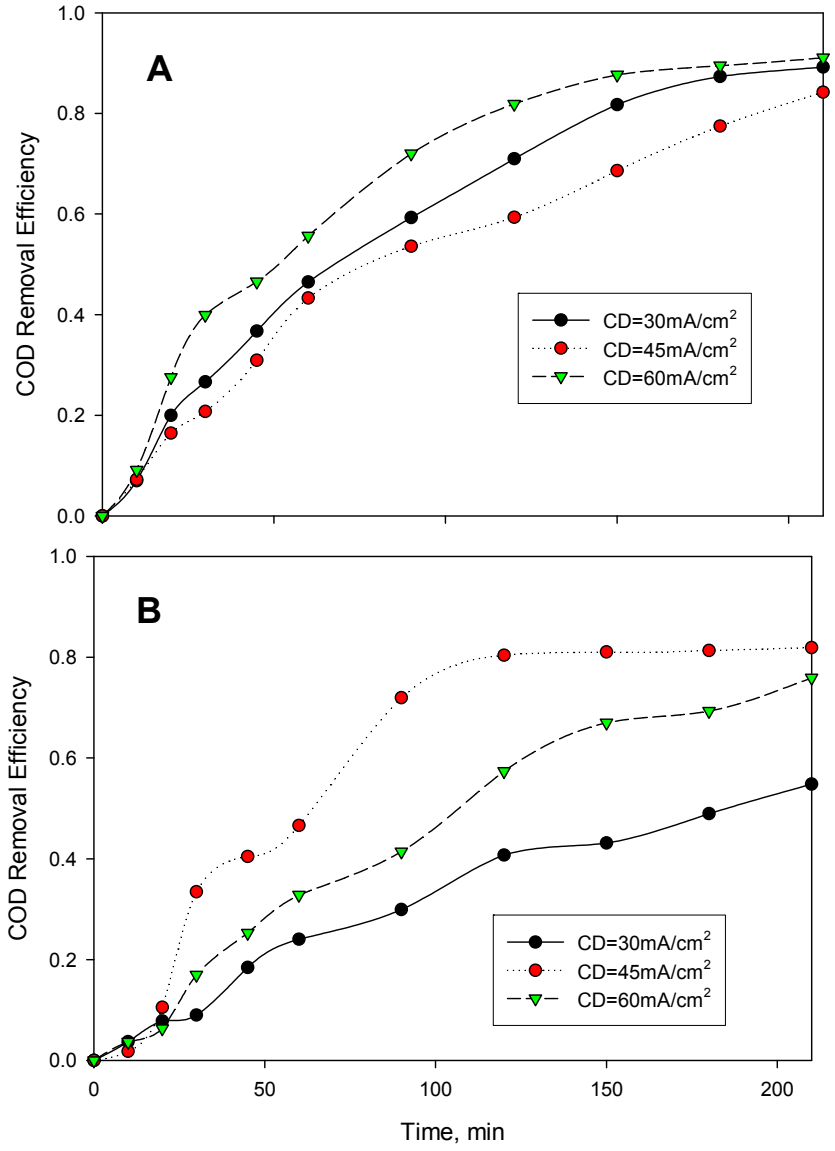

Figure 5.7: Effect of Current Density on COD Removal at (A) pH 7 and 3000 ppm Na_2SO_4 and (B) pH 2 and 5000 ppm Na_2SO_4

Moreover, with the exceptions of results at initial pH 12, the COD removal profiles as a function of applied current density were also kinetically controlled processes; longer treatment would ensure reaching steady state of complete elimination of COD under all experimental conditions. Conclusively, Figure 5.8 depicts the general idea pertaining to the influence of COD on phenol, TOC and COD removal at initial acidic pH 2 from the forgoing analysis. It suggests that increasing the current density mildly improve the decontamination process of the simulated wastewater within the range of investigated current density.

5.2.4 Effect of Initial pH on Removal of Phenol

Initial pH of solution is well known for its influence on reaction pathway(s) during electrochemical oxidation of phenol at different electrodes. In this study, Figures 5.9 and 5.10 signify the effect of initial pH on phenol removal efficiency during electrochemical oxidation of phenol at BDD anode. Results given in Figure 5.9A reveal that at fixed supporting electrolyte concentration of 1000 ppm Na_2SO_4 and irrespective of the current density, faster rate of removals for phenol were initially observed at initial pH 12 compared to the removal at initial pH 2, though at the end of the treatment, almost 100% removal was achieved in both cases. However, by increasing the concentration of the electrolyte by 5-fold (5000 ppm), the removal in the effluent dropped to less than 90% in both cases as shown in Figure 5.9B with no significant difference of the removal established between the two pH levels at 30 $mAcm^{-2}$. In contrast, operating at 60 $mAcm^{-2}$ CD as given in the same Figure 3.9, better removal rate was consistently recorded at initial pH 12 with 100% removal achievable in less than 180 minutes.

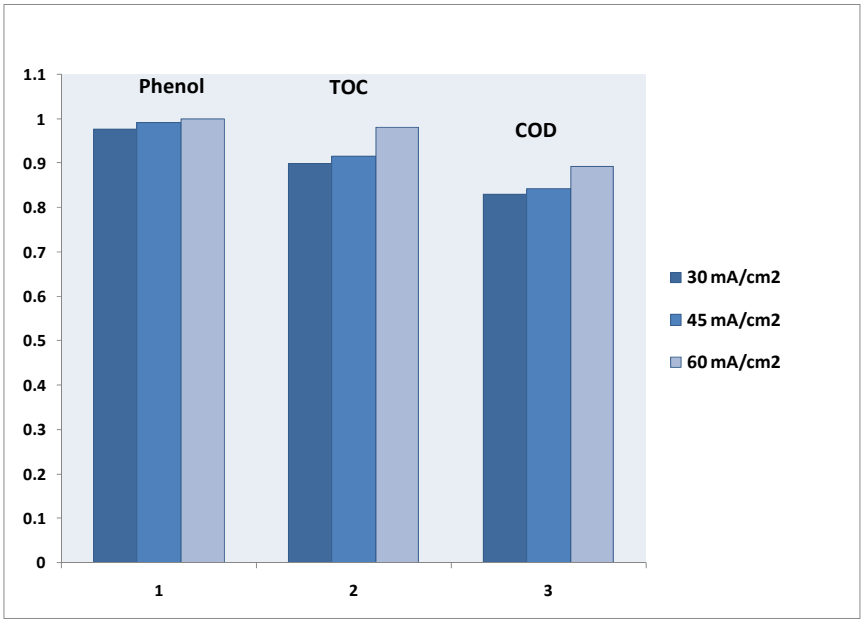

Figure 5.8: Influence of Current Density on Removal of Phenol, TOC and COD at pH 2 for Effluent at 210 minutes Retention Time

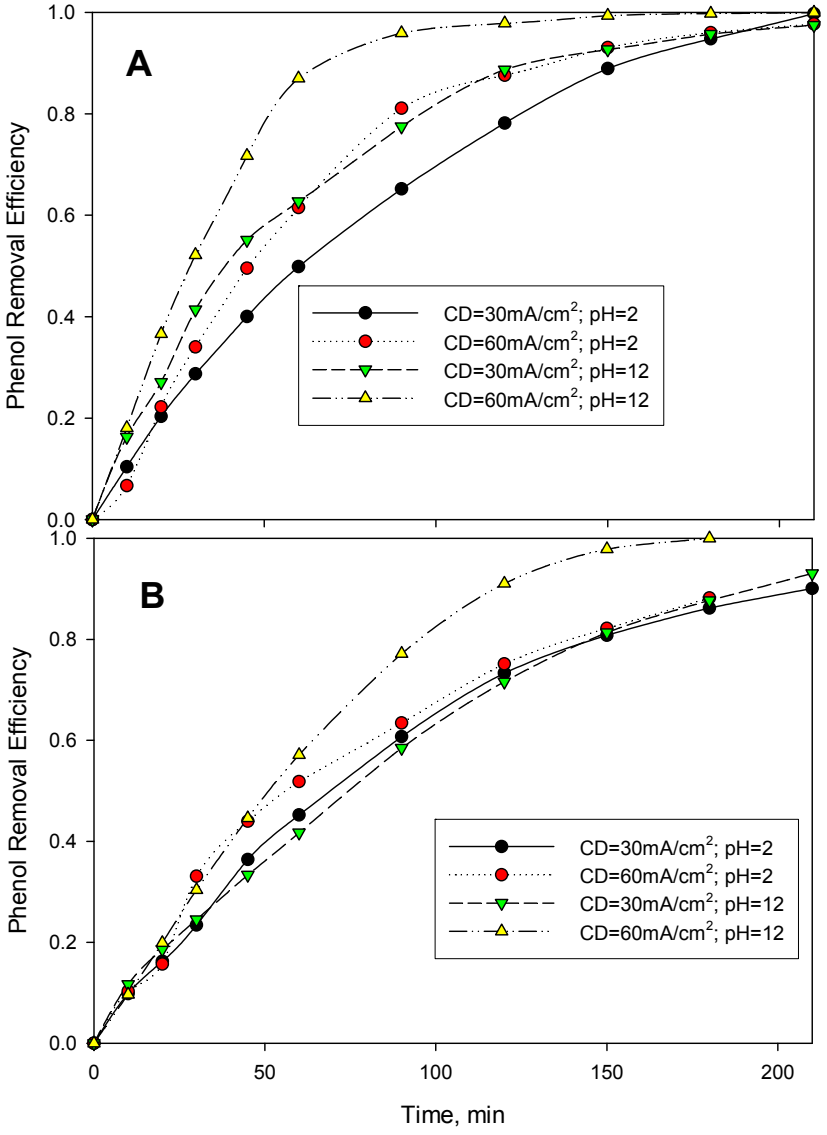

Figure 5.9: Effect of pH on Phenol Removal at (A) 1000 ppm Na_2SO_4 and (B) 5000 ppm Na_2SO_4

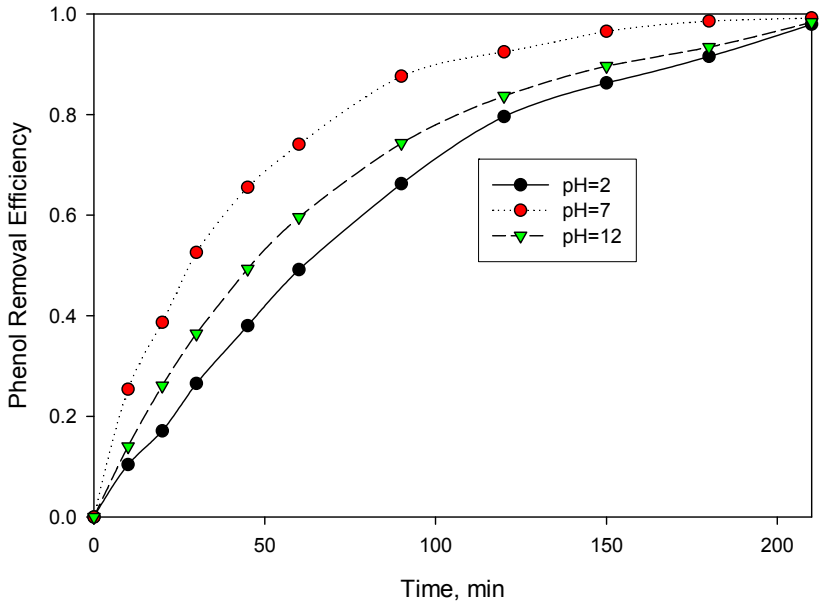

Figure 5.10: Effect of pH on Phenol Removal at 45 $mAcm^{-2}$ and 3000 ppm Na_2SO_4

Although, electrolysis at the central point of the design region (45 $mAcm^{-2}$ and 3000 ppm Na_2SO_4) shows that phenol removal rate at initial pH 7 was improved over that observed at pH 12 as shown in Figure 5.10, nonetheless, total elimination of phenol was almost steady under all the three pH values. Similarly, phenol removal trends as a function of initial pH is generally a kinetic controlled process with equilibrium been attainable at the 3.5 hours of electrolysis for the lower electrolyte concentrations. While at higher electrolyte concentration, the dwindling removal rate in some cases indicated that reaching equilibrium would necessitate time longer than the design retention time of 3.5 hours.

5.2.5 Effect of Initial pH on Removal of TOC

Figures 5.11A and 5.11B provide the variation of TOC removal efficiency with treatment time at supporting electrolyte concentration of 1000 ppm and 5000 ppm Na_2SO_4, respectively. For the 1000 ppm Na_2SO_4 while operating at initial pH 2, TOC was effectively reduced to approximately 21% of its original value at applied current density of 30 $mAcm^{-2}$ while increasing the current density to 60 $mAcm^{-2}$ substantially increased the removal to about 97%. Conversely, under initial pH 12, that TOC removal revealed entirely strange picture as it appeared that TOC removal was not possible throughout the treatment time. In the same manner, it can be seen that treatment at 5000 ppm Na_2SO_4 (Figure 5.11B) and initial pH 12 didn't lead to any appreciable reduction in TOC also, whereas for initial pH 2, TOC removal efficiency increases with time with distinctive features at 30 $mAcm^{-2}$ and 60 $mAcm^{-2}$. While at 30 $mAcm^{-2}$, the TOC removal trend smoothly varies with time throughout the process with unsteadied removal of 70%; however, by doubling the current density to 60 $mAcm^{-2}$, the removal rate was observed to be rapid below 120 minutes

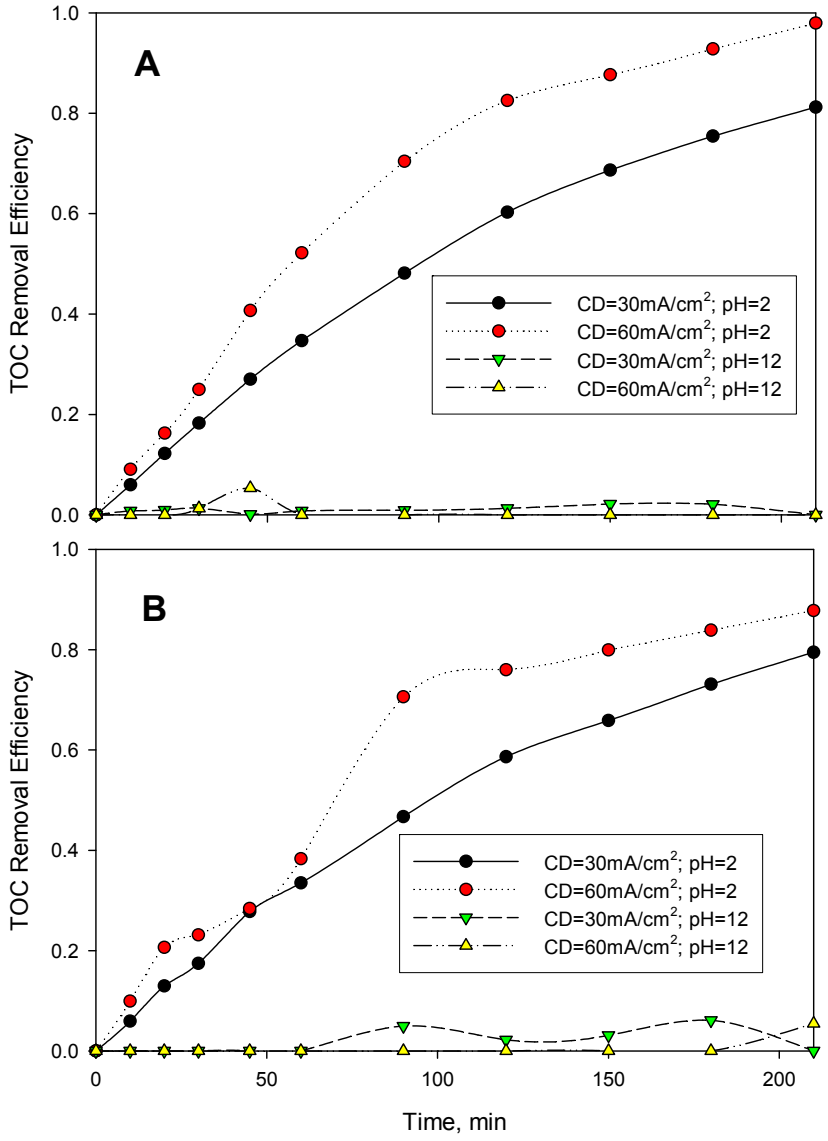

Figure 5.11: Effect of pH on TOC Removal for Electrolyte Concentration of (A) 1000 ppm and (B) 5000 ppm Na_2SO_4

and afterwards it slightly declined reaching the highest removal of about 85%. Based on these trends, it can be inferred that complete removal of TOC requires longer treatment time beyond the retention time of 3.5 hours considering that equilibrium was yet to be achieved under the investigated conditions. The effect of pH on TOC removal at 45 $mAcm^{-2}$ and 3000 ppm Na_2SO_4 displayed in Figure 5.12 suggests that no substantial difference existed in TOC removal between electrolysis at initial pH 2 and 7, while at initial pH 12, the impossibility to eliminate TOC was persistently perceivable. As speculated earlier, the inability to reduce the initial organic carbon content might be as an indication of conversion of phenol to other organic compounds rather than its oxidation to inorganic carbon, particularly CO_2.

5.2.6 Effect of Initial pH on Removal of COD

The effect of initial pH on COD removal efficacy depicted in Figures 5.13 and 5.14, collectively, reveal slight deviations from its effect on the TOC counterpart due to the observed improvements in the COD removal efficiency. At 1000 ppm and 5000 ppm Na_2SO_4 electrolyte concentrations (Figures 5.13A and 5.13B, respectively), much better removal efficiencies in the effluent were similarly obtainable at initial pH 2 compared to initial pH 12 which were susceptible to improving by increasing the current density from 30 $mAcm^{-2}$ to 60 $mAcm^{-2}$ for the former case. Figure 5.14 indicates that treatment at the mid levels of other factors (i.e., 3000 ppm Na_2SO_4 and 45 $mAcm^{-2}$) clearly shows that better removal efficiency of COD follows the order: pH 7 > pH 2 > pH 12 which also goes in line with the observed trends in the previous cases (phenol and TOC removals) at central points of the CDD design matrix. Although the removal efficiencies of COD

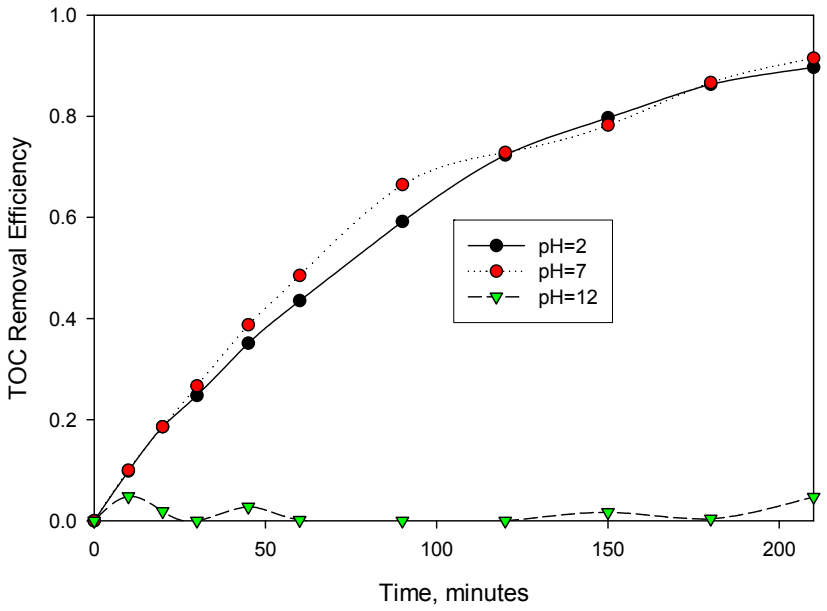

Figure 5.12: Effect of pH on TOC Removal at 45 $mAcm^{-2}$ and 3000 ppm Na_2SO_4

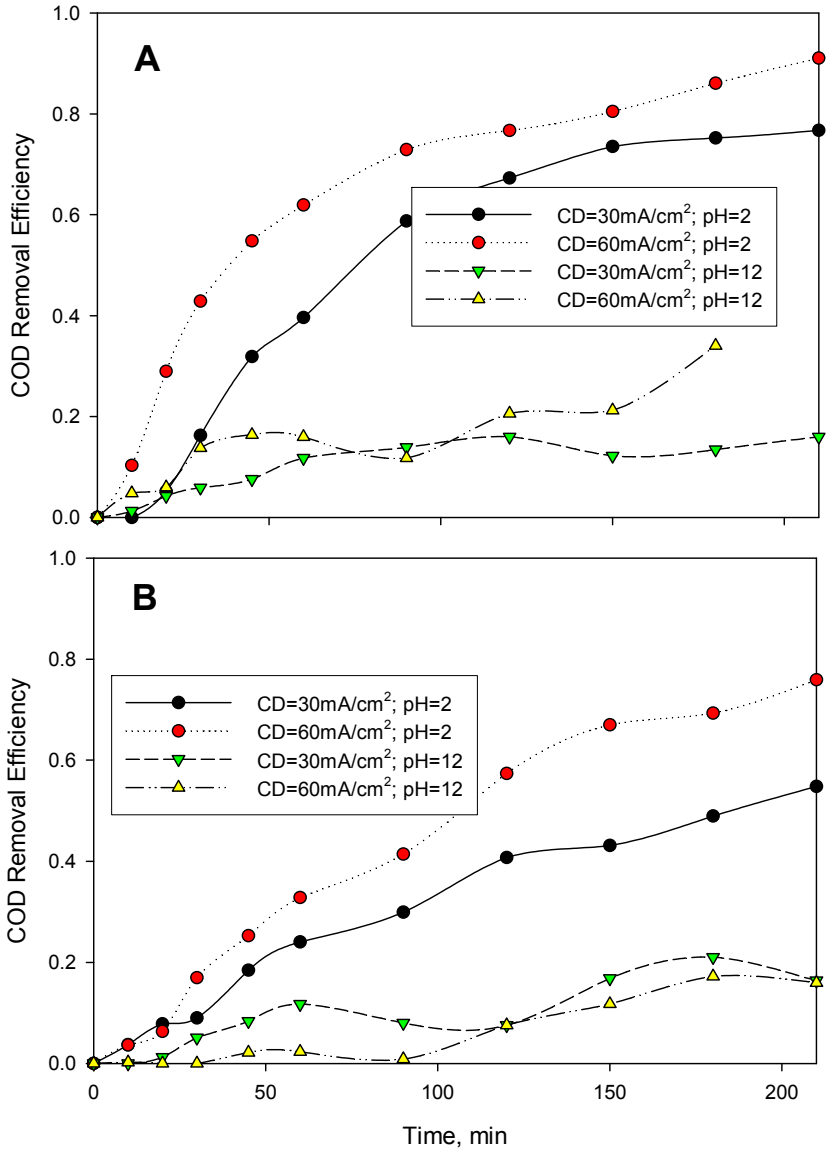

Figure 5.13 Effect of pH on COD Removal at Electrolyte Concentration of (A) 1000 ppm and (B) 5000 ppm Na_2SO_4

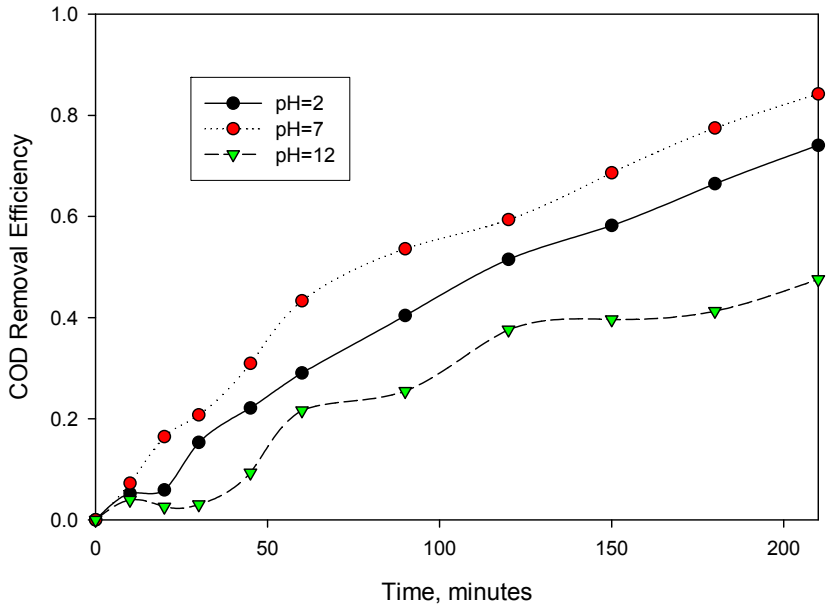

Figure 5.14: Effect of pH on COD Removal at 45 $mAcm^{-2}$ Current Density and 3000 ppm Na_2SO_4

at initial pH 12 substantiate the poor TOC removal presented earlier; however, the slightly better COD removal compared to the TOC could be attributed to two main reasons. First, the organic compounds resulting from phenol oxidation might be those that exert less oxygen demand than the parent compound. The second reason could be the relative higher percent error usually associated with the titrametric COD measurements employed in this study compared to the more accurate automated TOC measurement procedure used. Nonetheless, from the removal profiles presented above which are summarily depicted in Figure 5.15, the general perception of the effect of initial pH on COD removal are in direct support of the corresponding TOC removal profiles, thereby substantiating the idea that phenol oxidation was only severely hindered at pH 12.

5.2.7 Effect of Electrolyte Concentration on Removal of Phenol

At galvanostatic state of 30 $mAcm^{-2}$ and 60 $mAcm^{-2}$, respectively, Figures 5.16A and 5.16B display the results for increasing the electrolyte concentration from 1000 ppm to 5000 ppm Na_2SO_4 at the acidic and basic initial pH levels. In general, it is evident from these figures that better rate of phenol removal could be attributed to the low electrolyte concentration. The removal efficiency at 30 $mAcm^{-2}$ and initial pH 12 decreased by almost 10% as result of increase in the electrolyte concentration by 5-fold (Figure 5.16A). Similarly at the same current density and initial pH 2, the drop in the removal efficiency was about 14% as also depicted in Figure 5.16A. However, at the highest current density, such differences at the end of the 3.5 hours electrolysis are rendered to be insignificant (Figure 5.16B). Moreover, Figure 5.17 shows that at the mid-levels of the design matrix (i.e., 45 $mAcm^{-2}$ and pH 7), change in electrolyte concentration appeared to have insignificant effect on phenol removal.

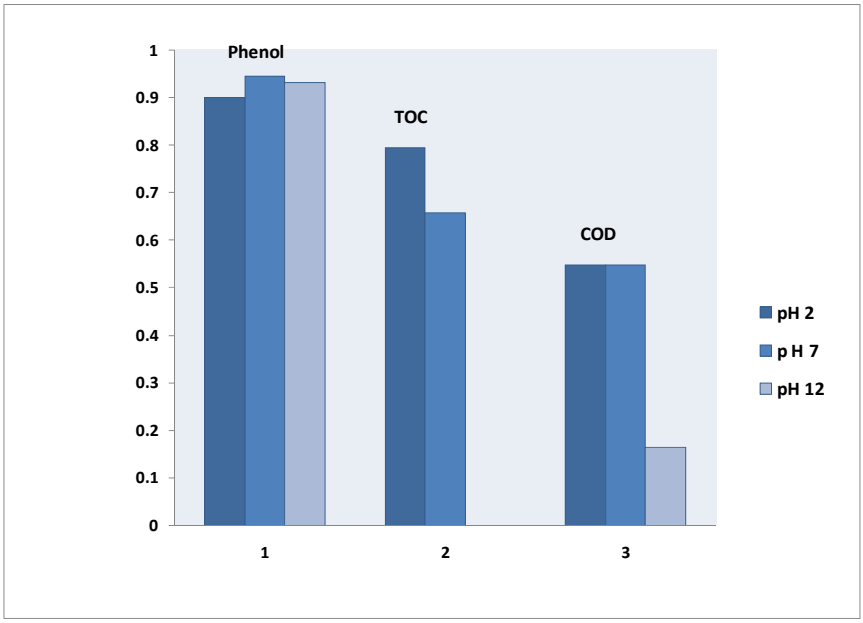

Figure 5.15: Influence of pH on Phenol, TOC and COD Removal Efficiencies for Effluent at 210 minutes Retention Time

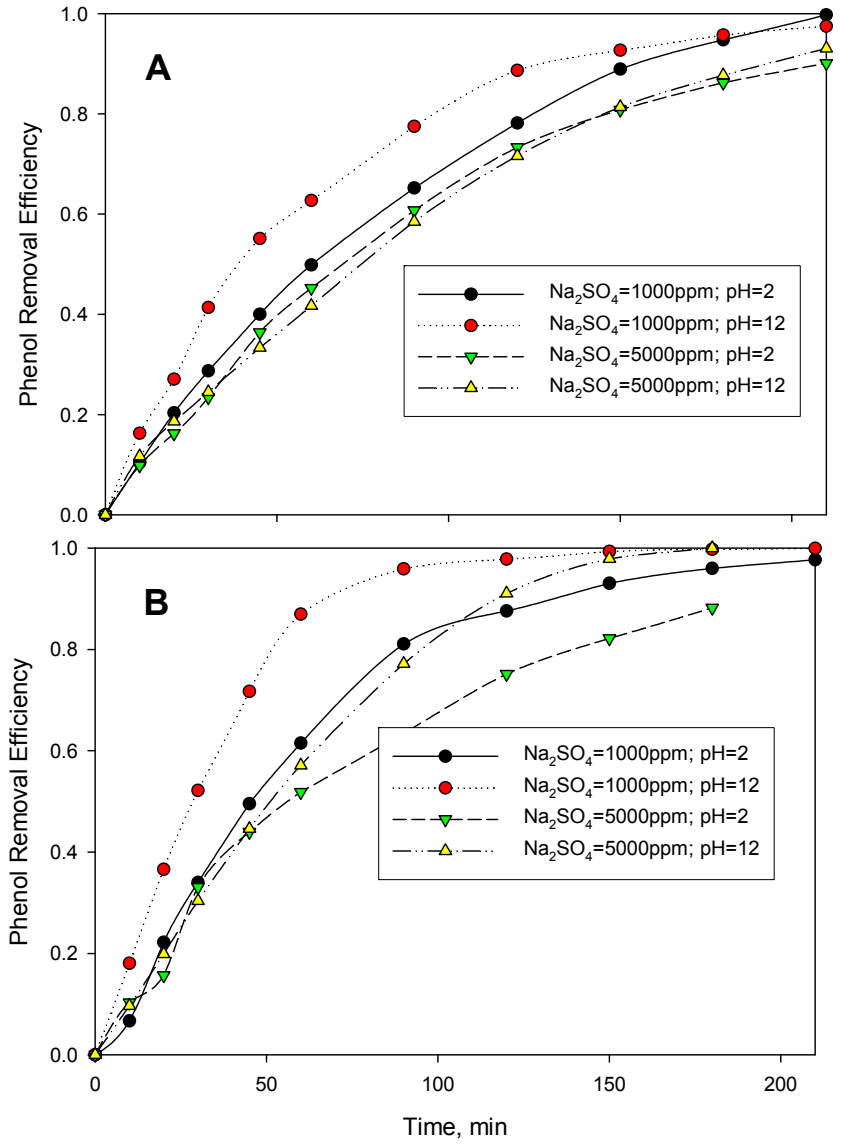

Figure 5.16: Effect of Electrolyte Concentration on Phenol Removal at (A) 30 $mAcm^{-2}$ and (B) 60 $mAcm^{-2}$

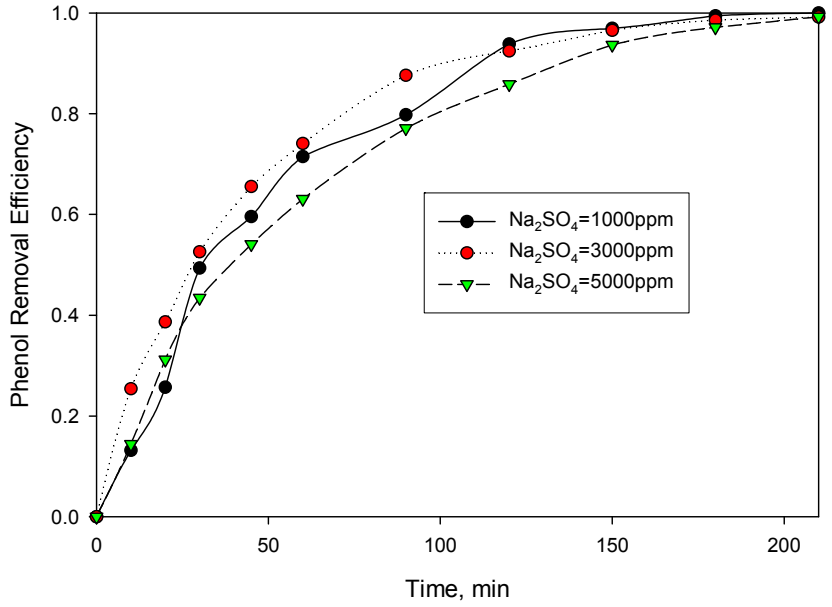

Figure 5.17: Effect of Electrolyte Concentration on Phenol Removal at 45 $mAcm^{-2}$ and pH 7

The Na_2SO_4 supporting electrolyte concentration was increased with the expectation that it would enhance the efficiency of both phenol elimination and oxidation from three distinctive perspectives. First, the electrochemical decomposition of Na_2SO_4 during electrolysis was anticipated to lead to the production of peroxodisulphate, a powerful oxidant which could effectively promote indirect phenol oxidation mechanism; thereby supplementing the default direct process (i.e., electron transfer reactions at the surface of the BDD anode). Second, presence of supporting electrolyte leads to increase in ionic conductivity which results in an increase in charge transport thereby resulting in an increase in mass transport. However, it became obvious from the results discussed earlier that increasing Na_2SO_4 concentration paradoxically led to the reduction in the rate of phenol removal. This can be an indication that the operating conditions and/or the cell design either didn't favor the peroxodisulphate production reactions or have led to production of weak and inactive peroxodisulphate. Moreover, the decline in the removal rate due to increase in Na_2SO_4 could be attributed to the confounding consequences of the mass transfer effect on the phenol not only due to hydrodynamic conditions but rather as result of blocking effects by other cohabiting species in solution with tendency to be more pronounced at higher concentration of the cohabiting species in solution. Third, in addition to ability to generate in-situ oxidant and mass transfer effects, at galvanostatic conditions, increase in concentration of supporting electrolyte increases the solution conductivity which invariably leads to decrease in applied voltage across the cell. This was expected to reduce the energy consumption thereby improving the overall current efficiency.

5.2.8 Effect of Electrolyte Concentration on Removal of TOC

The variation of TOC removal efficiency with time at 30 $mAcm^{-2}$ and initial pH 2 shows no significant improvement by lowering the Na_2SO_4 concentration from 5000 ppm to 1000 ppm (Figure 5.18A). However, Figure 5.18B shows that at 60 $mAcm^{-2}$ and initial pH 2, lowering the electrolyte concentration slightly led to better TOC removal efficiency as in the case of phenol. In clear support of previous observations, at initial pH 12, no substantial removal of TOC was achievable; thereby rendering the effect of electrolyte concentration on phenol oxidation unperceivable. Presence of supporting electrolyte was anticipated to improve the oxidation of phenol to CO_2 which could be indicated by reduction in TOC until steady of total removal is achieved. Result at the central point design (i.e., initial pH 7 at 45 $mAcm^{-2}$) as provided in Figure 5.19 reiterates the fact that changes in the electrolyte concentration slightly influenced the phenol oxidation process. These results are in absolute support of the hypothesis already put forward before which suggest that the presence of the Na_2SO_4 was immaterial in production of additional oxidants within the bulk of the solution to counter the mass transport effects that appeared to be the key rate limiting factor.

5.2.9 Effect of Electrolyte Concentration on Removal of COD

The effect of electrolyte concentration on removal of COD while operating at constant CD of 30 $mAcm^{-2}$ and 60 $mAcm^{-2}$ are displayed in Figures 5.20A and 5.20B, respectively; while Figure 5.21 depicts the results for the respective central point of the experimental design (initial pH 7 and 45 $mAcm^{-2}$). Most of the observable trends in these figures are to considerable extent similar to the observed trends in TOC removal due to the fact that TOC and COD are complementary indexes in serving as barometers to evaluate organic compound oxidation effectiveness.

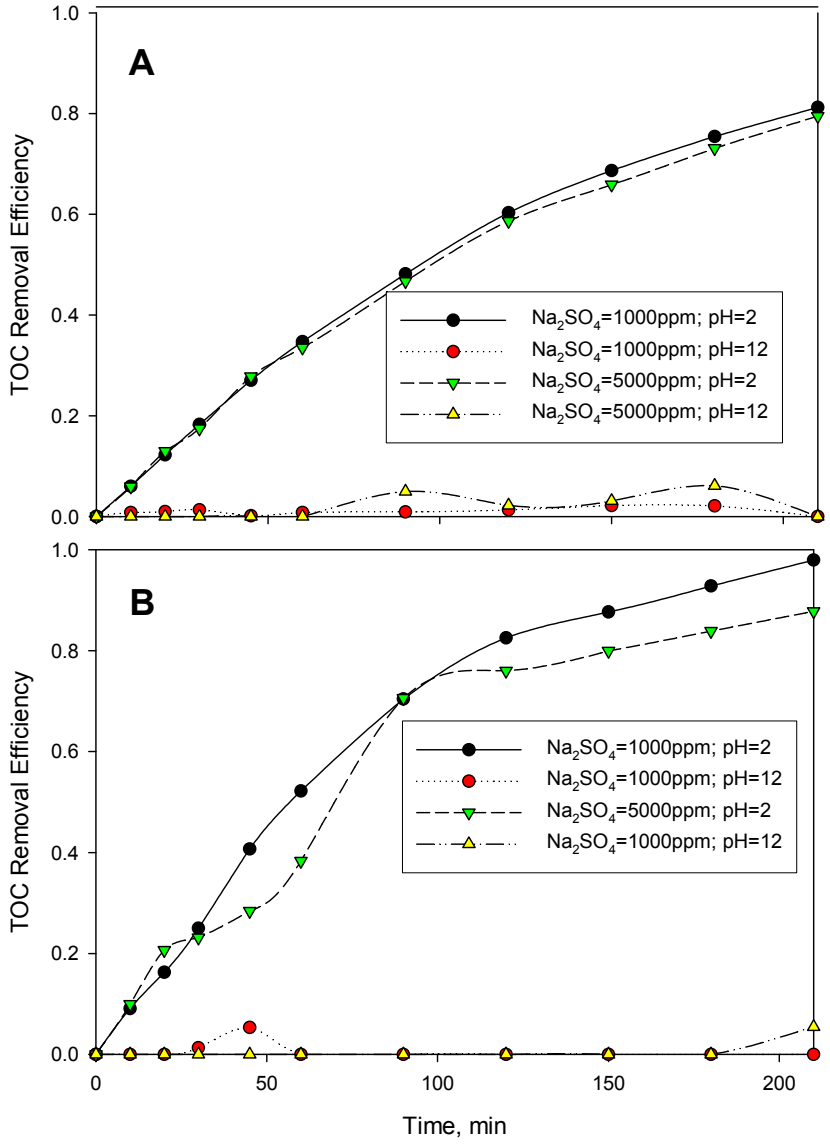

Figure 5.18: Effect of Electrolyte Concentration on TOC Removal at (A) 30 $mAcm^{-2}$ and (B) 60 $mAcm^{-2}$

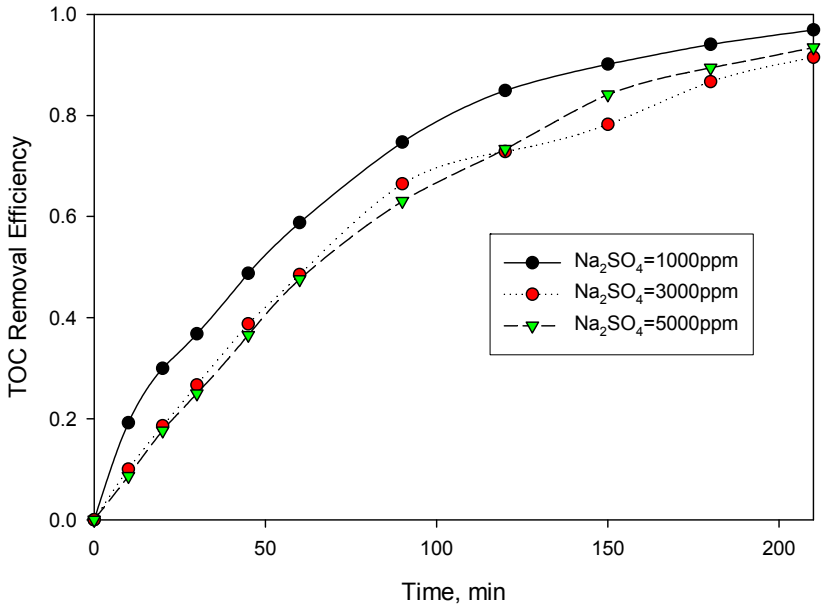

Figure 5.19: Effect of Electrolyte Concentration on TOC Removal at Initial pH 7 and 45 $mAcm^{-2}$

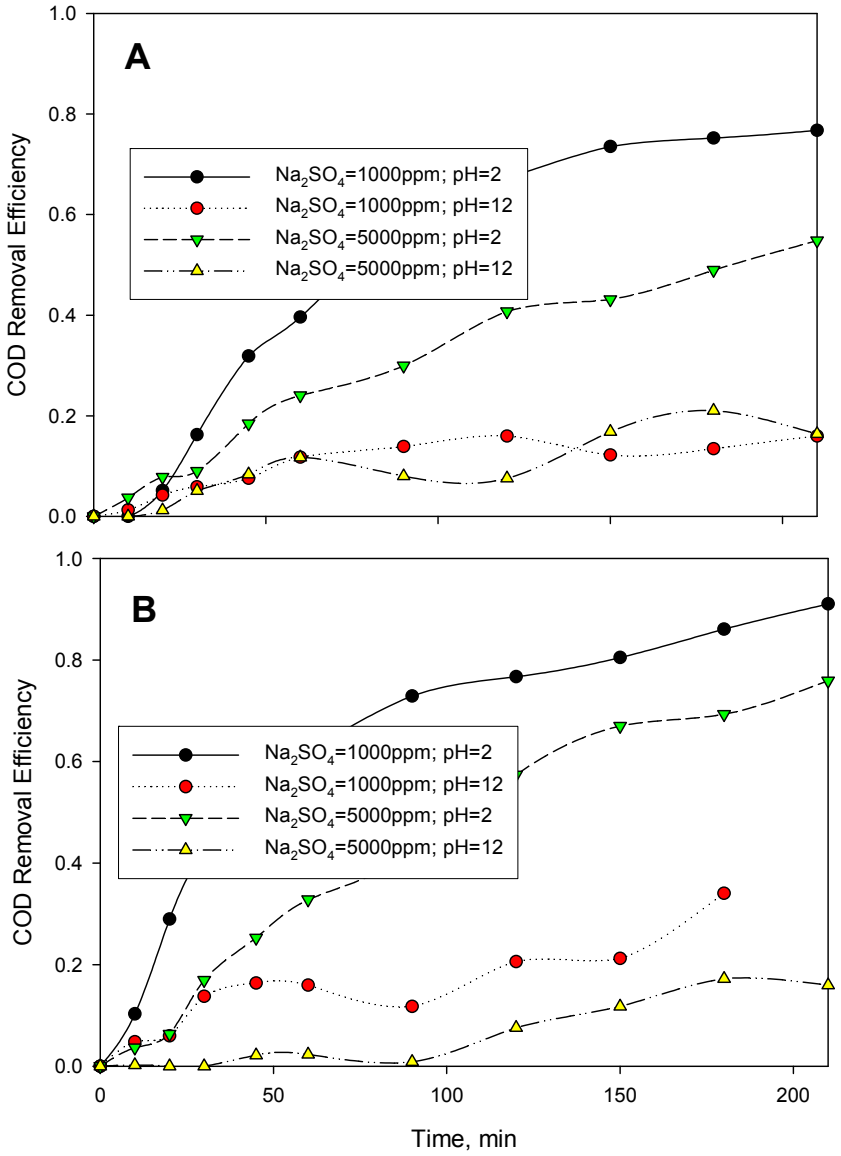

Figure 5.20: Effect of Electrolyte Concentration on TOC Removal at (A) 30 $mAcm^{-2}$ and (B) 60 $mAcm^{-2}$

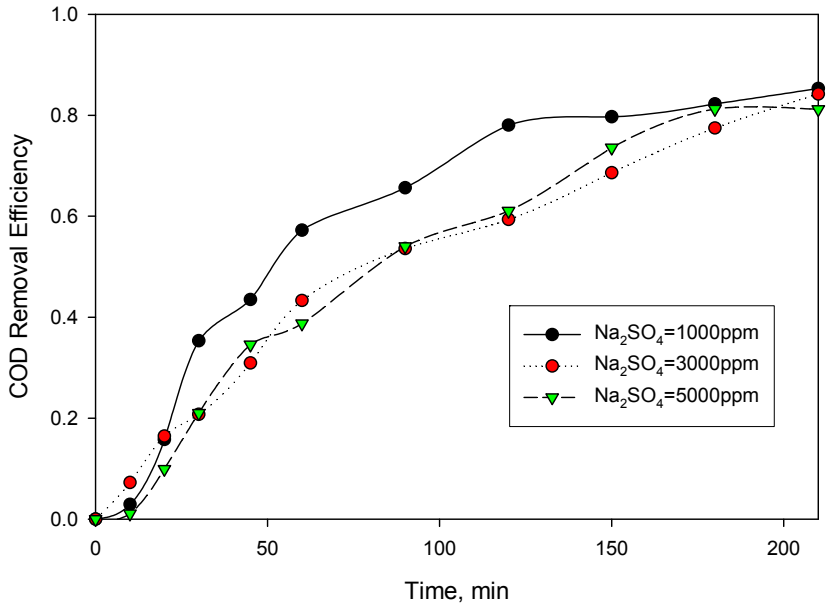

Figure 5.21: Effect of Electrolyte Concentration on COD Removal at Initial pH 7 and 45 $mAcm^{-2}$

Summarily, the COD removals in this case reiterate the fact that, generally, slightly better removal efficiencies are achievable at 1000 ppm Na_2SO_4 compared to both 3000 ppm and 5000 ppm Na_2SO_4 with no difference observable for treatment at 3000 ppm and 5000 ppm (Figure 5.22).

5.2.10 Effect of Initial Phenol Concentration on Removal of Phenol, TOC and COD

To assess the influence of initial phenol concentration on phenol, TOC and COD removal efficiencies, phenol concentration was increased by a factor of five (5) and ten (10) (i.e., to 500 ppm and 1000 ppm) and treated at two different experimental conditions. The results for the first tested operating condition (30 $mAcm^{-2}$ and initial pH 2) are provided in Figures 5.23A, 5.24A and 5.25A for phenol, TOC and COD, respectively. Although it can be deduced from these figures that the relative removal efficiencies for these quality parameters didn't follow any specific pattern in general, however, it appeared that the total moles of phenol removed drastically increases with increase in the initial concentration. The total percent removal for phenol, TOC and COD at the three levels of the initial phenol concentrations were (90.7, 93.22 and 76.22%), (79.47, 75.53 and 45.17%) and (54.82, 75.53 and 44.06%), respectively. On the other hand, Figures 5.23B, 5.24B and 5.35B depict the data for the effect of initial phenol concentration at 60 $mAcm^{-2}$ and initial pH 12, the second tested experimental condition. Very insignificant reduction in the relative percent removal of phenol was observed due to the increase in the phenol concentration. Interestingly, in contrast to the prevailing persistence of inability to remove TOC and COD at initial pH 12 for 100 ppm initial phenol concentration as observed earlier, tremendous removals of both TOC and COD were both achieved at 500 and 1000 ppm

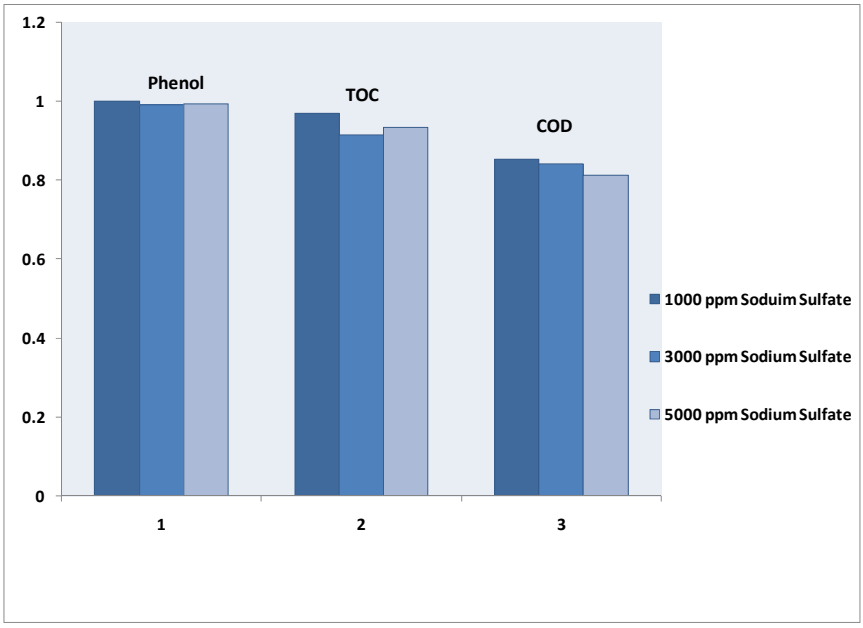

Figure 5.22: Influence of Electrolyte Concentration on Removal of Phenol, TOC and COD for Effluent at 210 minutes Retention Time

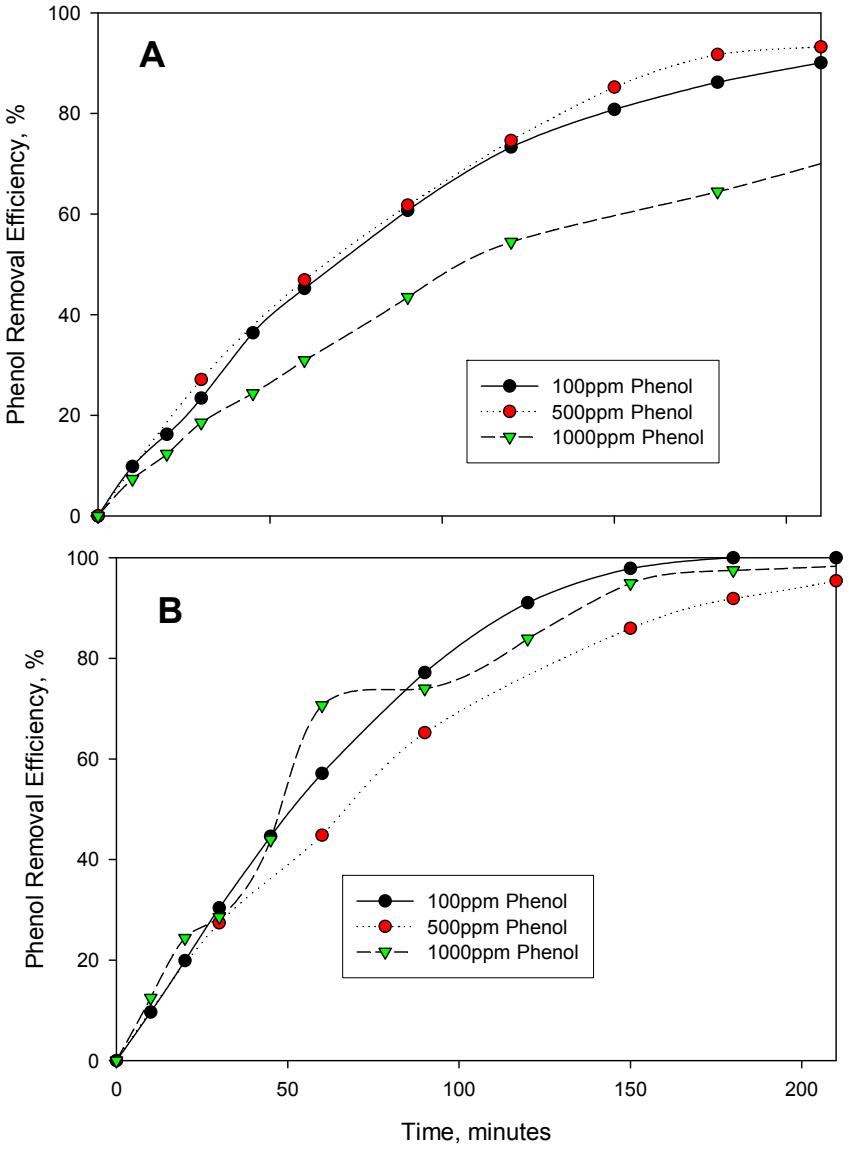

Figure 5.23: Effect of Concentration on Phenol Removal at (A) 30 $mAcm^{-2}$, pH 2; 5000 ppm Na_2SO_4 and (B) 60 $mAcm^{-2}$, pH 12; 5000 ppm Na_2SO_4

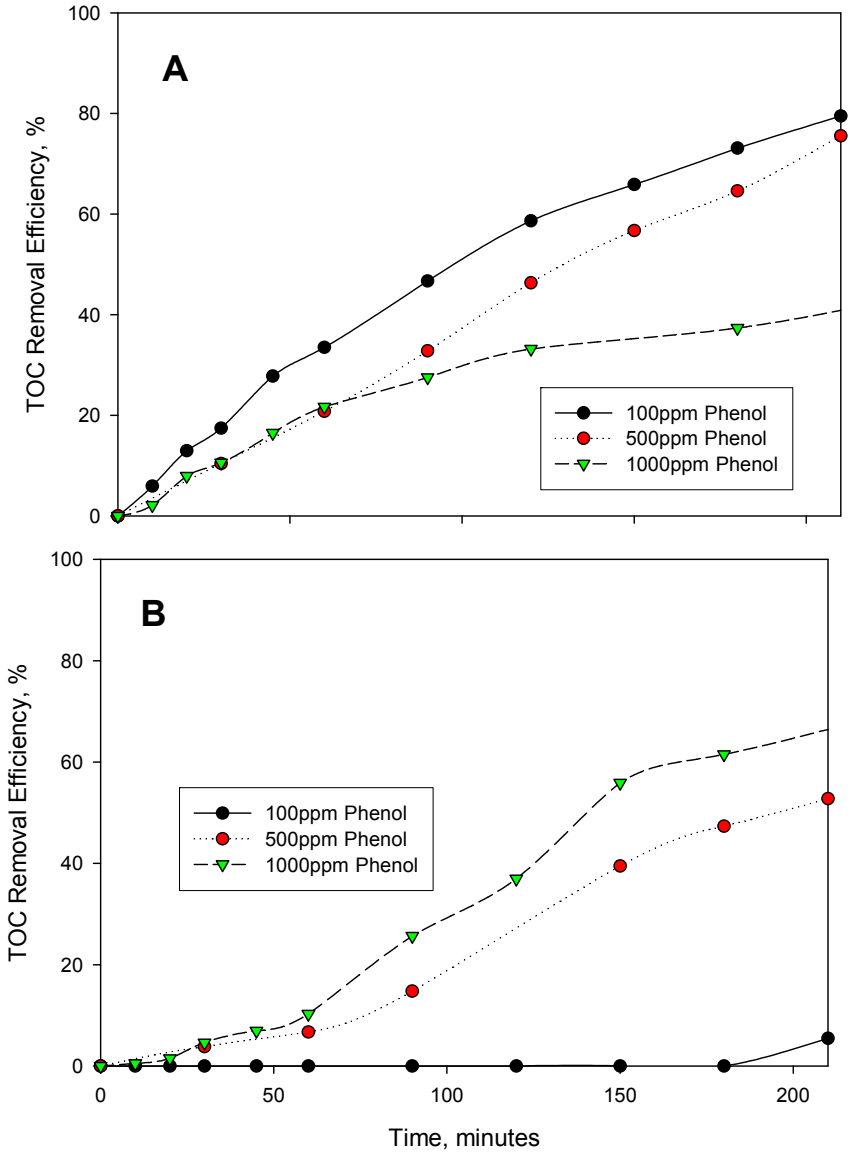

Figure 5.24: Effect of Initial Phenol Concentration on TOC Removal at (A) 30 $mAcm^{-2}$, pH 2; 5000 ppm Na_2SO_4 and (B) 60 $mAcm^{-2}$, pH 12; 5000 ppm Na_2SO_4

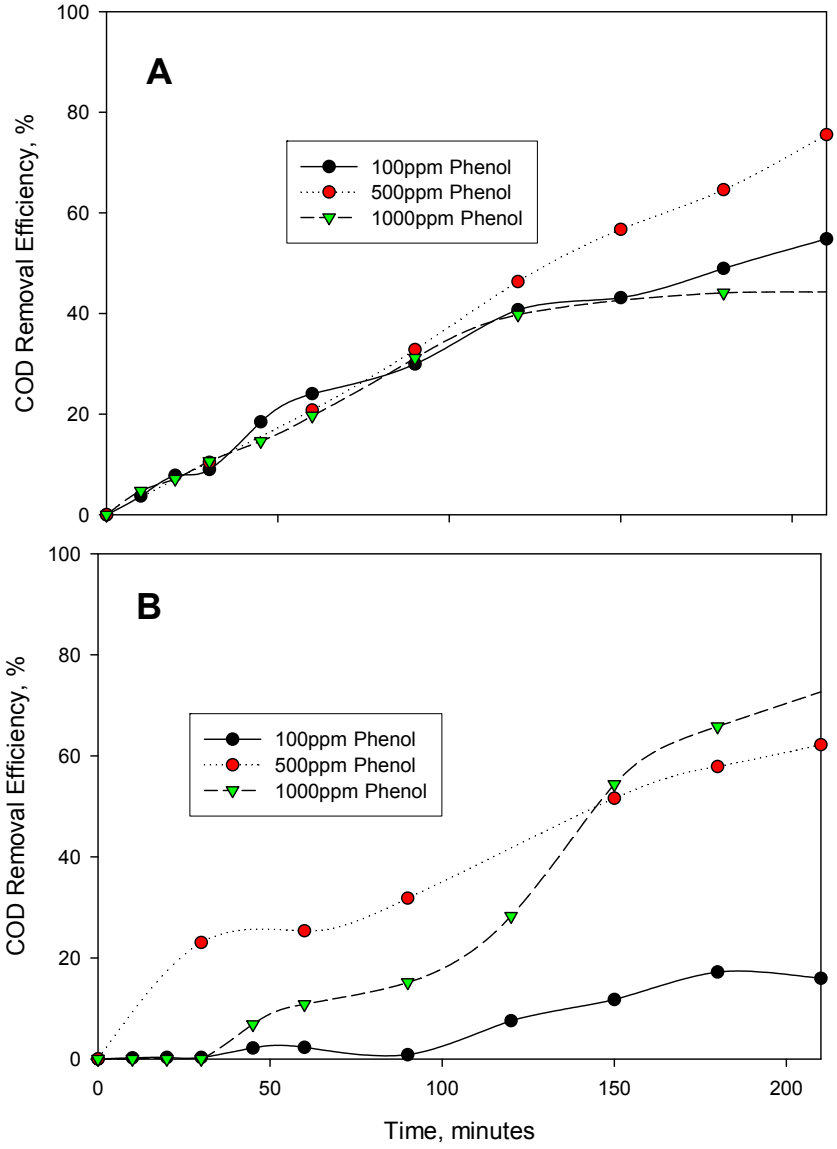

Figure 5.25: Effect of Initial Phenol Concentration on COD Removal at (A) 30 $mAcm^{-2}$, pH 2; 5000 ppm Na_2SO_4 and (B) 60 $mAcm^{-2}$, pH 12; 5000 ppm Na_2SO_4

initial phenol concentrations. In this case, both the removal efficiencies and total amount of phenol (and so also TOC and COD) removed increases with initial concentration. As illustrated in Figure 5.26, the total removal efficiencies in the effluent for phenol, TOC and COD at the three levels of phenol concentrations were (100, 95.40 and 99.26%), (5.44, 52.75 and 71.92%) and (15.97, 62.2 and 79.56%), respectively. For both the TOC and COD, definite removal patterns were obvious as the percent removals increase with increase in initial phenol concentration. Therefore, it is apparent that even at initial pH 12, treating higher phenol concentrations led to avoidance of hindering phenomenon which clearly prevailed at the lower concentration. In circumstances whereby oxidation hindrance was averted, increase in percent removals was due to better utilization of the oxidant(s) produced when the concentration of phenol was high as mass transfer effects was suspected to control the direct phenol oxidation mechanism on the BDD anode. More evidences of this phenomenon were experimentally verified and discussed in the next sections under this chapter.

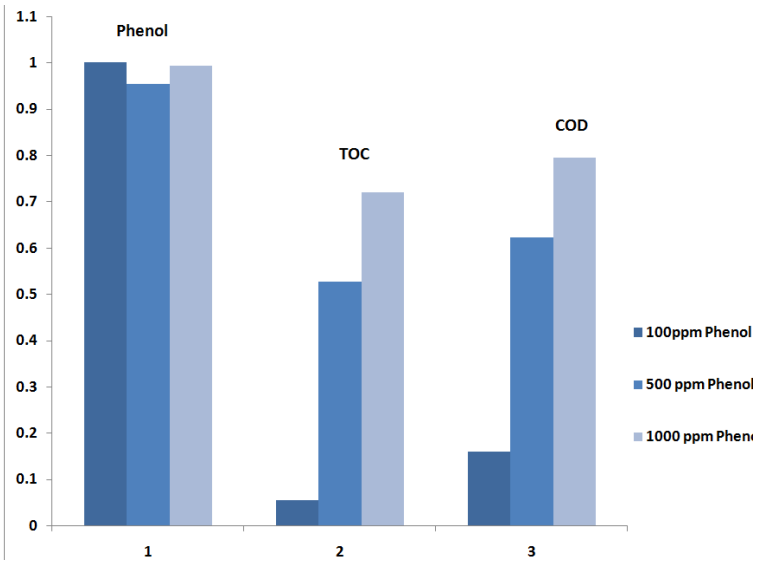

Figure 5.26: Influence of Initial Concentration on Phenol, TOC and COD Removal for Effluent at 210 minutes Retention Time

5.3 Mechanism of Electrochemical Oxidation of Phenol

The ability for BDD anode to generate $OH^{\bullet}$ radical on its surface provides rooms for heterogeneous advanced oxidation process for pollutant mineralization which mainly takes place within the vicinity of the BDD anode surface (Akira et al., 2005). This is the prevailing scenario once homogenous indirect oxidation process within the bulk solution is deliberately averted or not forthcoming (Akira et al., 2005). The evidence of direct oxidation can be directly manifested in the achievable current efficiency which renders current efficiency information an excellent barometric index to address mechanism of oxidation on anodic materials. Hence, the average current efficiency (ACE) data was employed for such purpose. The ACE was estimated based on the widely known relationship (Equation 5.1) that averages the amount of COD removed at any time interval and compares the current utilized in removing the COD to the total actual current supplied to the process. The relationship is given as:

$$ACE = \frac{\int_{t}^{0} ICE\, dt}{t} = \frac{\left(COD_0 - COD_t\right)}{8 I_{app} t} F V_r \qquad 5.1$$

Where ICE is the instantaneous current efficiency in %, F is the Faraday constant, COD_0 and COD_t are the COD values given in mg/L,at beginning of electrolysis at time zero and t, respectively, V_r is the reservoir or reactor volume and i_{app} is the applied current density.

5.3.1 Evidences of Direct Oxidation Mediated by $OH^{\bullet}$ Radicals

Figure 5.27 was clear evidence that the initial phenol concentration has a profound effect on the overall efficiency of the process. It was apparent that the utilization of supplied current was very low for treatment of 100 ppm phenol which contrasted the excellent utilization at 500 ppm and 1000 ppm initial phenol concentrations. For the 100 ppm phenol, the ACE continued to decay with the treatment time under all experimental conditions with maximum ACE of 19.1% attainable at the end of the experiment. However, for the higher initial phenol concentrations, 100% ACE was observed almost throughout the experiments conducted at 30 $mAcm^{-2}$ and initial pH 2 (Figure 5.27A). These observations reaffirmed that at sufficiently high phenol concentration, 100% current efficiency is achievable using BDD anode as reported by other authors (Gherardini et al., 2001). While for the case of operating at 60 $mAcm^{-2}$ and initial pH 12 (Figure 5.27B), the ACE was less than 10% for 100 ppm phenol which also was significantly lower than the ACE obtained at the higher concentrations (i.e., 40% and 76.97% respectively); these ACE values were low when compared to those estimated for the former case (30 $mAcm^{-2}$ and initial pH 2) due to the reduction in COD removal obtained in this later case.

Conclusively, observations from the ACE data evidently suggest that the dominant mechanism for the electro-oxidation of phenol was the direct mechanism mediated by $OH^{\bullet}$ radical attack. This mechanism for inactive electrodes, previously shown in Figure 2.1 in chapter two, is a heterogeneous process that takes place within the vicinity of the surface of the BDD anode as the electro-generated $OH^{\bullet}$ radicals produced were mainly responsible for the oxidation of phenol and its intermediate byproducts.

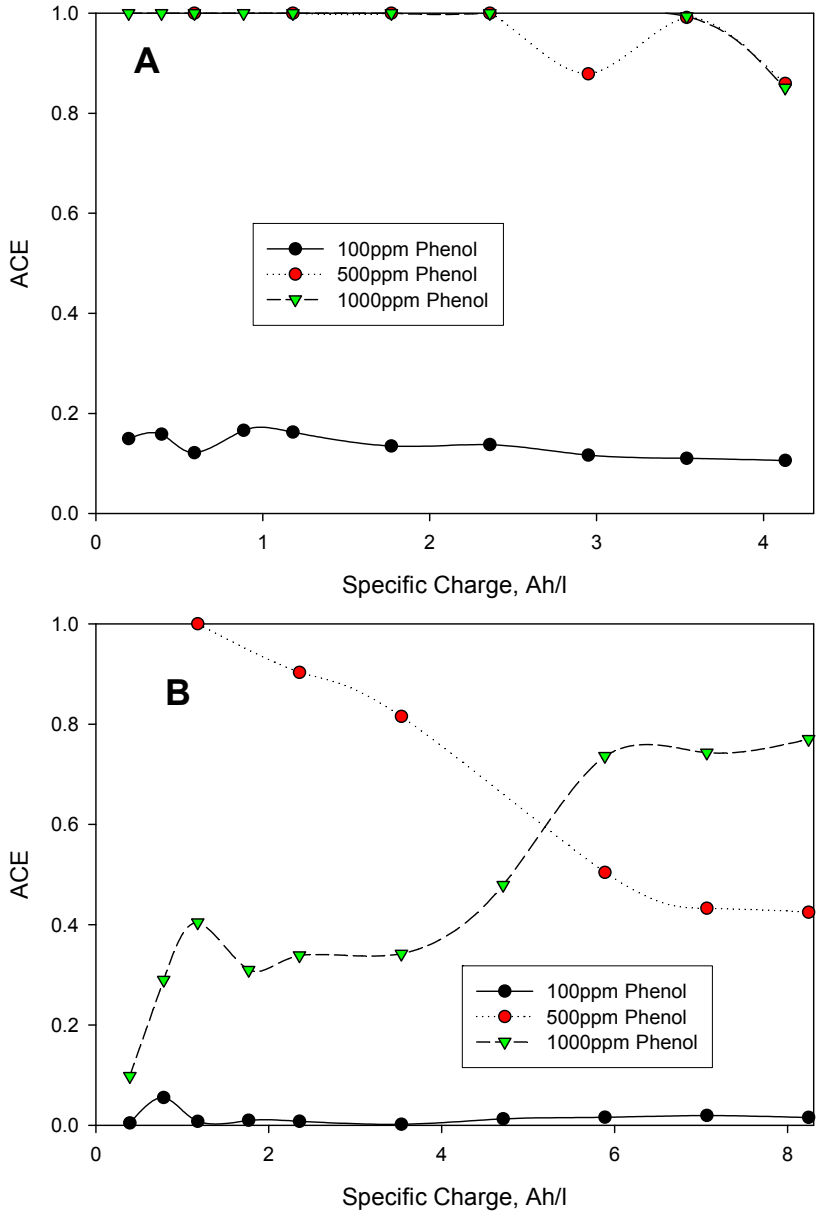

Figure 5.27: Average Current Efficiency vs Specific Charge Passed at 5000 ppm Na_2SO_4 (A) 30 $mAcm^{-2}$, pH 2 and (B) 60 $mAcm^{-2}$, pH 12

Other investigators reported that additional in-situ produced oxidants that can promote indirect electrolysis can also negatively scavenge $OH^{\bullet}$ radicals thereby reducing the oxidation potential of the whole process (Akira et al., 2005; Jin-Fang et al., 2003; Marselli et al., 2003; Murugananthan et al., 2008). Murugananthan et al (2008) lamented that part of the electro-generated $OH^{\bullet}$ at BDD can be wasted at higher applied current by parallel parasite reactions such as O_2 evolution and production of peroxodisulfate ($S_2O_8^{2-}$) and/or hydrogen peroxide as $S_2O_8^{2-}$ (produce according to Equation 5.2) and H_2O_2 are weaker oxidants compared to $OH^{\bullet}$. In fact, these authors found such intermediary oxidants ($S_2O_8^{2-}$ and H_2O_2) to have insignificant impact on mineralization of some organic compounds. Marselli et al. (2003) also showed that the $OH^{\bullet}$ radicals were mainly responsible for oxidation on BDD anode, and they clearly proved that the $OH^{\bullet}$ radicals can also combine according to Equation 5.7 to significantly generate H_2O_2 that either diffuse into the bulk solution or oxidize to O_2 according to Equations 5.8 and 5.9, respectively. In another separate study, $S_2O_8^{2-}$ was also found to have decomposed to O_2, monopersulfate and H_2O_2 according to Equations 5.3 to 5.5 (Akira et al., 2005). All these suggest that the formation of these in-situ generated oxidants can mediate secondary reactions that are capable of impairing the mineralization efficiency as they are susceptible to promoting unwanted side reactions that diminish the current efficiency.

Due to the competing side reactions, the efficiency of the electrochemical production of peroxodisulfate (E_o=2.0 V vs. SHE) strongly depends on electrode material and BDD anode is known to be an effective candidate material. However, other operating conditions particularly, temperature and concentration of the source of the precursor ions (SO_4^{2-}) are found to be the major controlling parameters in the production of active and effective $S_2O_8^{2-}$ for aqueous

oxidation of pollutants. Using sulfuric acid and at applied current density of 23 $mAcm^{-2}$, Serrano and co-investigators (Serrano et al., 2002) showed that the main anodic reaction was oxidation of sulfate to $S_2O_8^{2-}$ at higher concentration of sulfuric acid (> 2 mol/l H_2SO_4) and optimum operating temperature was 9 ^oC, while lower concentration of the H_2SO_4 mainly led to the decomposition of the $S_2O_8^{2-}$ (according to Equations 5.3 and 5.5). Other investigators (Michaud et al., 2000) have shown that high current efficiency for peroxodisulfuric acid formation can be achieved in concentrated H_2SO_4 (7.5 mol dm^{-3}) using high current densities (200 mA cm^{-2}) at near room temperature of 25 ^oC.

$$2HSO_4^- + 2OH^\bullet \rightarrow S_2O_8^{-2} + H_2O \qquad 5.2$$

$$S_2O_8^{-2} + H_2O \rightarrow 2HSO_4^- + \tfrac{1}{2}O_2 \qquad 5.3$$

$$S_2O_8^{-2} + H_2O \rightarrow SO_5^{-2} + SO_4^{-2} + 2H^+ \qquad 5.4$$

$$SO_5^{-2} + H_2O \rightarrow H_2O_2 + SO_4^{-2} \qquad 5.5$$

$$2\,H_2O \rightarrow O_2 + 4\,H^+ + 4\,e^- \qquad 5.6$$

$$OH^\bullet + OH^\bullet \rightarrow H_2O_2 \qquad 5.7$$

$$(H_2O_2)_{BDD} \rightarrow (H_2O_2)_{solution} \qquad 5.8$$

$$H_2O_2 \rightarrow O_2 + 2H^+ + 2\,e^- \qquad 5.9$$

Moreover, data reported by Vatistas and co-investigators (Vatistas et al., 2005) indicated that a high organic compound oxidation rate using in-situ generated peroxodisulfate can be reached by increasing the reaction temperature from 25 to 70 ^oC due to activation of the

$S_2O_8^{2-}$ at higher temperature. They showed that at sufficiently high temperature, the oxidation of sulfate ions (from H_2SO_4) to peroxodisulfate is capable of suppressing the side reaction of oxygen evolution and homogenous AOP can be achieved in the bulk of the wastewater to supplement the heterogeneous direct process on the BDD anode. Eventhough, effect of other different sources of the SO_4^{2-} ions on activation of the $S_2O_8^{2-}$ in the previous studies was not taken into account, however, it can be deduced from the forgoing analysis that activation of electro-generated $S_2O_8^{2-}$ didn't occur in the present study in spite of the high concentration of the electrolyte used (5000 ppm). Therefore, the most likely reason for the inability for the generated $S_2O_8^{2-}$ to be active could be due to the operating temperature and current density in the present study were probably not in the ranges to favor the activation.

Conclusively, there is indication that mass transfer of the phenol species to the BDD anode surface was very essential in controlling the mineralization efficiency of the phenol molecules. This implies that, the greater ability of the phenol molecules to reach the electrode surface, the better the oxidation potentials of the overall process. A high mass-transport process can guarantee greater uniformity of high pollutant concentration in the reaction layer near the electrode surface where the oxidation was believed to mainly take place. For such reason, the higher the initial concentration the more oxidizable species are expected to be transferable to the electrode surface to get access to the available $OH^{\bullet}$ radicals which mediate in the oxidation process; this ensures better phenol oxidation as well as effective utilization of current (i.e., high ACE). Considering that all the removal trends of phenol consistently showed an exponential decay with time (i.e., first-order kinetics) indicates a mass transfer controlled process. Initially due to high concentration of species in solution, the mass transfer

control effects would be less compared to the later part of the treatment time. As the concentration continuously reduces with time, the removal rate decays as well which manifested in the first order kinetics, hence, proving that the anodic oxidation of phenol on the BDD anode was mainly diffusion controlled process. Moreover, evidence of mass transfer control of the system was portrayed in the fact that phenol, TOC and COD removals were more inclined to increase with increase in applied current density. An increase in the current in an electrolytic solution causes increase in charge transported through the electrolyte to the electrode thereby increasing the mass transported to the electrode surface increases (Marselli et al., 2003). In addition, increasing applied current results in more gas evolution at the anode which will additionally increase the stirring of the solution more vigorously leading to a decrease in the diffusion layer, δ (Michaud et al., 2000). Considering the mass transfer coefficient to be equal to the diffusion coefficient divided by the thickness of diffusion layer, any parameter that decreases δ will increase the mass transfer coefficient. Although the rate-limiting step of the process could be ascribed to the chemical reaction for phenol oxidation which was time dependent (kinetic control as observed earlier), but it became apparent that the reaction limiting step corresponds to hydrodynamics that influenced the phenol molecules reaching the BDD anode surface (mass-transfer control) where the reaction heterogeneously takes place.

The observations above suggest that for the 500 ppm and 1000 ppm initial phenol concentrations, due to the availability of phenol molecules at the electrode surface (as direct oxidation is the dominant mechanism suggested by the data in this study) more supplied current was used for the electro-oxidation of phenol by getting attacked by the $OH^{\bullet}$ radicals,

hence, the lesser the amount of $OH^{\bullet}$ likely be wasted and/or consumed in side reactions i.e., the competing hydroxyl radical-mediated reactions (Jin-Fang et al., 2003; Marselli et al., 2003) and current wastage was minimized. But on contrary, for the 100 ppm, due to greater influence by the mass transfer limitations, much fewer phenol molecules could reach the electrode surface and the consequence was that most of the $OH^{\bullet}$ radicals generated became wasted either due to not been optimally utilized or in competing side reactions.

5.3.2 Experimental Validation of Direct Oxidation Mediated by $OH^{\bullet}$ Radicals

The claim of direct oxidation via $OH^{\bullet}$ mediation could be supported by the experimentally established fact presented earlier in this study that increasing the electrolyte concentration didn't yield better removal of phenol. It was initially anticipated that an increase in the Na_2SO_4 electrolyte would promote the production of active in-situ generated oxidants, such as $S_2O_8^{2-}$ leading to indirect oxidation in the bulk of solution to supplement the direct oxidation process; thereby increasing the efficiency of the treatment process. However, the productions of the expected oxidants ($S_2O_8^{2-}$ and H_2O_2) do not always lead to better mineralization. Moreover, they are only effective when they do not act negatively as scavengers of $OH^{\bullet}$ radicals, reaction routes that could lead to promoting other undesirable secondary reactions that reduce process efficiency. Once promoting the secondary side reactions due to generation of these oxidants becomes the prevailing scenario, it is likely to be more pronounced at higher concentration of the supporting electrolyte a possible reason for lower phenol removal (as well as oxidation) rate observed at higher concentrations of the Na_2SO_4. Consequently, it can be understood that, the indirect oxidation appeared to be mildly harnessed and hence, at lower

initial phenol concentration, mass transfer limitation further contributed significantly to inefficient oxidation of phenol thereby rendering the ACE to become very low. Moreover, the increase in mineralization rate with increase in current density that was observed earlier suggests an increase in $OH^{\bullet}$ with increase in current density bearing in mind that all experiments were conducted at galvanostatic conditions (Brillas et al., 2004); reaffirming that $OH^{\bullet}$ was the key mediator in the process.

The hypothesis that the process in this present study was mainly dominated by direct electro-oxidation of phenol via $OH^{\bullet}$ attack was further substantiated by employing three additional experiments. The three (3) experiments were conducted included one without addition of any supporting electrolyte and two others with the addition of 1000 ppm Na_2SO_4 and 1000 ppm NaCl as supporting electrolyte separately. The NaCl supporting electrolyte was tested in order to explore the feasibility of harnessing the indirect mechanism due to generation of different in-situ generated oxidants (Cl_2 and hypochlorite) instead of the peroxodisulphate. Considering the results provided in Figures 5.28A and 5.28B for phenol and TOC removal, respectively, it can be deduced that adding 1000 ppm Na_2SO_4 didn't improve the phenol oxidation to any appreciable degree. For the 1000 ppm NaCl, although phenol was removed completely in less than 40 minutes, conversely, the TOC removal was below the two former cases. Hence, the removal of phenol in the presence of the NaCl initially suggested that the additional generated oxidant beside $OH^{\bullet}$ in such a case were more active compared to those produced due to the presence of Na_2SO_4 as supporting electrolyte. However, by comparing the TOC removals for these two different cases it became apparent that for the NaCl the good phenol removal didn't commensurate with its TOC counterpart, thereby refuting the earlier

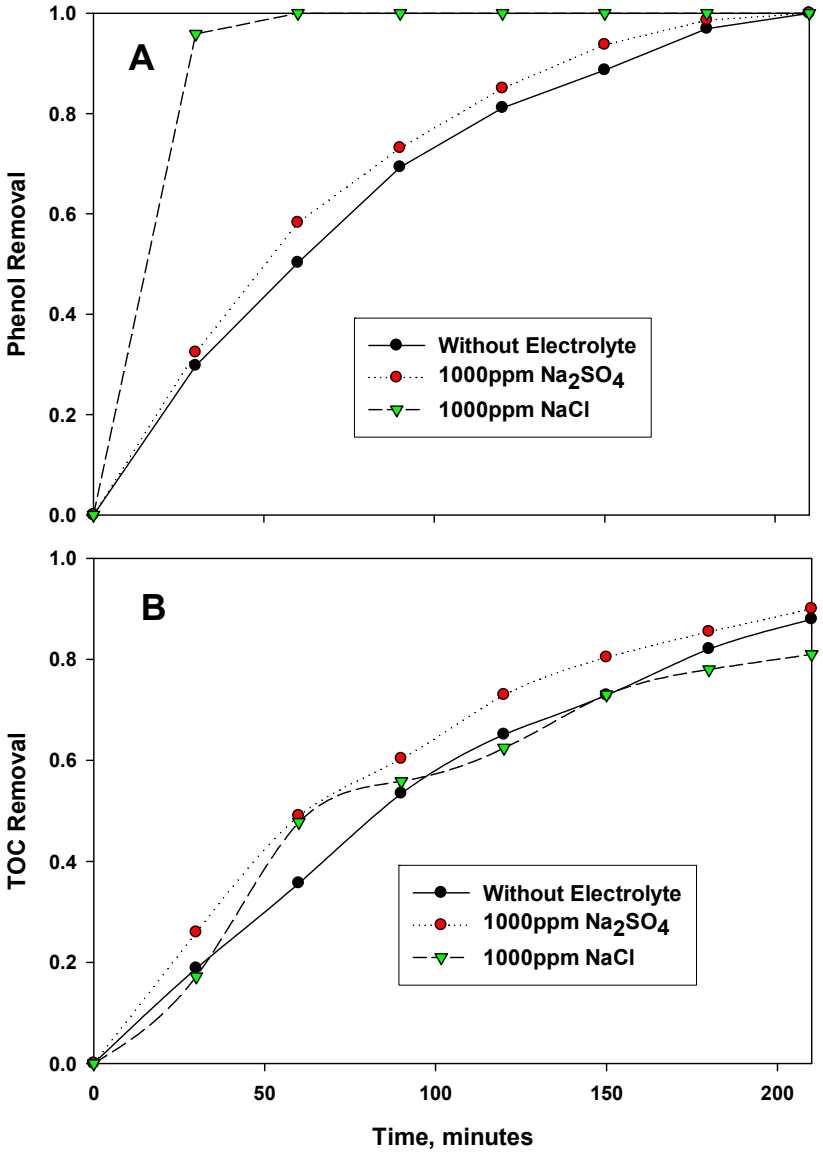

5.28: Effect of Different Electrolytes on Oxidation of Phenol Using BDD anode

indication that the oxidants generated due to presence of NaCl might be more effective in enhancing the indirect process. Although the removal of phenol was gradual and slower in case of Na_2SO_4 electrolyte, however, the overall phenol oxidation appeared to be slightly more effective eventually. Therefore, these results apparently substantiated the assertion that adding supporting electrolytes didn't enhance the oxidation process to a considerable degree, and they evidently supported the suggestion that $OH^{\bullet}$ was the key mediator in the phenol oxidation process.

5.4 Detailed Analysis of Mechanism of Phenol Oxidation

The TOC removal data presented earlier highlighted that no considerable change in the original organic content for experiments conducted at initial pH 12 which contrasted the good removal observed at initial pH values of 2 and pH 7. Based on that, it was speculated that the conversion of phenol to other organic compounds at lower oxidation state and their fate was responsible for the observed TOC removal discrepancies. In order to substantiate such hypothesis, analyses of phenol disappearance in relation to the evolution of its oxidation byproducts were brought into play for the different experimental conditions. Phenol and its aromatic oxidation intermediary byproducts where monitored and quantified using HPLC instrument. Their respective concentrations were determined based on calibration curves developed using standard samples prepared from high purity reagents (See APPENDIX for the calibration curves). Regression coefficients for (R^2) for the calibration curves for phenol, benzoquinone, hyroquinone and catechol were on the average of 0.999, 0.946, 0.9918 and 0.9975, respectively. Two separate plots for typical superimposed HPLC chromatograms for samples drawn and analyzed corresponding to two different experiments are given in Figure 5.29. These plots illustrate typical

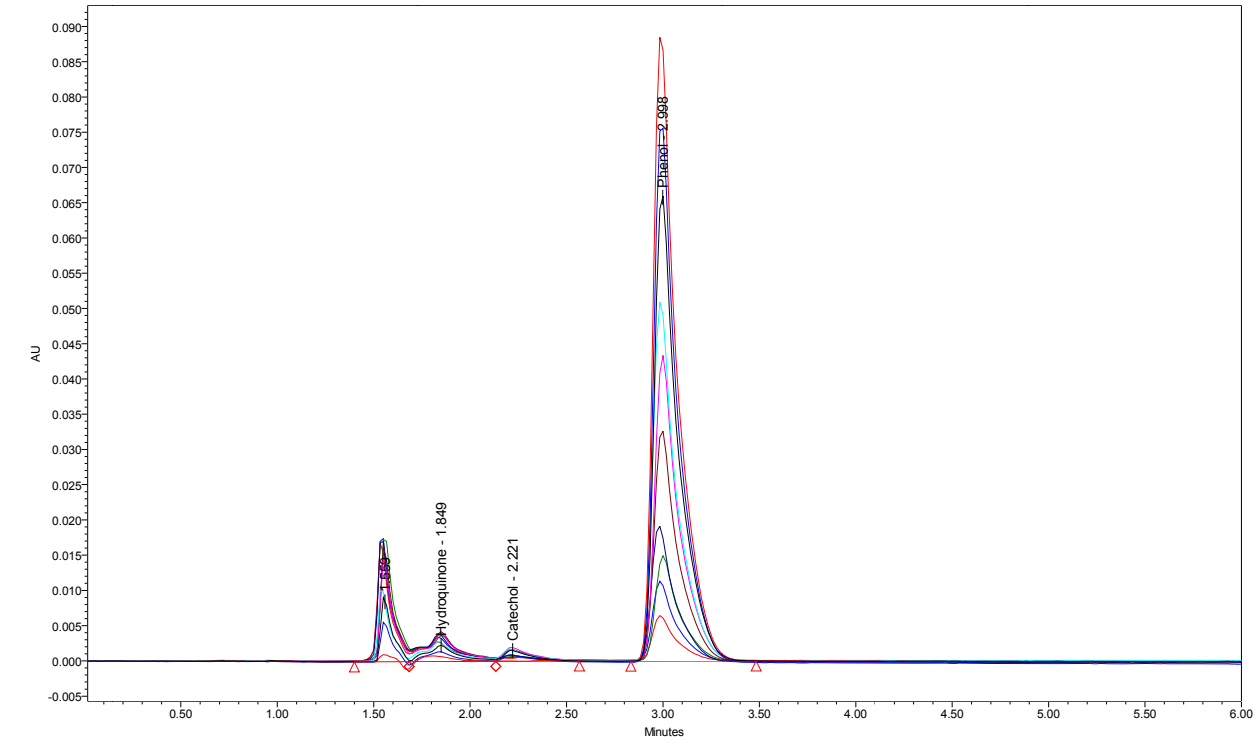

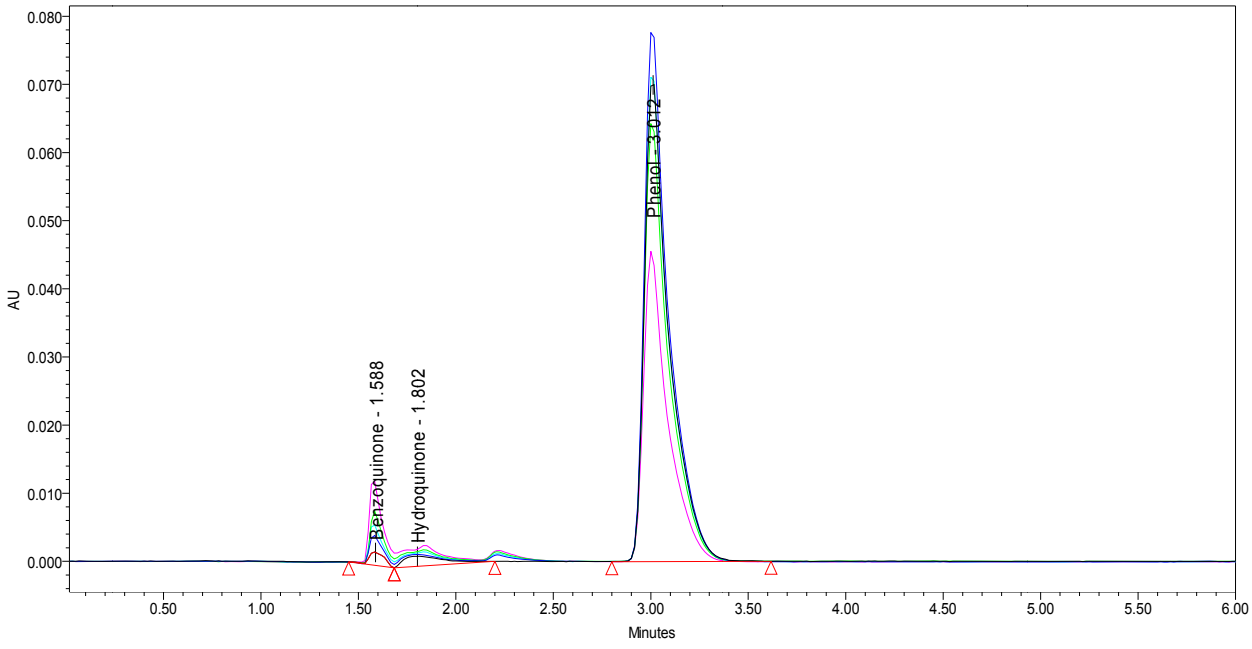

(1.561minutes) Benzoquinone
(1.842minutes) Hydroquinone
(2.214 minutes) Catechol
(2.99 minutes) Phenol

Figure 5.29: Typical HPLC Chromatograms during Oxidation of Phenol

evolutions of phenol and the aromatic byproducts. It can be seen that, benzoquinone, hydroquinone, catechol and phenol separated in the C18 column were well detected at eluding times of 1.581, 1.86, 2.296 and 3.055 minutes, respectively. For each sample analyzed, the respective concentration of each of these components was directly proportional to the area under its chromatogram in relation to the area under the chromatogram of its pure standards.

Figures 5.30 to 5.33, noticeably, display the different relevant profiles during oxidation of phenol at initial pH 12 under different experimental conditions. It can be seen that each of these figures is composed of three distinct plots designated as A, B and C which correspond to percent removals (for phenol, TOC and COD), phenol and aromatics intermediates concentration profiles and percent composition of generated byproducts, respectively. The percent phenol converted to CO_2 and aromatic intermediates, relative to oxidized phenol were calculated from the TOC data, respectively, using the relationships in Equations 5.10 and 5.11 (Iniesta et al., 2001b; Noureddine and André, 1998).

$$\%CO_2 = \frac{\left\{[TOC]_0 - [TOC]_t\right\}/6}{[Phenol]_0 - [phenol]_t} \times 100 \qquad 5.10$$

$$\%\,Aromatics = \frac{[Aromatics]}{[phenol]_0 - [phenol]_t} \times 100 \qquad 5.11$$

Where $[TOC]_0$ and $[TOC]_t$ are the total organic carbon in $mmoldm^{-3}$ at times 0 and t, respectively, $[Phenol]_0$ and $[Phenol]_t$ the concentration of phenol in $mmoldm^{-3}$ at times 0 and t,

respectively. The term $\{[TOC]_0-[TOC]_t\}/6$ represents the mole number of phenol converted to CO_2 where [Aromatics] is the concentration of aromatic intermediates (1,4 benzoquinone, hydroquinone and catechol) in mmol dm^{-3}.

Hence, based on stoichiometric mass balance, the percentage of unaccounted byproduct can be estimated from Equation 5.12:

$$\%Other\ Byproducts = 100 - \%CO_2 - \%Aromatics \qquad 5.12$$

Irrespective of the applied current density and electrolyte concentration, treatment at initial pH 12 was found to have led to the accumulation of aromatics and other byproducts yet to be identified till later part of the study (Next Section). At this initial pH, the rate of phenol reduction was found to be very good as established earlier and also reported by a number of authors (Panizza and Cerisola, 2004; Tian et al., 2006). Total phenol elimination was observed in less than 180 minutes, particularly at the highest applied current density (i.e., 60 $mAcm^{-2}$) as shown in Figures 5.30 to 5.31. Conversely, the effectiveness of phenol destruction was undermined by the inability to further mineralize the generated byproducts to the desired final oxidation byproduct (i.e CO_2). The percent compositions of the byproducts depicted in Figures 5.30B to 5.33B suggest that, phenol was firstly oxidized to aromatic byproducts which were further converted to other intermediary byproducts with negligible conversion to CO_2. It was be observed that the decline in the aromatic byproducts is proportional to the rise in other unaccounted byproducts while corresponding CO_2 evolution is virtually zero in all the cases; evidently indicating that oxidation of the parent compound had been severely hindered.

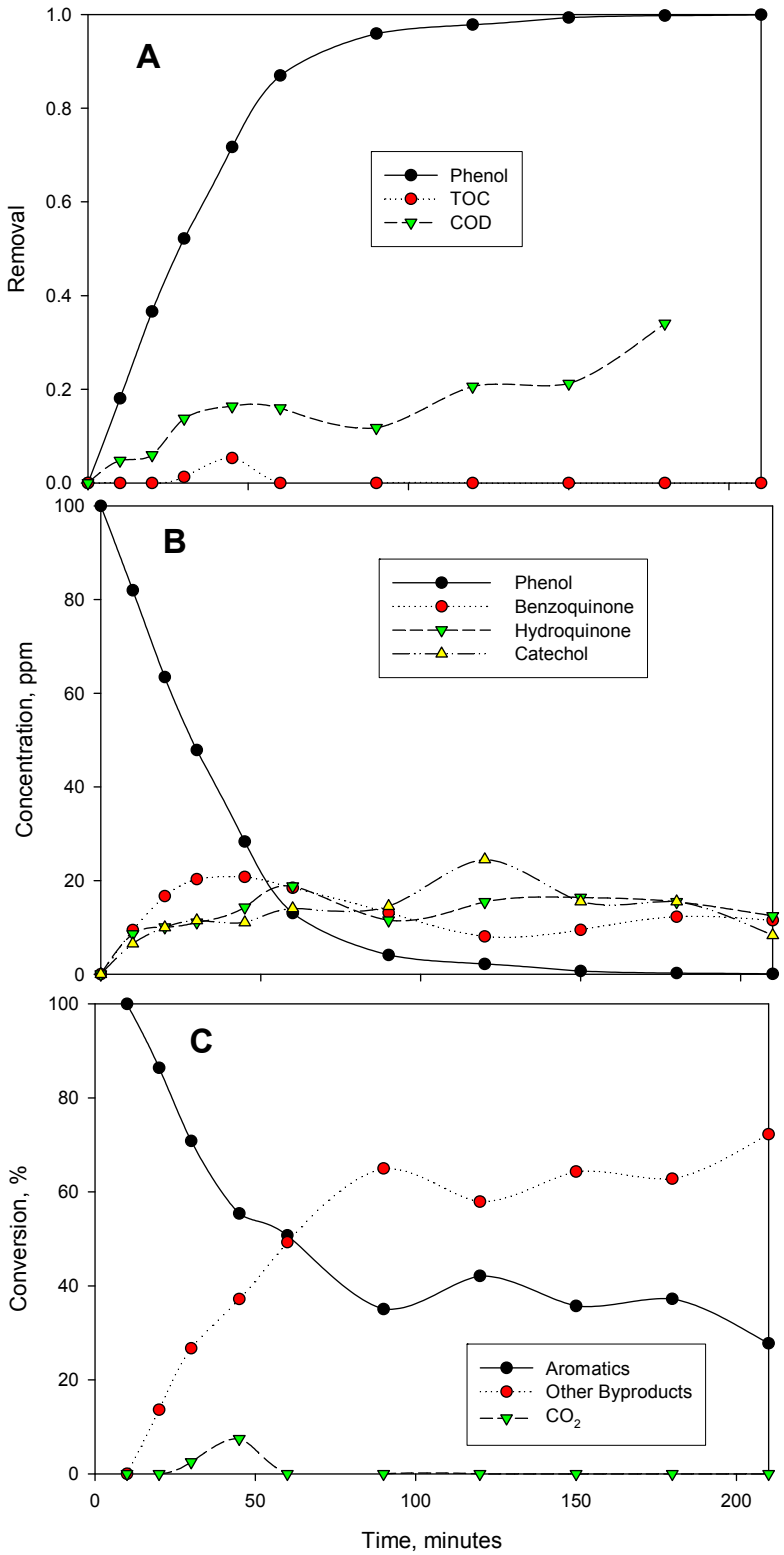

Figure 5.30: Profiles for Oxidation of Phenol at pH 12; 60 $mAcm^{-2}$; 1000 ppm Na_2SO_4

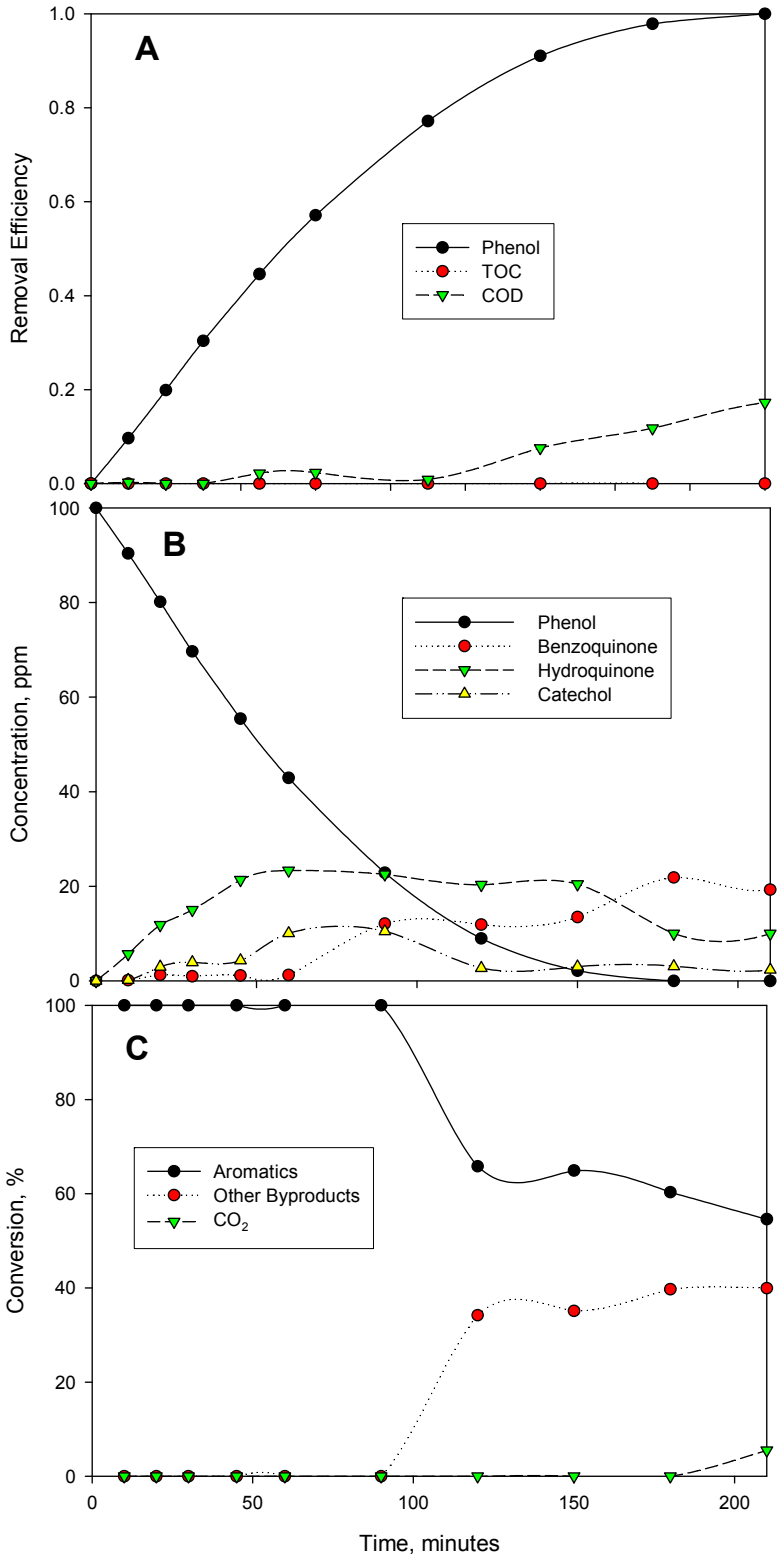

Figure 5.31: Profiles for Oxidation of Phenol pH 12; 60 $mAcm^{-2}$; 5000 ppm Na_2SO_4

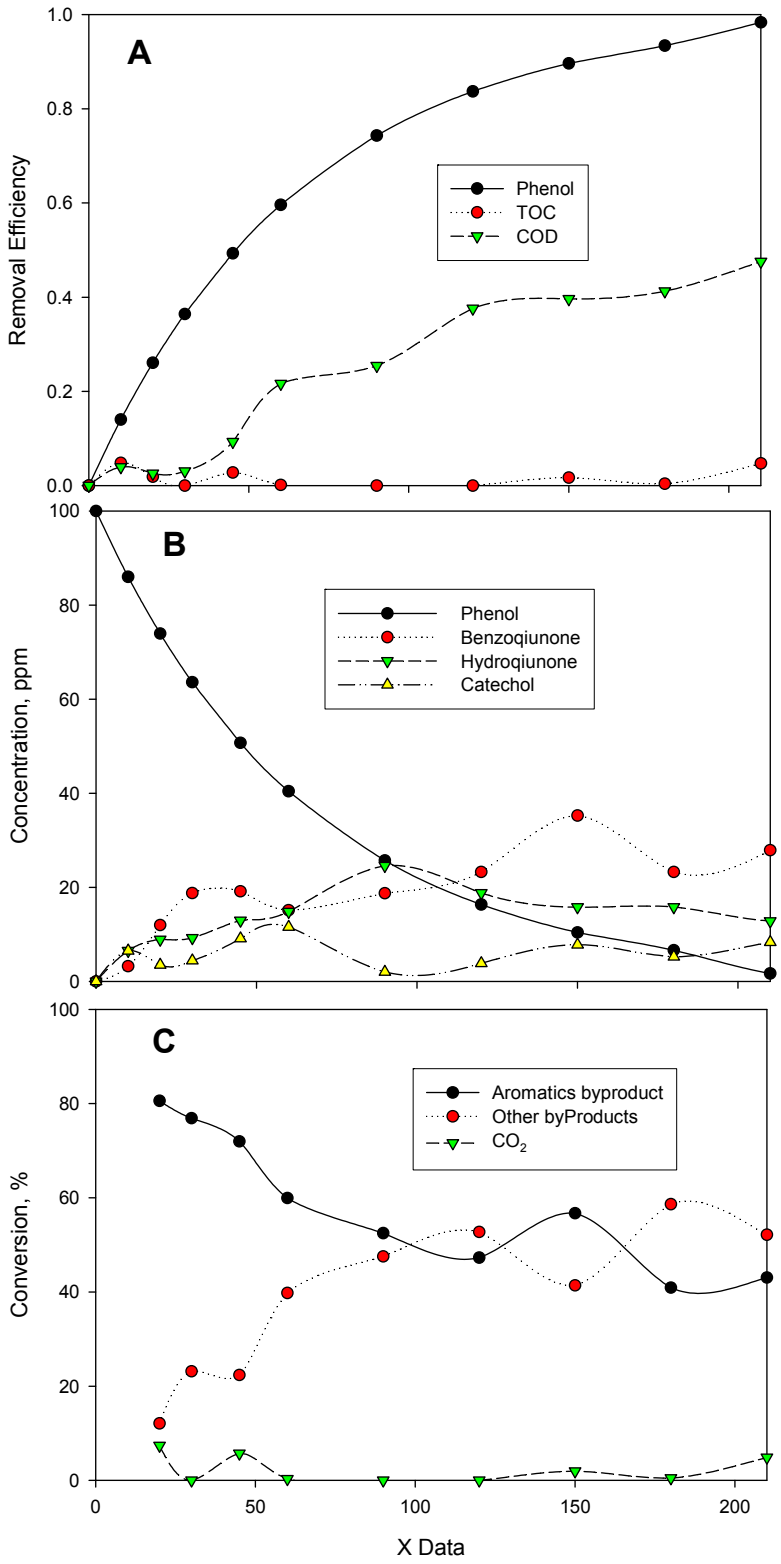

Figure 5.32: Profiles for Oxidation of Phenol pH 12; 45 $mAcm^{-2}$; 3000 ppm Na_2SO_4

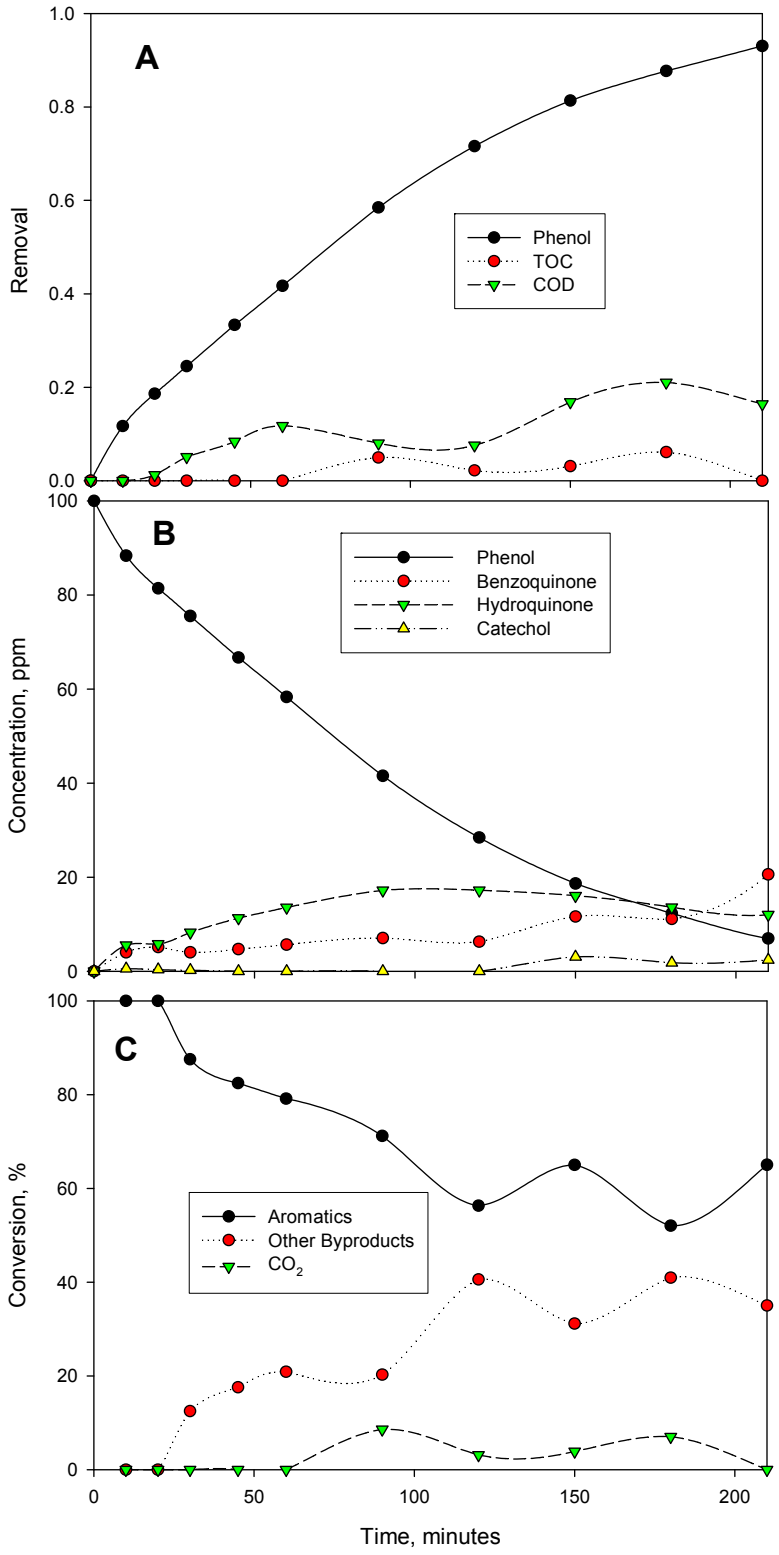

Figure 5.33: Profiles for Oxidation of Phenol; pH 12; 30 $mAcm^{-2}$; 5000 ppm Na_2SO_4

The poor TOC and COD (Figures 5.30A to 5.33A) removals also corroborate the aforementioned fact that it was phenol conversion to byproducts that took place rather than its oxidation to CO_2. The concentrations levels of the byproducts vis-à-vis TOC and COD removals markedly go in agreement with the stoichiometric byproducts conversion compositions as depicted in Figures 5.30C to 5.33C.

In obvious deviation from the evidences that were against effective oxidation at initial pH 12, combined analysis of the TOC, COD and percent composition of generated byproducts in relation to phenol elimination strongly indicated that effective oxidation of phenol was achieved at higher initial phenol concentration investigated even at initial pH 12. As respectively, depicted in Figures 5.34 and 5.35, there exists strong evidence to corroborate the previous suggestion that increasing the initial phenol concentration from 100 to 500 and 1000 ppm, significantly, led to effective phenol oxidation. It can be deduced from the profiles presented in these figures that the oxidation of phenol at higher initial phenol concentration was also initiated by generation of hydroxylated byproducts of phenol (hydroquinone and catechol) which were further converted to other intermediary byproducts at higher oxidation states such as benzoquinone. Further oxidation of these byproducts led to the gradual and continuous production of the final oxidation byproduct, CO_2; with clear indication that the process was kinetically controlled, and hence, complete oxidation of phenol was quite possible at higher concentrations.

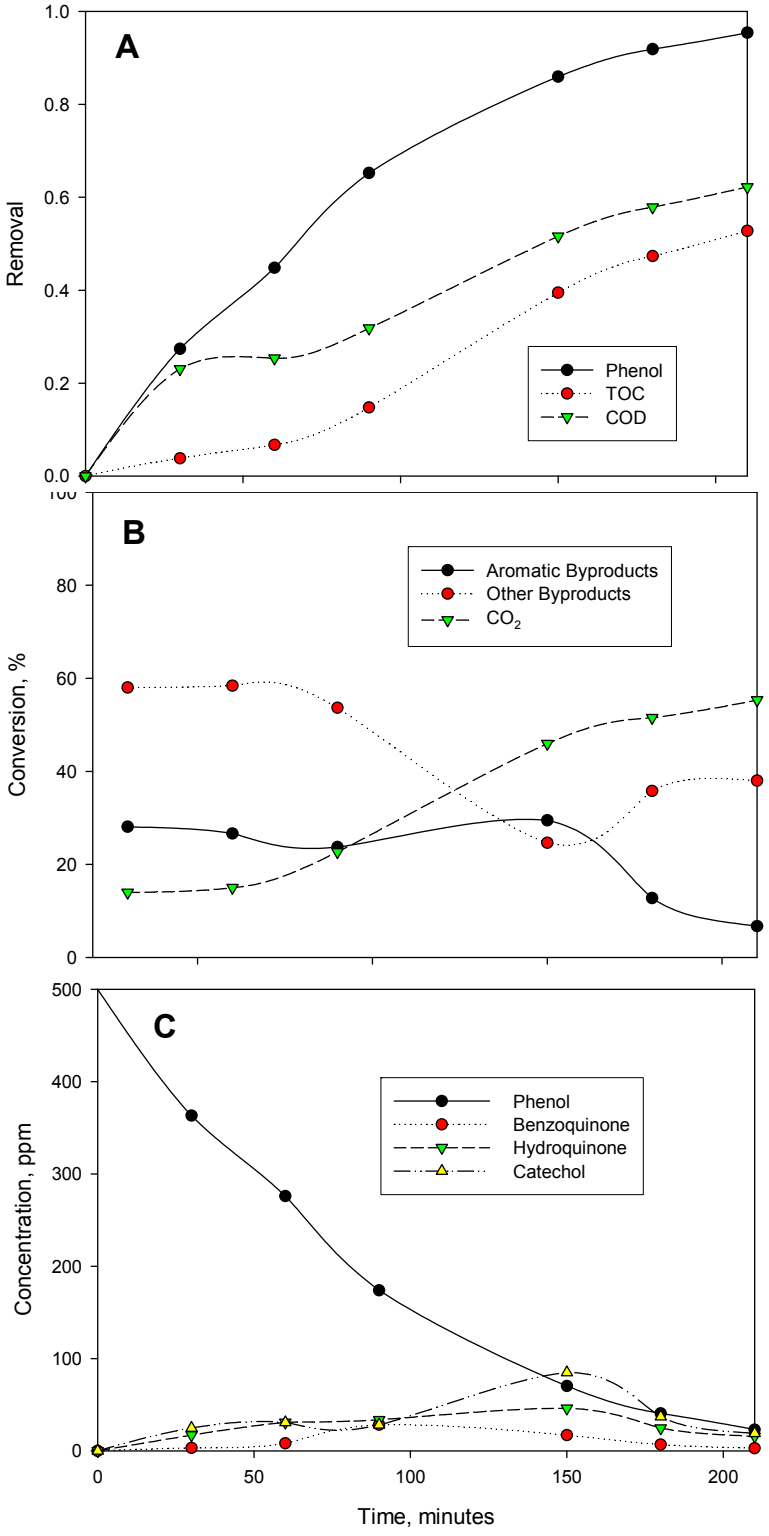

Figure 5.34: Profiles for Oxidation of 500 ppm Phenol: pH 12, 60 $mAcm^{-2}$, 5000 ppm Na_2SO_4

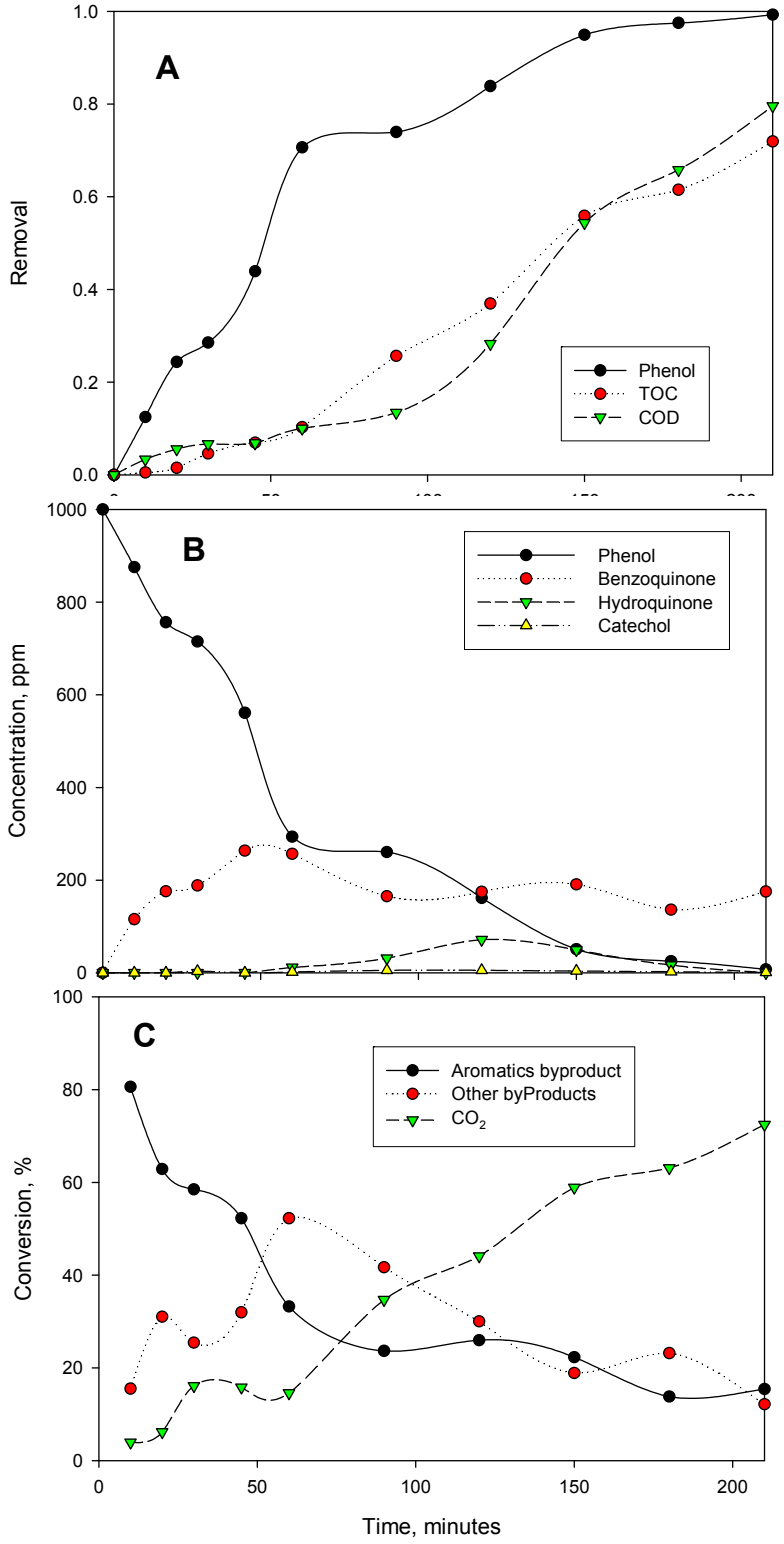

Figure 5.35: Profiles for Oxidation of 1000 ppm Phenol: pH 12, 60 $mAcm^{-2}$, 5000 ppm Na_2SO_4

However, in the cases of initial pH 2 and 7, initial phenol concentration didn't appear to have negatively hindered phenol oxidation as clear contrasting behavior was noticed compared to the data presented for pH 12. Even though, trends for the rate of phenol removal were slightly lower at initial pH values of 2 and 7, but it appeared that the generation and accumulation of intermediate byproducts were by far lesser regardless of other experimental conditions. As provided in Figures 5.36 to 5.39, in most cases both the aromatics and other byproducts were completely eliminated or else lower residual concentrations were observed at the end of the treatment process with clear indication of complete disappearance if the electrolysis time were extended beyond 3.5 hours. It was thought that phenol might have been converted to other unidentifiable byproducts. However, by invoking the residual TOC and COD data in relation to the byproducts composition, sufficient evidence can be established that oxidation of phenol to CO_2 was the dominant phenomenon as depicted in Figures 5.36C to 5.39C; The removals of TOC and COD (Figures 5.36A to 5.39A) commensurate well with the phenol removal trends, reaffirming that electrochemical destruction of phenol took place. Similar results from electrolysis of aromatic intermediates of phenol oxidation were reported elsewhere (Nasr et al., 2005) that clearly indicated that at acidic pH, BDD anode is very effective in complete oxidation of phenol rather than its conversion to other unwanted products that could be more toxic and/or more difficult to be oxidized. This suggest that at pH values of 2 and 7, more active $OH^{\bullet}$ radicals are likely to be generated that can effectively attack and prevent the accumulation of intermediary byproducts (which might be more refractory in nature) and/or the formation of polymeric products (Xiao-yan et al., 2005).

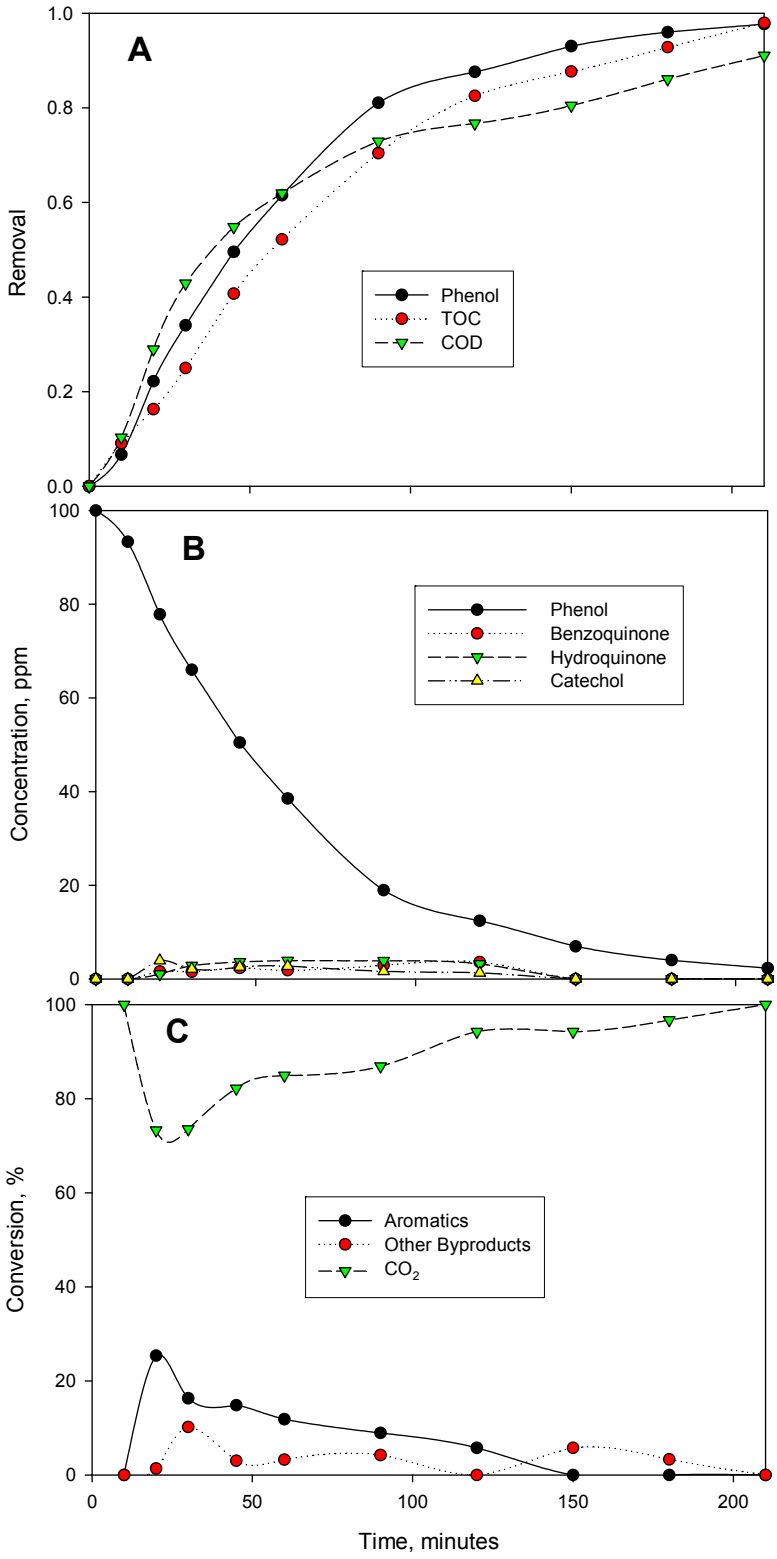

Figure 5.36: Profiles for Oxidation of Phenol: pH 2; 60 $mAcm^{-2}$; 1000 ppm Na_2SO_4

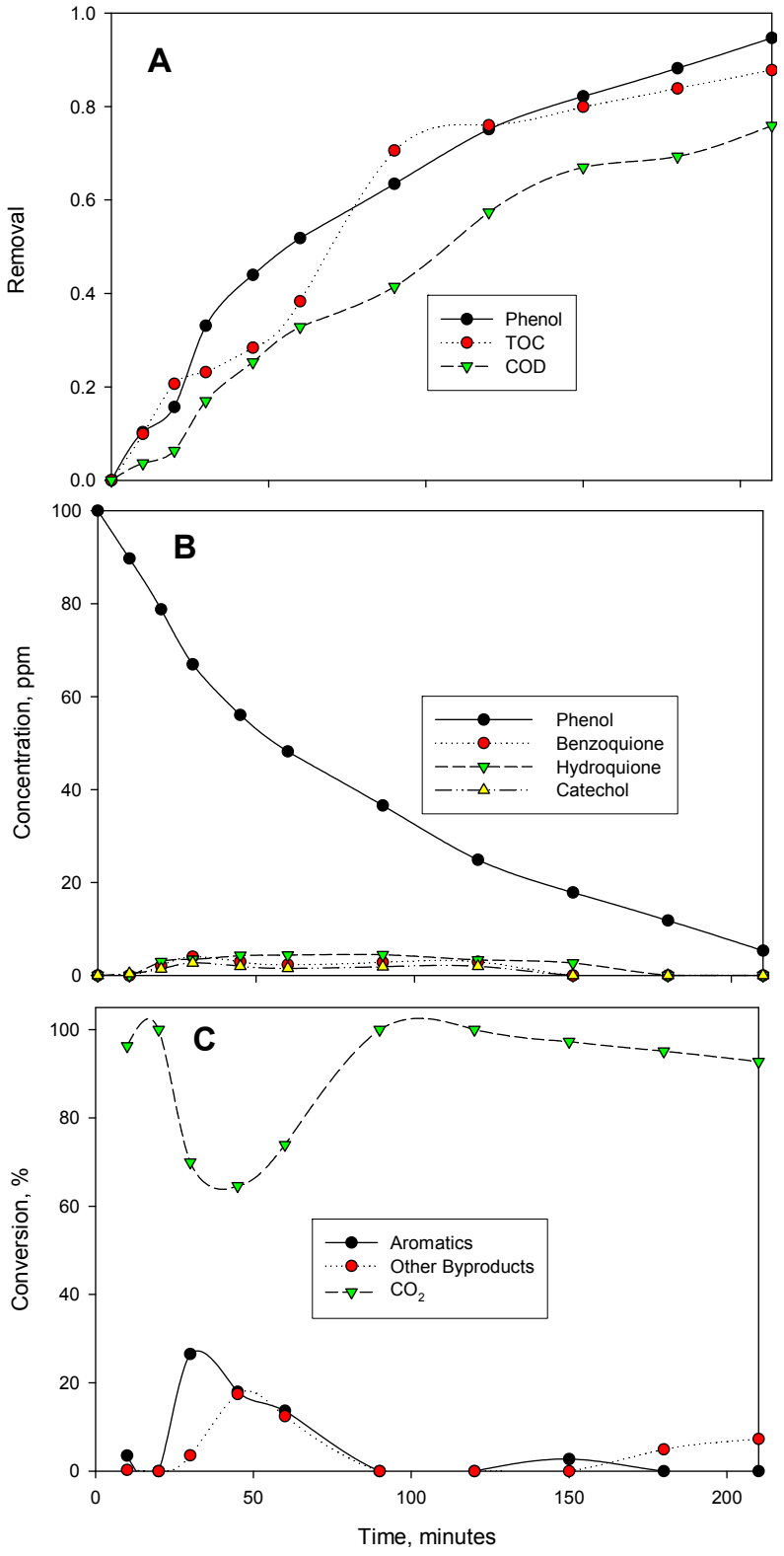

Figure 5.37: Profiles for Oxidation of Phenol; pH 2; 60 $mAcm^{-2}$; 5000 ppm Na_2SO_4

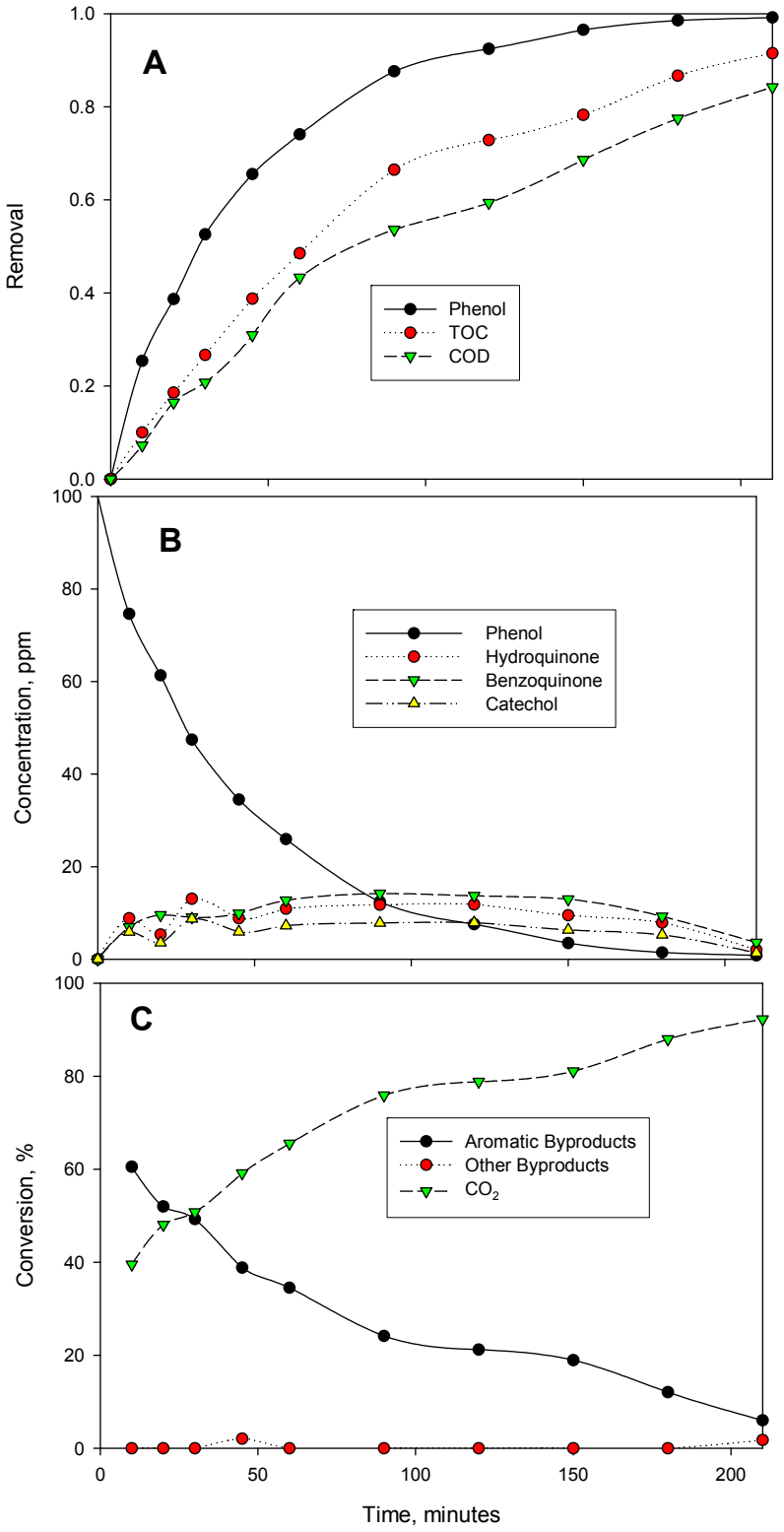

Figure 5.38: Profiles for Oxidation of Phenol; pH 7; 45 $mAcm^{-2}$; 3000 ppm Na_2SO_4

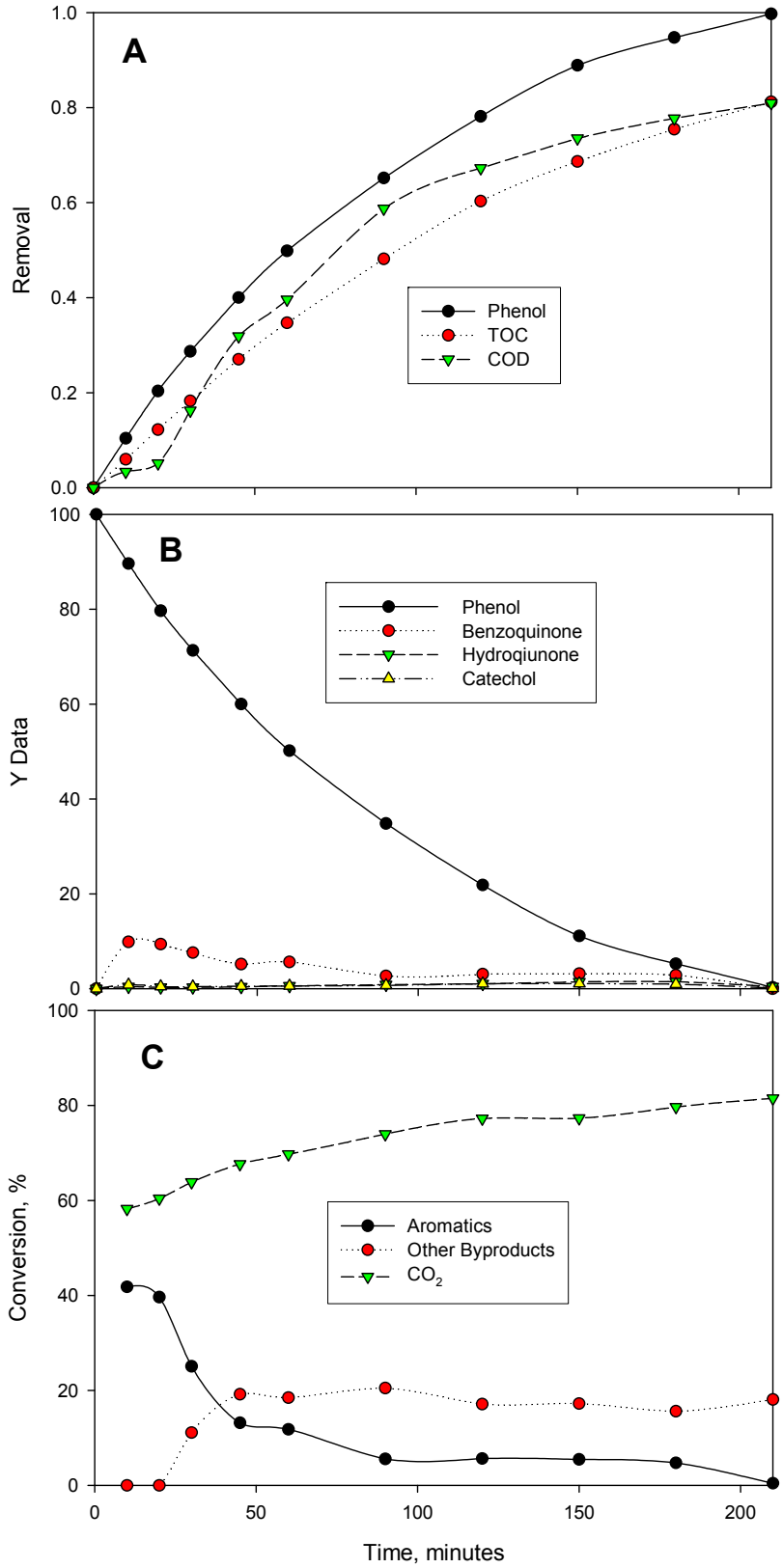

Figure 5.39: Profiles for Oxidation of Phenol; pH 2; 30 $mAcm^{-2}$; 1000 ppm Na_2SO_4

During electrochemical treatment of wastewater, interaction between organic pollutant in solution and anode surface is influenced by solution pH. It strongly controls the pathway for the oxidation determining whether the parent pollutants and subsequent generated intermediates will absorb onto the surface of the anode and possibility of further destruction. Comninellis and Pulgarin (1991) reported that the formation of polymeric film on BDD anode surface depends on the experimental conditions. Under their experimental conditions, they pointed out that alkaline media (pH > 9), low current density (< 30 $mAcm^{-2}$), high temperatures (> 50 ^{o}C) and high phenol concentration (> 50 mM) favored film formation. In complete contradiction to these claims**,** despite using similar experimental set-up and BDD anode, Canizares et al.(Canizares et al., 2002a) reported complete mineralization at pH 12 regardless of other experimental conditions. Their operating conditions were temperature range of 15- 60 ^{o}C, initial phenol concentration range of 10-40.2 mM and current density range of 15-60 $mAcm^{-2}$. Similarly, at initial COD of 1170 ppm (12.45 mM phenol), Tian et al. (2006), effectively, degraded phenol on Ti/BDD anode irrespective of initial pH (1.1, 6.1 and 12.1) with applied CD of 20 $mAcm^{-2}$ and operating temperature of 30 ^{o}C. A different research findings published by other authors (Gattrell and Kirk., 1990) supportively buttressed Comninellis and Pulgarin (1991) assertion by lamenting that polymer formation due to phenol oxidation could be combated by operating at low pH and high potential (though with reduced activity) and also selection of electrode materials that favor other reaction pathways over polymerization.

Relatively, data presented earlier in this study was a compromise between the findings of these previous authors. In a nutshell, the earlier observations herein suggested that mineralization of phenol at room temperature range (20-28 ^{o}C) was only persistently hindered at initial pH 12 for

low initial phenol concentration (i.e., 1.06 mM) regardless of the current density (30-60 $mAcm^{-2}$) with the mineralization potentials increases with increasing in initial phenol concentration (1.06, 10.6 and 21.2mM) and the trends strongly indicated possible attaining of equilibrium at longer electrolysis time. The discrepancies between the present study and the reports by the authors can be attributed to two main reasons. First, the difference in cell design could be a contributing factor. Studies by the other authors used stainless steel (an active electrode) as the cathode material, while in the present study graphite (non-active) was used instead. It is known and experimentally proven that counter electrode material used during oxidation of phenolic compounds can also influence anodic oxidation process significantly (Azzam et al., 1999) rather than just being passive means for completing the electric circuit as usually being assumed. Second, in the present study, the initial pH of solution was neither buffered nor maintained constant by any other means which differed from the other studies in which constant pH were maintained by using appropriate amount of acid and/or base during electrolysis to maintain constant solution pH. The degree of pH fluctuations of solution is susceptible to control the nature of byproducts to be generated and also the reaction pathways.

Iniesta et al. (2001b) highlighted the unique characteristics of BDD anode once operated at the potential region of water decomposition (E > 2.3V vs. SHE) in acidic environment of evading polymerization which usually leads to BDD anode deactivation. In addition to that, it was also demonstrated by (Marselli et al., 2003) that water discharge on BDD usually led to the production of hydroxyl radicals that oxidized the polymeric film on its surface according to Equation 5.13:

$$H_2O \rightarrow OH^* + H^+ + e^- \qquad 5.13$$

$$Polymeric\ film + OH^* \rightarrow H_2O + CO_2$$

Attempts made to accurately set the lowest operating potential at the least potential for water discharge were to no avail due to limitation of the potentiostat instruments available during the course of this work. The maximum current for the potentiostat of 1A was far below the current required to set the minimum current for the BDD electrode area used (i.e., 78 cm^2 or 12 $mAcm^{-2}$). Moreover, the DC power supply having maximum current capacity of 5A (i.e., maximum of applied current density of 64 $mAcm^{-2}$) limited the choice of higher current density range to be used to ensure that the BDD anode was optimally operated. The optimal and most effective operating potential regime would guarantee that all experiments were conducted at potential region of water decomposition to avoid the possibility of polymer generation.

Phenol is slightly acidic in nature possessing pK_a of 9.89, and as consequence, at pH > 9.89, phenol deprotonates yielding phenolate ions and hydroxyl ion. The relative composition of phenol to the phenolate ion is pH dependant, with basic pH (pH > 9.89) yielding more stable phenolate ions due to resonant stability of the phenolate ions in that range of pH (Figure 3.40). While at pH around 12, phenol in molecular form is expected to totally convert to the phenolate ions, thereby favoring the ability to transform the mechanisms of molecular phenol oxidation completely. Nonetheless, other authors (Vermillion and Pearl, 1964) opined that even at pH < 9.89, the bi-electronic discharge of phenol molecules leads to the formation of phenoxonium cations according to Equation 5.14:

$$C_6H_5OH \rightarrow C_6H_5O^- + H^+ + 2e^- \qquad 5.14$$

According to these authors, phenoxonium cations can react to form polymeric products in acidic medium while phenoxy radicals initiate polymerization in alkaline medium. A number of other investigators reported that both phenoxonium cations and phenoxy radicals generated at the anode are electrophiles capable of reacting with either the starting phenol molecule or another radical by C–C and/or C–O coupling, giving dimmers (Noureddine et al., 2009; Noureddine and André, 2009; Wang et al., 1998).

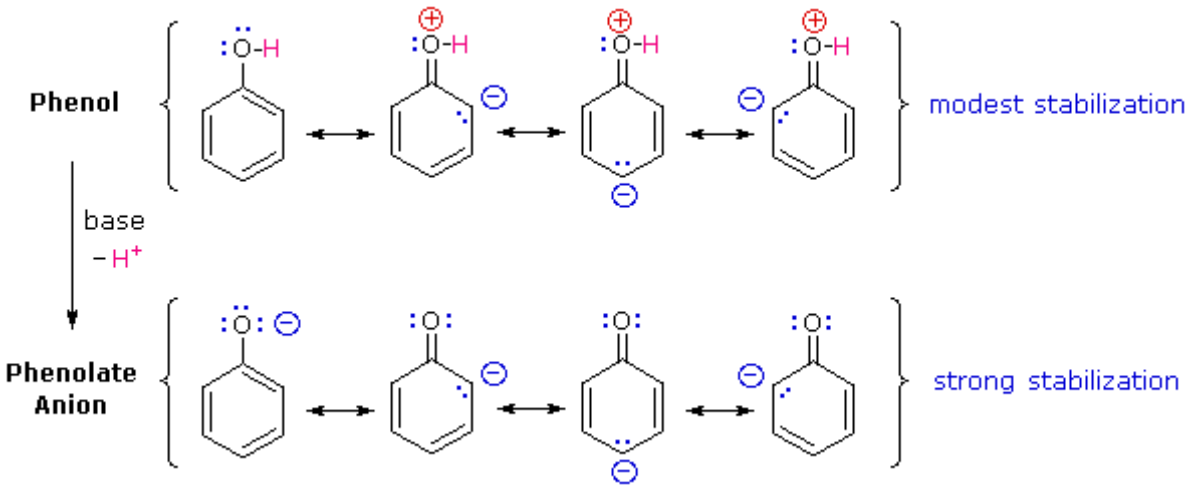

Figure 5.40: Phenol Speciation and Resonance Stability

It can be deduced from these facts that oxidation of phenol on BDD effectively achievable at pH < 9.89; while at more basic pH, phenol oxidation is more likely to be hindered as results of persistent build-up of byproducts that are difficult to be oxidized thereby negatively impairing

BDD anode performance. This may be used to provide clarification for the inability to oxidize phenol at initial pH 12 in this study. However, the paradox was the fact that this was only observed at 100 ppm (1.06 mM) initial phenol concentration and was not the case when it was increased to 500 and 1000 ppm (10.6 and 21.2 mM, respectively). Eventhough, the cell design used in this study was entirely different from that used by (Iniesta et al., 2001b), but this observation completely contradicts the concentration range suggested by these authors as all the initial phenol concentration considered here were far below 50 mM. The speculation that the white material that was observed on the surface of the BDD after several experimental runs were generated polymeric products that adsorbed more onto the electrode surface at higher phenol concentrations compared to at lower concentration, thereby leading to reduced organic contents (TOC and COD) of the solution at higher concentration couldn't be substantiated. However, the distinctive property of phenol that is pH dependent was anticipated to be more responsible for phenol oxidation hindrance as well as disparity observed for phenol oxidation at the different levels of initial phenol concentration under the basic medium (i.e., pH 12). In addition, a more complex radical mechanism might be involved which could have persistently hindered the phenol oxidation at the low phenol concentration and pH 12. Hence, this is a subject for further in-depth investigation. The foregoing observations can provide explanation for why most researches on electrochemical oxidation of phenol on BDD anode were not instituted on basic media (mainly limited to either acidic or neural media).

Also under the experimental conditions in this present study, it was speculated that the dominant mechanism involved in the oxidation of phenol and intermediately byproducts was heterogeneous direct oxidation reactions on the surface of the BDD anode. The presumed in-situ generated oxidants (peroxodisulfate) produced due to presence of Na_2SO_4 supporting electrolyte and the

hydrogen peroxide generated on the BDD anode appeared to be inactive to have catalyzed the oxidation process via indirect mechanism. Hence, effective degradation of phenol, its oxidation intermediates byproducts and the inorganic species were mainly mediated by the $OH^{\bullet}$ radicals generated on the BDD anode.

The data on the operating parameters effects on phenol oxidation on BDD anode presented in this chapter underscored the essence of defining region of interest for an electrochemical process and thoroughly navigating it according to a popular experimental design matrix. The findings may imply that, under similar experimental conditions, most experimenters consider the effect of operating parameters at one point of certain region while neglecting the other points; and thereby rendering researchers reporting effect of certain parameter(s) differently.

5.5 Effect of Operating Parameters on Current Efficiency and Specific Energy Consumption

5.5.1 Average Current Efficiency (ACE)

ACE is certainly of great concern for industrial economic considerations for adopting electrochemical process as a viable wastewater treatment option. The ACE (also estimated based on Equation 5.1) variation with specific charge passed during experiments are illustrated in Figure 5.41 which complements the ACE data already provided in Figure 5.27. The overall perceivable idea based on these trends was that the ACE decreases with increase in current density, electrolyte concentration and pH (Figure 5.41) while it increases with increase in initial phenol concentration (Figure 5.27). Considering Figure 5.41 which pertains to low initial phenol

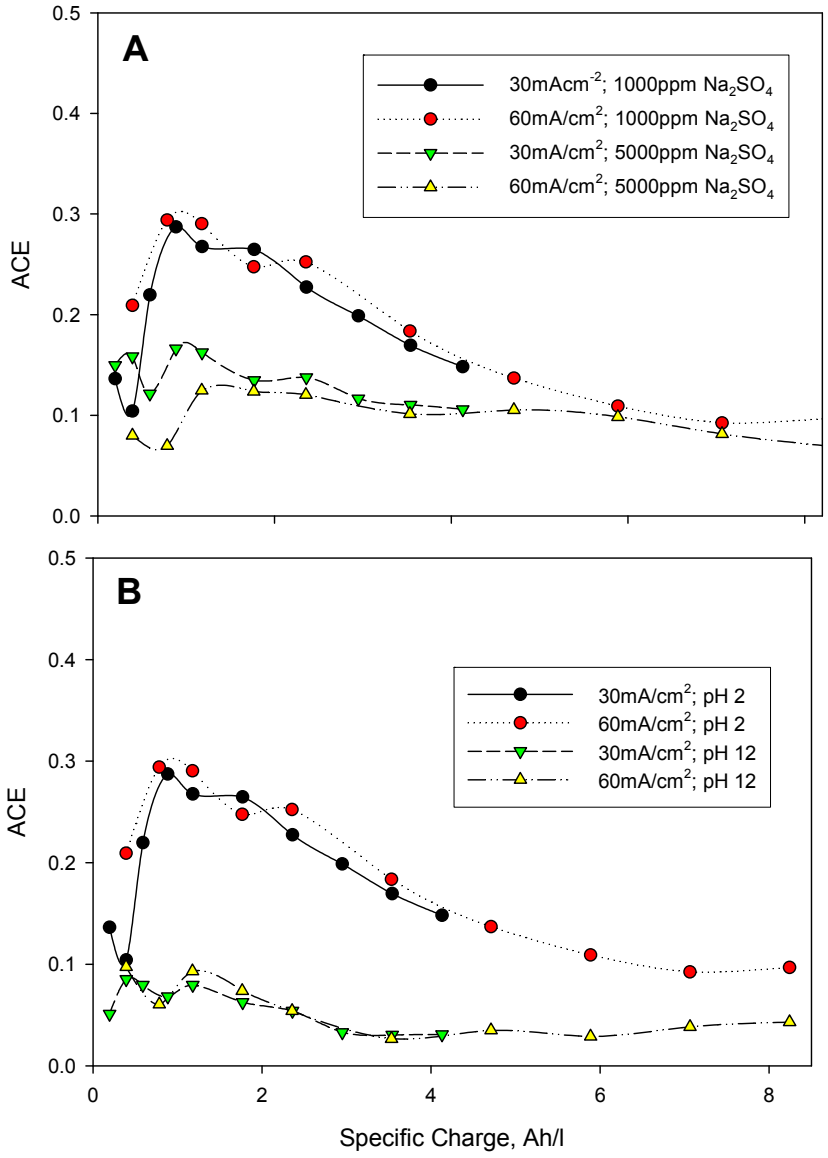

5.41: Average Current Efficiency vs Specific Charge Passed at (A) pH 2 and (B) 1000 ppm Na_2SO_4

concentration (100 ppm) under different experimental conditions, the ACE initially increases with specific charge passed until overall maximum ACE of 30% was observed at 1.5 Ah/L. Thereafter, the ACE continued to decline as the experiments were approaching steady state. It is interesting to observe that, despite the fact that the lowest specific charge passed during the 210 minutes electrolysis was at 30 $mAcm^{-2}$, the overall highest ACE of about 19.1% was achievable at the end of the experiment at such current density. However, for the higher initial phenol concentrations, 100% ACE was maintained almost throughout the experiments conducted at 30 $mAcm^{-2}$ and initial pH 2 (Figure 5.27A). The predominant trend of decrease in ACE as result of increase in current density was also reported by a number of authors (Panizza et al., 2001). In the case of this study, it could be mainly attributed to the fact that not all the additional current was utilized in the oxidation process and/or the side reactions (such as oxygen evolution reactions and production of inactive oxidants as discussed in previous sections) that compete with the phenol electro-oxidation in consuming the extra supplied current. The implication of the presented ACE data is that the oxidizable pollutant loading of wastewater are liable to control the cost-effectiveness of this process's viability which needs to be thoroughly evaluated. In this regard, it suggests that the higher the loading, the better the ACE would be anticipated; while low loading necessitates optimization and some trade-offs.

5.5.2 Specific Energy Consumptions

Electrochemical treatment process is undoubtedly an energy intense process and its efficiency could be evaluated in terms of specific energy consumption (SEC) which is defined as the amount of energy consumed per unit mass of pollutant removed. Hence, in addition to removal and current efficiencies, adopting electrochemical process for industrial wastewater treatment would

also be influenced by the SEC as it may control the economic viability of such a process that can render it competitive with other treatment processes. Two key SEC of interest during electrochemical oxidation of phenol are the SEC with respect to phenol removal and COD removal mathematically expressed in Equations 5.15 and 5.16, respectively.

$$E_{Phenol} = \frac{\int_{t}^{0} \frac{IV_C}{W}\, dt}{3600\, X\, 1000} \qquad 5.15$$

$$E_{COD} = \frac{4FV_C}{3600EOI} \qquad 0 \le EOI \le 1 \qquad 5.16$$

Where E_{phenol} and E_{COD} are the specific energy consumption in kWh/kmol COD and kWh/g-phenol, respectively, I is the supplied current, W is the weight of phenol removed at time t, F is the Faraday's constant in C mol^{-1}, V_c is the cell potential in Volt and EOI is the electrochemical oxidation index (which is equal to ACE as given in Equation 5.1).

5.5.3 Phenol Removal Specific Energy Consumption

It can be clearly inferred from the SEC with regard to phenol removal as illustrated in Figures 5.42 and 5.43 that the SEC was adversely influenced by the experimental operating conditions. The trends broadly suggest that the SEC increases with increase in current density and pH and decreases with increase in electrolyte concentration and initial phenol concentration.

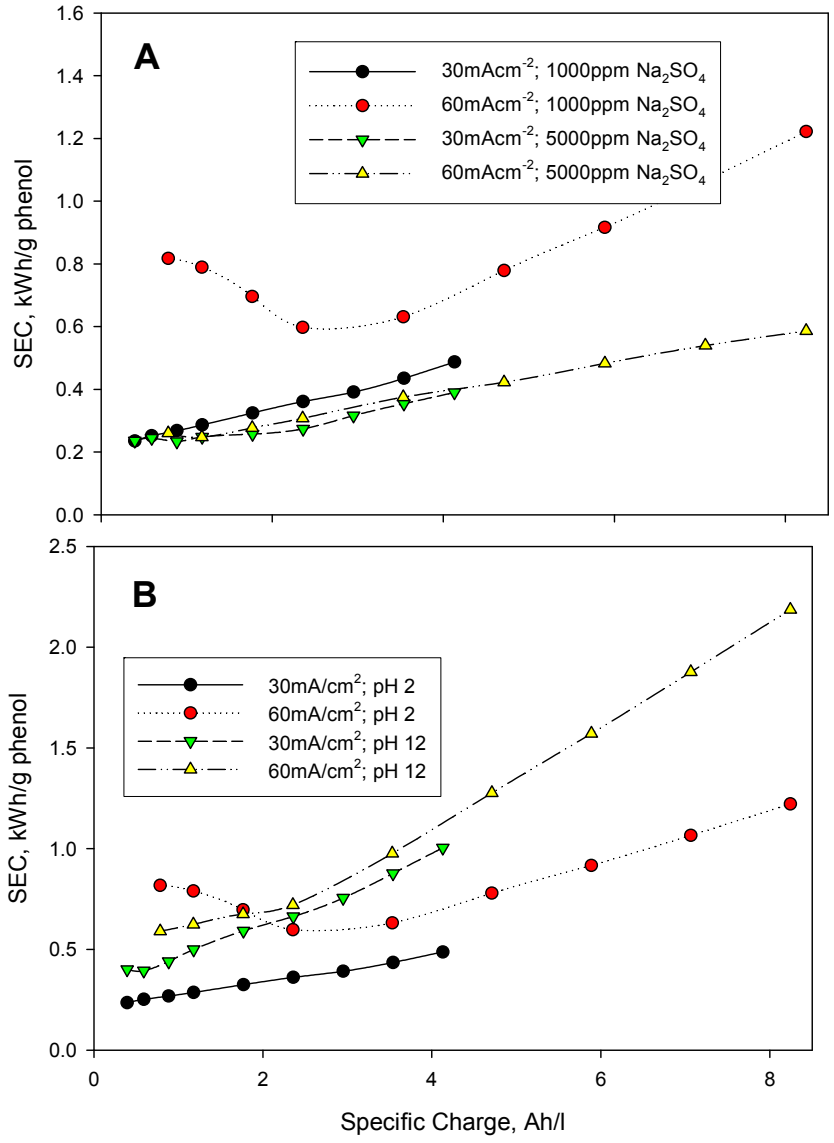

Figure 5.42: Energy Consumption with Respect to Phenol Removal at (A) pH 2 and (B) 1000 ppm Na_2SO_4

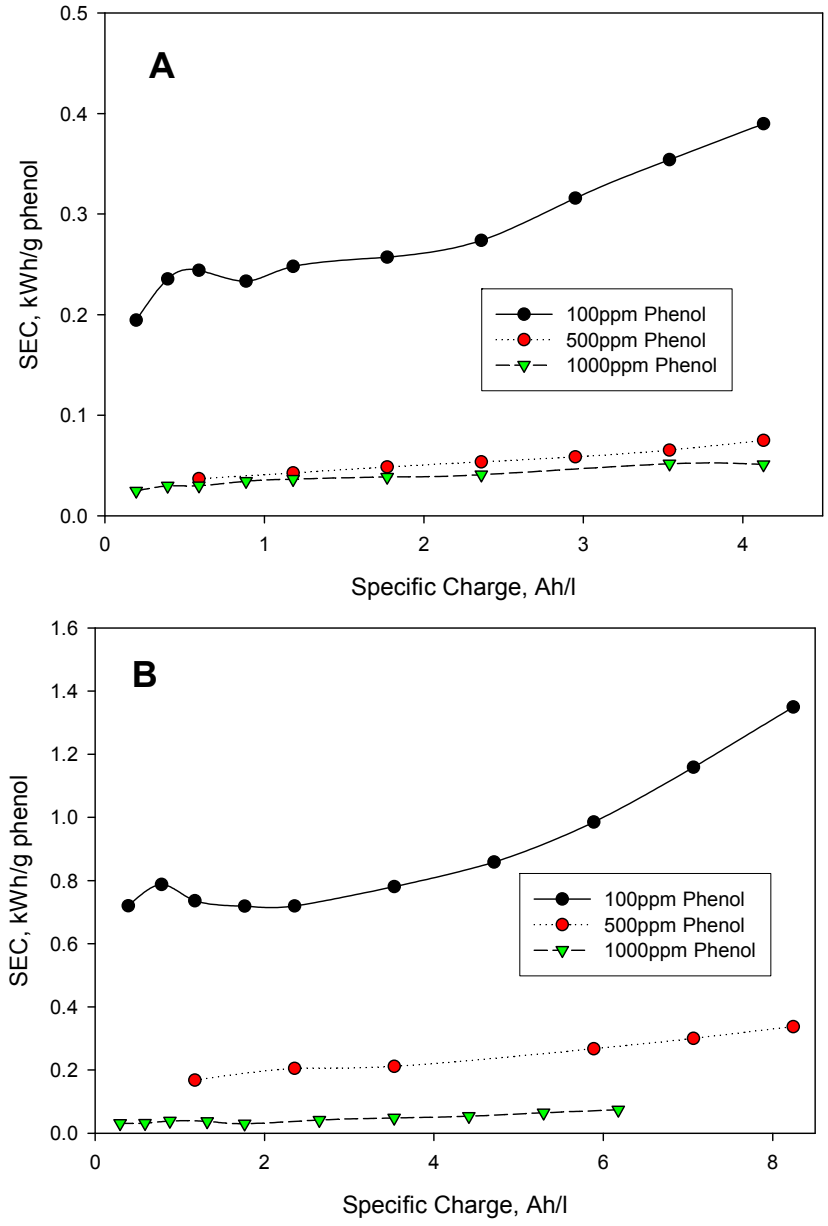

Figure 5.43: Energy Consumption With Respect to Phenol Removal at 5000 ppm Na_2SO_4 (A) 30 $mAcm^{-2}$ and pH 2 and (B) 60 $mAcm^{-2}$ and pH 12

Taken into account Figure 5.42 for low initial phenol concentration, increase in current density demanded higher potential across the cell, while the slight improvement on phenol removal rate (as established earlier) as result of the current increment couldn't compensate for the overall energy exerted. Hence, increase in current density improved the phenol oxidation but at the expense of reduced current efficiency and higher specific energy consumptions. Moreover, at fixed applied current density, increase in electrolyte concentration invariably led to enough drop in voltage across the cell due to rise in solution conductivity that may canceled the effect of lower phenol removals, thereby leading to more effective utilization of energy. Even though good removal of phenol was achieved under most of the experimental conditions, however, bearing in mind that the overall minimum SEC was approximated at 389kWh/kg phenol, it is worthy to mention that the SEC in all the cases were excessive compared to most of the reported values by other authors (Panizza and Cerisola, 2008; Urtiaga et al., 2009). This was attributed to the lower initial concentration of phenol, an assertion substantiated by considering the SEC at higher initial phenol concentrations of 500 ppm and 1000 ppm as provided in Figure 5.43. The SEC was found to decrease considerably with increase in phenol initial concentration. At 60 $mAcm^{-2}$ and initial pH 12 the SEC drastically lowered from 1349 to 337 and 74 kWh/kg-phenol, respectively. While decreasing both the current density and pH (at 30 $mAcm^{-2}$ and initial pH 2), the SEC was reduced from 389 to 74.9 and 50.9 kWh/kg-phenol, respectively. Hence, by considering these cases, values of the SEC obtained were quite comparable with values reported elsewhere (Panizza and Cerisola, 2008; Yao et al., 2008). The SEC decreases with initial phenol concentration due to the fact that the total amount of phenol removed was directly proportionally to initial phenol concentration; and it was found to significantly increase when the concentration was raised from 100 ppm to 500 and 1000 ppm. Consequently, in addition to ACE, the data presented here also

reiterated the idea that loading of a given wastewater is one of the major controllers of the viability of adopting organic pollutant's treatment with BDD anode. The higher the loading, the better the SEC; while for substantially low pollutant loading, optimization and some trade-offs also become necessary for ensuring process cost-effectiveness.

5.5.4 COD Removal Specific Energy Consumption

The SEC in terms of COD removal as a holistic approach for evaluating the overall energy consumption takes into cognizance the energy utilization in removing not only phenol, but rather all oxidizable species in a wastewater stream. As provided in Figures 5.44 and 5.45, generally, the trends are to a greater extent comparable to energy consumption due to phenol removal. Increase in current density and initial pH led to more energy demands for eliminating COD and vice versa for increase in electrolyte and initial phenol concentration. The reasons for such variations at different operating conditions are similar to those provided for the SEC in terms of phenol removal with the exception of the influence of the initial pH. The drastic increase in the SEC at initial pH 12 was due to the fact established previously that at such pH value, phenol was mainly converted other organic compounds rather than its effective oxidation to CO_2. The undulating profiles for some of the SEC at pH 12 correspond to the fluctuations in the COD values with treatment time. Similarly, the least energy consumed estimated as 84.07 kWh/kg-COD observed at 30 $mAcm^{-2}$ and initial pH 2 drastically reduced, respectively, to 11.6 and 10.29 kWh/kg-COD at the higher initial phenol concentration (i.e., 500 and 1000 ppm) as shown in Figure 5.45A. However, for operating at 60 $mAcm^{-2}$ and initial pH 12 (Figure 5.45B), SEC was reduced from 1109 to 48.1 and 24.4 kWh/kg-COD, respectively.

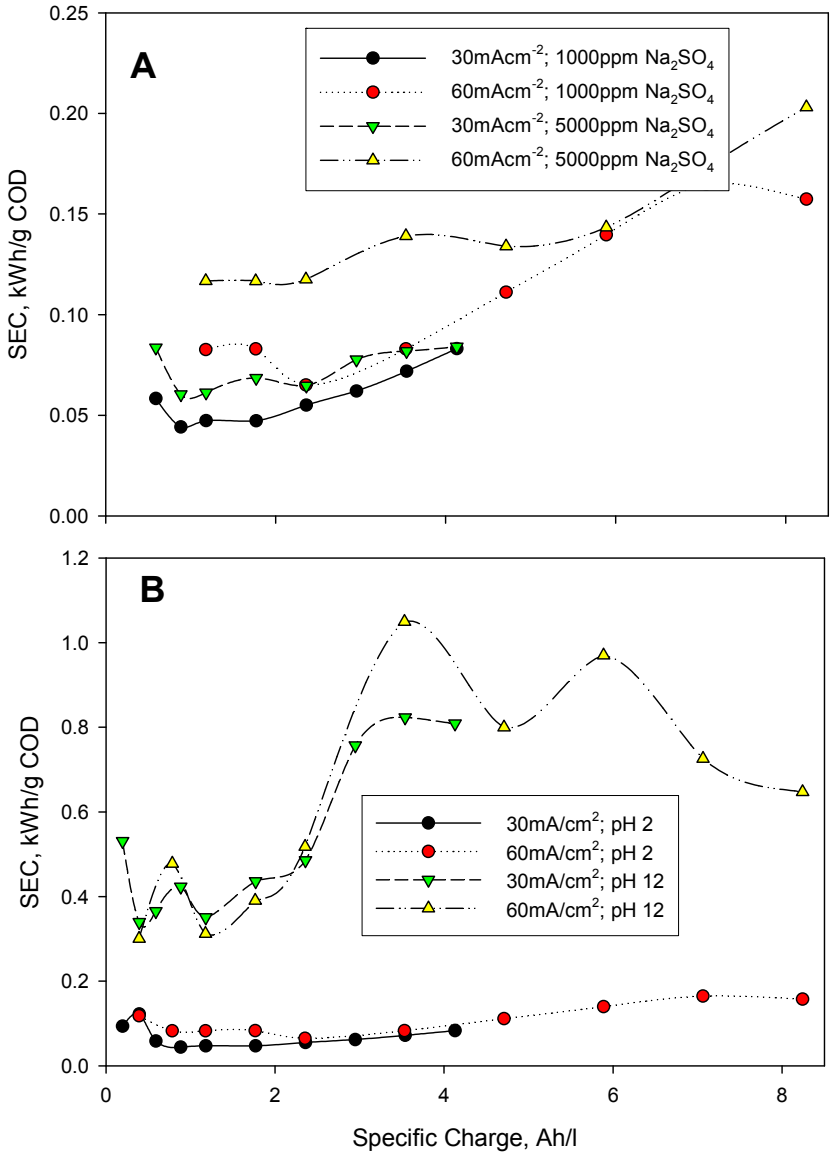

Figure 5.44: Energy Consumption With Respect to COD Removal at (A) pH 2 and (B) 1000 ppm Na_2SO_4

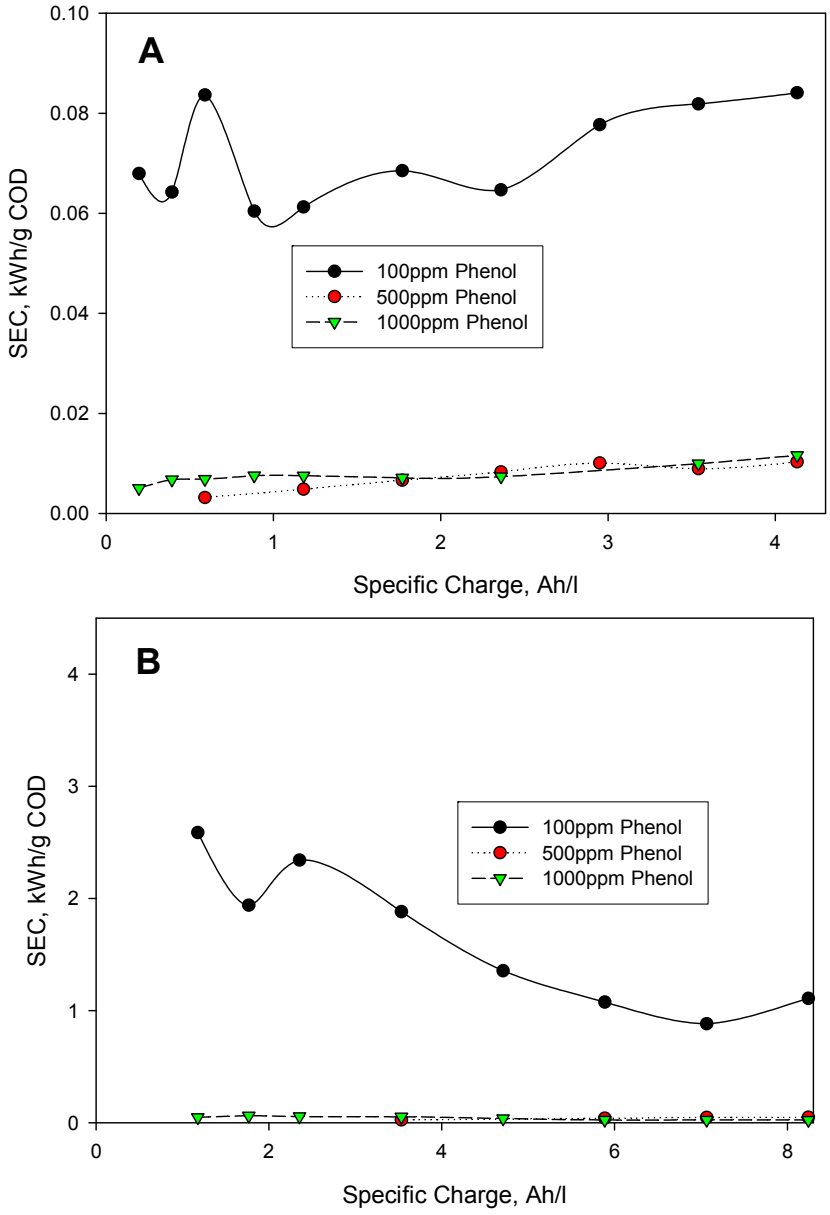

Figure 5.45: Energy Consumption with Respect to COD Removal at 5000 ppm Na_2SO_4 (A) 30 $mAcm^{-2}$ and pH 2 (B) 60 $mAcm^{-2}$ and pH 12

These foregoing observations reiterated the fact that better utilization of current and energy during electrochemical treatment of wastewater at BDD anode are expected at higher pollutant loadings. Consequently, for cost-effectiveness, this would definitely necessitate process optimization in situations whereby low phenol or oxidizable pollutant loadings are encountered.

Chapter 6

Kinetics and Mechanism of Phenol Oxidation in Different Mix Matrixes

6.1 Introduction

Electrochemical oxidation of phenol in the presence of NH_4^+, CN^- and S^{2-} ions in different mix matrixes was undertaken at optimum operating conditions obtained from the RSM modeling (see Chapter Seven). Details for the simulated wastewaters' characteristics used are provided in Table 4.1.They mainly composed of two batches of experiments conducted in presence of 200 ppm and 100 ppm of each of the inorganic species at binary, ternary and quaternary combinations with phenol. In spite of the presence of 200 ppm of each of the inorganic species, excellent oxidation of phenol was obtained. However, all the results obtained later for the second set of experiments pertaining low initial concentration (i.e., 100 ppm) of each of the inorganic species appeared to be unexpectedly lower than the corresponding former cases. At higher initial concentrations of the inorganic species, it was more logical that there would be higher competitiveness for the electro-generated radicals by the various species in solution which was more liable to impair phenol oxidation. Paradoxically, reverse was consistently the case for all the various mix matrixes. In view of that, it was observed that a white deposit appeared to have covered some portion of the BDD anode (as shown in Figure 6.1B) just before starting the later set of experiments which differ from the former cases (Figure 6.1A). Iniesta and co-researchers (Iniesta et al., 2001b) attributed this type of surface modification of the BDD anode to the adsorption of generated oxidation byproducts that have affinity to BDD anode surface during electrochemical oxidation

of phenols which happens particularly after long electrolysis time. In order to provide better explanation for such observation, cyclic voltammogram (CV) scans using PCI4/300 Gamry potentiostat instrument were conducted in 1M H_2SO_4 on small portion of the BDD anode (about 5 cm^2) during the two batches of experiments. Results for the CV scans are provided in Figures 6.2A and 6.2B, respectively. For the first condition as depicted in Figure 6.2A, it can be observed that almost all the superimposed cycles for the five consecutive scans are not far from one another (with the exception of the first one). The maximum measured anodic currents from the five scans range was 0.4 - 0.54 A. In contrast, for the second condition (Figure 6.1B), the wider cycles' separations are obvious and the anodic current range has substantially increased (0.31 - 0.82 A). Consequently, it was speculated that the experiments for the latter case were undertaken at reduced activity of the anode. Hence, that appeared to be the main reason for the low removal efficiencies encountered in the later set of the experiments despite lowering the concentrations of the inorganic species by half. Limitation of the potentiostatic instrument constrained the ability to set the experimental conditions at E > 2.3 vs SCE; the potential region for water decomposition which would have prevented accumulation and subsequent adherence of polymer byproducts on the anode which apparently led to the decline in the anode activity. Therefore, due to the apparent differences in physical appearance and activity of the anode during the two distinct set of experiments, the BDD anodes were designated as BDD1 and BDD2, respectively. To further validate the claim of the decline in the anode activity, two experiments for BDD1 (one for single phenol matrix and the other for ternary mix matrix of phenol-CN-NH_4^+) were repeated using the BDD2. In the ternary mix matrix experiment, the initial concentration of each of the inorganic species was set at 200 ppm instead of 100 ppm. The plots depicted in Figures 6.3A and 6.3B, respectively, compare the results from these two later experiments with those obtained earlier

A 

B 

Figure 6.1: Physical Appearance for the BDD Anodes Used during Experiments for Inorganic Species Initial Concentrations of (A) 200 ppm and (B) 100 ppm

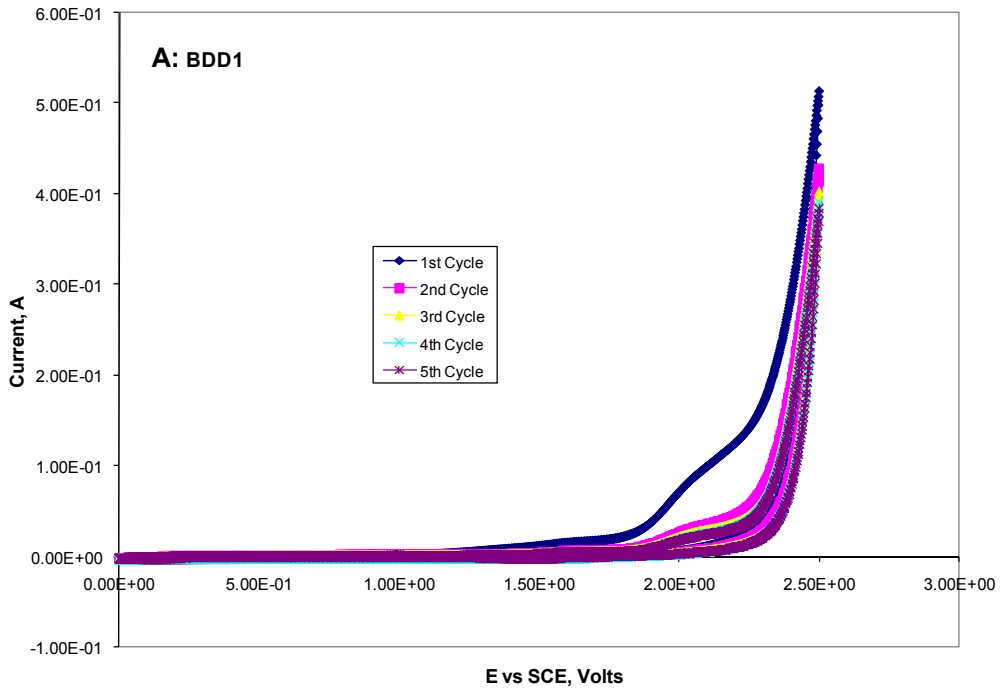

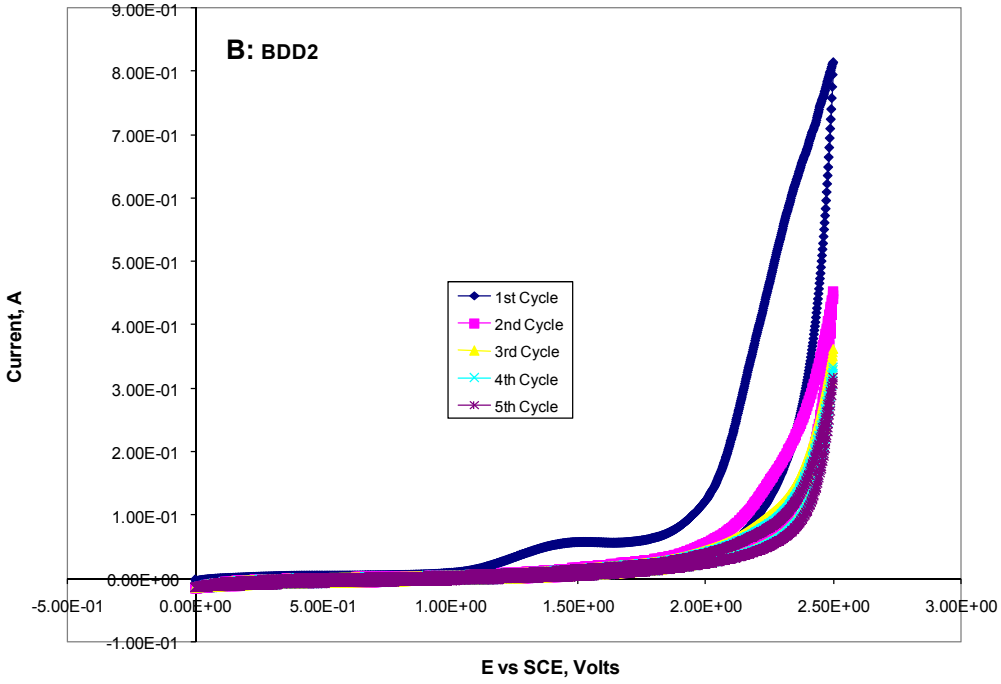

Figure 6.2: Cyclic Voltammogram Scans in 1M H_2SO_4 During Experiments at Initial Concentrations of Inorganic Species of (A) 200 ppm and (B) 100 ppm

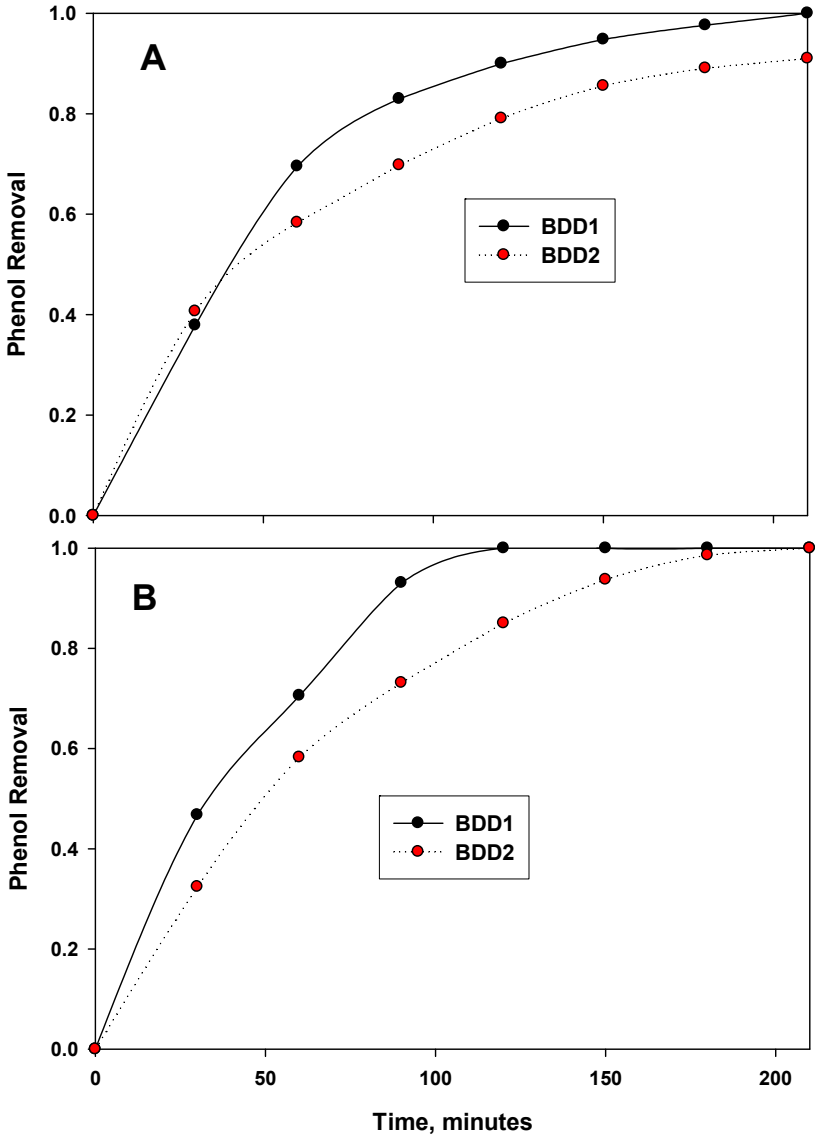

6.3: Experimental Runs Replicated Using BDD2 for (A) Single Phenol Matrix and (B) Ternary Matrix of Phenol, Cyanide and Ammonium

using BDD1. In the first case, phenol removal at 3.5 hours retention time was found to decrease from 100% to 84%; while for the second case, the time for the 100% removal of phenol increased from 120 to 180 minutes, respectively. The wide disparity and irreproducibility of the data from these different sets of experiments are clear evidence supporting each other. They support the claim that decline in BDD activity was responsible for the strange results discrepancies observed by for the two separate batches of experiments cohabiting phenol with 200 ppm and 100 ppm concentrations of each of the inorganic species in the different mix matrixes experiments.

For the two scenarios (i.e., BDD1 and BDD2), the effects of the inorganic species presences on the kinetics and process efficiency in the different mix matrixes were evaluated based on the removal of phenol, TOC and COD vis-à-vis profiles for intermediary byproducts generations. Similarly, the ACE and SEC data in absence and presence of the inorganic species were also compared. While summary of the results are given in APPENDIXES A, B and C, detailed analyses are provided in the next sections.

6.2 Development of Kinetic Models for Phenol, TOC and COD Removal

Degradation kinetics for phenol, TOC and COD were studied based on the data obtained from the different mix matrixes experiments. Firstly, several kinetic models were used to fit concentration versus time data with the help of SIGMAPLOT regression tool from which the best fitted models were identified. The best fitted models for phenol, TOC and COD consistently showed that there exist good linearity between $\log(C/C_0)$ and the treatment time as all the removal trends of these parameters predominantly showed exponential decay trends. Hence, under the present

experimental conditions, presence of the inorganic species in the different mix matrixes appeared not to have altered the predominantly pseudo-first-order reaction kinetics of phenol and TOC and COD degradation as widely reported in the literature. This implies that the initial concentration of phenol in solution was very essential for phenol oxidation; the higher the initial concentration, the faster the rate of disappearance and oxidation was expected.

Consequently, working at galvanostatic conditions, it can be adequately assumed that the concentration of $OH^{\bullet}$ radicals (which were mainly responsible for the AOP in this study) were approximately in a steady state and therefore, the oxidation rate can be expressed according to Equation 6.1 (Brillas et al., 2004);

$$\frac{d[C_0]}{dt} = k[OH^*][C] \qquad 6.1$$

Integrating Equation 6.1 yields Equation 6.2:

$$\ln\left[\frac{C_t}{C_0}\right] = k_{app}t \qquad 6.2$$

Where k_{pp} is the apparent observed pseudo-first-order rate constant.

Typically, for the electrochemical cell employed in this study and in case of first order degradation kinetics, the mass transfer coefficient (k_m), a parameter that can adequately define the

hydrodynamic nature of the electrochemical system can be estimated from the slope of ln(C/C_0) vs time graph. Accordingly, both Equations 6.1 and 6.2 can be re-written as Equation 6.3:

$$\frac{d[C_0]}{dt} = \frac{A}{V_r} k_m [C] \qquad 6.3$$

Hence, for any system that can be described by Equation 6.3, the mass transfer coefficient is directly proportional to the apparent decay constant and for that, it can be expressed as:

$$k_m = \frac{V_r}{A} k_{app} \qquad 6.4$$

Where V_r is the reactor volume; A is the electrode surface area.

As previously established, the oxidation of phenol in the present study was mainly a heterogeneous direct process that took place on the anode surface. The solution within the electrochemical cell was vigorously stirred in order to eliminate the mass transport effect so as to render the process to be mainly kinetically controlled. However, data presented earlier suggested that the overall decontamination process was a kinetically controlled process with was subject to mass transport of species in solution to the surface of the BDD anode. Therefore, in the second phase of the kinetic modeling, the rate limiting technique was employed to identify the best parameter among phenol, TOC and COD that could be used to model in order to satisfactorily understand and also determine the operating regime (either kinetic or mass transfer controlled) for

phenol oxidation both in absence and presence of the inorganic species. Generally, the rate-limiting step of a process, basically, corresponds to either chemical reaction (kinetic control) or to transfer of the component to surface or region where reaction takes place (mass-transfer control). For electrochemical oxidation process of organic pollutants, the limiting current approach takes into account the nature and concentration of pollutant(s) under study as well as the experimental (hydrodynamic) conditions in relation to the degradation efficiency. For an organic compound in a single matrix aqueous system, the limiting current density, an index which delineates the key operating regimes can be estimated according to Equation 2.10 directly using the organic compound concentration (in case of fast and direct conversion to CO_2 with no or negligible generation of other undesired byproducts). Otherwise, the global parameter COD in Equation 2.11 is employed. Moreover, depending on the operating regime, the temporal evolution of either organic concentration or COD can be estimated using Equations 2.12 and 2.14, respectively. These models were found to conveniently fit experimental data for different phenolic compounds under certain laboratory operating conditions (Boye et al., 2002; Comninellis and Pulgarin, 1991; Gherardini et al., 2001; Panizza et al., 2001; Rodrigo et al., 2001). Unfortunately, these equations were short of addressing circumstances where an organic compound in solution is cohabited with other oxidizable inorganic species that also exert oxygen demand. Under such scenarios, the temporal COD removal cannot be a sole attribute of the organic compound removal. Beside that fact, organic compound removal cannot also be used directly as a yardstick to indicate effective oxidation of any organic compound under study. Moreover, presence of the inorganic species definitely invalidates the applicability of both Equations 2.10 and 2.11, thereby rendering the organic compound kinetic modeling and estimating the operating regime delineator (i.e., $i_{\lim}$) for

its oxidation to be more difficult and challenging. These observations collectively suggest the need for a different approach in tackling this vital issue.

Consequently, SIGMAPLOT regression capabilities were employed to develop empirical models for TOC and COD from experimental data obtained both in absence and presence of the inorganic species. Knowing that in both absence and presence of the inorganic species, phenol mineralization (i.e., oxidation) was predominantly not very fast and direct conversion of phenol to CO_2 (without generation of intermediary byproducts) was mainly not realistic, phenol removal data were disregarded in this approach as they cannot provide meaningful mineralization or oxidation information. It was interesting to find that, for both parameters considered (TOC or COD), analyses of the regression output revealed that the exponential decay models for nearly all the data could be better if represented mathematically by Equation 6.5:

$$C_t = aC_0 \exp\left(-bt + d\right) \tag{6.5}$$

Where a, b and d are unknown model's constants. The similarity between this model and Equation 2.14 is comprehensible by considering $a = \alpha$, $b = \alpha A k_m / V_r$ and $d = (1- \alpha)/ \alpha$. Finding that $d = (1- \alpha)/ \alpha \approx (1- a)/ a$ in most of the cases and knowing the values of A and V_r which are constant for a given set-up, the values of α and k_m can be easily estimated. Thus, based on the presented models, two values of k_m can be calculated either directly from Equation 6.3 or indirectly from Equation 6.5, respectively, designated as $k_{m\ exp}$ and $k_{m\ model}$. The corresponding α can now be conveniently estimated indirectly. Intuitively, amongst the two obtainable values of α

(i.e., from TOC and COD data), the best estimator of its corresponding k_m can be assumed to be the best regime delineator from which the limiting current can be estimated (only under galvanostatic conditions).

For the single phenol matrix at applied current density of 60 $mAcm^{-2}$ and initial pH 12, regardless of phenol initial concentration, it was found that temporal evolution of COD was the best estimator of the k_m. The high $R^2_{Adjusted}$ values for the plots in Figure 6.4 indicate the goodness of models' fits, respectively. The values of the $k_{m\ exp}$ and $k_{m\ model}$ for 1000 ppm initial phenol concentration are 0.08153 and 0.0876 cm-$minutes^{-1}$, while for 100 ppm are 0.09899 and 0.1009 cm-$minutes^{-1}$ respectively. The respective α value of 1.3221 and 1.0785 revealed that the applied constant current is greater than the i_{lim}, thereby suggesting that the oxidation process was within the mass-transfer controlled regime.

For the case of the higher mix matrixes, detailed results for phenol, TOC and COD removal efficiencies and the kinetic modeling results are presented in the next sections.

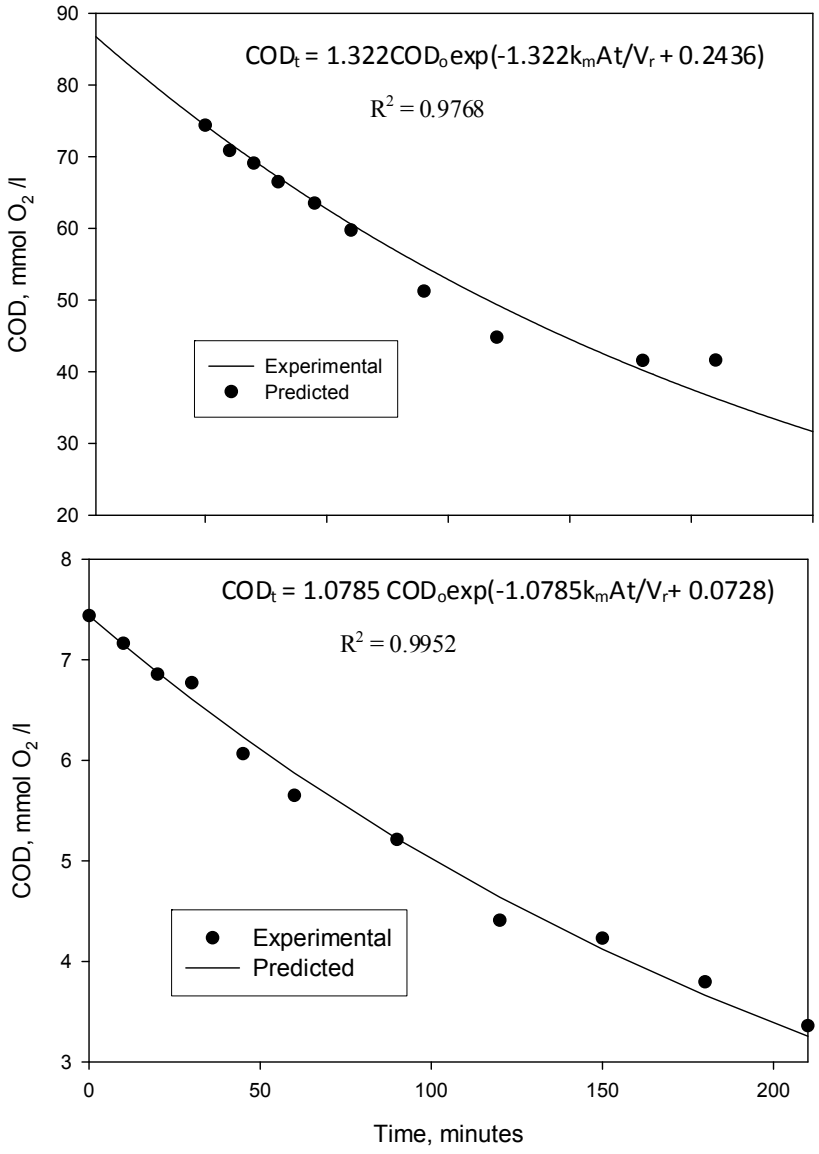

Figure 6.4: Experimental vs Model's Prediction for COD Evolution at initial Phenol Concentration of (Top) 1000 ppm and (Bottom) 100 ppm

6.3 Analysis of Phenol Removal Kinetics in Different Mix matrixes

The key phenol degradation kinetic and hydrodynamic parameters (k_{pp}, $k_{m\ exp}$,$t_{1/2}$ and R^2) for the fitted first-order models were calculated from the slope of lines given in Figures 6.5 and 6.6 for BDD1 and BDD2, respectively. The values of these parameters are listed in Table 6.1 from which the phenol degradation kinetics in presence of the inorganic species can be compared. Moreover, the estimated values of $k_{m\ model}$ are provided in the table, respectively. The statistical analysis for the models' adequacies show that all the regression coefficients (R^2) are in good agreement with the $R^2_{adjusted}$. Also all the *p*-values supported the acceptance of the hypothesis that the coefficients are significant parameters in the models.

6.3.1 Phenol Removal Kinetics in Binary Mix Matrixes

Removals of phenol in binary mix matrixes in the presence of NH_4^+, CN^- and S^{2-} at the optimized conditions are depicted in Figures 6.7A and 6.7B for the BDD1 and BDD2, respectively. Similarly, the entire removal trends in these cases show an exponential decay of phenol concentration with time as the previous single phase cases. It is inferable that phenol removal was reduced at different degrees in almost all the cases for both BDD1 and BDD2, with the observed reduction for BDD2 being more pronounced. In the presence of NH_4^+ ions, it appeared that the removal efficiency of phenol was slightly reduced in both cases; from 100% to 95.07% and 97.26%, respectively, for BDD2 and BDD1. The decrease in removal efficiency in the presence of CN^- is more noticeable for BDD2 as it was lowered from 100% to 89.82%. Conversely, remarkable improvement of phenol removal was observed for BDD1 which even surpassed that of the single phase matrix. In this later case, 100% removal was achieved at 150 minutes (i.e., $t_{1/2}$

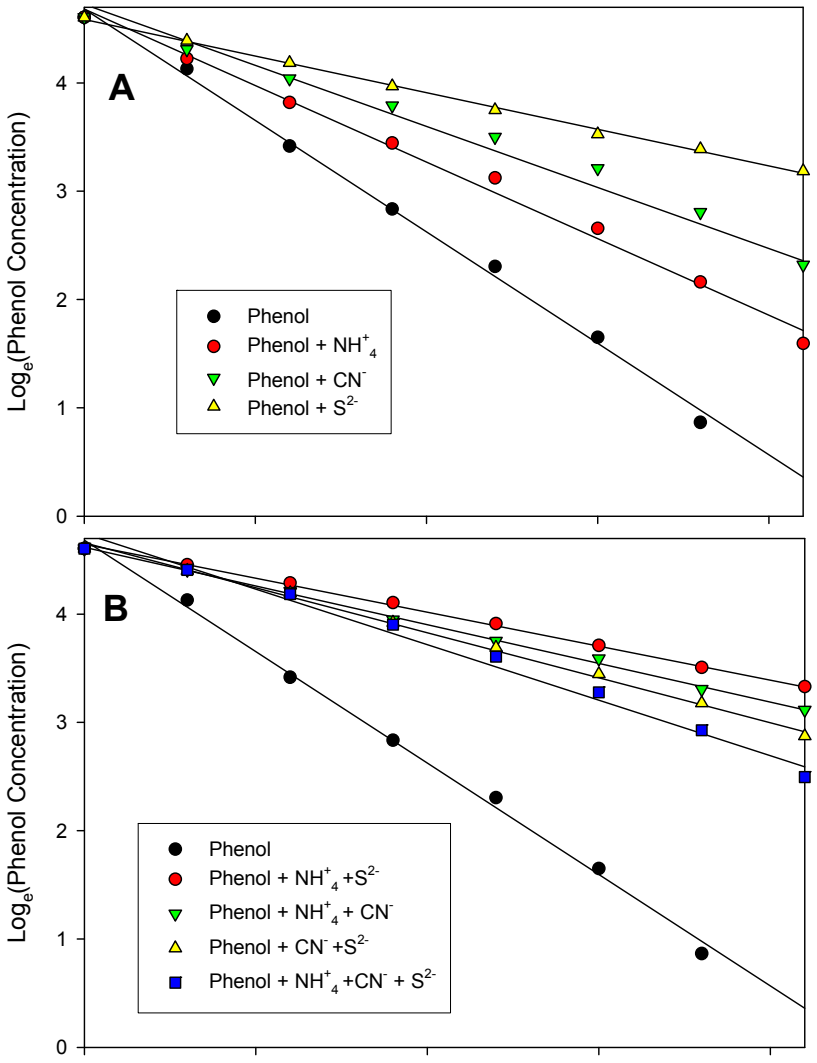

Figure 6.5: First Order Kinetic Fits for Phenol in Different Mix Matrixes for BDD2

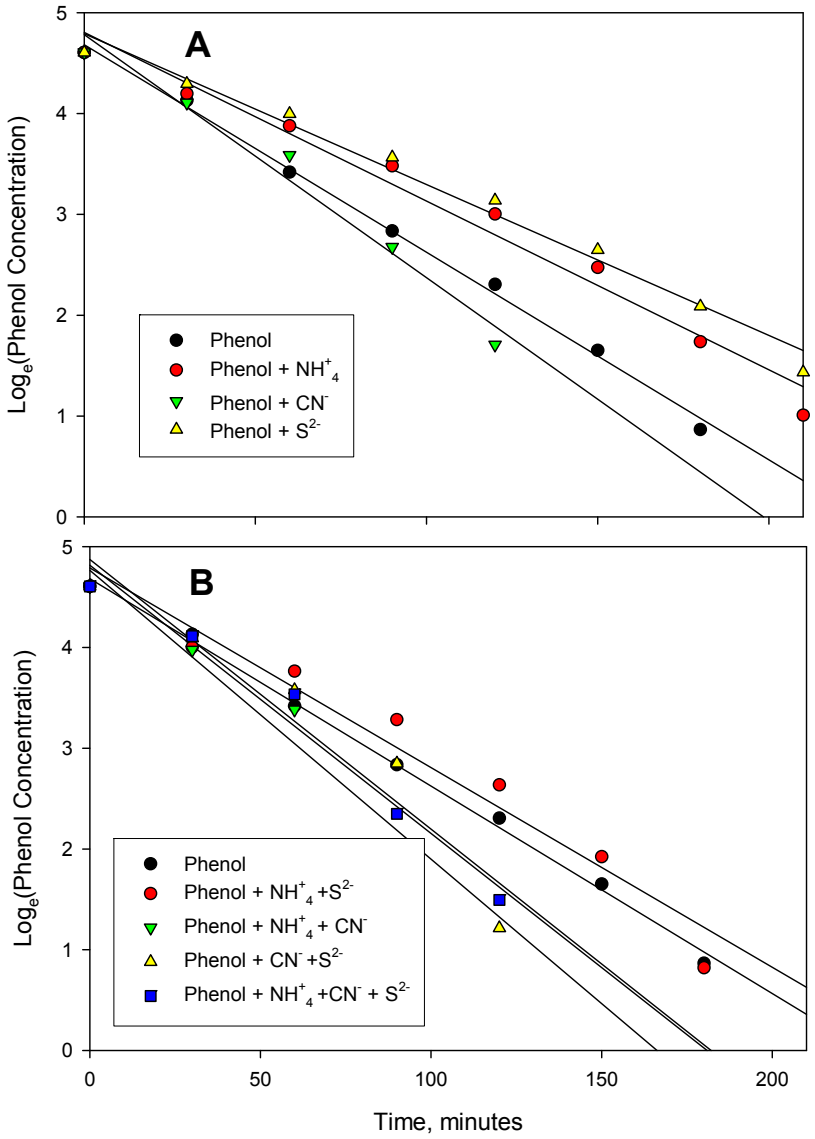

Figure 6.6: First Order Kinetic Fits for Phenol in Different Mix Matrixes for BDD1

Table 6.1: Phenol Removal Kinetic and Hydrodynamic Parameters for (Top) BDD1 and (Bottom) BDD2

Matrix Nature	Component (s)	k_{app} min^{-1}	$K_{m\ exp}$ cm/min	$t_{1/2}$ minutes	R^2	$R^2_{Adjusted}$	p-Value
Single	Phenol	0.019	0.4822335	36.48	0.996	0.9953	<0.0001
Binary	Phenol, NH_4^+	0.0134	0.3401015	51.73	0.9948	0.9939	<0.0001
	Phenol, CN^-	0.0197	0.5	35.19	0.9883	0.9864	<0.0001
	Phenol , S^{2-}	0.0122	0.3096447	56.82	0.9916	0.9901	<0.0001
Ternary	Phenol, NH_4^+, S^{2-}	0.0161	0.4086294	43.05	0.9868	0.9846	<0.0001
	Phenol, NH_4^+,CN^-	0.0236	0.5989848	29.37	0.9881	0.9861	<0.0001
	Phenol, CN^-, S^{2-}	0.0197	0.5	35.19	0.9879	0.9858	<0.0001
Quaternary	Phenol, NH_4, S^{2-}, CN^-	0.0206	0.5228426	33.65	0.9855	0.9831	<0.0001

Matrix Nature	Component (s)	k_{app} min^{-1}	$K_{m\ exp}$ cm/min	$t_{1/2}$ minutes	R^2	$R^2_{Adjusted}$	p-Value
Single	Phenol	0.0156	0.397522	44.43	0.9917	0.9903	<0.0001
Binary	Phenol, NH_4^+	0.013	0.3312102	53.32	0.9991	0.999	<0.0001
	Phenol, CN^-	0.0097	0.2471338	71.46	0.9955	0.9949	<0.0001
	Phenol , S^{2-}	0.007	0.1783439	99.02	0.9991	0.999	<0.0001
Ternary	Phenol, NH_4^+, S^{2-}	0.006	0.1528662	115.52	0.9973	0.9969	<0.0001
	Phenol, NH_4^+,CN^-	0.0071	0.1808917	97.63	0.9984	0.9982	<0.0001
	Phenol, CN^-, S^{2-}	0.0078	0.1987261	88.87	0.9972	0.9968	<0.0001
Quaternary	Phenol, NH_4, S^{2-}, CN^-	0.0087	0.2216561	79.67	0.9894	0.9876	<0.0001

of 35.18 minutes) which was much lower than the 210 minutes required to attaining 100% removal in the single phase. However, the removal trends for BDD2 in the presence of either NH_4^+ or CN^- indicate that the process nearly reached steady state of complete elimination of phenol ($t_{1/2}$ = 51.72 and 35.18 and $t_{1/2}$ = 53.31 and 71.45, for BDD1 and BDD2, respectively). In the presence of S^{2-}, the decline in phenol removal efficiency is more conspicuous compared to the two previous scenarios, particularly for the BDD2. The removal efficiency of about 75.79% was found to be the maximum achievable for BDD2, while for BDD1, the removal was observed to be 95.1%. Moreover, the removal trend in case of the presence of S^{2-} for the BDD2 implies that reaching equilibrium (i.e., achieving 100% removal of phenol) would have required longer retention time.

Considering Table 6.1 for the binary mix matrixes, the k_{app} and the mass transfer coefficient observed ($k_{m\ exp}$) in the single matrix were apparently reduced by 29-36% and 17-55% while the $t_{1/2}$ was increased by 41-55 and 20-123% for BDD1 and BDD2, respectively. The negative effects of the inorganic species predominantly following the order Phenol-NH_4^+ < Phenol-CN^- < Phenol-S^{2-}.

For the binary mix matrixes using BDD1, phenol concentration was increased from 100 ppm to 500 ppm and treated at a basic pH of 12 for comparative reasons. The result depicted in Figure 6.8 demonstrates that the removal trends didn't deviate from the corresponding previous cases (Figure 6.7A) despite the change in pH of the solution and phenol concentration. The removal efficiency of phenol appeared not to be affected due to the presence of NH_4^+ and CN^-, while in the presence of S^{2-}, phenol removal was profoundly deteriorated. These observations suggest that,

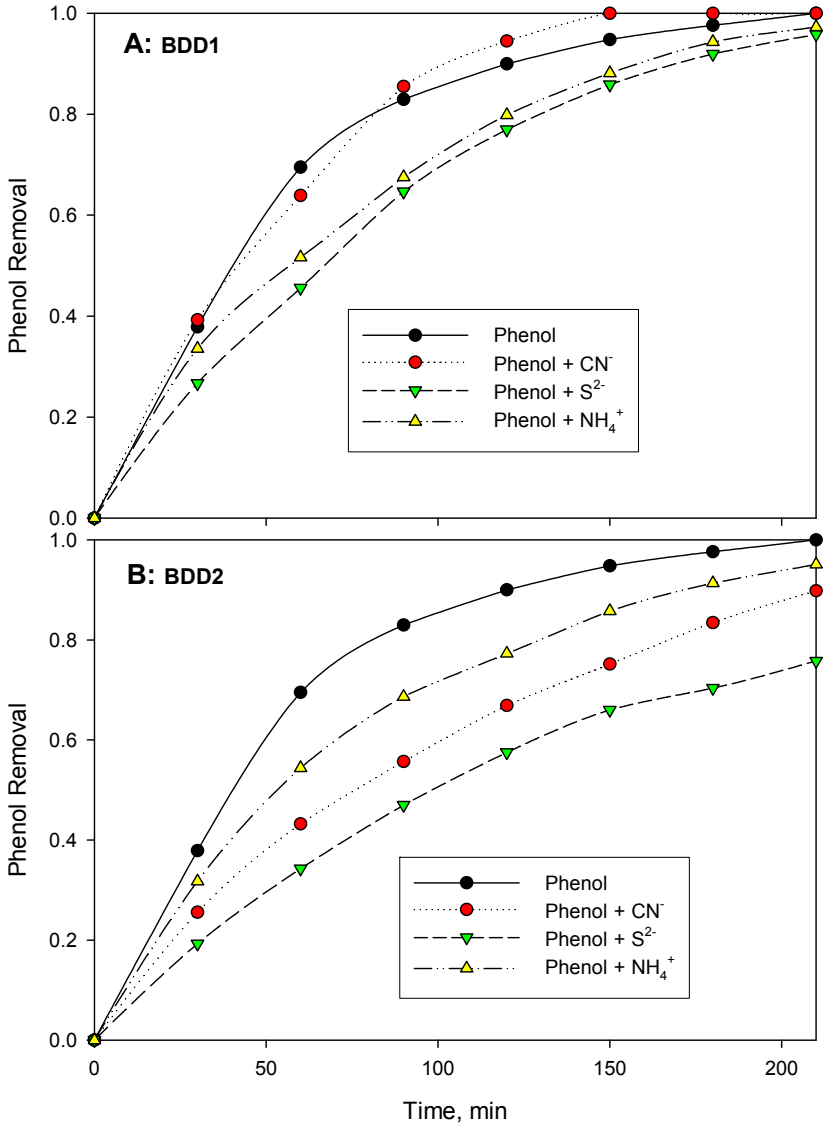

Figure 6.7: Phenol Removal Efficiency in Binary Mix Matrixes

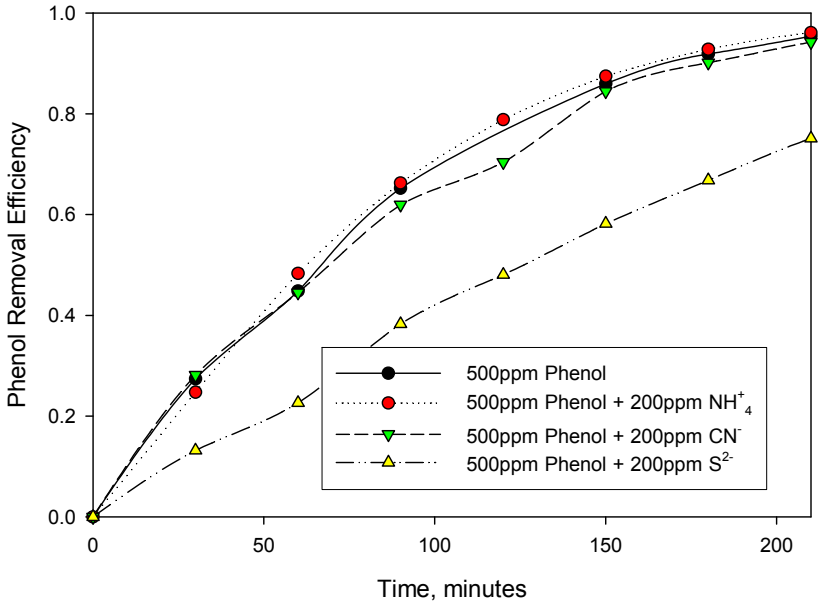

Figure 6.8: Phenol Removal Efficiency in Binary Mix Matrix for 500 ppm Initial Phenol Concentration

in the binary mix matrixes, presence of S^{2-} is likely to have more tendencies toward impairing the removal of phenol compare to the effect of the presence of NH_4^+ or CN^- ions. Moreover, the mechanism of phenol oxidation is not likely to be affect by the initial pH at higher initial phenol concentration even in the presence of the inorganic species.

6.3.2 Phenol Removal Kinetics in Ternary and Quaternary Mix Matrixes

Figures 6.9A and 6.9B depict phenol removal considering the different combinations of the cohabiting inorganic species for BDD1 and BDD2, respectively. Data for BDD1 as depicted in Figure 6.9A reveals that, for most of the different mix matrixes, 100% phenol removal was achieved in less than 180minutes with maximum $t_{1/2}$ of 43.05 minutes. This rendered the phenol removal rates in these cases to mostly surpass that of the single matrix. In clear contrast, for the BDD2, the phenol removal was significantly hampered in all the investigated situations at varying degree (Figure 6.9B). In such cases, the ternary combinations removal efficiencies for final effluent follow the order $(CN^- + S^{2-}) > (CN^- + NH_4^+) >(NH_4^+ + S^{2-})$ i.e., 82.3%, 77.49% and 72% , respectively; whereas the quaternary mix matrix removal was found to be better than all the ternary cases with removal of 87.87%. As a result, these observations were directly reflected in the reduction of the kinetic and the hydrodynamic constants by 50, 54.48, 61.5 and 44.23% with corresponding increase in the $t_{1/2}$ (i.e., 88.86, 97.6, 115.5 and 79.67 minutes, respectively). The various phenol decay profiles, supportively, reveal that the removal trends were kinetically controlled and that the attainment of steady state would be more challenging compared to the binary matrixes.

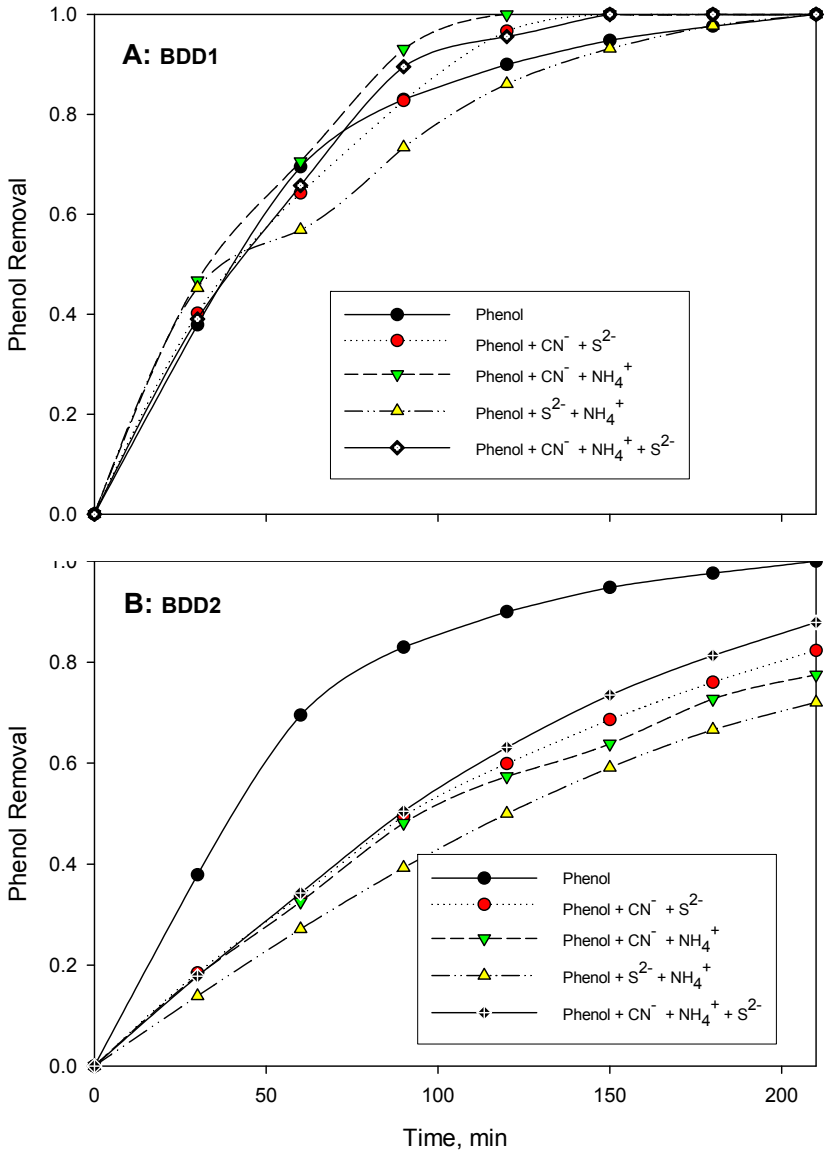

Figure 6.9: Phenol Removal Efficiency in Ternary & Quaternary Mix Matrixes

Inferably, the assumption that the decrease in the phenol removal potentials of the BDD anode during the treatment process was due to competitiveness of the various species in consuming the electro-generated oxidants can be nullified considering the unexpectedly higher removal encountered in some of the mix matrixes (Figure 6.9A). Nonetheless, the decline in the removal rates was mainly attributed to the reduced activity of the BDD2. For the excellent removal associated with BDD1, autocatalytic activities would have been involved due to presence of the inorganic species or oxidation byproducts generated during the treatment process. Otherwise, the reduction in voltage across the cell observed as more species were added led to the increase in solution conductivity which reduced the energy exerted for the BDD activity thereby improving its performance.

6.4 Analysis of TOC Removal Kinetics in Different Mix Matrixes

Similarly, the TOC degradation kinetic parameters (k_{pp}, $t_{1/2}$ and $R^2_{adjusted}$) for the fitted pseudo-first-order models were calculated from the slope of ln(TOC\TOC$_0$) vs time plots. The hydrodynamic parameters (α, $k_{m\ exp}$ and k_{mmodel}) estimated from the corresponding models derived from Equation 6.5 are given in Table 6.2 for BDD1 and BDD2, respectively. The statistical analysis of the models' adequacies showed that all the regression coefficients (R^2) are in good agreement with the $R^2_{adjusted}$. Also, the *p*-values supported the acceptance of the hypothesis that the coefficients are significant parameters in the models. Based on the ability of the semi-empirical models' accuracies in estimating the k_m obtained from the experimental data, the suitability and accuracies of employing TOC data on predicting behaviors of phenol oxidation kinetics and operating regime in presence of the inorganic species was assessed. The details are provided below.

6.4.1 TOC Removal Kinetics in Binary Mix Matrixes

The TOC removal data for the binary matrixes containing phenol and the inorganic ions for BDD1 and BDD2 are provided in Figures 6.10A and 6.10B, respectively. The trends suggest that there exist a significant decline in the TOC decay rate in the presence of the inorganic species for all the different binary combinations. As depicted in Figure 6.10A for BDD1, the TOC removal was significantly reduced and with no single case for any improvement. These results clearly contrasted with the corresponding cases for phenol removals (Figure 6.7A). With decreased in removal from 100% to 87.49, 90.8 and 82.35% in the presence of NH_4^+, CN^- and S^{2-} ,respectively, the corresponding decrease in k_{app} (as well as $k_{m\ exp}$) and increase in $t_{1/2}$ were found in the range of 20-45.7% and 24-84.2%, respectively. These suggest that the presence of the cohabiting inorganic ions have tremendous negative influence on the rate at which phenol can be oxidized. For the case of BDD2 in presence of NH_4^+ (Figure 6.10B), the TOC removal rate was observed to initially improve before eventually declining and finally reaching 86.63% overall removal at the end of the experiment (a value less than that for the single matrix i.e., 100%). In addition, for BDD2 in presence of CN^- and S^{2-}, TOC removals show a similar trend with reduction in removal down to 63.39% and 57.83%, respectively. Larger measured deviations (compared to deviations ascribed to BDD1) of 55.6 – 62.92% and 124-167% were observed for k_{app} and $t_{1/2}$, respectively. Remarkably, in line with the observations for phenol removal, the least TOC removal was also associated with the matrixes containing sulfide ion for both BDD1 and BDD2. These corroborating observations for phenol and TOC removal suggest that, both effective phenol elimination as well as its oxidation are prone to be more negatively affected in the presence of sulfide rather than in the presence of the other two investigated cohabiting inorganic species.

Table 6.2: TOC Removal Kinetic and Hydrodynamic Parameters for (Top) BDD1 and (Bottom) BDD2

Matrix Nature	Component (s)	k_{app} min^{-1}	$t_{1/2}$ minutes	$K_{m\ exp}$ cm/min	$K_{m\ model}$ cm/min	α	$R^2_{adjusted}$	p-Value
Single	Phenol	0.014	49.51	0.35533	0.2921	1.2195	0.9912	<0.0001
Binary	Phenol, NH_4^+	0.0089	77.88	0.22589	0.1862	1.2187	0.9909	<0.0001
	Phenol, CN^-	0.0112	61.89	0.28426	0.2501	1.1409	0.9986	<0.0001
	Phenol , S^{2-}	0.0076	91.20	0.19289	0.1383	1.3941	0.9825	<0.0001
Ternary	Phenol, NH_4^+, S^{2-}	0.0065	106.64	0.16497	0.1125	1.4568	0.9717	<0.0001
	Phenol, NH_4^+,CN^-	0.0161	43.05	0.40863	0.321	1.2251	0.9896	<0.0001
	Phenol, CN^-, S^{2-}	0.0144	48.14	0.36548	0.3341	1.1388	0.9959	<0.0001
Quaternary	Phenol, NH_4, S^{2-}, CN^-	0.0111	62.45	0.28173	0.1988	1.4201	0.9716	<0.0001

Matrix Nature	Component (s)	k_{app} min^{-1}	$t_{1/2}$ minutes	$K_{m\ exp}$ cm/min	$K_{m\ model}$ cm/min	α	$R^2_{adjusted}$	p-Value
Single	Phenol	0.0108	64.18	0.27481	0.2391	1.1966	0.9984	<0.0001
Binary	Phenol, NH_4^+	0.0111	62.45	0.28244	0.323	1.2195	0.8983	0.0006
	Phenol, CN^-	0.0048	144.41	0.12214	0.1242	1	0.9972	<0.0001
	Phenol , S^{2-}	0.004	173.29	0.10178	0.0876	1.1633	0.9961	<0.0001
Ternary	Phenol, NH_4^+, S^{2-}	0.0042	165.04	0.10687	0.0842	1.256	0.984	<0.0001
	Phenol, NH_4^+,CN^-	0.0046	150.68	0.11705	0.0936	1.2426	0.9941	<0.0001
	Phenol, CN^-, S^{2-}	0.0046	150.68	0.11705	0.0938	1.236	0.9959	<0.0001
Quaternary	Phenol, NH_4, S^{2-}, CN^-	0.0047	147.48	0.11959	0.0974	1.2315	0.996	<0.0001

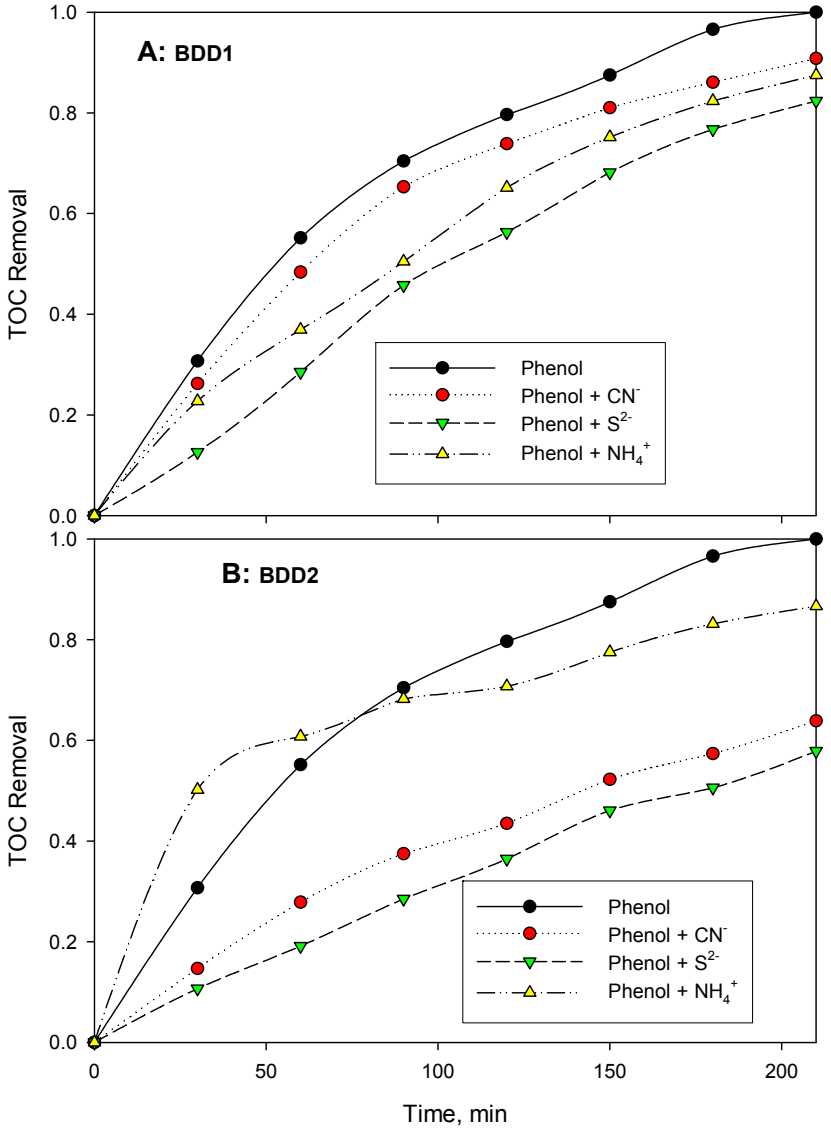

Figure 6.10: TOC Removal Efficiency for Binary Mix Matrixes

By comparing $k_{m\ model}$ and $k_{m\ exp}$ in Table 6.2, the excellent predictions of the k_m values from the modified models that employ TOC data in place of traditional COD data suggest that TOC was a reliable predictor of the operating regime in the binary mix matrixes for both BDD1 and BDD2. As illustrated in Figures 6.11 through 6.13, the models decay trends are in good agreement with the experimental data. The least $R^2_{Adjusted}$ was 0.9997; while all the *p*-values are in outright support of the acceptance alternate hypothesis. For that, the estimated values of α which are all greater than unity suggests that the applied current was in the range greater than the limiting current above which the operating becomes under mass transport controlled. The estimated ACEs values of 44.34-58.75% and 29.53-33.99% for BDD1 and BDD2, respectively, support the models' predictions that the mass transport of phenol towards BDD anode surface was the rate-limiting step to the kinetics of the phenol oxidation in the binary mix matrixes.

6.4.2 TOC Removal Kinetics in Ternary and Quaternary Mix Matrixes

TOC removal results obtained for higher mix matrixes revealed that presence of the inorganic species in the different mix matrixes was prone to impair the organic carbon content removal efficiency, particularly for BDD2. Figure 6.14B demonstrates comparable drops in the TOC removal trends for the various mix matrixes as they show no significant differences with regard to the respective maximum removal efficiencies which was reduced from 100% to within 61.3 to 63%. It appears that much longer time was required to ensure equilibrium of total conversion of all the initial carbon content to CO_2 was achieved. On the other hand, for BDD1, significant drop in the TOC removal was observed to be mainly associated with the ternary combination of phenol with S^{2-} and NH_4^+ (78.16%); the mix matrix that persistently revealed the highest drops in

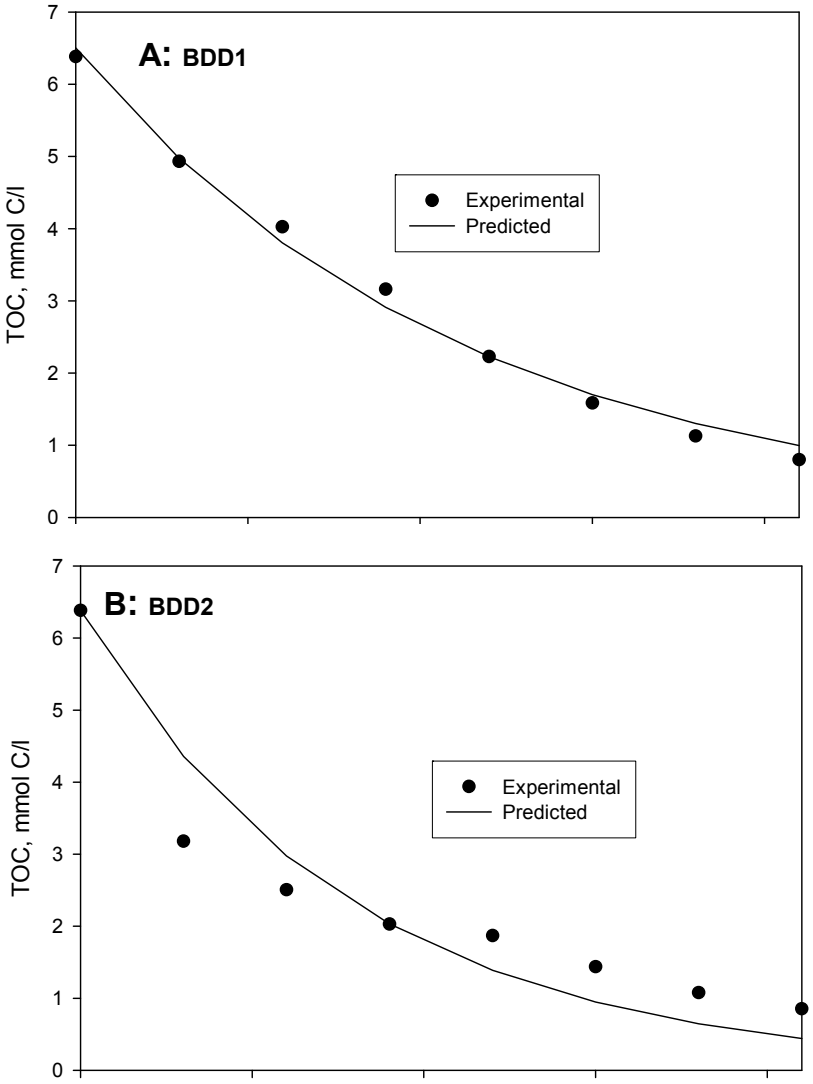

Figure 6.11: Experimental vs Model's Prediction for TOC Evolution during Phenol Oxidation on BDD anode in Presence of NH_4^+

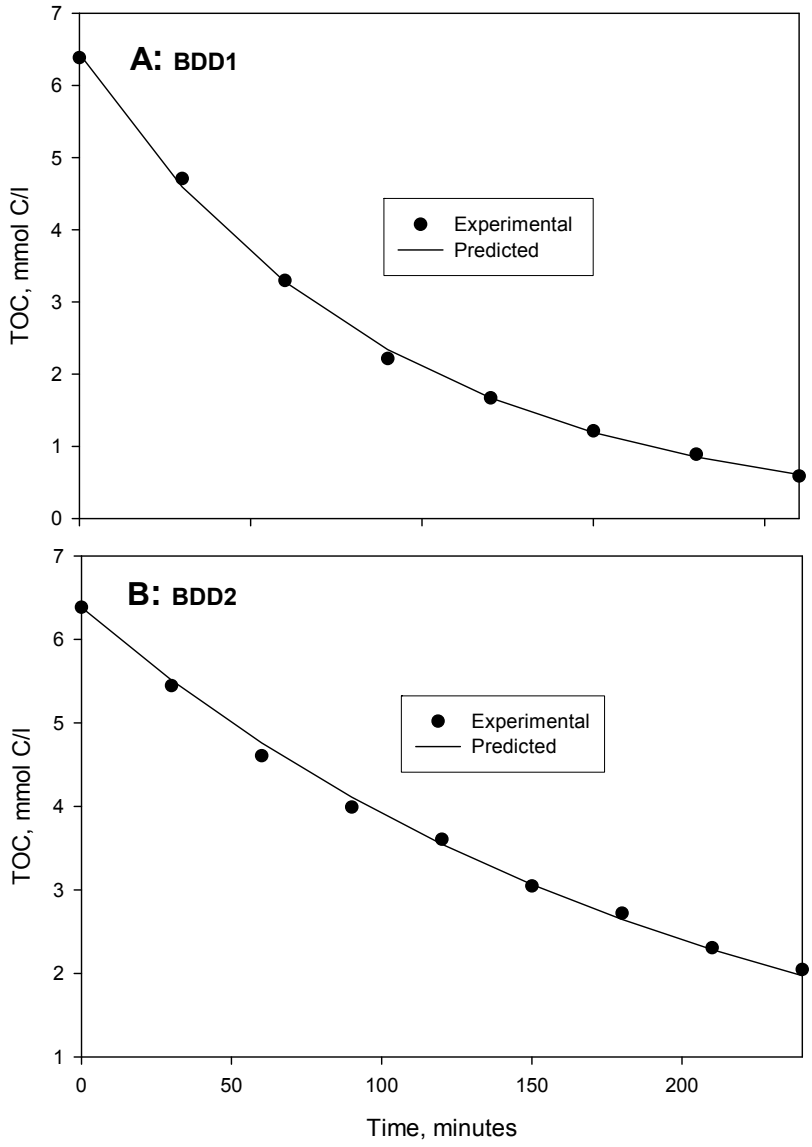

Figure 6.12: Experimental vs Model's Prediction for TOC Evolution during Phenol Oxidation on BDD anode in Presence of CN^-

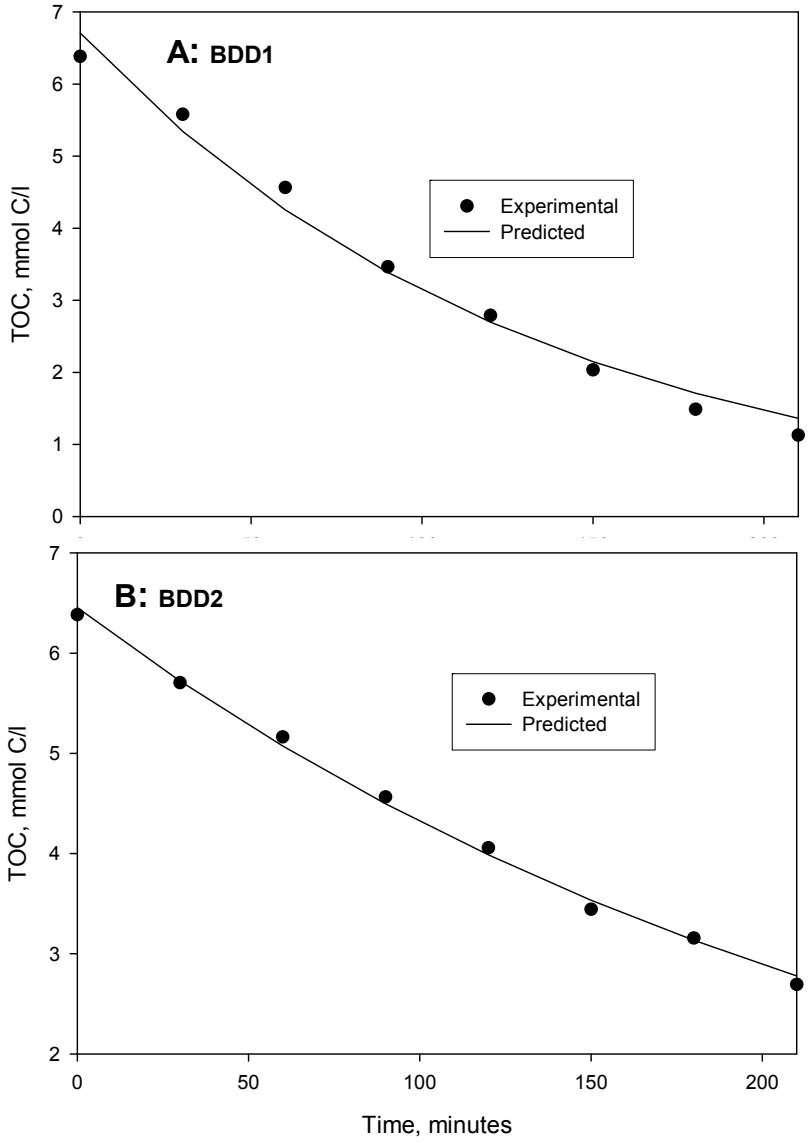

Figure 6.13: Experimental vs Model's Prediction for TOC Evolution during Phenol Oxidation on BDD anode in Presence of S^{2-}

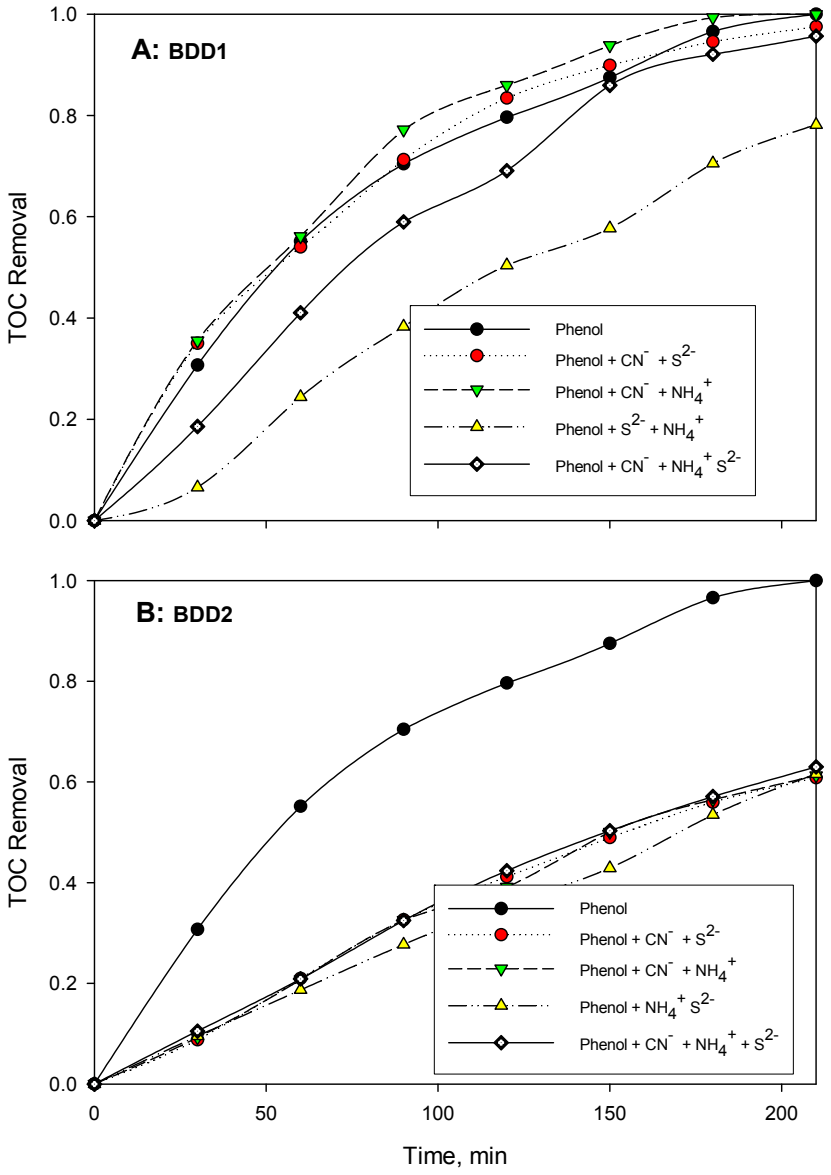

Figure 6.14: TOC Removal Efficiencies for Ternary and Quaternary Mix Matrixes

the TOC removal for both BDD1 and BDD2 (as in the case for phenol removal as given in Figure 6.9). However, good removal was obtained in the ternary cases of CN^--S^{2-} and CN^--NH_4^+ and the quaternary matrix that nearly reached steady state with overall removals of 97.53, 100 and 95.67%, respectively. As result, these are reflected in the change in kinetic and hydrodynamic parameters for BDD1 that showed improvements in k_{app} (as well as $k_{m\ exp}$) and decrease in $t_{1/2}$ values for phenol-CN^--NH_4^+ and phenol-CN^--S^{2-} while vice versa for phenol-NH_4^+-S^{2-} and phenol- CN^--NH_4-S^{2-} (Table 6.2). However, for BDD2, substantial deterioration in the TOC removal is evident in the drastic drops in the kinetic and hydrodynamic parameters by 57.5 to 61% and increase in the $t_{1/2}$ values by 134-157%. The obvious discrepancies visible by comparing the results for the binary and higher mix matrixes clearly suggest that the decline in BDD anode activity was the main factor that can retard effective phenol oxidation under present study. Moreover, this negative effect is likely to be more pronounced in the cases of the higher mix matrixes.

The remarkable agreements that also exist between values of $k_{m\ model}$ and $k_{m\ expt}$ (Table 6.2), indicate the excellent predictions of the k_m from the modified models for the ternary and quaternary mix matrixes that employed TOC data instead of COD data. These further suggest that using TOC as a substitute for COD can be adequately extended beyond binary matrixes to cater as well for the higher mix matrixes for better understanding kinetics of organic pollutant oxidation using BDD anode in the presence of inorganic ions. This is evident in the comparative trends depicted in Figures 6.15 to 6.18 which clearly reveal the good agreements of the models' decay patterns with that of the experimental data with corresponding $R^2_{Adjusted}$ mainly in the range of 0.99 while all the *p*-values are also in outright support of the acceptance alternate

hypothesis. For that, the estimated values of α (all > 1) led to the conclusion that the applied current was in the range greater than the limiting current. Hence, the treatment processes for the various higher mix matrixes were also under mass transport controlled. Supportively, all the respective ACEs were well below 100% ranging between 44.34-58.78% and 58.88-79.26% for the binary and higher mix matrixes, respectively.

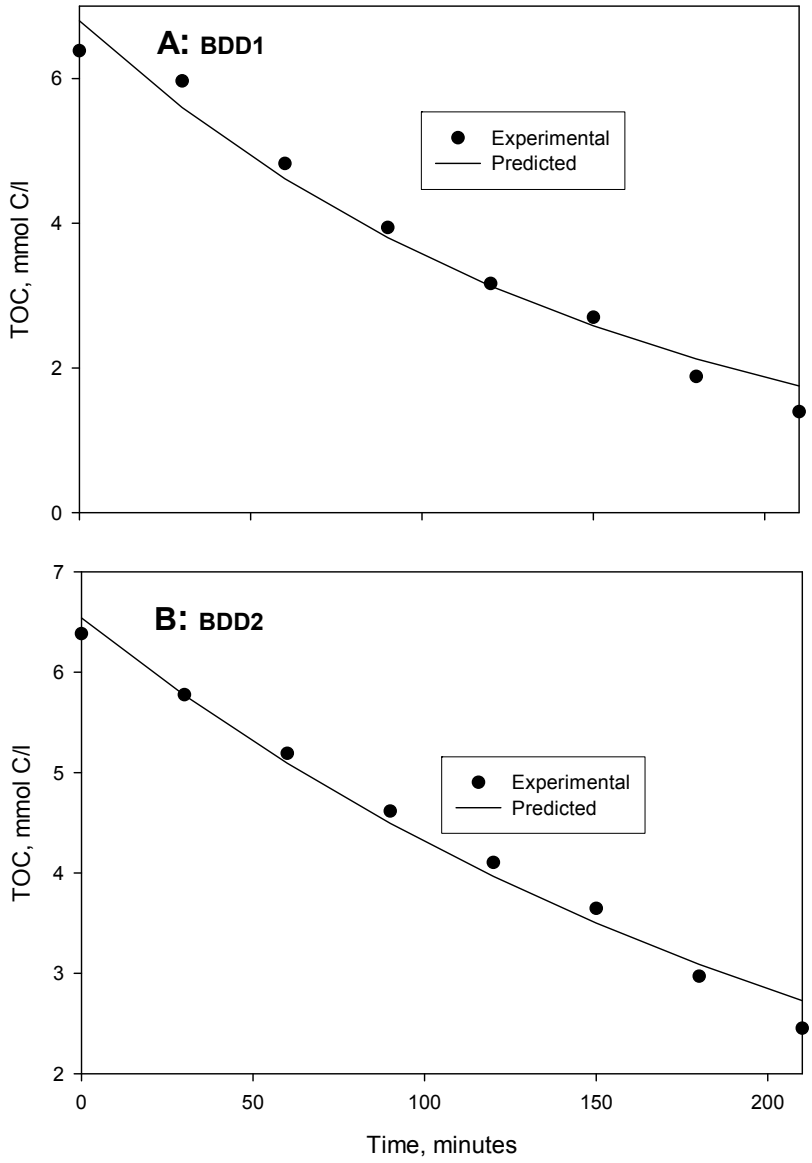

Figure 6.15: Experimental vs Model's Prediction for TOC Evolution during Phenol Oxidation on BDD anode in Presence of NH_4^+ and S^{2-}

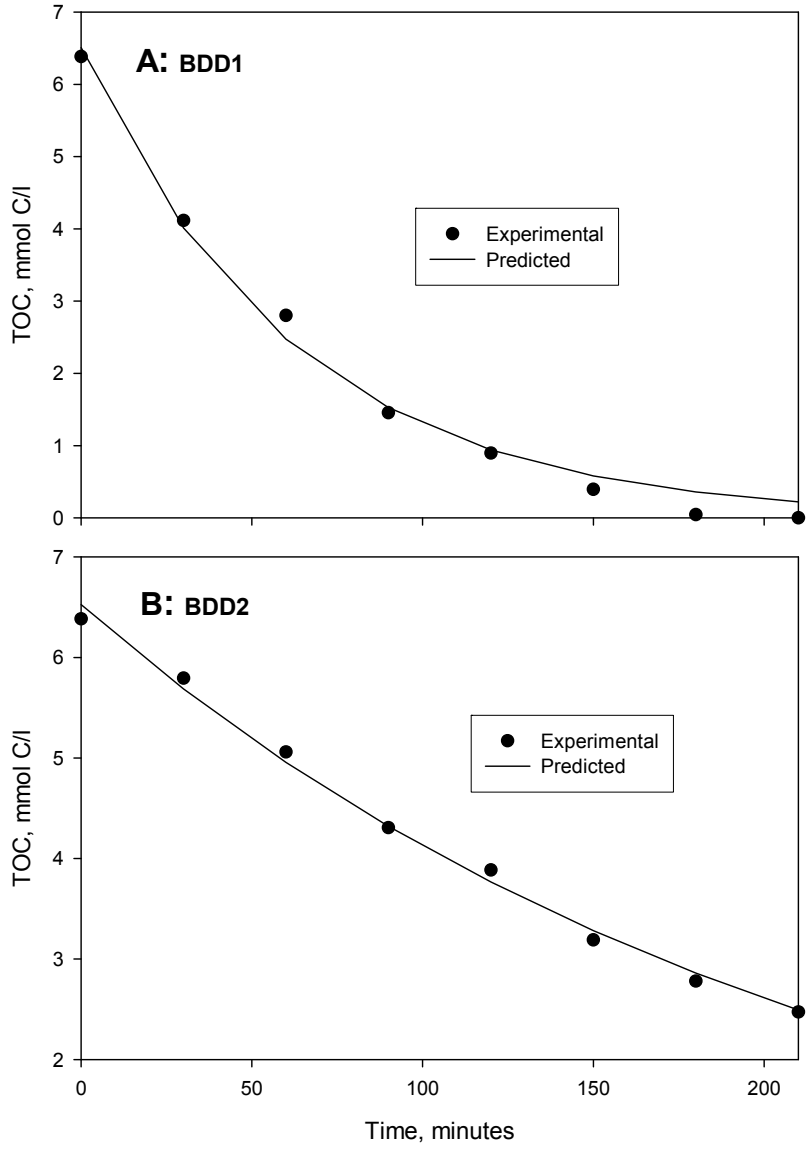

Figure 6.16: Experimental vs Model's Prediction for TOC Evolution during Phenol Oxidation on BDD anode in Presence of NH_4^+ and CN^-

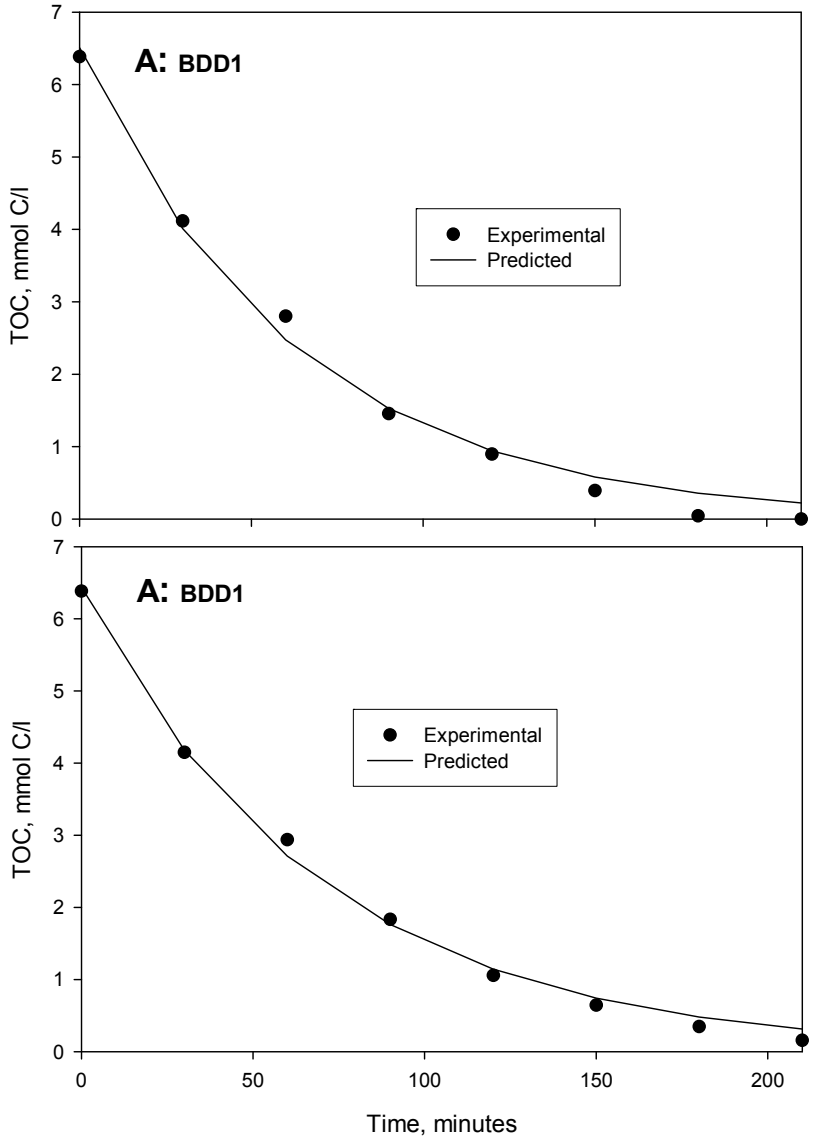

Figure 6.17: Experimental vs Model's Prediction for TOC Evolution during Phenol Oxidation on BDD anode in Presence of CN^- and S^{2-}

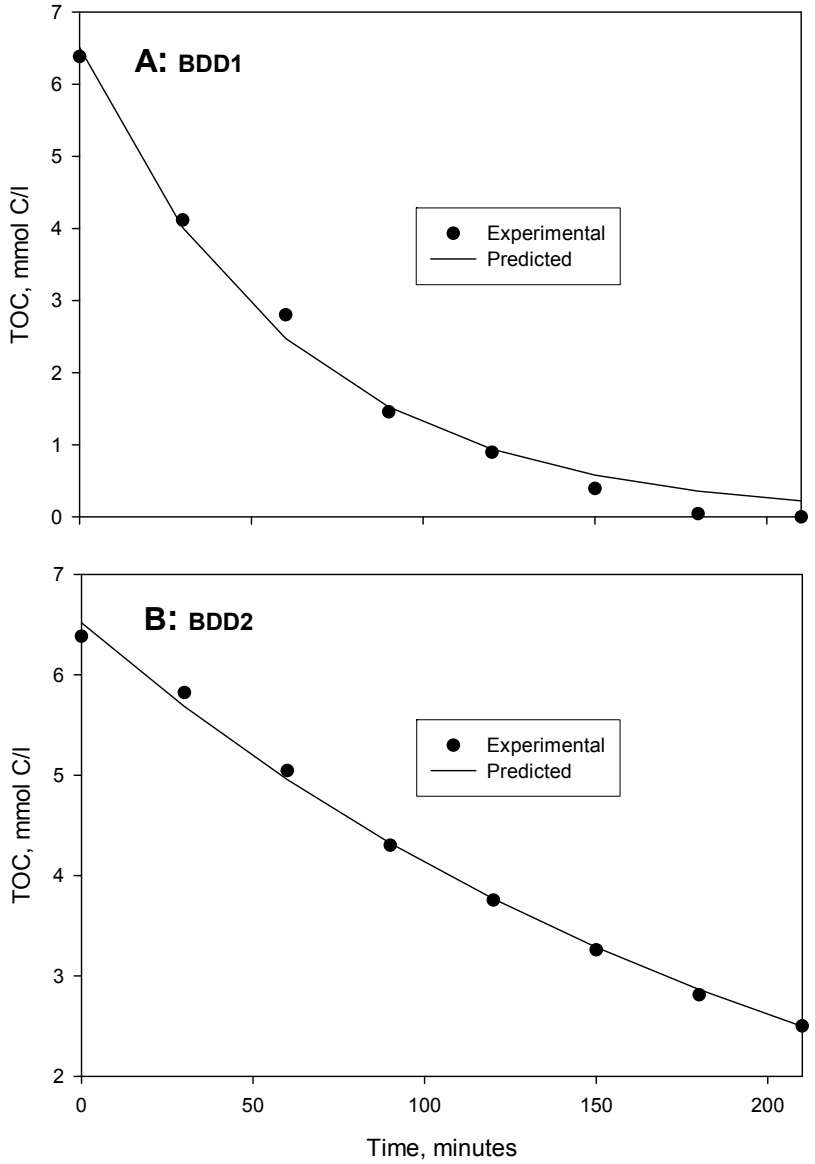

Figure 6.18: Experimental vs Model's Prediction for TOC Evolution during Phenol Oxidation on BDD anode in Presence of NH_4^+, CN^- and S^{2-}

6.5 Analysis of COD Removal Kinetics in Different Mix Matrixes

6.5.1 COD Removal Kinetics in Binary Mix Matrixes

In contrary to TOC of aqueous solutions, one of the major consequences of the presence of NH_4^+, CN^- and S^{2-} is the drastic increase in initial COD (COD_0) according to the added species in solution (see APPENDIX A). This is due to the fact that such inorganic species in aqueous systems exert oxygen demand thereby rendering them environmental quality parameters of great concerns. The theoretical COD equivalents per molar of these species in aqueous solutions are 3.55, 1-2.9 and 2, respectively. These values were found to be in good agreement (to considerable extent) with the respective measured COD at time zero for the different mix matrixes. Generally, slight discrepancies were observed to exist between the declines in relative decay profiles for the various mix matrixes. As provided in Figure 6.19, the trends, essentially, were not influenced by the condition of the BDD anode (i.e., BDD1 or BDD2) used as well as the nature of cohabiting specie in solution. In addition, lower COD removals were obtained in the presence of inorganic species compared to their respective TOC counterparts (whose initial values were not influenced by the presence of the inorganic species). Significant drop in COD removal efficiency was observed in all the different scenarios with the efficiency increasing with decrease in COD_0; though the total amount of COD removed increases with increase in the COD_0.

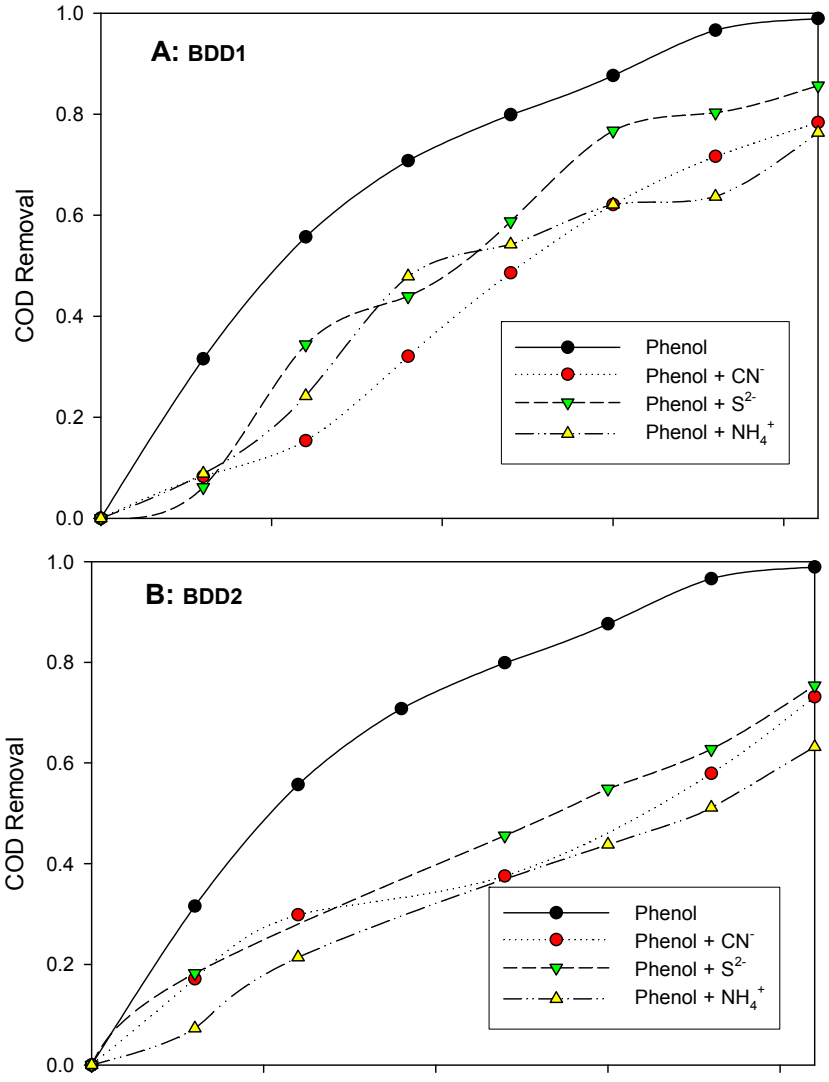

Figure 6.19: COD Removal Efficiency in Binary Mix Matrixes

Considering the results for BDD2 displayed in Figure 6.19B, for the case of binary matrix with NH_4^+ -which has the highest measured COD_0 (i.e., 638.5 ppm) - the maximum removal was 63.32%, while for CN^- and S^{2-}, the removal dropped to 73.12% and 75.32% (from 98.92% for the single matrix), respectively. Hence, these values were better than that of phenol-NH_4^+ matrix due to the lower COD_0 estimated as 573 ppm and 483 ppm for the other two binary cases, respectively. This observation underscores the fact that, better removal of COD is achievable at higher $COD_{0;}$ a fact further buttressed by considering the result for BDD1 display in Figure 6.19A. This figure further substantiates clearly that, the total amount of COD removal was directly proportionally to the initial COD. With COD_0 of 818, 638, and 949 ppm, the COD removal efficiencies were 78.36, 85.66 and 76.32% in the presence of CN^-, S^{2-} and NH_4^+, respectively.

The corresponding changes in kinetic and hydrodynamic parameters for both BDD1 and BDD2 show that presence of the inorganic species considerably influenced the efficiency of the overall decontamination process. Based on the kinetic information provided in Table 6.3, with the exceptions phenol-S^{2-} for BDD1, the decrease in the k_{app} (as well as $k_{m\ exp}$) and increase in the $t_{1/2}$ values for the other mix matrixes are very obvious. The low decline in the k_{app} and the $k_{m\ exp}$ values compared to those obtained for TOC were due to higher amount of removal associated with COD that increases with the COD_0. Figures 6.20, 6.21 and 6.22 clearly reveal good agreements of the COD models' decay patterns with the experimental data with statistically acceptable $R^2_{Adjusted}$ and *p*-values. On the contrary, the wide differences existing between $k_{m\ model}$ and $k_{m\ expt}$ estimates (Table 6.3) indicate that the prediction of the k_m from the actual COD temporal models were not satisfactory for the binary mix matrixes. These observations may

Table 6.3:COD Removal Kinetic and Hydrodynamic Parameters for (Top) BDD1 and (Bottom) BDD2

Matrix Nature	Component (s)	k_{app} min^{-1}	$t_{1/2}$ minutes	$K_{m\ exp}$ cm/min	$K_{m\ model}$ cm/min	α	$R^2_{adjusted}$	p-Value
Single	Phenol	0.0141	49.16	0.35787	0.2596	1.1959	0.9933	<0.0001
Binary	Phenol, NH_4^+	0.0093	74.53	0.23604	0.2975	1	0.8557	0.0013
	Phenol, CN^-	0.0077	90.02	0.19543	0.1172	1.6711	0.8771	0.0012
	Phenol , S^{2-}	0.0146	47.48	0.37056	0.2984	1	0.9538	0.0001
Ternary	Phenol, NH_4^+, S^{2-}	0.0132	52.51	0.33503	0.2357	1	0.9869	<0.0001
	Phenol, NH_4^+,CN^-	0.0113	61.34	0.2868	0.2383	1.249	0.9916	<0.0001
	Phenol, CN^-, S^{2-}	0.0117	59.24	0.29695	0.3247	1	0.943	0.0001
Quaternary	Phenol, NH_4, S^{2-}, CN^-	0.0127	54.58	0.32234	0.281	1.1461	0.9739	<0.0001

Matrix Nature	Component (s)	k_{app} min^{-1}	$t_{1/2}$ minutes	$K_{m\ exp}$ cm/min	$K_{m\ model}$ cm/min	α	$R^2_{adjusted}$	p-Value
Single	Phenol	0.01051	65.95	0.26743	0.2996	1.1959	0.9933	<0.0001
Binary	Phenol, NH_4^+	0.0094	73.74	0.23919	0.344	1	0.9728	0.0007
	Phenol, CN^-	0.0057	121.60	0.14504	0.266	1.1488	0.9609	0.0007
	Phenol , S^{2-}	0.0047	147.48	0.11959	0.2864	1	0.7552	0.0204
Ternary	Phenol, NH_4^+, S^{2-}	0.007	99.02	0.17812	0.301	1	0.9256	0.0003
	Phenol, NH_4^+,CN^-	0.0147	47.15	0.37405	0.262	1.4116	0.9469	0.0006
	Phenol, CN^-, S^{2-}	0.0058	119.51	0.14758	0.2568	1	0.8549	0.0244
Quaternary	Phenol, NH_4, S^{2-}, CN^-	0.0052	133.30	0.13232	0.3383	1	0.9727	0.0002

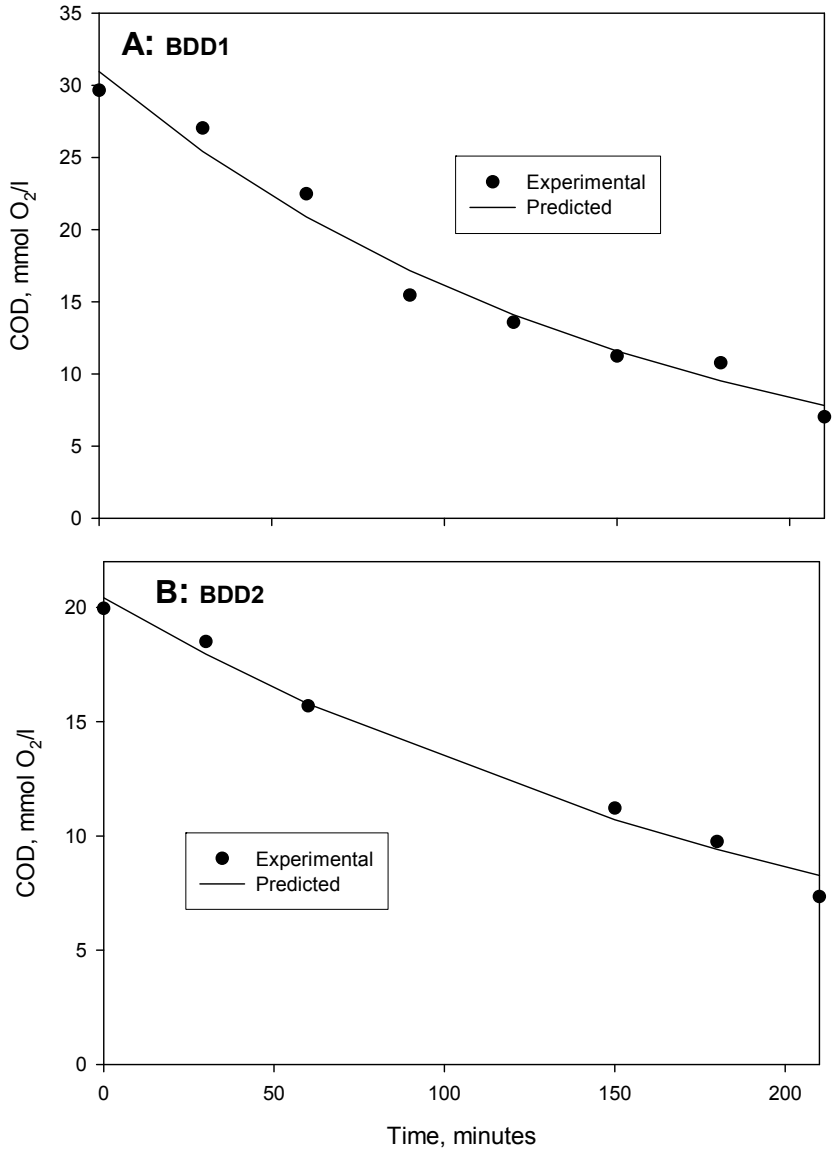

Figure 6.20: Experimental vs Model's Prediction for COD Evolution during Phenol Oxidation on BDD anode in Presence of NH_4^+

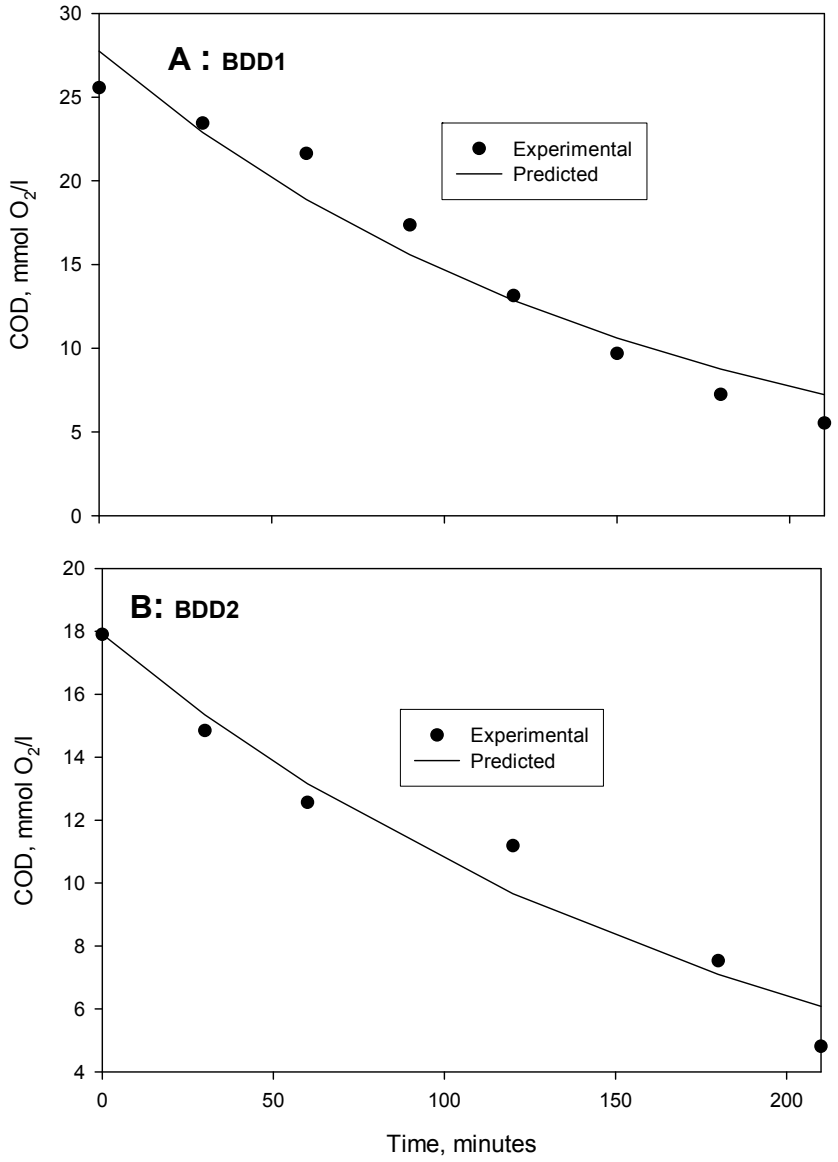

Figure 6.21: Experimental vs Model's Prediction for COD Evolution during Phenol Oxidation on BDD anode in Presence of CN^-

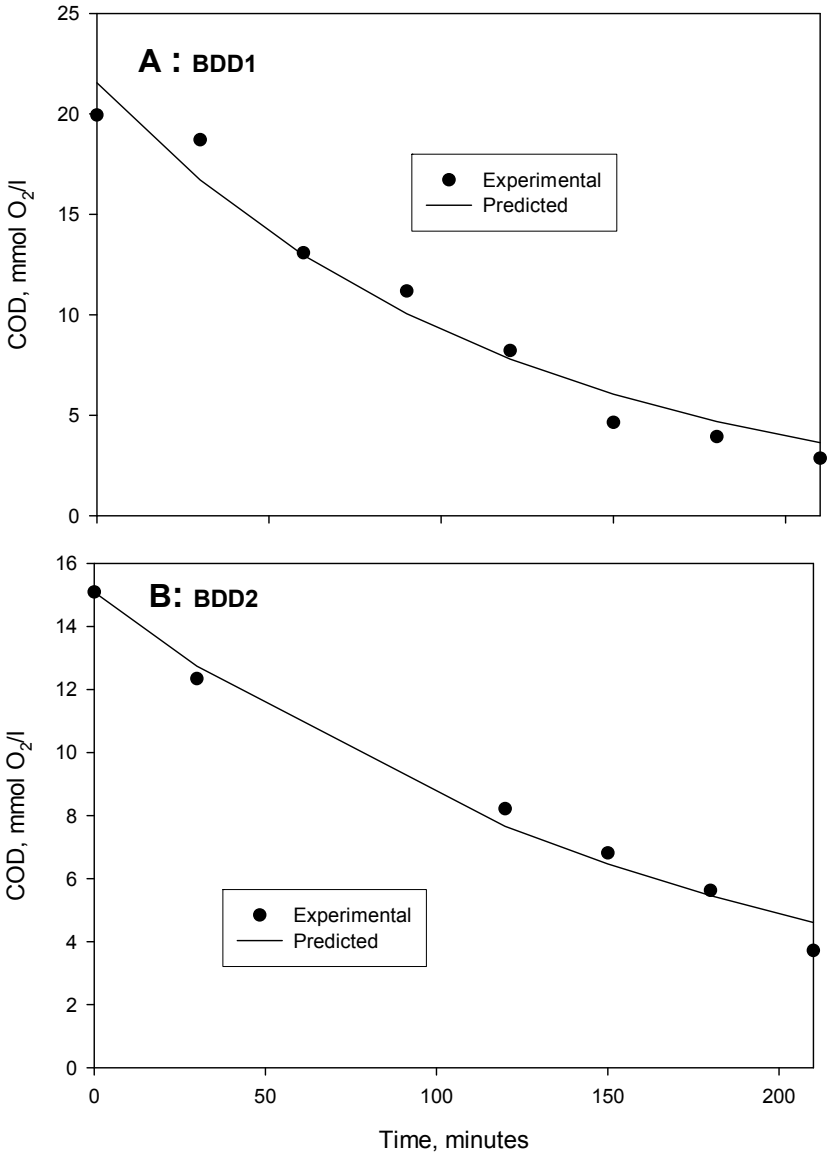

Figure 6.22: Experimental vs Model's Prediction for COD Evolution during Phenol Oxidation on BDD anode in Presence of S^{2-}

suggest that the α values estimated from COD data are not liable to be reliable predictors of the kinetics of phenol oxidation (as well as operating regime) once inorganic species are present in the simulated phenolic wastewaters. In apparent support of this conclusion, it can be observed that most of the estimated α values are equal to unity; suggesting that the applied current density was exactly or approximately equal to the limiting current density. Considering Equation 2.11, the incorrectness of this idea suggested by some of the COD models' was quite clear due to the fact the limiting current density is directly proportional to COD_0 as well as the number of exchangeable electrons (*n*) for oxidation of all oxidizable components. As such, the i_{lim} in the presence of the inorganic was expected to increase rather than to decrease. However, it can be seen from the results provided by the COD model's predictions that reduction in i_{lim} was the predominant case. Thus, it becomes apparent that for the binary mix matrixes TOC data appeared to be a better parameter for kinetic modeling of electrochemical oxidation of phenol. This is due to the fact that, in such cases, the data presented here suggest that the more global oxidation indicator parameter (i.e., COD) is not likely to provide accurate or acceptable judgments.

6.5.2 COD Removal Kinetics in Ternary and Quaternary Mix Matrixes

Similarly, for all the cases of ternary and quaternary mix matrixes, there exist tremendous drops in COD removals which were more pronounced for BDD2 (Figure 6.23B). In addition, the COD removal efficiency decreases with increase in COD_0 while the total amount of COD removed increases with increase in COD_0 similar to previous observations with the binary mix matrixes. The least drop in COD removal (i.e., from 98.92% to 54.37%) was observed with the ternary combination of phenol with S^2 and CN^- while the percent removals for the remaining matrixes (Phenol-NH_4^+-CN^-, Phenol-NH_4^+-S^{2-} and Phenol-CN^--NH_4^+-S^{2-}) were 51.22, 52.40 and 48.25%,

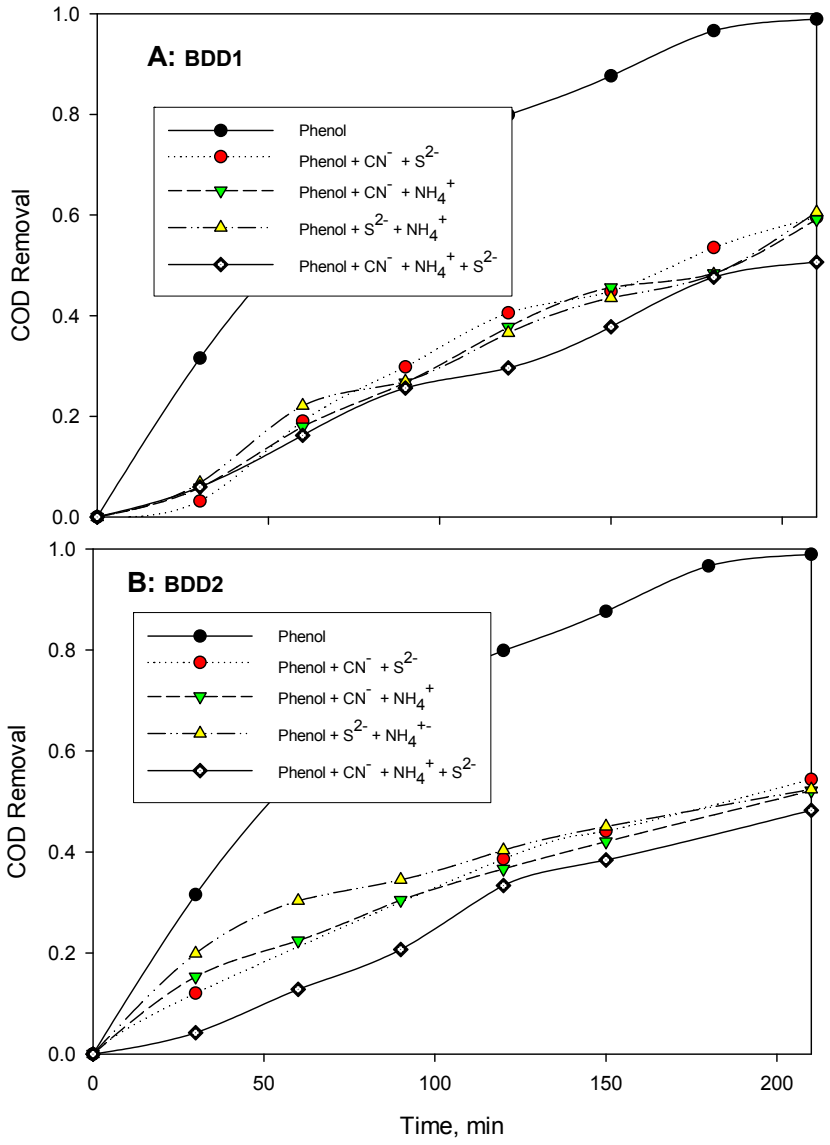

Figure 6.23: COD Removal Efficiencies in Ternary and Quaternary Mix Matrixes

respectively. However, the corresponding removals for all BDD1 cases (Figure 6.23A), the estimated COD removals were much better. For the ternary combinations they were in range of 59.52.-60.56% though these values are much lower than 98.92% obtained for the single matrix. For the quaternary matrix, the decrease in the removal was below 50.65%. It is noteworthy to point out that the presence of the inorganic species have drastically increase the time required to attain equilibrium of 100% COD removal; thereby rendering it difficult to meet the COD target discharge limit (120 ppm), particularly, for the ternary and quaternary mix matrixes. The observations for both binary and higher mix matrixes can hint at possible negative synergies on phenol oxidation due to the inorganic species presence which are yet to be neither quantifiable nor fully comprehensible. Also they imply that within the framework of the designed retention times, complete simultaneous electro-oxidation of both phenol and the inorganic species didn't occur. Hence, based on the COD data presented, it can be understood that, the inability of the effective oxidation of all species in solution to occur was at the expense of conversions of the species to other unaccounted byproducts (that exert lesser oxygen demands).

As a result of the increase in the species in solution in the ternary and quaternary mix levels, the change in kinetic and hydrodynamic parameters for BDD1, respectively, showed 6.38-19.86% and 6.84-24.20% decline in k_{app} (as well as $k_{m\ exp}$) and increase in $t_{1/2}$. Predictably, for BDD2, higher decline were approximated at 33.4-50.5% and 50-102.2%, respectively. Similarly, the obvious discrepancies visible by comparing the results for the BDD1 and BDD2 reiterated the fact that, decline in the BDD anode activity was one of the key factor that impaired effective phenol oxidation which was inclined to be more pronounced in the cases of the higher mix matrixes. The wider deviations predominantly existing between $k_{m\ model}$ and $k_{m\ expt}$ (Table 6.3)

and observing that most of estimated α values were equal to unity for the higher mix matrixes apparently further support the inappropriateness of using COD data for the kinetic modeling of phenol oxidation (as also suggested by the kinetic data of the binary mix matrixes). Similarly, this was the case despite good agreements of existing between the COD models' decay patterns and the experimental data with statistically acceptable $R^2_{Adjusted}$ and *p*-values which demonstrate good predictions as depicted in Figures 6.24 to 6.27. As result of that, this observation which is common with the majority of the different mix matrixes is tangible justification and basis for reaching a generalized conclusion of inaccuracy of estimating α for phenol oxidation directly from the COD data. Therefore, irrespective of nature of the mix matrixes, analysis presented here suggest that TOC is more appropriate for kinetic modeling of electrochemical oxidation of phenol in the presence of the inorganic species as COD is liable to providing erroneous predictions.

The percent decrease in phenol, TOC and COD removals as discussed previously are illustrated in Figure 6.28 which comparatively summarizes the decline in efficiency of phenol oxidation as well as the overall decontamination efficiency for the different mix matrixes.

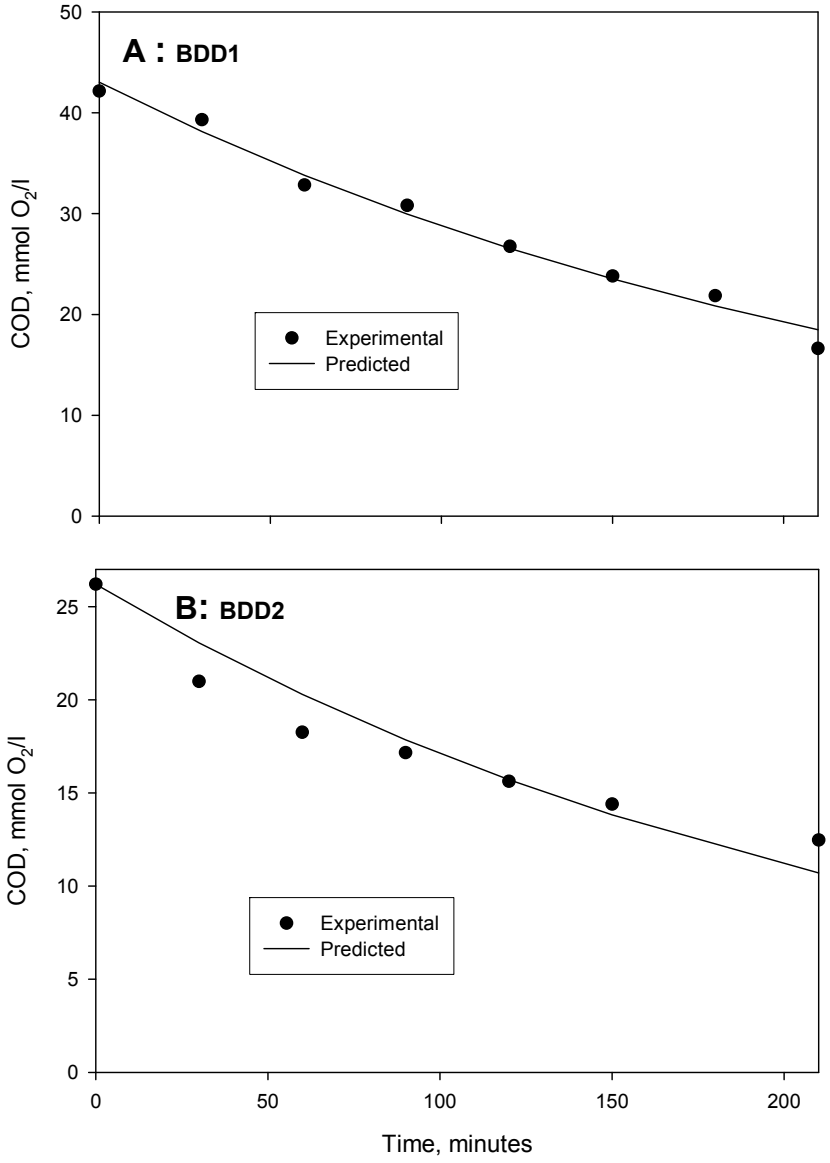

Figure 6.24: Experimental vs Model's Prediction for TOC Evolution during Phenol Oxidation on BDD anode in Presence of NH_4^+ and S^2

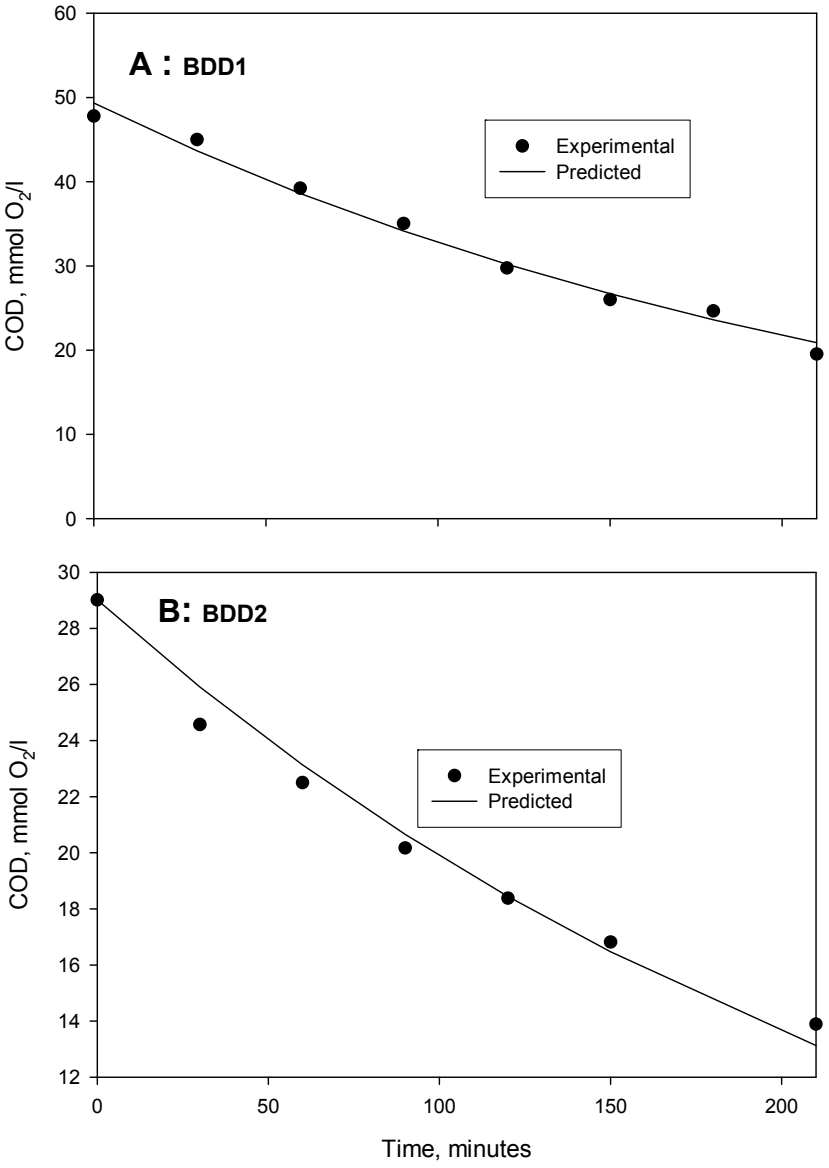

Figure 6.25: Experimental vs Model's Prediction for TOC Evolution during Phenol Oxidation on BDD anode in Presence of NH_4^+ and CN^-

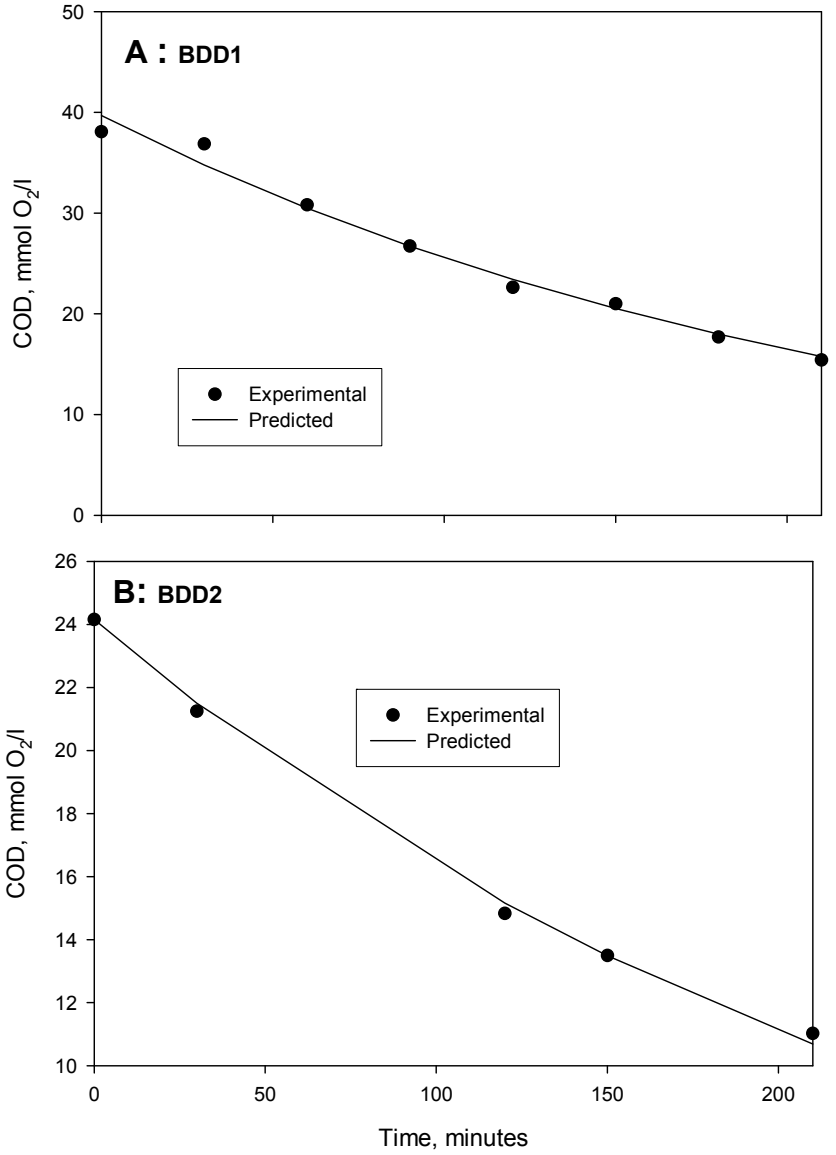

Figure 6.26: Experimental vs Model's Prediction for TOC Evolution during Phenol Oxidation on BDD anode in Presence of CN^- and S^{2-}

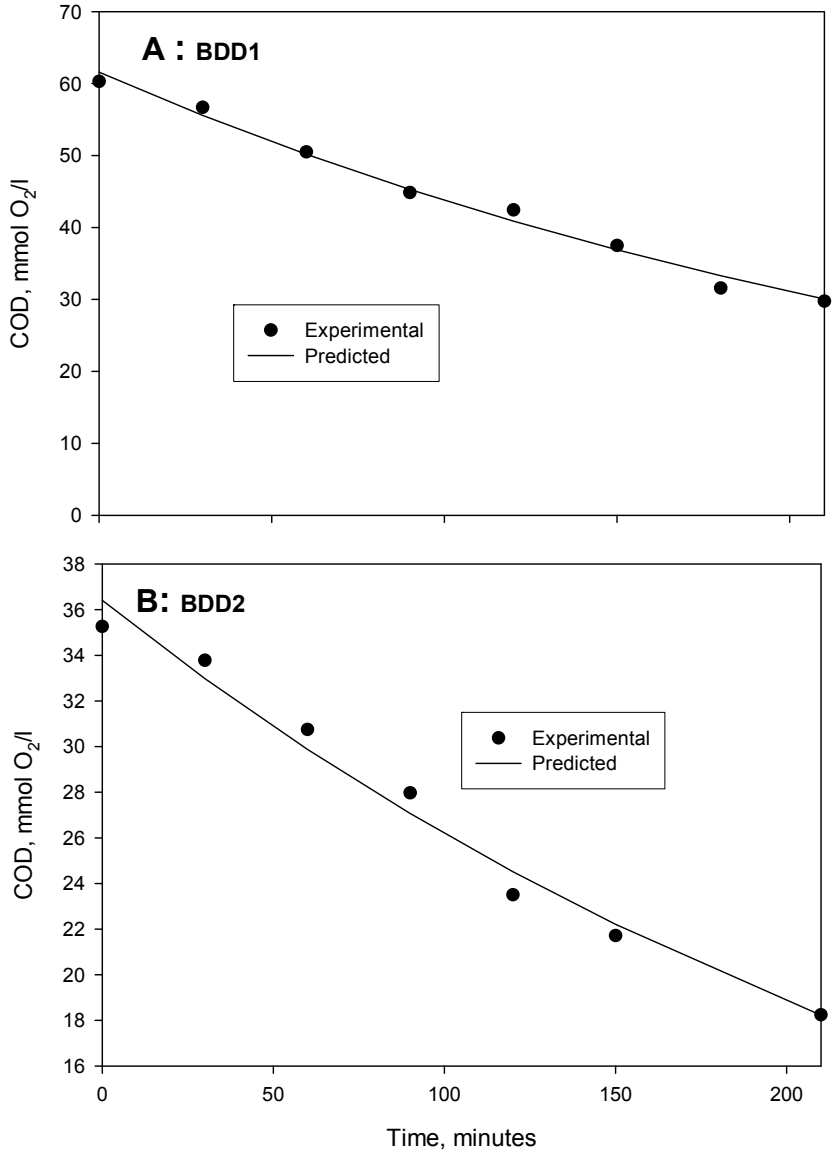

Figure 6.27: Experimental vs Model's Prediction for TOC Evolution during Phenol Oxidation on BDD anode in Presence of NH_4^+, CN^- and S^{2-}

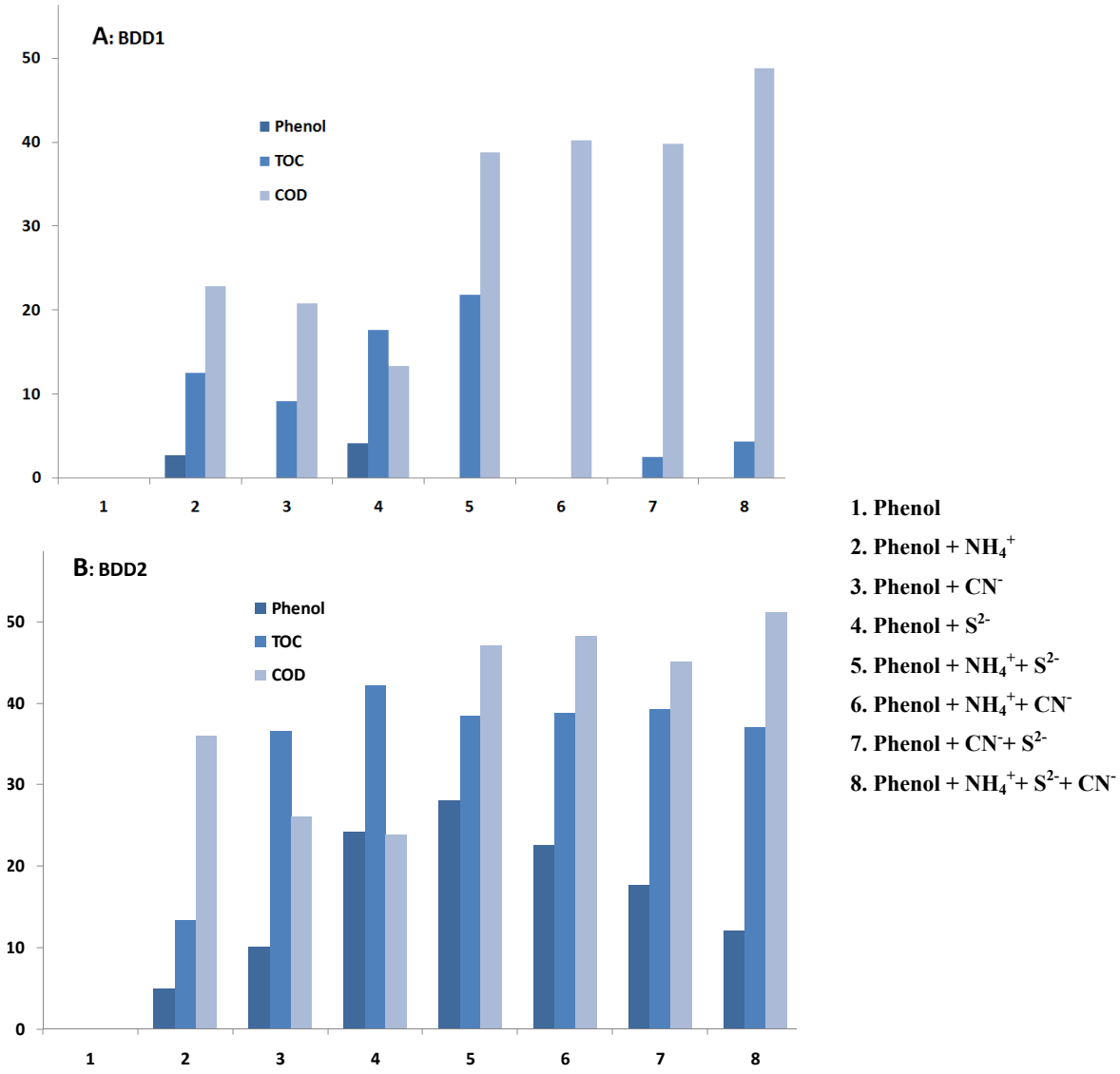

Figure 6.28: Summary of Percent Decrease in Phenol, TOC and COD Removal in Different Mix Matrixes

6.6 Mechanism of Phenol Oxidation in Different Mix Matrixes

This section evaluates the mechanism of electrochemical oxidation of phenol in presence of NH_4^+, CN^- and S^{2-} in the different mix matrixes. The amount of phenol removed vis-à-vis the decay in corresponding TOC and COD values and the percent compositions of byproducts generated that jointly provide yardstick for assessing the efficacy of the process are presented. For operating at the optimum condition in the absence of the inorganic species, the various profiles for phenol oxidation are depicted in Figure 6.29. It can be deduced from such plots that complete mineralization of phenol was achieved as residual phenol and TOC were both zero, while COD removal was around 99% (Figure 6.29A). Also, the byproduct compositions plots show that the aromatic intermediates evolved as the pioneer oxidation byproducts were converted to higher intermediates prior to gradual and eventual conversion to CO_2 (Figure 6.29B). Steady state was achieved at the end of the 3.5 hours electrolysis time as the percent composition of byproducts (Figure 6.29C) clearly indicate that both phenol and the byproducts generated were completely oxidized to CO_2

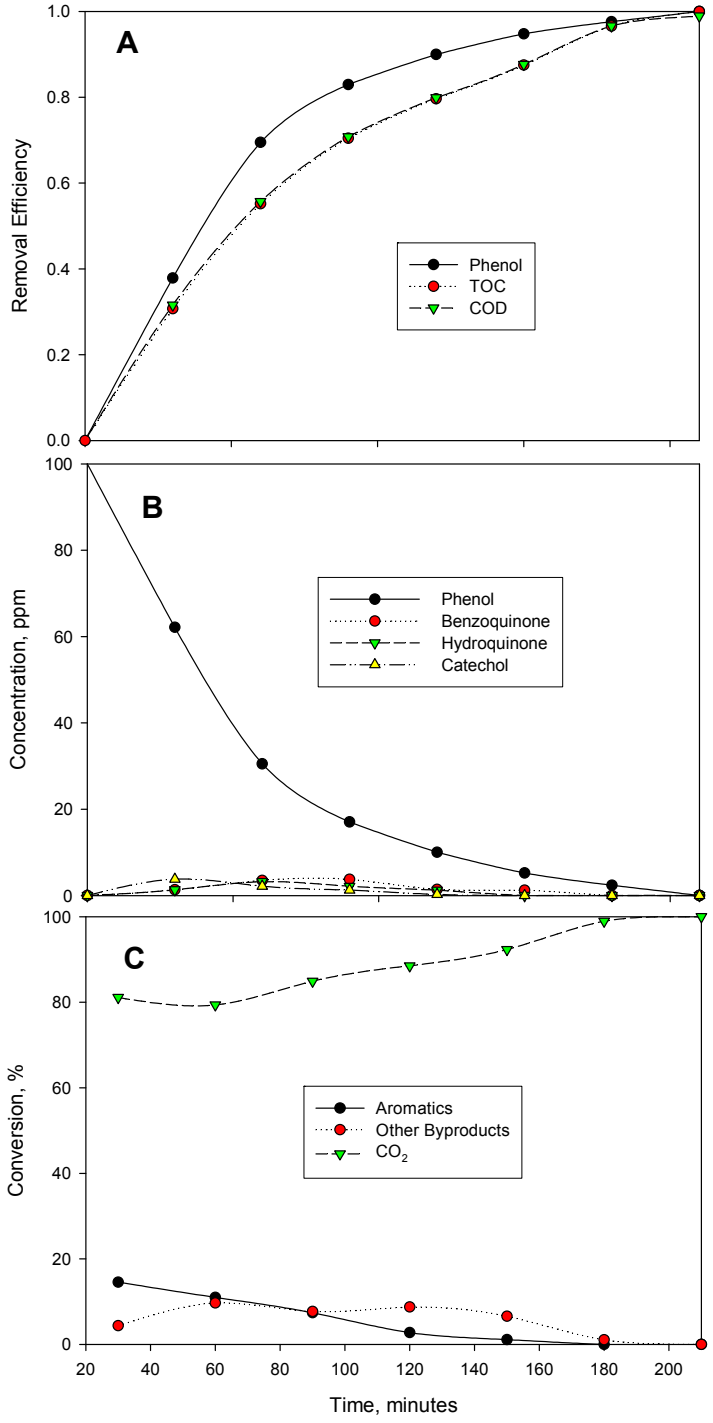

Figure 6.29: Profiles for Oxidation of Phenol in Single Matrix at Optimum Condition

6.6.1 Phenol Oxidation Byproducts in Binary Mix Matrixes

Figures 6.30 to 6.35, elaborately, display the different relevant profiles during oxidation of phenol in the presence of CN^-, S^{2-} and NH_4^+, each for BDD1 and BDD2, respectively. Each of these figures also comprises of three distinct plots designated as A, B and C for removals trends (of phenol, TOC and COD), concentration profiles (of phenol and aromatic byproducts) and percent composition of generated byproducts, respectively. It can be observed that all the three binary mix cases suggest that a common oxidation pattern for the two conditions of the BDD anode. For BDD2, Figures 6.31, 6.33 and 6.35, corroborate the idea that phenol was mainly converted to CO_2 via production of the measured aromatic compounds as the major intermediate byproducts. Moreover, equilibrium was yet to be attained as removal of phenol was partial (i.e., 75.79 - 95.01%), complete oxidation of the generated aromatic byproducts was unattainable and the overall conversion to CO_2 of the phenol removed was 72.2, 76.3 and 91.1%, respectively, for phenol-CN^-, phenol-S^{2-} and phenol-NH_4^+ mix matrixes. Contrary to the foregoing observations, considering Figures 6.30, 6.32 and 6.34, for BDD1, direct phenol oxidation to CO_2 was favored as being the most suggested dominant oxidation mechanism. Although, both the identified aromatic compounds and other unknown byproducts persisted in the effluent at the 3.5 hour retention time, but their compositions was found to be low. In these cases, phenol removal was better (98.1 - 100%) and eventually conversion to CO_2 was estimated at 95.4, 93.1, and 95.4%, respectively.

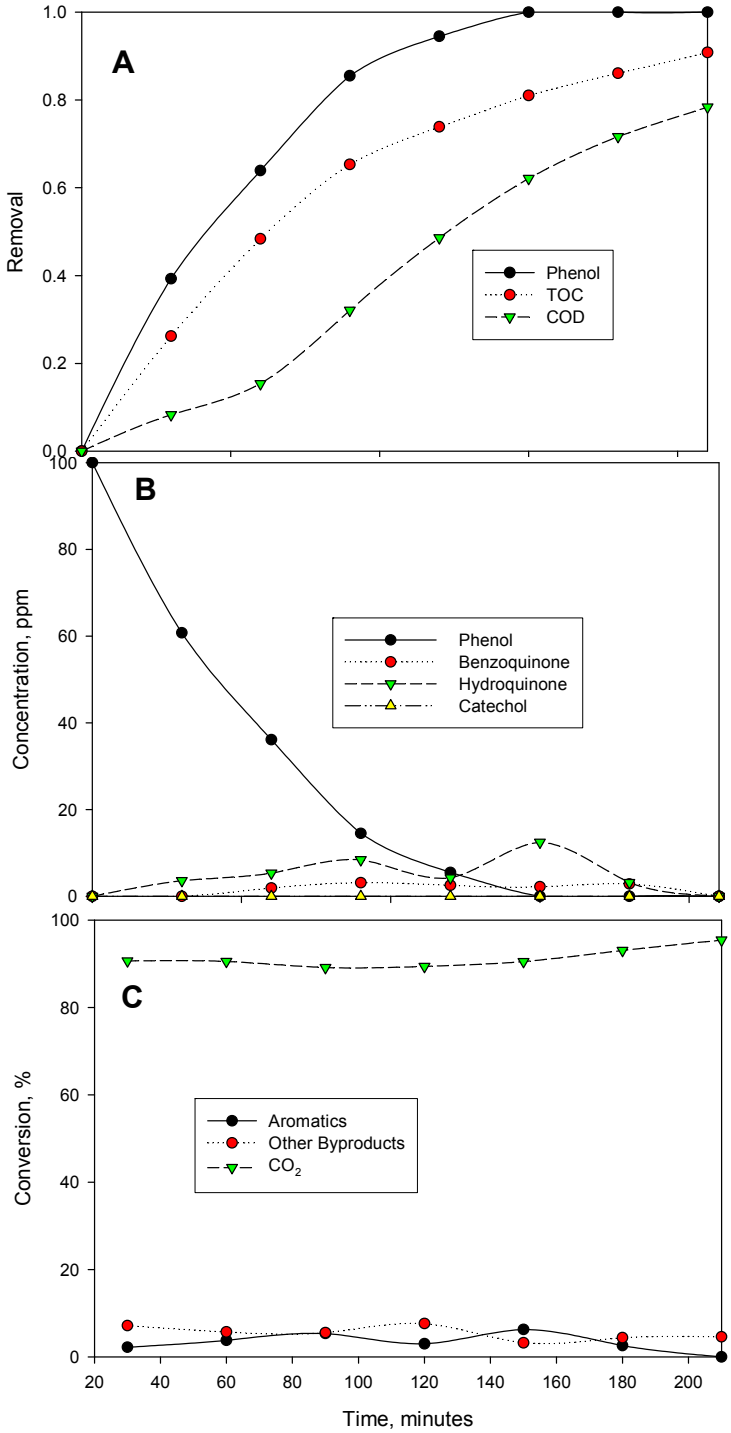

Figure 6.30: Profiles for Oxidation of Phenol in Presence of CN^- for BDD1

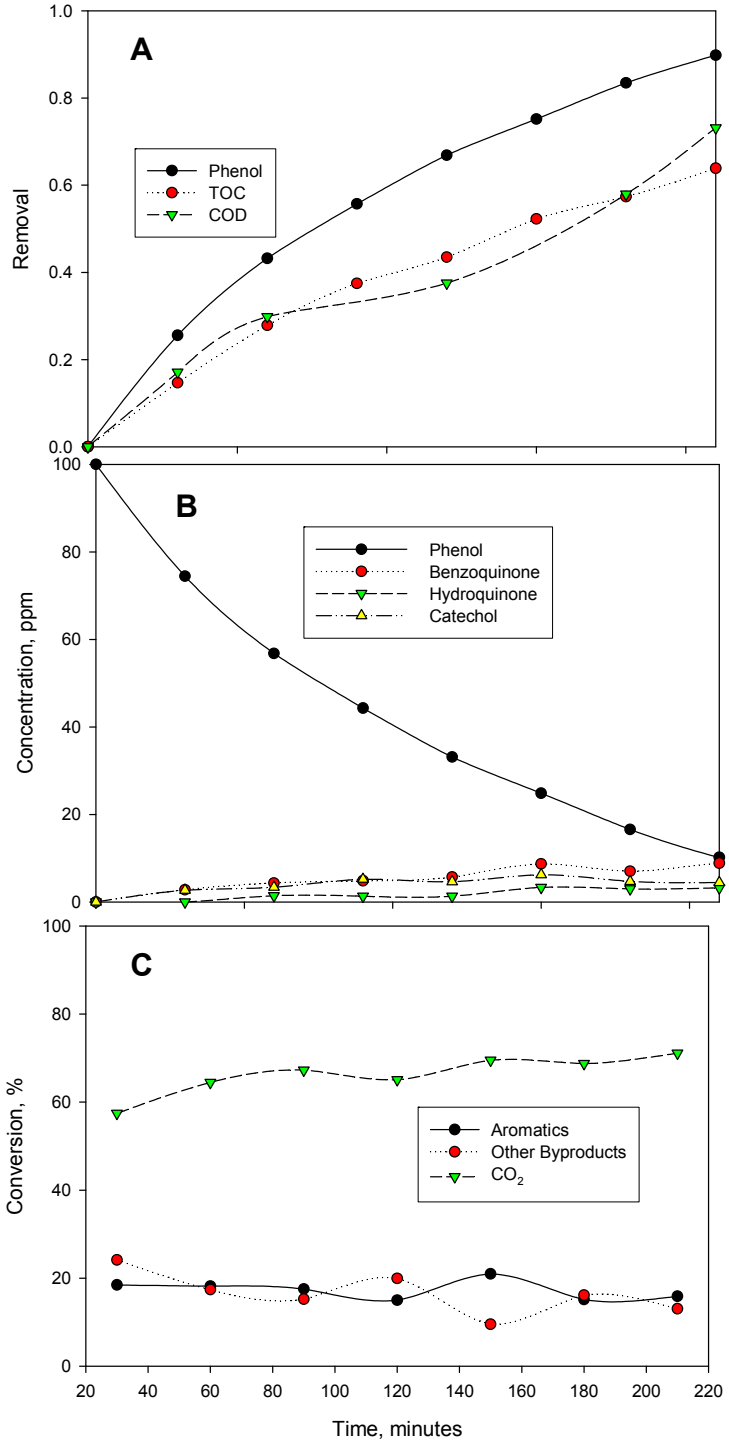

Figure 6.31: Profiles for Oxidation of Phenol in Presence CN^- for BDD2

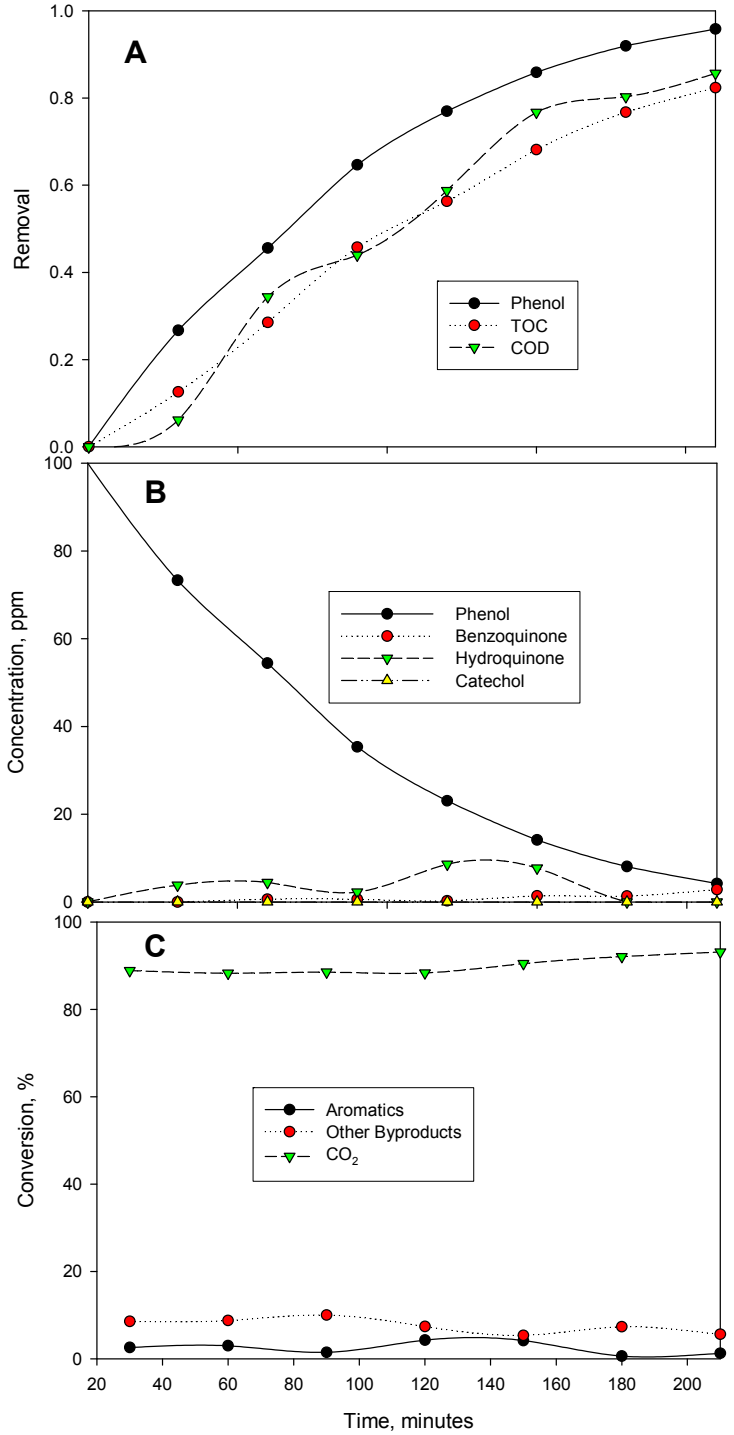

Figure 6.32: Profiles for Oxidation of Phenol in Presence of S^{2-} for BDD1

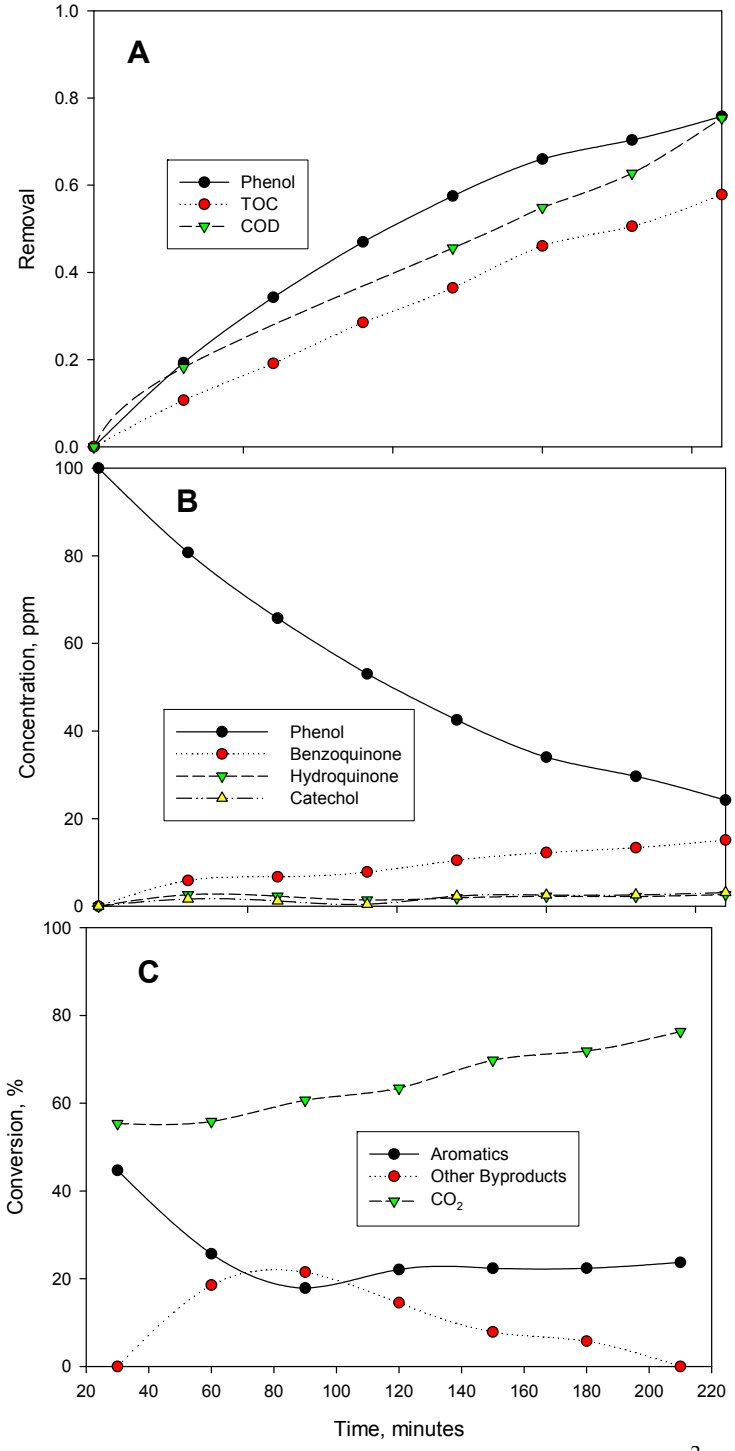

Figure 6.33: Profiles for Oxidation of Phenol in Presence of S^{2-} for BDD2

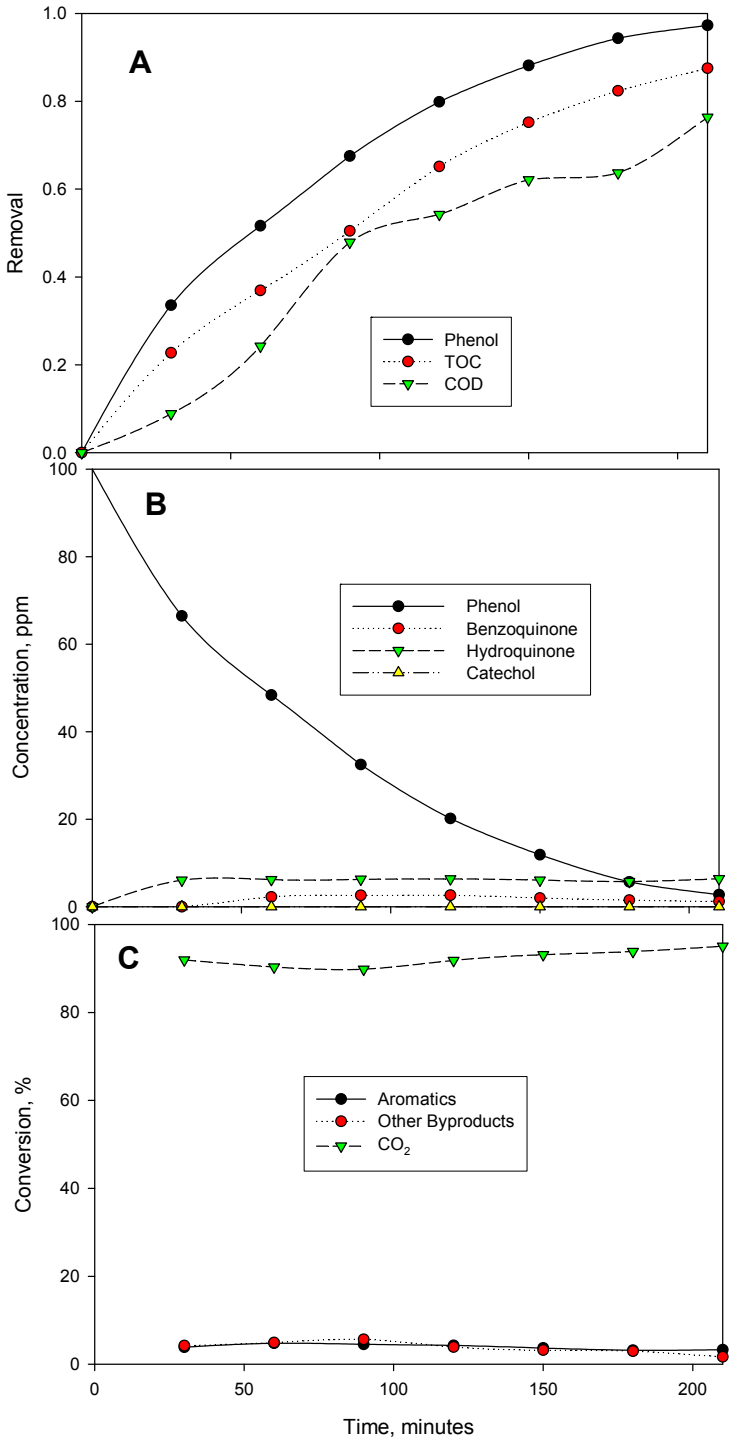

Figure 6.34: Profiles Oxidation of Phenol in Presence of NH_4^+ for BDD1

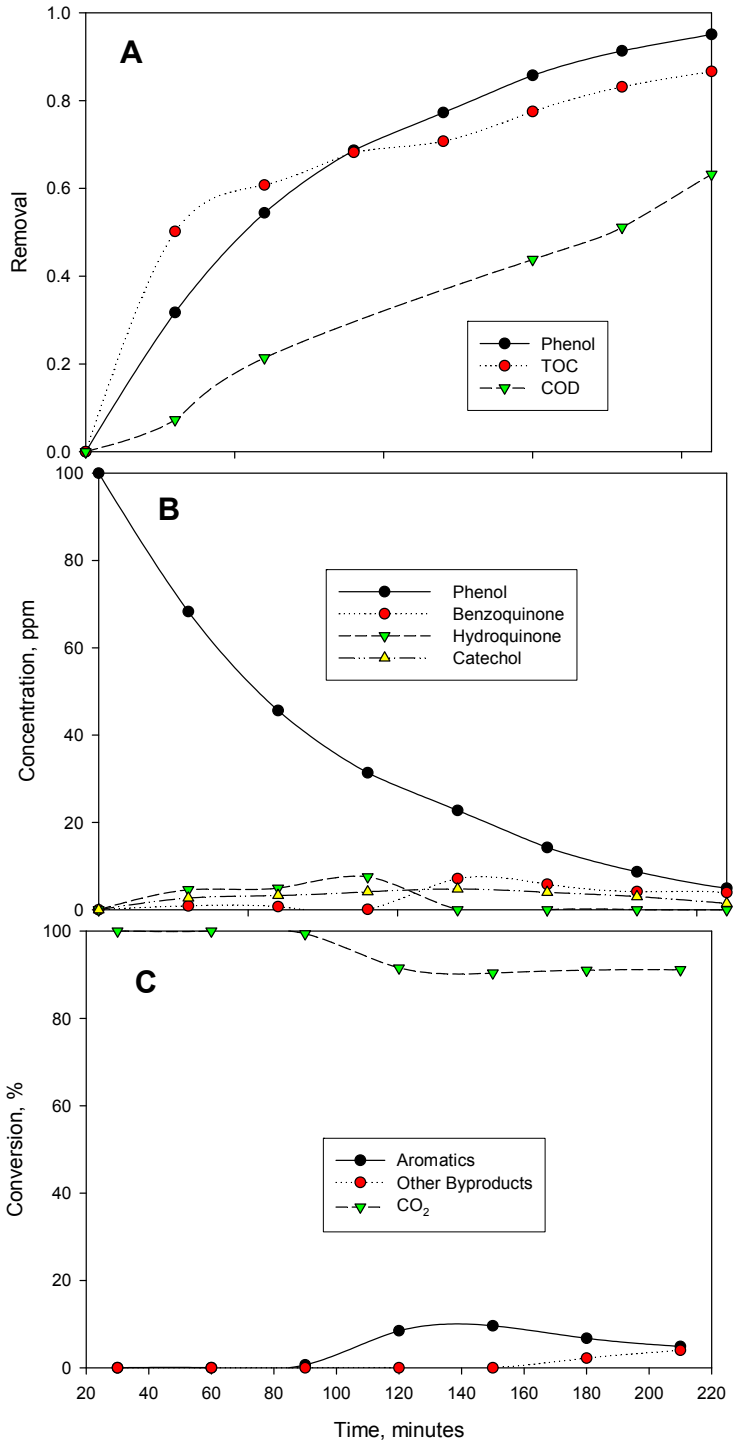

Figure 6.35: Profiles for Oxidation of Phenol in Presence of NH_4^+ for BDD2

Supportively, considering the relationship between phenol removal and the corresponding TOC and COD evolutions profiles also suggest that, phenol oxidation was mainly favored over its conversion during the treatment process in all the various binary mix matrixes. The low COD removals in most of the cases were due to the existence of the inorganic species in the mix matrixes which were appeared to be partially oxidized to other species that exert lesser oxygen demand.

6.6.2 Phenol Oxidation Byproducts in Ternary and Quaternary Mix Matrixes

At the two levels of initial concentrations of the inorganic species, data for the oxidation of phenol in the higher mix matrixes (ternary and quaternary) suggest similar mechanisms as observed in the binary mix cases. Figures 6.36 through 6.43 depict the different relevant profiles (also designated as A, B and C) during oxidation of phenol using BDD1 and BDD2 for the three ternary cases CN^-+ S^{2-}, CN^- + NH_4^+ and S^{2-} + NH_4^+ and the quaternary matrix matrixes, respectively. For BDD2, Figures 6.37, 6.39, 6.41 and 6.43 indicate that phenol was mainly converted to CO_2 via the measured aromatic compounds as the initial major intermediate byproducts which were apparently transformed into other byproducts. Moreover, removal of phenol was partial (i.e., 72.03 – 87.87%), complete oxidation of the generated byproducts was not feasible and the overall conversion to CO_2 was much lower (i.e., 73.9, 79.1, 85.1 and 71.7%, respectively).

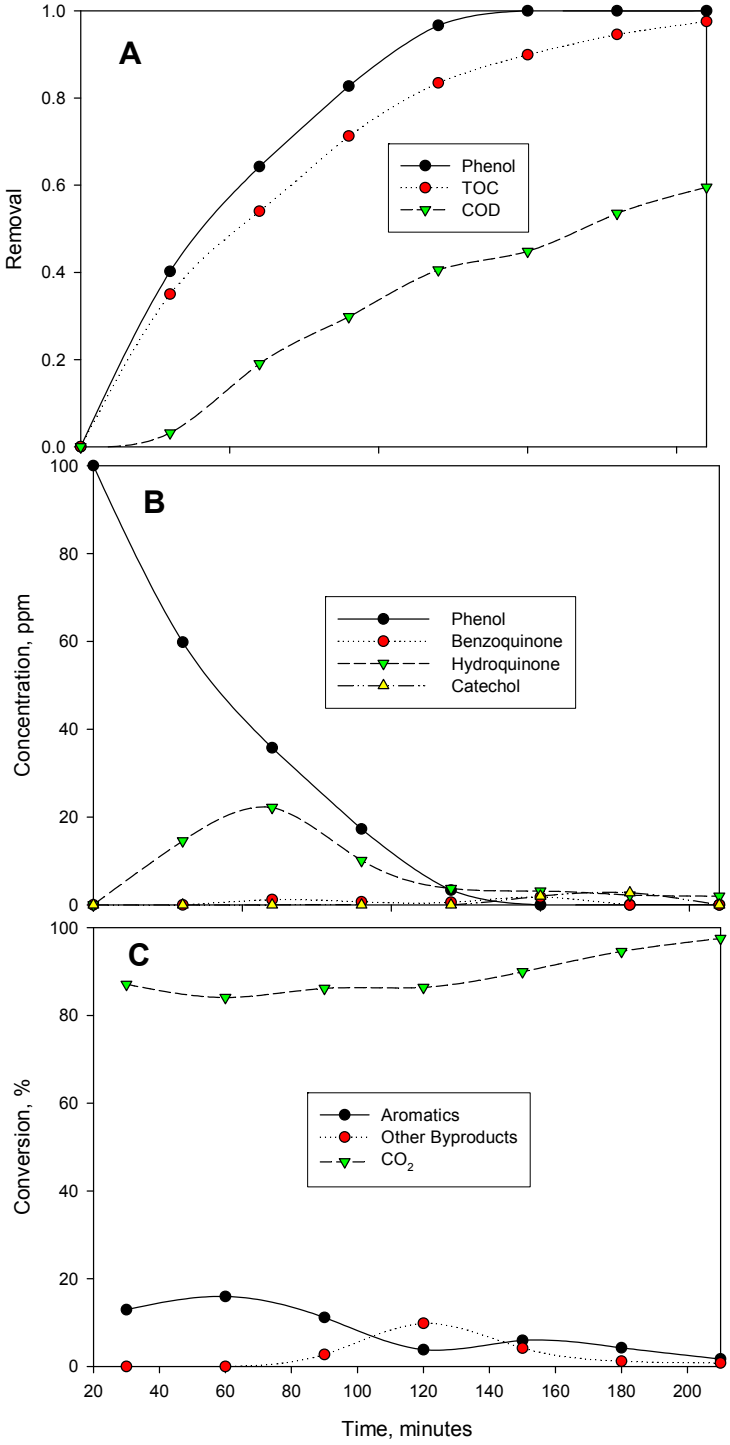

Figure 6.36: Profiles for Oxidation of Phenol in Presence of CN- and S^{2-} for BDD1

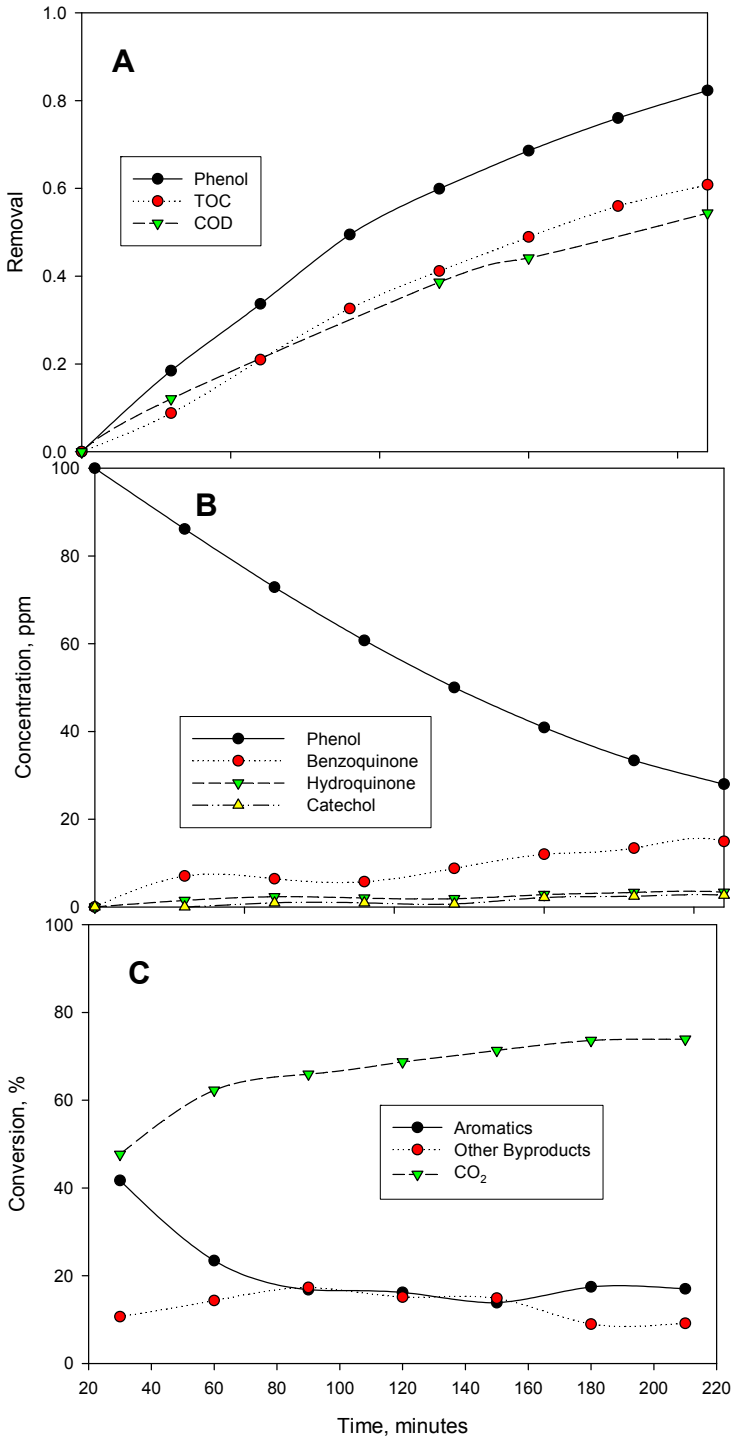

Figure 6.37: Profiles for Oxidation of Phenol in Presence of CN^- and S^{2-} for BDD2

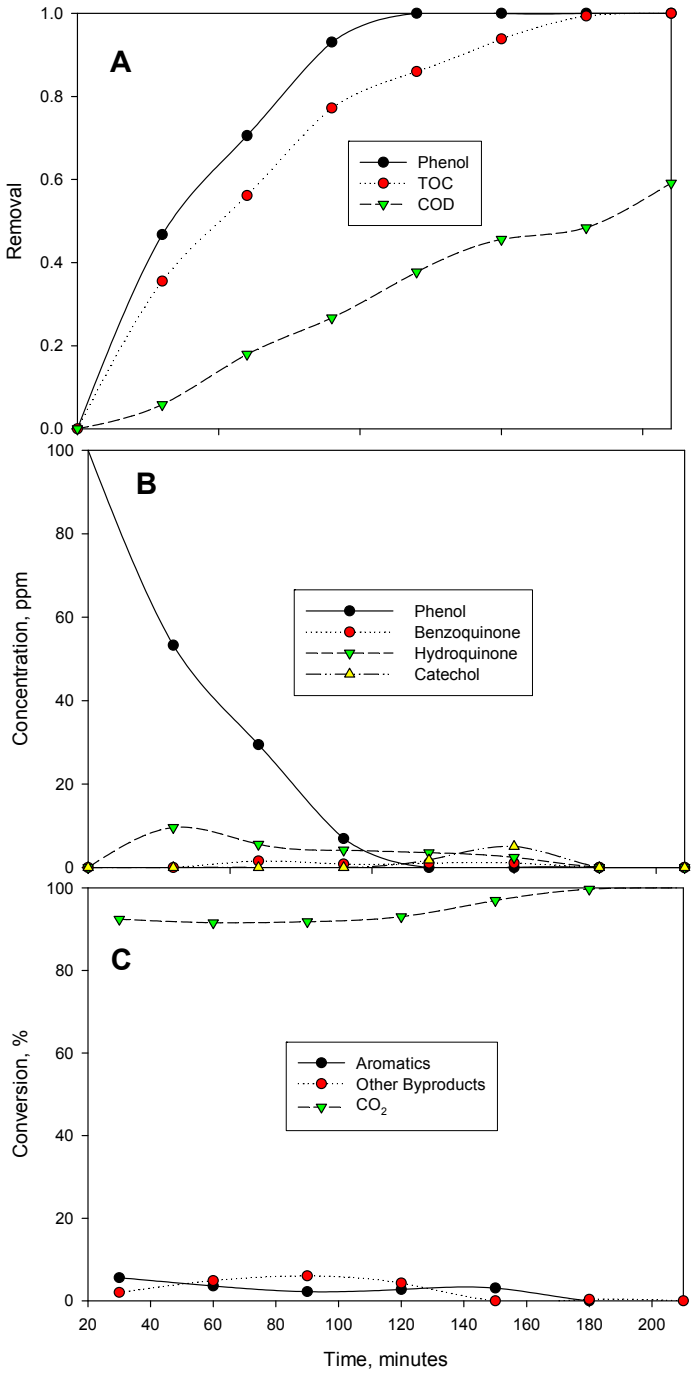

Figure 6.38: Profiles for Oxidation of Phenol in Presence of CN- and NH_4^+ for BDD1

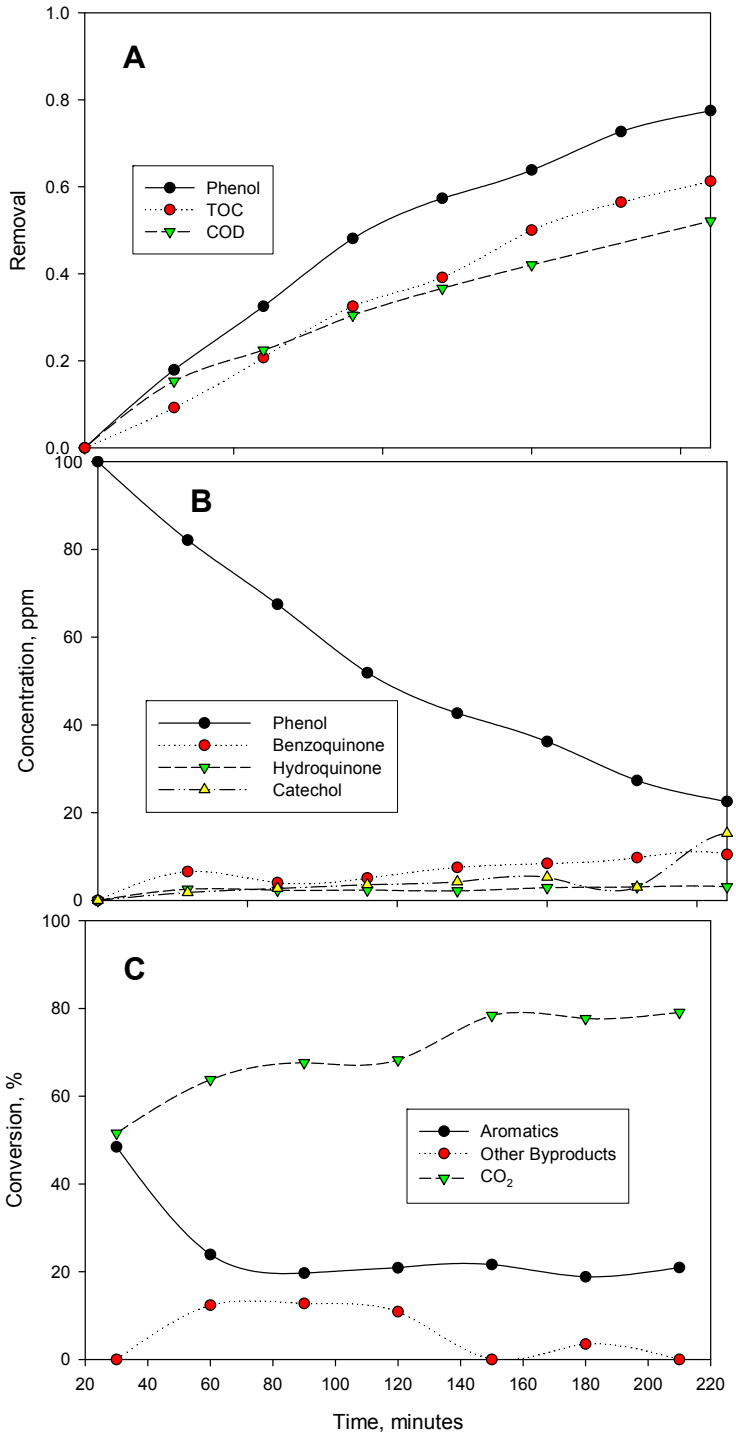

Figure 6.39: Profiles for Oxidation of Phenol in Presence of CN- and NH_4^+ for BDD2

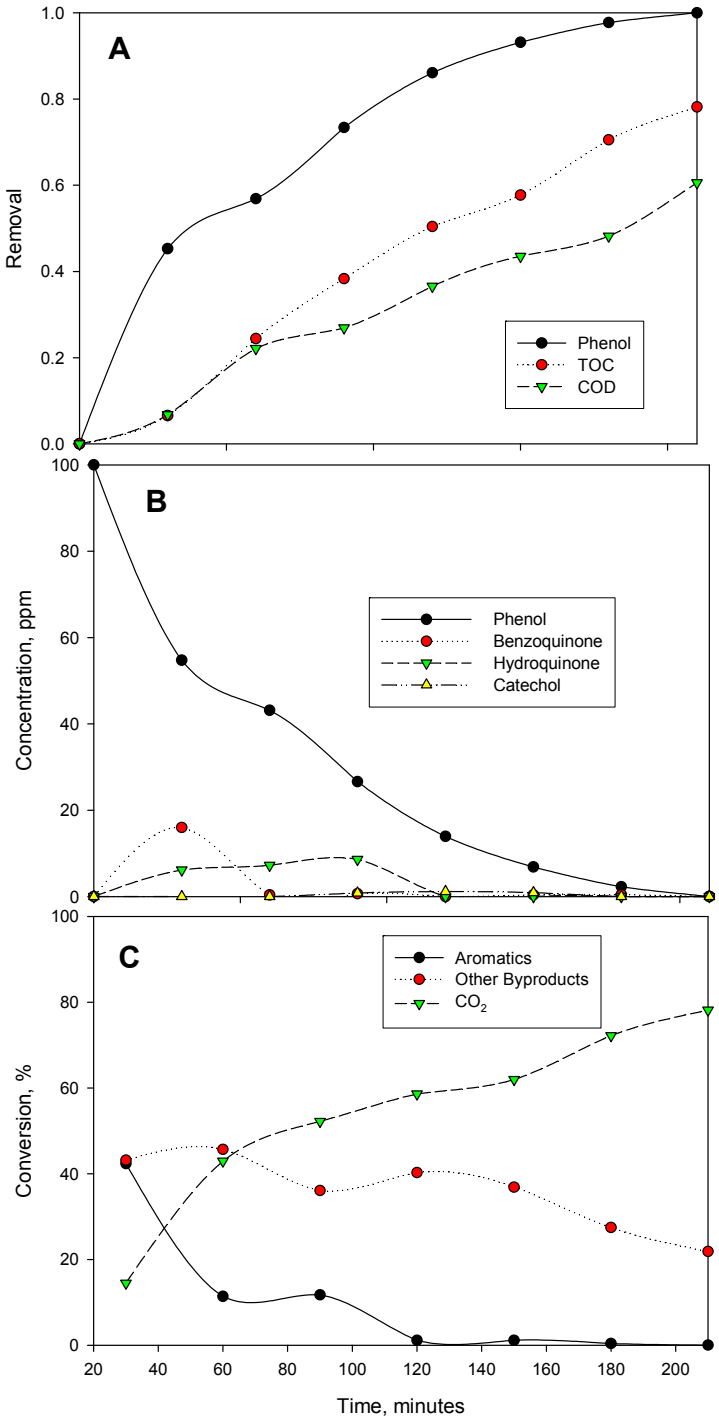

Figure 6.40: Profiles for Oxidation of Phenol in Presence of NH_4^+ and S^{2-} for BDD1

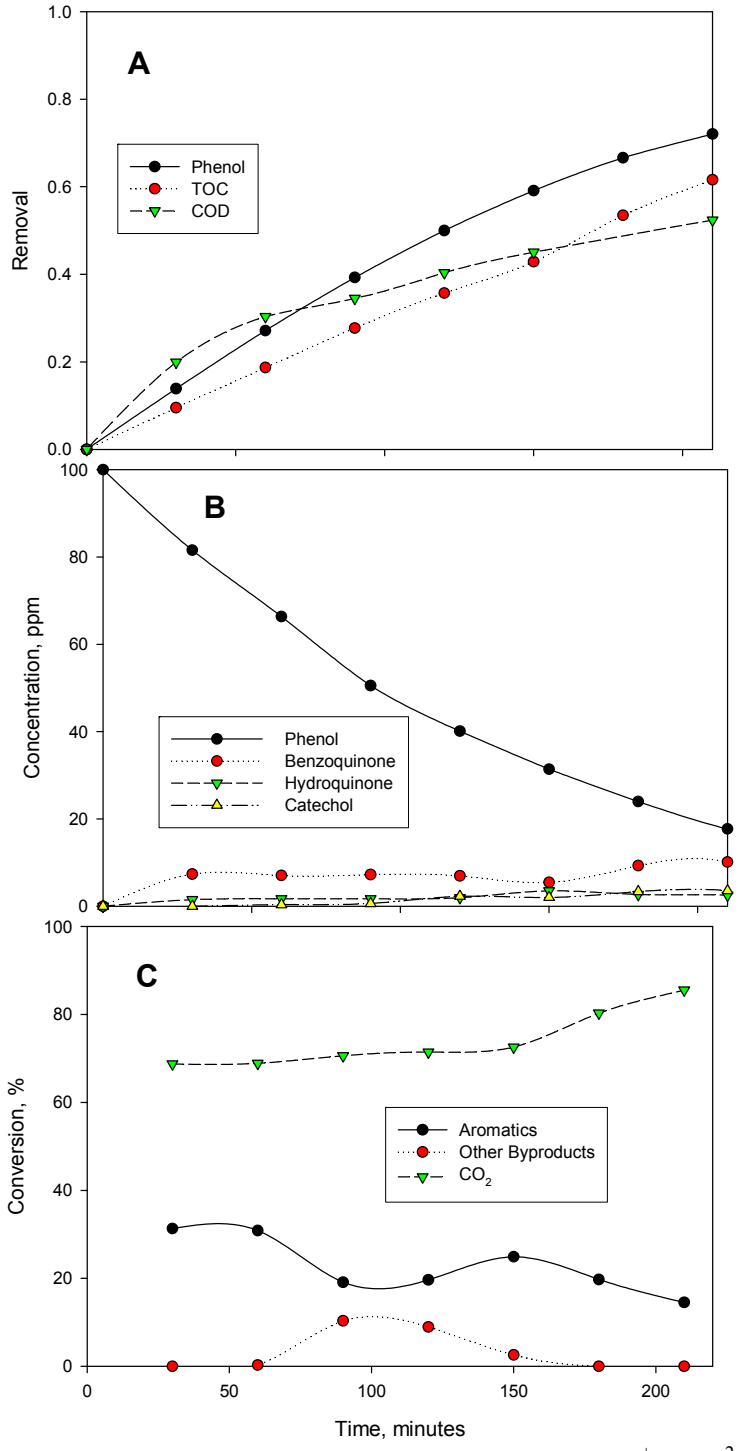

Figure 6.41: Profiles for Oxidation of Phenol in Presence of NH_4^+ and S^{2-} for BDD2

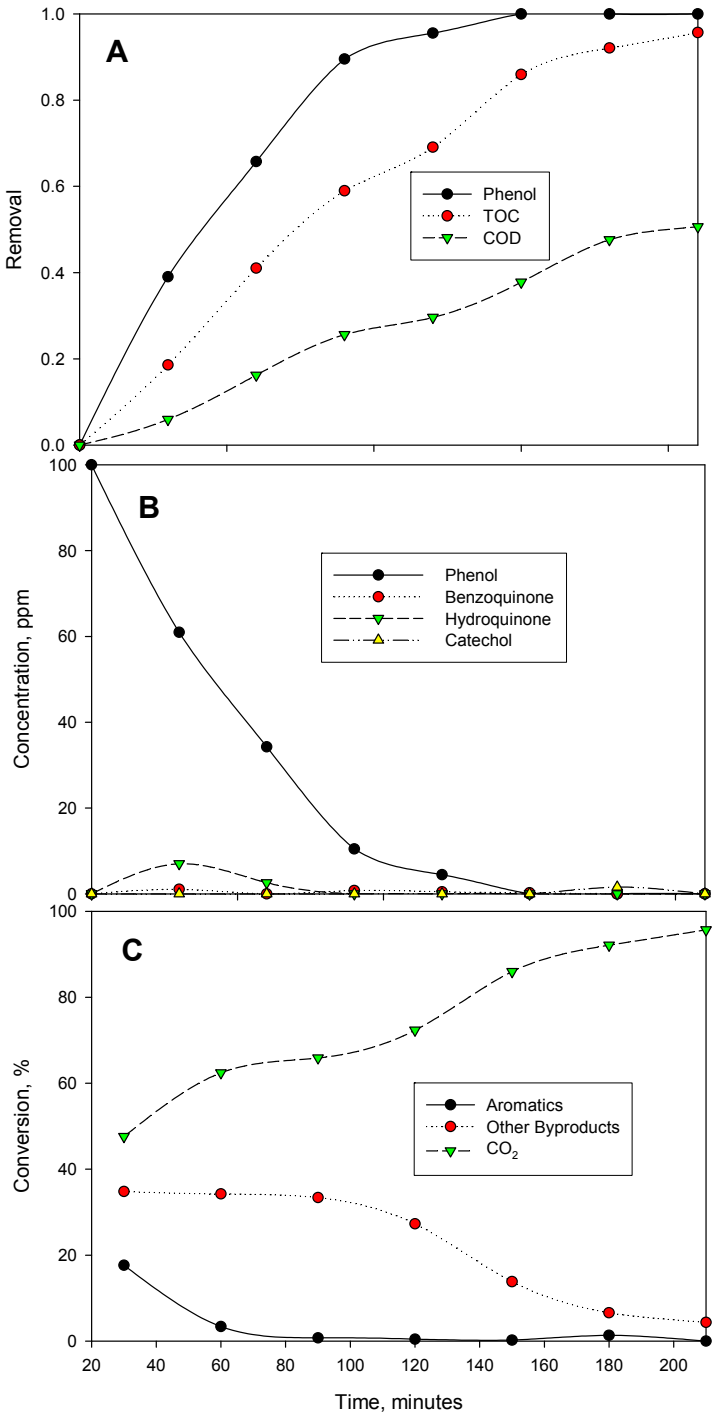

Figure 6.42: Profiles for Oxidation of Phenol in Presence of CN^-, NH_4^+ and S^{2-} for BDD1

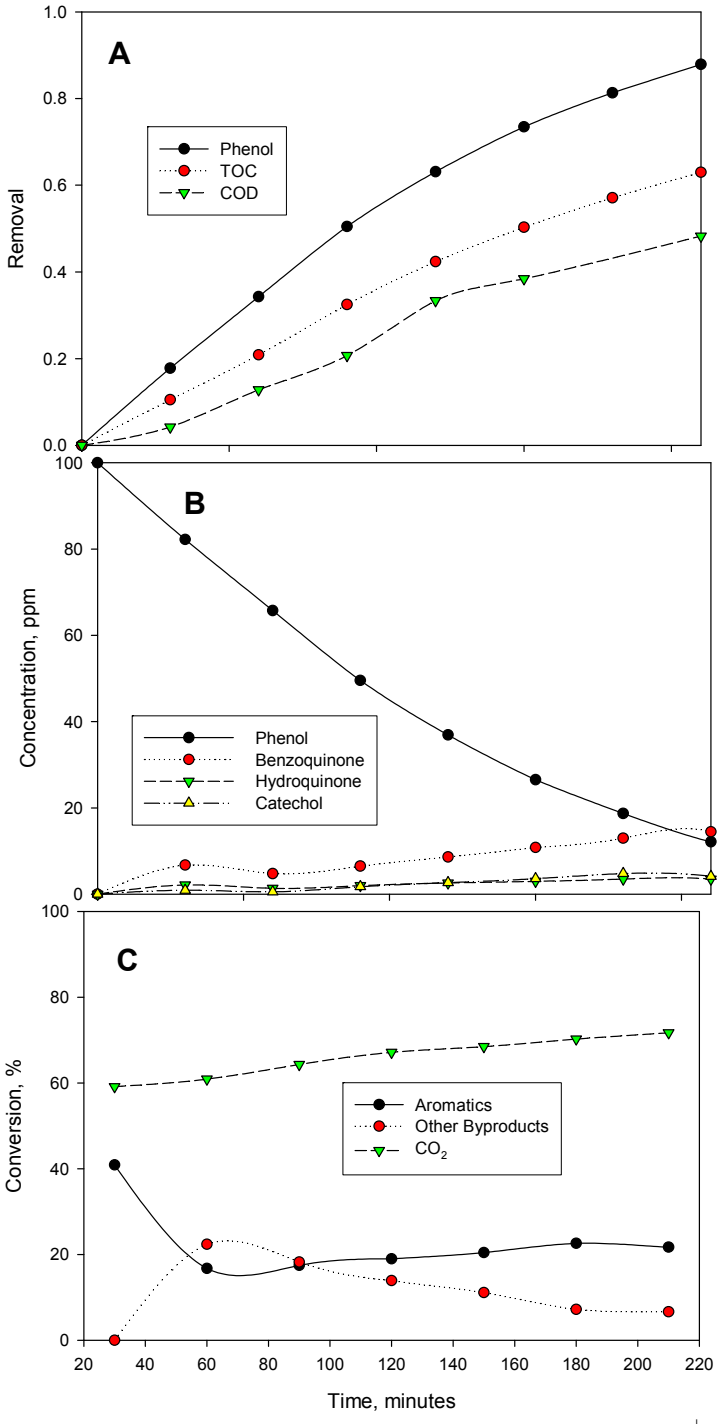

Figure 6.43: Profiles for Oxidation of Phenol in Presence of CN^-, NH_4^+ and S^{2-} for BDD2

For BDD1, in deviation from these observations also as observed earlier in the cases of the binary mix matrixes, taken into account the profiles in Figures 6.36, 6.38, 6.40 and 6.42, direct conversion to CO_2 was also the most favorable suggestible dominant means of phenol oxidation. It is noteworthy here to mention that the identified aromatic compounds and other unknown byproducts in the effluent compositions were mainly found to be lower than the later cases. In these cases, phenol was completely removed and eventual conversion to CO_2 was estimated at 97.5, 100, 78.2 and 95.7%, respectively. Similarly, it is well noticeable to observe that the COD removal has substantially decreased for the BDD1 as result of higher concentration of the inorganic species. Figure 6.44 provides the summary for the byproducts breakdown for the different mix matrixes from it is inferable that, regardless of the nature of the mix matrix, once the BDD anode is active, the presence of the inorganic species is not likely to significantly hamper the BDD anode's pollution mitigation potentials during electrochemical treatment of the simulated phenolic wastewaters.

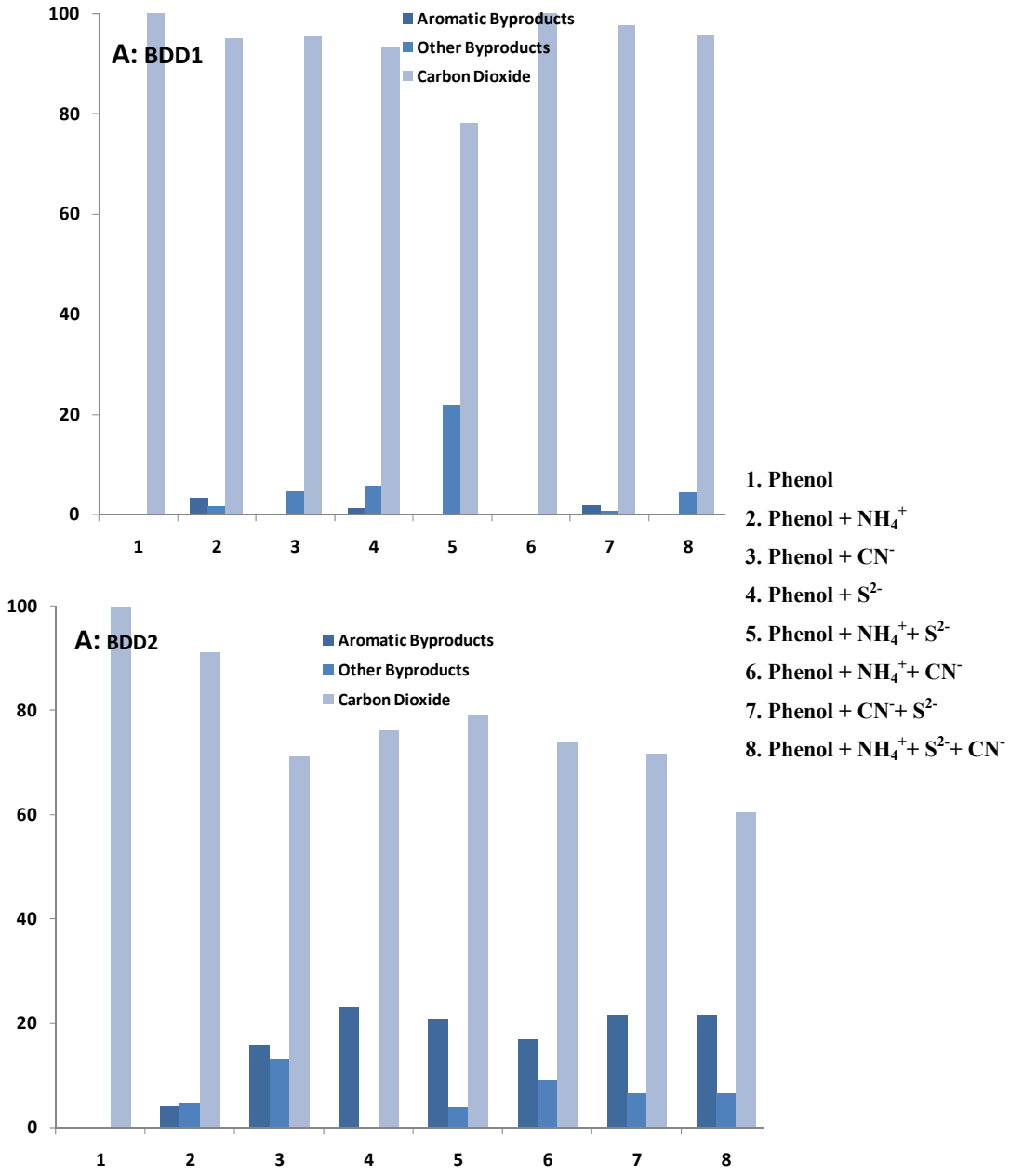

Figure 6.44: Summary of Percent Composition of Byproducts Generated for the Different Mix Matrixes

6.7 Pathways for Phenol Oxidation in Different Mix Matrixes

6.7.1 Introduction

Nature and concentration of byproducts generated during electrochemical oxidation of phenol are adversely influenced by the experimental conditions (Agnieszka et al., 2008; Iniesta et al., 2001b). The most efficient process involves generation of carbon dioxide and water as the sole byproducts with negligent or no production of intermediary byproducts (i.e., direct and fast destruction or mineralization). This depends generally on the oxidation pathways followed as well as the kinetics of disappearance of more toxic generated aromatic intermediates, quinonic compounds and higher intermediates prior to final conversion to carbon dioxide and water. Iniesta et al (2001b) and several other authors (Boye et al., 2002; Comninellis and Pulgarin, 1991; Gherardini et al., 2001; Rodrigo et al., 2001) found that at low current density and high phenol concentration or operating electrolysis within potential region of water stability, formation of aromatic intermediates dominates the process as phenol conversion to such intermediates mainly took place. This was in contrast to bulk electrolyses at high current density and low phenol concentration or within potential region of water decomposition where they reported no intermediates were practically formed and phenol was directly combusted to CO_2. .

Therefore, based on experimental conditions that invariably affect the phenol oxidation process, three distinctive possible oxidation scenarios for phenol oxidation could be (i) the generation and build-up of intermediates with no prospect for their further destruction, (ii) a

kinetically controlled process whereby sufficient electrolysis time can lead to a steady state of total mineralization of phenol and all the generated byproducts and (iii) the most efficient process, whereby the oxidation process is very fast and the pathway is "virtually" direct conversion of the parent organic compound to carbon dioxide and water with negligible or no generation of intermediates. Consequently, the build-up of oxidation intermediates byproducts and the inability to effectively convert them to CO_2 pave the way to inefficient electrochemical oxidation of phenol. As global parameters; TOC and also COD in synthetic organic wastewater free from inorganic species (exerting oxygen demand), can provide holistic information regarding wastewater's organic content. Their removal trends can be invoked in order to confirm and/or provide more accurate judgment regarding the fate of the parent compound; whether the oxidation process led to generation of organic byproducts derived as result of conversion of the parent compound rather than its mineralization to carbon dioxide (Canizares et al., 2009).

6.7.2 Comprehensive Determination of Oxidation Byproducts in Different Mix Matrixes

Partial analyses of phenol oxidation intermediary byproducts using HPLC analysis revealed evolution of benzoquinone, hydroquinone, catechol and phenol at eluding times of 1.581, 1.86, 2.296 and 3.055 minutes ,respectively, as depicted earlier in Figure 5.29. In addition to that, comprehensive qualitative byproducts' analyses were conducted using gas

chromatograph device equipped with mass spectrophotometer detector (GC-MS) and auto-sampler. Several samples drawn from the different experiments were analyzed in order to supplement the HPLC analyses. Sample extraction was performed based on standard method procedure (EPA Method 3510C). For each sample, pH was adjusted to 2 using H_2SO_4 then followed by extracting 50ml of the sample into 50ml of dichloromethane by shaking the mixture in separation funnel in three sequential steps; 20, 20 and 10ml of the dichloromethane for 5 minutes each. Afterwards, the extract was concentrated to 5 ml before injection into the GS-MS where the analysis was made.

The GC-MS analyses for samples from the several mix matrixes experiments showed that the aromatics intermediates were mainly compounds with the highest quality of detection beside the phenol. Nonetheless, very small peaks for other unconfirmed compounds were observed in some of the samples. Typically, phenol (m/e = 94), benzoquinone (m/e = 108) and catechol or resorcinol (m/e = 110) were detected, though the retention times were not always consistent. Supplementary HPLC analysis was undertaken for determining individual extraction efficiencies for phenol and the aromatic byproducts in standards as well as in some experimental samples. Typical results for these experimental samples' analyses revealed 80-90 % recovery for phenol. However, for the aromatics hydrocarbons, recovery was in the order the benzoquinone > catechol > hydroquinone with benzoquinone showing moderate recovery (around 25%) while catechol and hydroquinone possessing lesser recoveries (less

than 10%). In the other hand, for freshly prepared pure standard samples of the aromatic intermediates, the recoveries of these compounds were found to be on the average side (20-35%). For the known organic acids such as oxalic, maleic and fumeric acids which were also notably detected by the GC-MS, the recoveries of their pure samples were far below (2-5%). This could be the reason why phenol, benzoquinone, hydroquinone and catechol were the most identifiable compounds with the GC-MS analysis. However, because of the concentrations of the phenol and aromatics as found from the HPLC analyses were usually by far beyond the detection limit of the GC-MS, these lower recoveries didn't pose much problem for qualitative identification purpose.

Some of the GC-MS chromatograms obtained from the analyzed samples are displayed in Figures 6.45 to 6.59. The analyses of the peaks in conjunction of library matching were used to identify the most probable corresponding compound(s) in the samples qualitatively. The peak of phenol at zero minute of electrolysis for all the mix matrixes was observed to appear at 3.9 minutes (Figure 6.45). However, this peak shifted to 5.38 minutes for most of the samples from the treated synthetic wastewater laden with the inorganic species; this particular peak usually disappears gradually with time of electrolysis. The disappearance of the phenol peak is concurrently occurring with appearance of other smaller peaks that persisted in most cases till the end of the electrolysis; which matched nearly all the HPLC data. Analyses for some of the peaks are detailed below.

For phenol-NH_4^+-S^{2-} ternary mix system, though peaks were noticeable at 2.45, 2.98, 3.9, 5.37 and 10.76 minutes (Figures 6.46, 6.47 and 6.48); qualitatively, only the peaks at 5.37 and 10.76 minutes were, respectively, attributed to phenol and benzoquinone compound with certainty. Benzoquinone persisted till the end of 210 minutes which goes in line with the concentration profile presented earlier in Figure 6.43. Dimethylamine (C_2H_7N), butanoic acid 2-oxo ($C_4H_6O_3$), ethane, 1,2-dimethoxy- ($C_4H_{10}O_2$) and carbonic acid dimethyl ester ($C_3H_6O_3$) appeared to be the suggested compounds at 2.988 minutes; though their library match qualities were very low (< 7%). Likewise the case was for peak at 2.45 and 3.39 minutes. For 2.45 minutes, the most probable compounds were propanoic acid, 2-methyl-ethyl ester ($C_6H1_2O_2$) and cyclohexanethiol ($C_6H_{12}S$); with the propanoic acid been the most acceptable likely compound due to its higher match quality. While for the peak at 3.39 minutes, the best library matches were cyclohexanethiol ($C_6H_{12}S$) and Hydrazinecarboxylic acid, methyl ester ($C_2H_6N_2O_2$).

Similarly, for the ternary matrixes of phenol with NH_4^+ and CN^- as depicted in Figures 6.50, 6.51 and 6.52, major peaks were at 2.99, 4.59, 5.37 and 10.45 minutes with benzoquinone, phenol and resorcinol at 4.59, 5.37 and 10.45 minutes, respectively. It can be observed that the peak of benzoquinone have now shifted backward and also all peaks for the three identified compounds have completely disappeared at 180 minutes; also confirming the profile given in Figure 6.38. As in the previous case, carbonic acid dimethyl ester ($C_3H_6O_3$)

and dimethylamine (C_2H_7N) appeared to have eluded 2.99 minutes; though with low library match quality.

The peaks for ternary and quaternary mix matrixes of phenol-CN^--S^{2-} and phenol-CN-NH_4^+-S^{2-} are depicted in Figures 6.52 to 6.55 and Figures 6.56 to 6.59, respectively. The analyses for nature of the byproducts from the chromatograms depicted in these figures showed that they were not quite different from those found in the scenarios analyzed above. Similarly, the qualitative detections of the aromatic byproducts in these cases were also well in conformity with those obtained previously from the HPLC quantitative analyses.

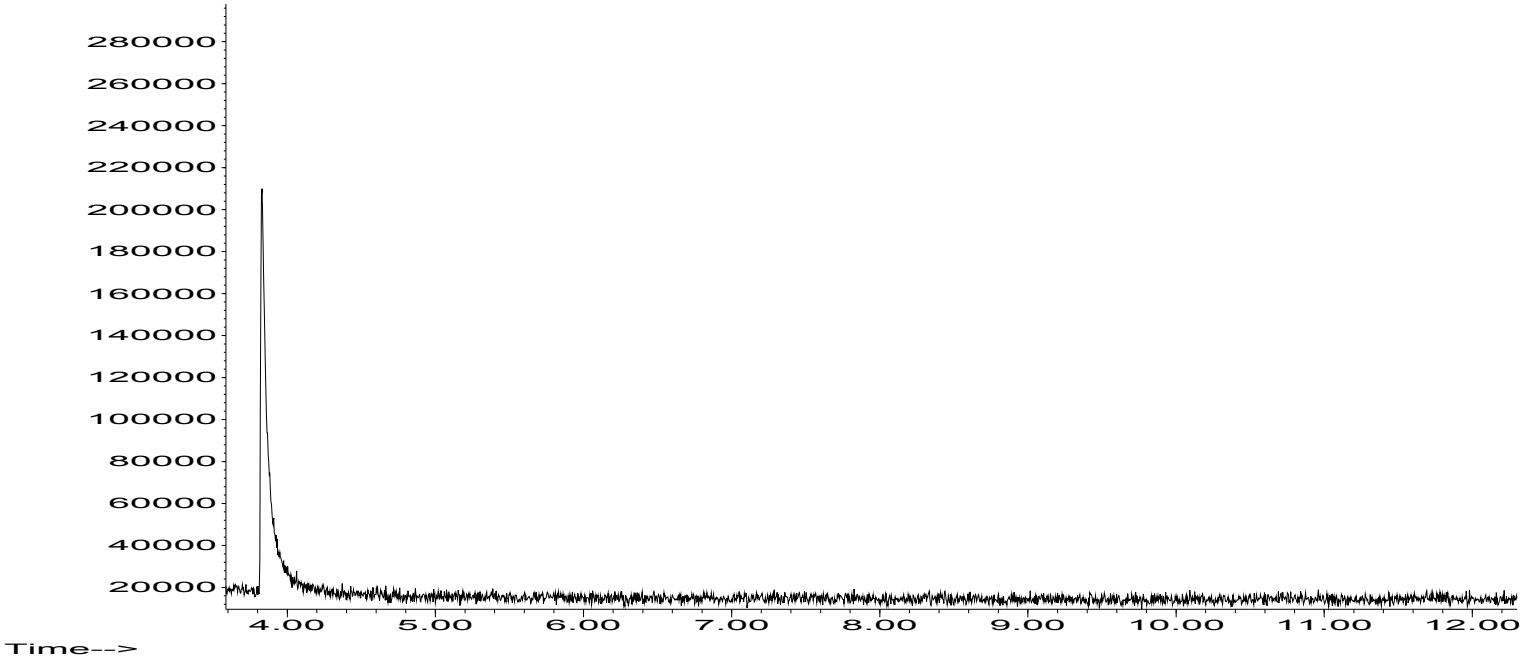

Figure 6.45: GC-MS Peak for Phenol at 0 minutes

- **(3.9 minutes)** Phenol

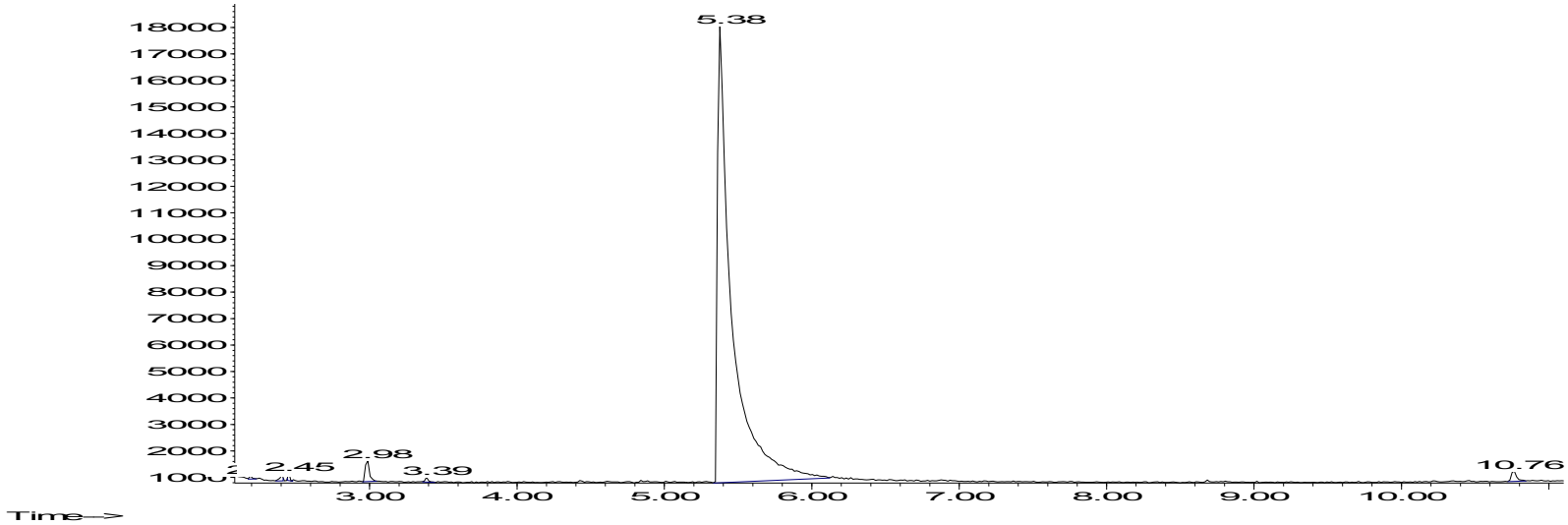

Figure 6.46: GC-MS Chromatogram for Phenol Oxidation in Presence of NH_4^+ and S^{2-} at 60 minutes

- **(2.45 minutes) (1)** Propanoic acid, 2-methyl-ethyl ester ($C_6H1_2O_2$) **(2)** Cyclohexanethiol ($C_6H_{12}S$)
- **(2.98 minutes) (1)** Dimethylamine (C_2H_7N), **(2)** Butanoic acid 2-oxo ($C_4H_6O_3$), **(3)** Ethane, 1,2-dimethoxy- ($C_4H_{10}O_2$) **(4)** **C**arbonic acid dimethyl ester ($C_3H_6O_3$)
- **(3.39 minutes) (1)** Cyclohexanethiol ($C_6H_{12}S$) **(2)** Hydrazinecarboxylic acid, methyl ester ($C_2H_6N_2O_2$)
- **(5.37 minutes)** Phenol
- **(10.76 minutes)** p-Benzoquinone

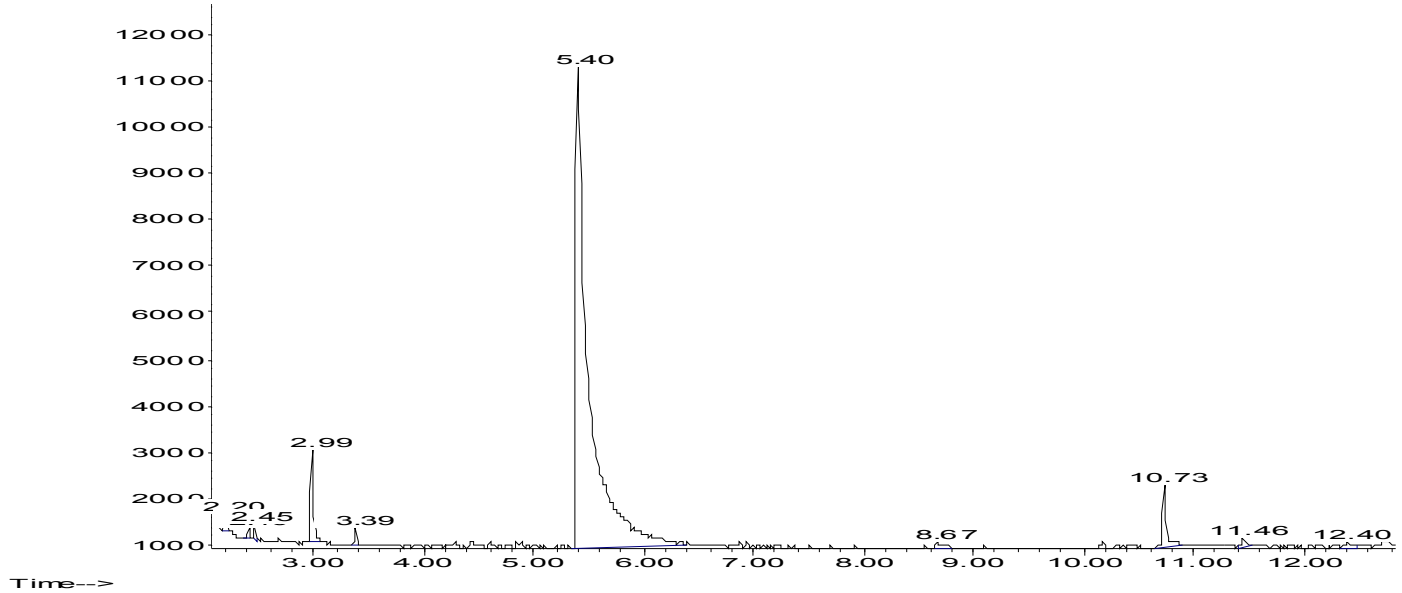

Figure 6.47: GC-MS Chromatogram for Phenol Oxidation in Presence of NH_4^+ and S^{2-} at 120 minutes

(2.45 minutes) (1) Propanoic acid, 2-methyl-ethyl ester ($C_6H1_2O_2$) **(2)** Cyclohexanethiol ($C_6H_{12}S$)

- **(2.98 minutes) (1)** Dimethylamine (C_2H_7N), **(2)** butanoic acid 2-oxo ($C_4H_6O_3$), **(3)** Ethane, 1,2-dimethoxy- ($C_4H_{10}O_2$) **(4)** Carbonic acid dimethyl ester ($C_3H_6O_3$)
- **(3.39 minutes) (1)** Cyclohexanethiol ($C_6H_{12}S$) **(2)** Hydrazinecarboxylic acid, methyl ester ($C_2H_6N_2O_2$)
- **(5.37 minutes)** Phenol
- **(10.76 minutes)** p-Benzoquinone

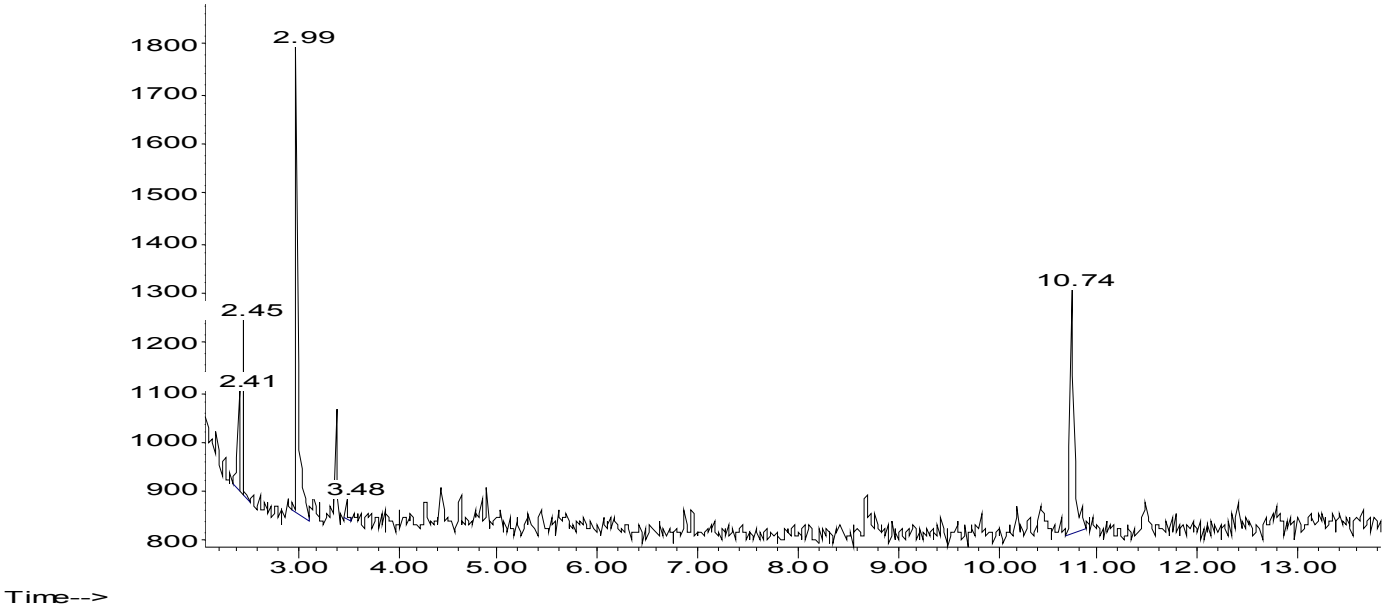

Figure 6.48: GC-MS Chromatogram for Phenol Oxidation in Presence of NH_4^+ and S^{2-} at 210 minutes

(2.45 minutes) (1) Propanoic acid, 2-methyl-ethyl ester ($C_6H1_2O_2$) **(2)** Cyclohexanethiol ($C_6H_{12}S$)

- **(2.98 minutes) (1)** Dimethylamine (C_2H_7N), **(2)** Butanoic acid 2-oxo ($C_4H_6O_3$), **(3)** Ethane, 1,2-dimethoxy- ($C_4H_{10}O_2$)
  - **(4)** carbonic acid dimethyl ester ($C_3H_6O_3$)
- **(3.39 minutes) (1)** Cyclohexanethiol ($C_6H_{12}S$) **(2)** Hydrazinecarboxylic acid, methyl ester ($C_2H_6N_2O_2$)
- **(5.37 minutes)** Phenol
- **(10.76 minutes)** p-Benzoquinone

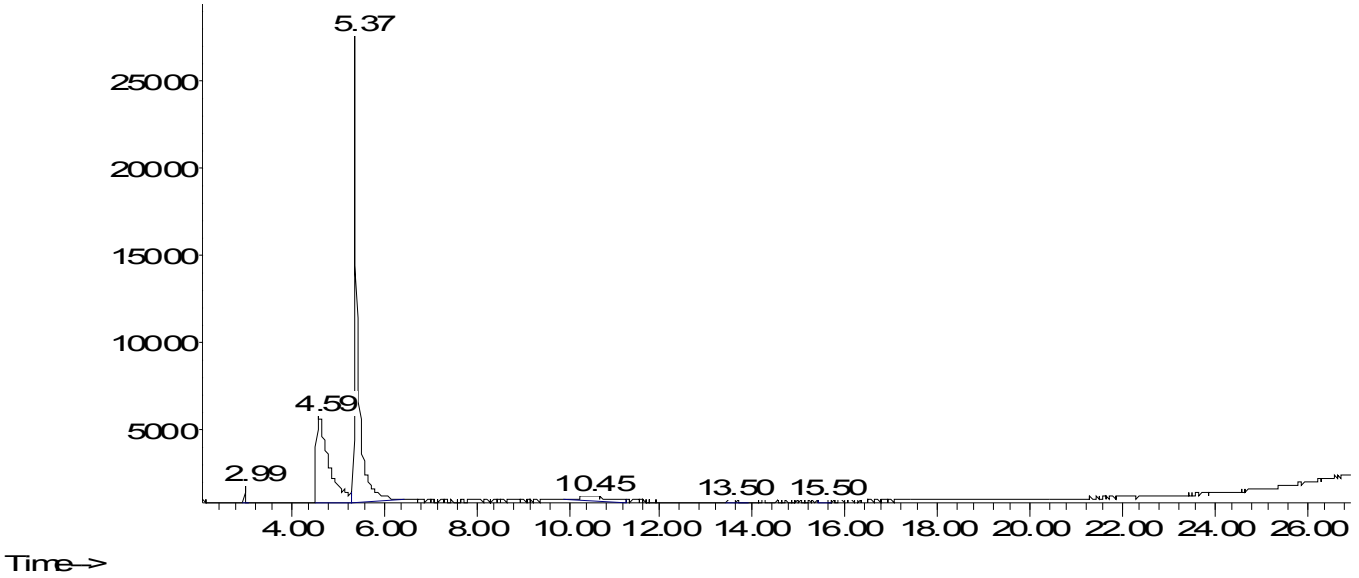

Figure 6.49: GC-MS Chromatogram for Phenol Oxidation in Presence of NH_4^+ and CN^- at 30 minutes

- **(2.98 minutes) (1)** Dimethylamine (C_2H_7N), **(2)** Butanoic acid 2-oxo ($C_4H_6O_3$), **(3)** Ethane, 1,2-dimethoxy- ($C_4H_{10}O_2$) **(4)** carbonic acid dimethyl ester ($C_3H_6O_3$)
- **(4.59 minutes) (1)** Resorcinol **(2)** Cyclohexanethiol ($C_6H_{12}S$) **(3)** Hydrazinecarboxylic acid, methyl ester ($C_2H_6N_2O_2$)
- **(5.37 minutes)** Phenol
- **(10.45 minutes)** p-Benzoquinone

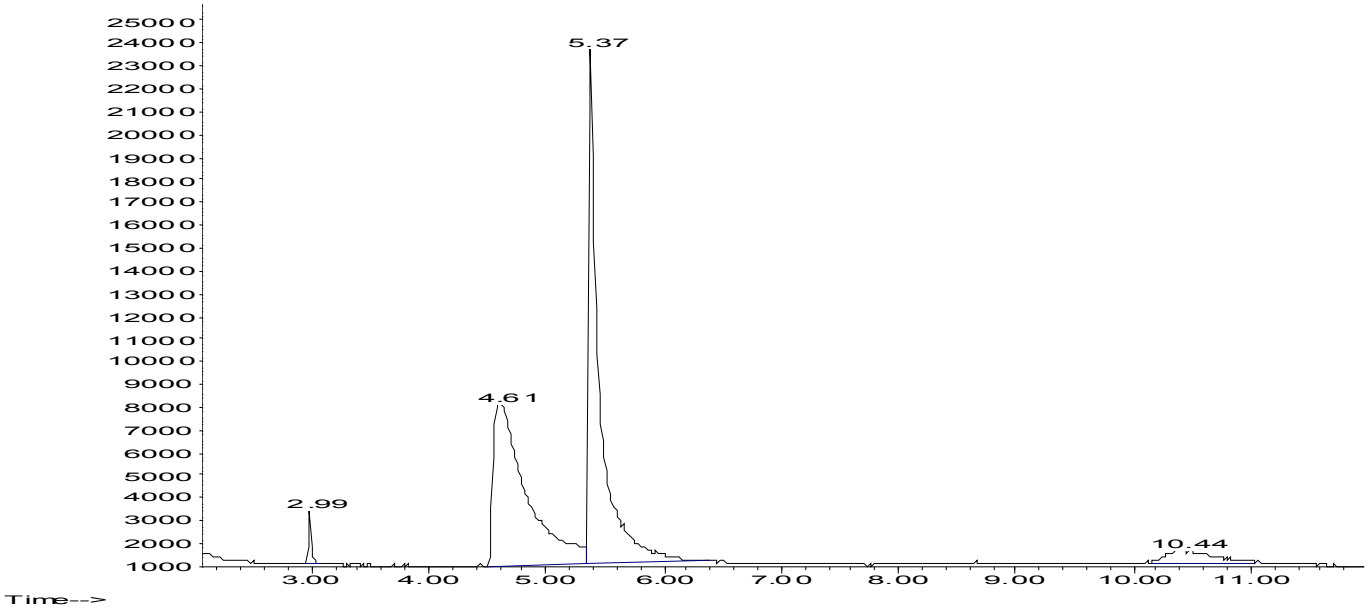

Figure 6.50: GC-MS Chromatogram for Phenol Oxidation in Presence of NH_4^+ and CN^- at 60 minutes

- **(2.98 minutes) (1)** Dimethylamine (C_2H_7N), **(2)** Butanoic acid 2-oxo ($C_4H_6O_3$), **(3)** Ethane, 1,2-dimethoxy- ($C_4H_{10}O_2$) **(4)** carbonic acid dimethyl ester ($C_3H_6O_3$)
- **(4.59 minutes) (1)** Resorcinol **(2)** Cyclohexanethiol ($C_6H_{12}S$) **(3)** Hydrazinecarboxylic acid, methyl ester ($C_2H_6N_2O_2$)
- **(5.37 minutes)** Phenol
- **(10.45 minutes)** p-Benzoquinone

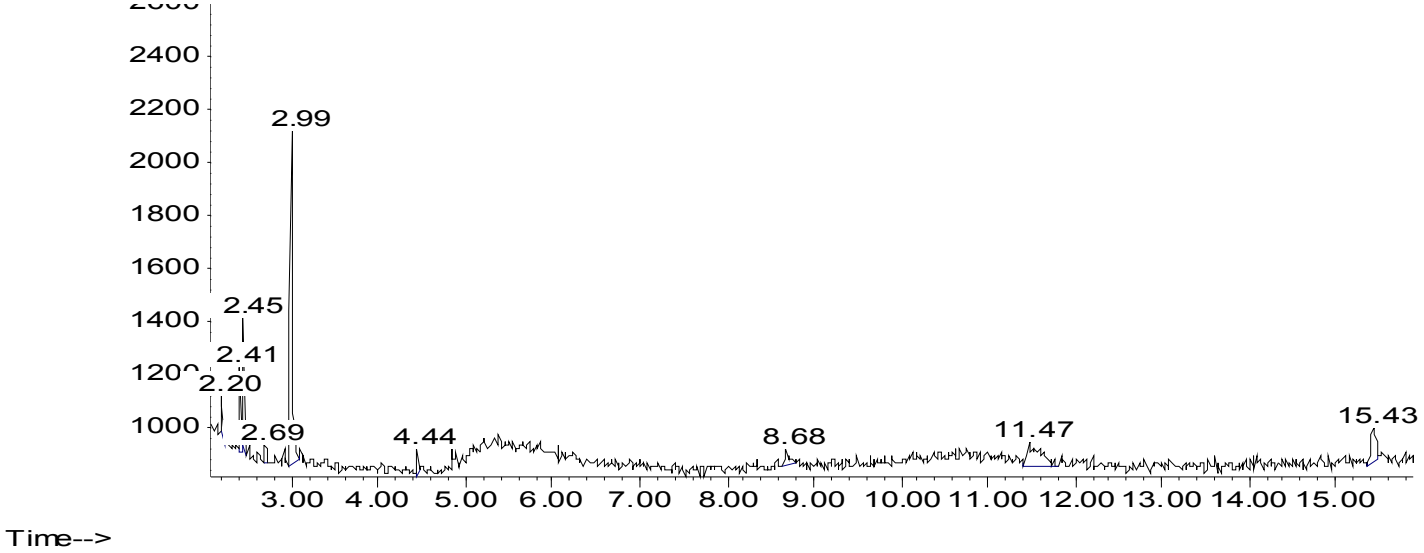

Figure 6.51: GC-MS Chromatogram for Phenol Oxidation in Presence of NH_4^+ and CN^- at 180 minutes

- **(2.99 minutes) (1)** Dimethylamine (C_2H_7N), **(2)** Butanoic acid 2-oxo ($C_4H_6O_3$), **(3)** Ethane, 1,2-dimethoxy- ($C_4H_{10}O_2$) **(4)** carbonic acid dimethyl ester ($C_3H_6O_3$)

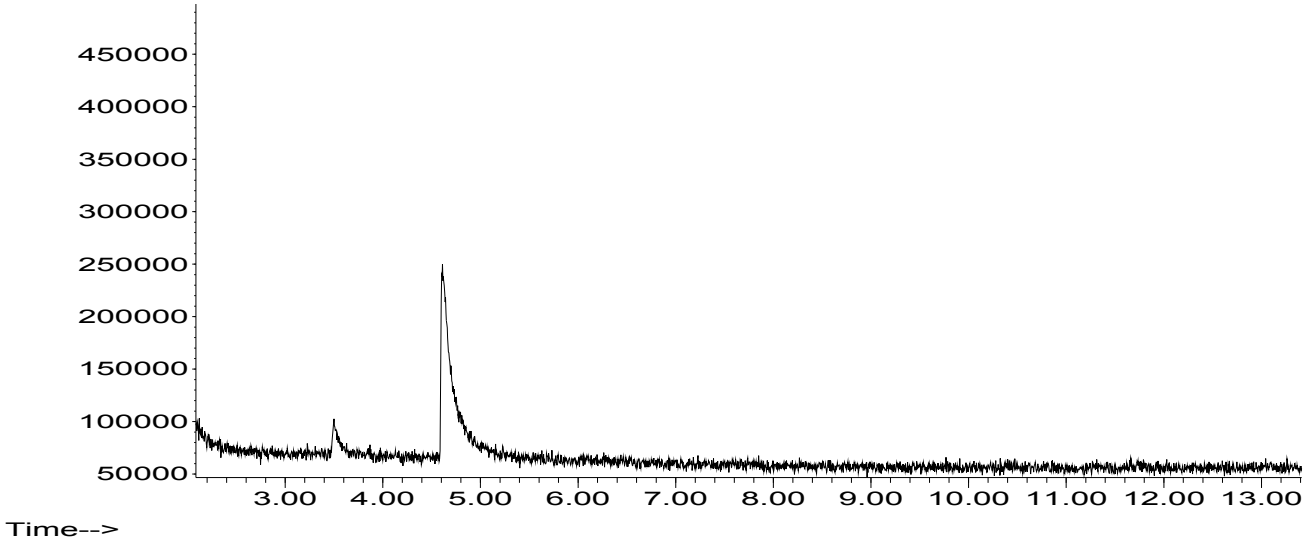

Figure 6.52: GC-MS Chromatogram for Phenol Oxidation in Presence of CN^- and S^{2-} at 30 minutes

- **(4.8 minutes)** phenol
- **(3.5 minutes) (1).**Bicyclo[4.2.0]octa-1,3,5-triene and **(2)** Acetic acid, 2-phenylethyl ester

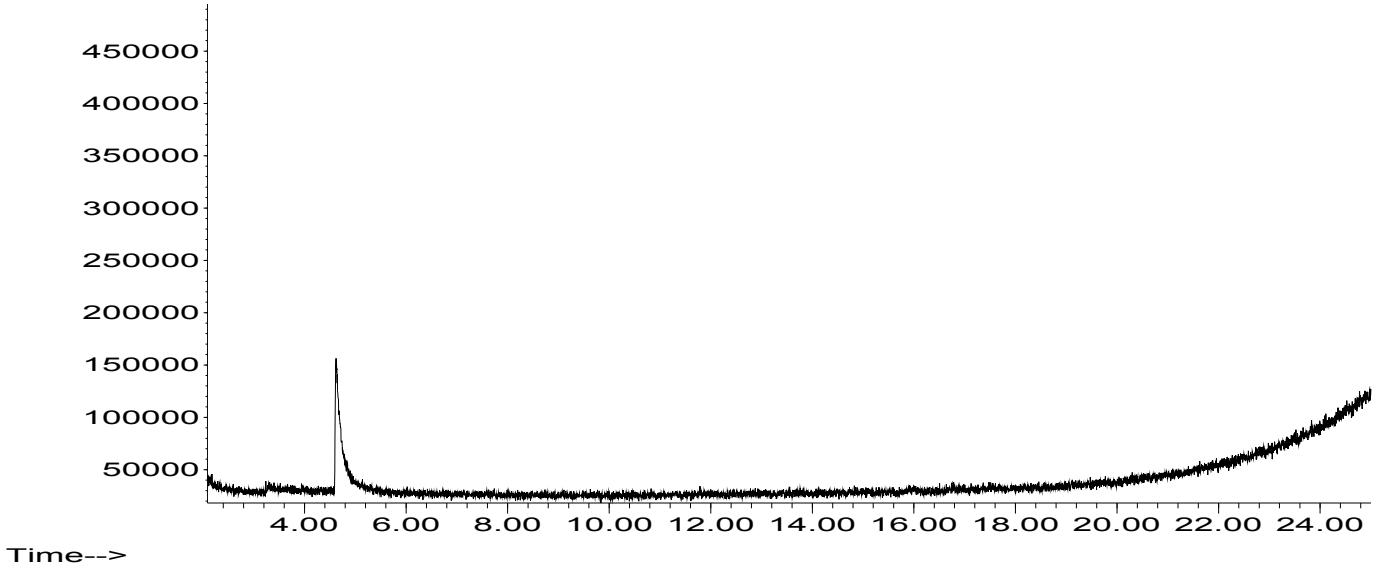

Figure 6.53: GC-MS Chromatogram for Phenol Oxidation in Presence of CN^- and S^{2-} at 90 minutes

- **(4.8 minutes)** phenol

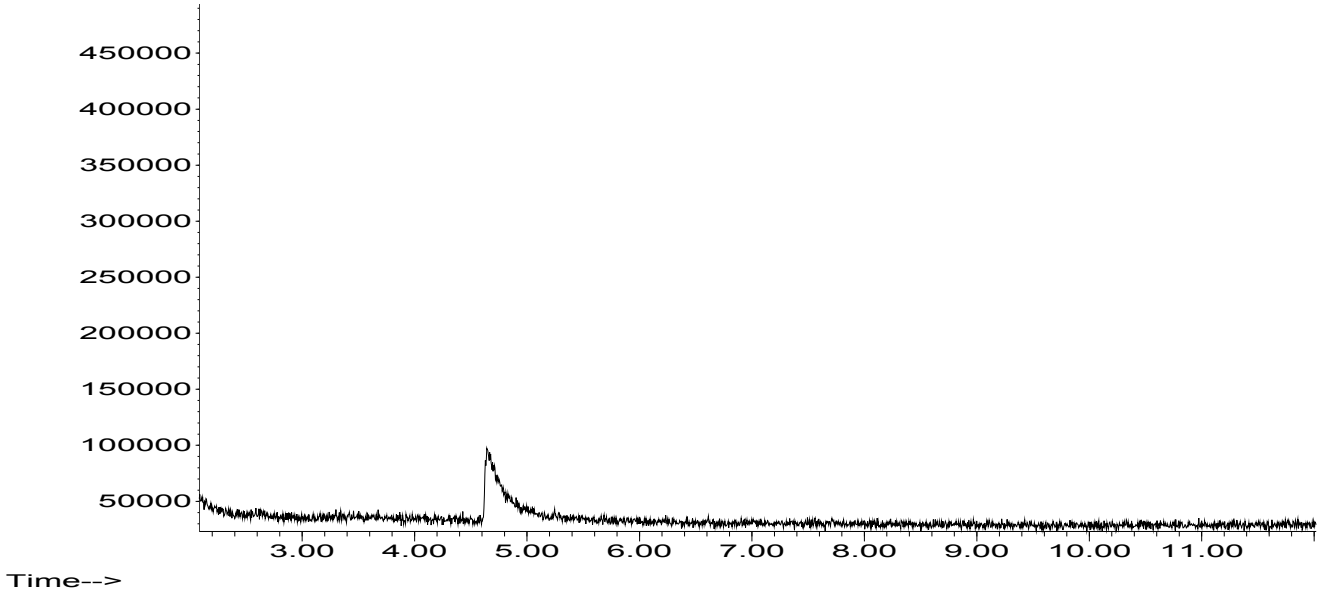

Figure 6.54: GC-MS Chromatogram for Phenol Oxidation in Presence of CN^- and S^{2-} at 120 minutes

- **(4.8 minutes)** phenol

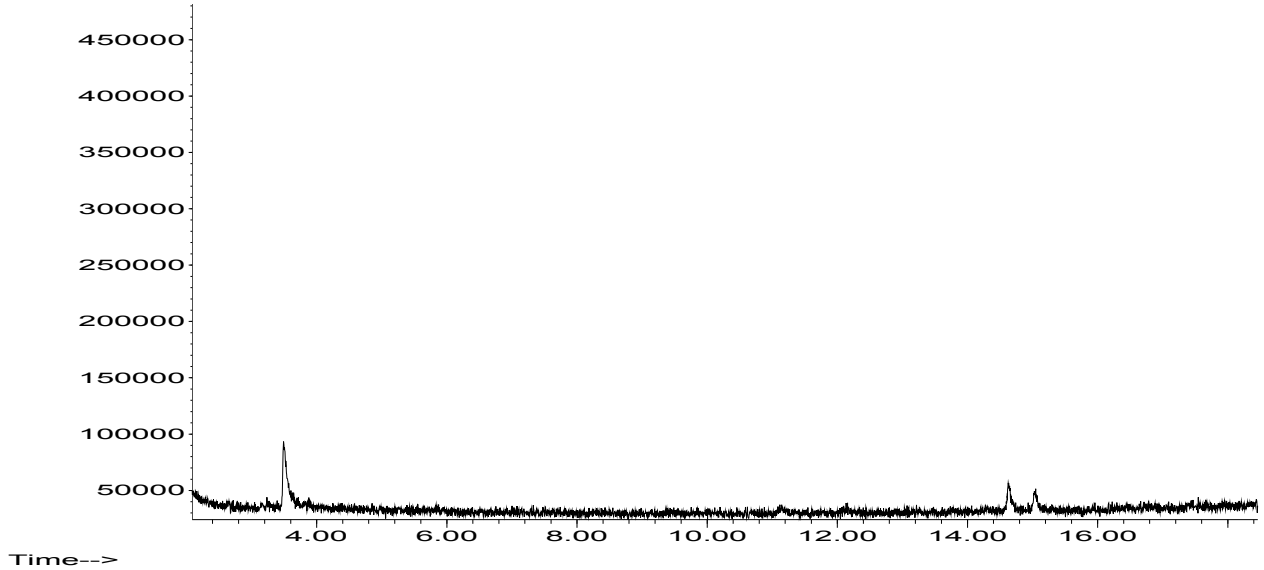

Figure 6.55: GC-MS Chromatogram for Phenol Oxidation in Presence of CN^- and S^{2-} at 210 minutes

- **(3.845 minutes)** Butanedioic acid, phenyl
- **(14.63 minutes) (1)**.Butanoic acid, 2-benzyl-3-{[benzyloxy)carbonyl]amino}-, methyl ester, **(2).**Carbamic acid, N-(3-methylphenyl)-, benzyl ester, and **(3)**-Propenoic acid, 3-[(phenylmethyl)thio]-, methyl ester
- **(15.44 minutes**) Paracyclophane

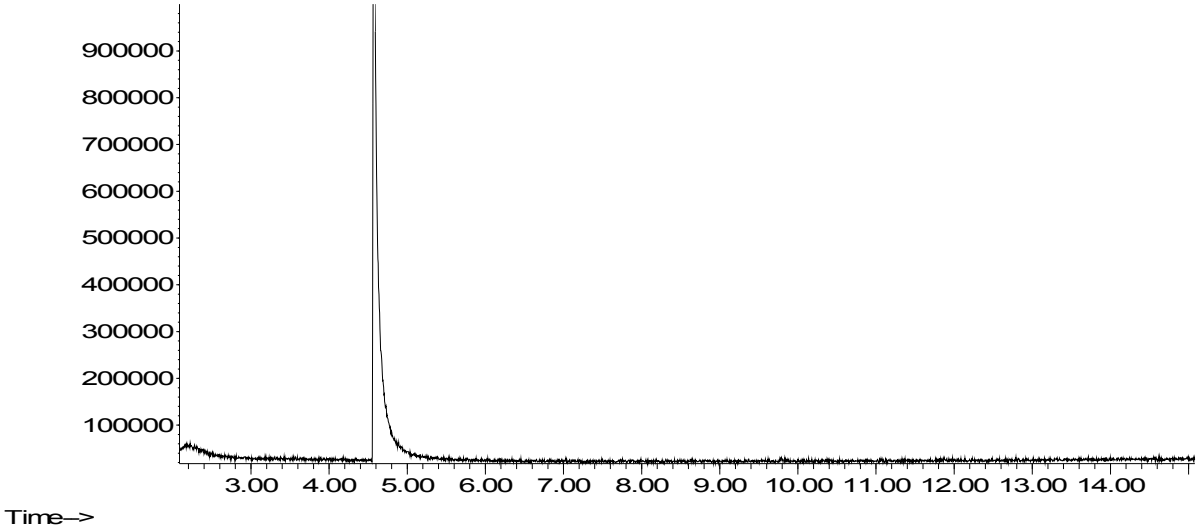

Figure 6.56: GC-MS Chromatogram for Phenol Oxidation in Presence of NH_4^+, CN^- and S^{2-} at 30 minutes

- **(5.37 minutes)** phenol

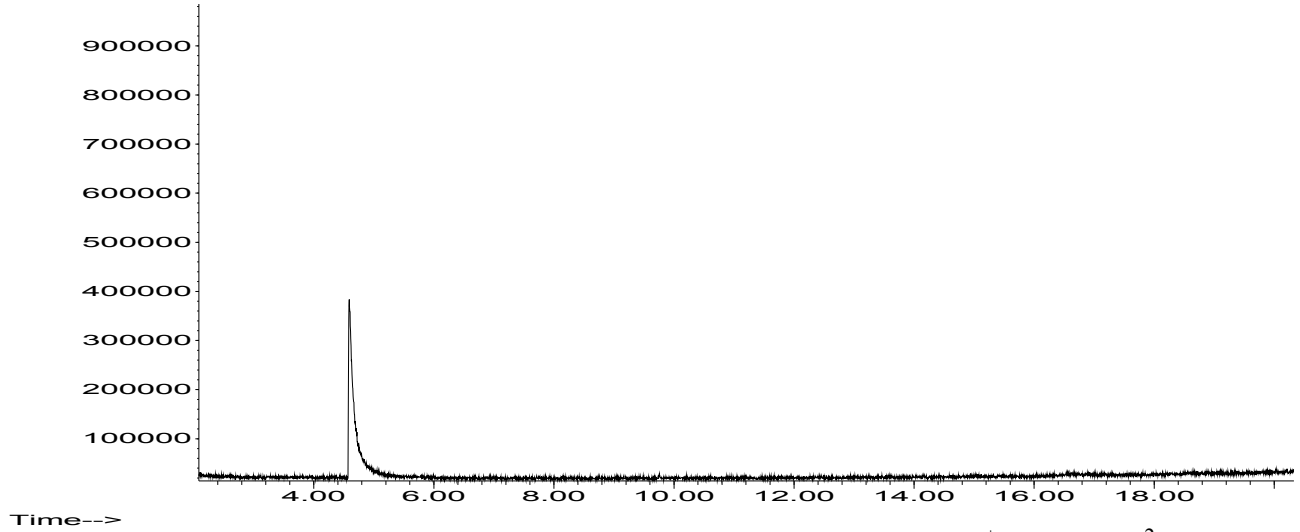

Figure 6.57: GC-MS Chromatogram for Phenol Oxidation in Presence of NH_4^+, CN^- and S^{2-} at 60 minutes

- **(5.37 minutes)** phenol

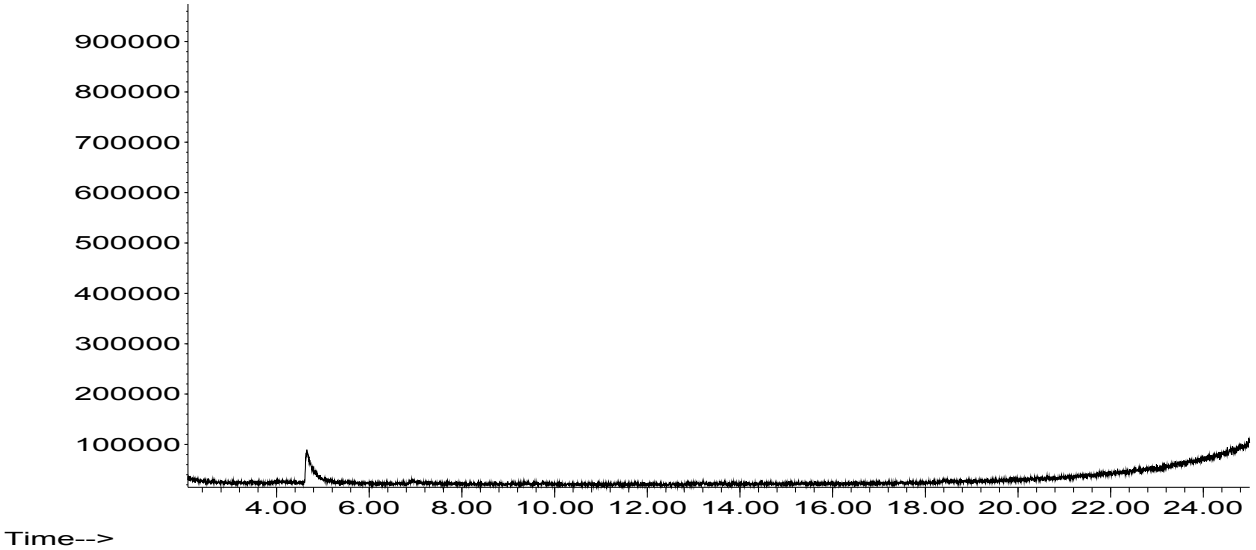

Figure 6.58: GC-MS Chromatogram for Phenol Oxidation in Presence of NH_4^+, CN^- and S^{2-} at 90 minutes

- **(5.37 minutes)** phenol

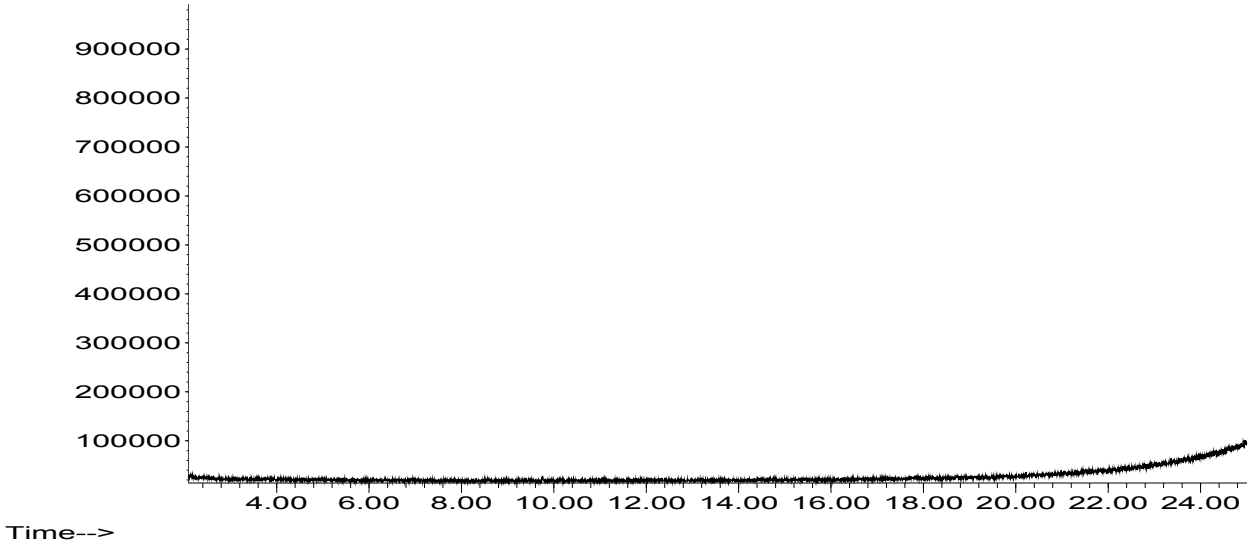

Figure 6.59: GC-MS Chromatogram for Phenol Oxidation in Presence of NH_4^+, CN^- and S^{2-} at 180 minute

6.7.3 Pathways for Phenol Oxidation in Different Mix Matrixes

The dominant oxidation mechanism involved in this study for the oxidation of phenol was the direct oxidation on surface of the BDD anode by electro-generated hydroxyl radicals. As anticipated, the presence of Na_2SO_4 supporting electrolyte didn't appear to have led to the production of effective in-situ oxidations (peroxoxisulphate, hydrogen peroxide etc) or hypochlorite (when NaCl electrolyte was used) which would have additionally mediated and catalyzed the oxidation process via indirect mechanism. Hence, destructive attack on phenol, its intermediates byproducts as well as the inorganic species was mainly by the $OH^{\bullet}$ radicals generated on the BDD (as the $OH^{\bullet}$, the only assumed effective oxidant, weakly interacted with the BDD anode). Based on the qualitative and quantitative byproducts analysis from the GC-MS and HPLC, it was concluded that oxidation of phenol was gradual with mass transport to the electrode surface been the rate-limiting step for the kinetically controlled process. Direct combustion of phenol to CO_2 rarely occurred, but rather, it was through succession of generation of intermediates byproducts prior to eventual complete oxidation to CO_2.

The byproducts distribution and the reaction pathways during electrochemical oxidation of phenols are known to be affected by the following factors (i.e., concentration of phenolic compounds, electrode material, pH, current density, potential, etc). For the present study, the foregoing analyses confirmed that initial phenol concentration and pH were the main controllers of the likely pathway(s) followed during the oxidation of phenol. Consequently, the primary stage in the oxidation of phenol was mainly pH-dependent as the speciation of the phenol molecules took place with respect to its inherent pK_a in pure water solution.

As shown in Figure 6.60, for initial pH < pK_a, oxidation of phenol was initiated by phenol molecule losing an electron to produce phenoxonium cation which kinetically favored the oxidation pathway A1→A2→A3→A4→A5 to be followed until steady state of complete oxidation was achieved. This pathway averted polymerization from occurring. It was speculated that hydroxylation (chemical process that introduces one or more hydroxyl group ($OH^{\bullet}$) into a compound or radical) of phenolic ring of the phenoxonium cation (→A2) was responsible for the formation of the catechol, resorcinol and hydroquinone compounds which were further converted to benzoquinone (→A3) (Cui et al., 2009; Murugananthan et al., 2008); all these compounds were well detected (HPLC peaks and also GS-MS mass spectrums consistently showed species at m/e = 110 and m/e=108). Other investigators earlier suggested that only hydroquinone could be expected from the phenol hydroxylation (Canizares et al., 2005c; Murugananthan et al., 2008). However, the assertion by this authors was not the case in this study owing to the fact that hydroquinone wasn't the only expected phenol hydroxylation products that was found. Subsequently, the hydroxylated compounds were further oxidized to form quinone compound by dehydrogenation reaction with $OH^{\bullet}$ radicals (Canizares et al., 2005c; Murugananthan et al., 2008). Consequently, the entire generated phenolic ring molecules were further oxidized and converted to ring cleavage small fragmented products via aromatic ring openings which eventually gave short chain aliphatic acids (maleic, fumaric, oxalic, acetic and formic acid) (→A4) by the $OH^{\bullet}$ attack (Canizares et al., 2005c). Though, not all the formations of these aliphatic acids specifically were not readily identified, but it can be easily understood that, that was the predominant case bearing in mind that some aliphatic acids appeared to be the most probable identifiable compounds in the GC-MS qualitative analyses; and also the pH decay during the galvanostatic electrolysis as observed earlier (Figure 4.1B).

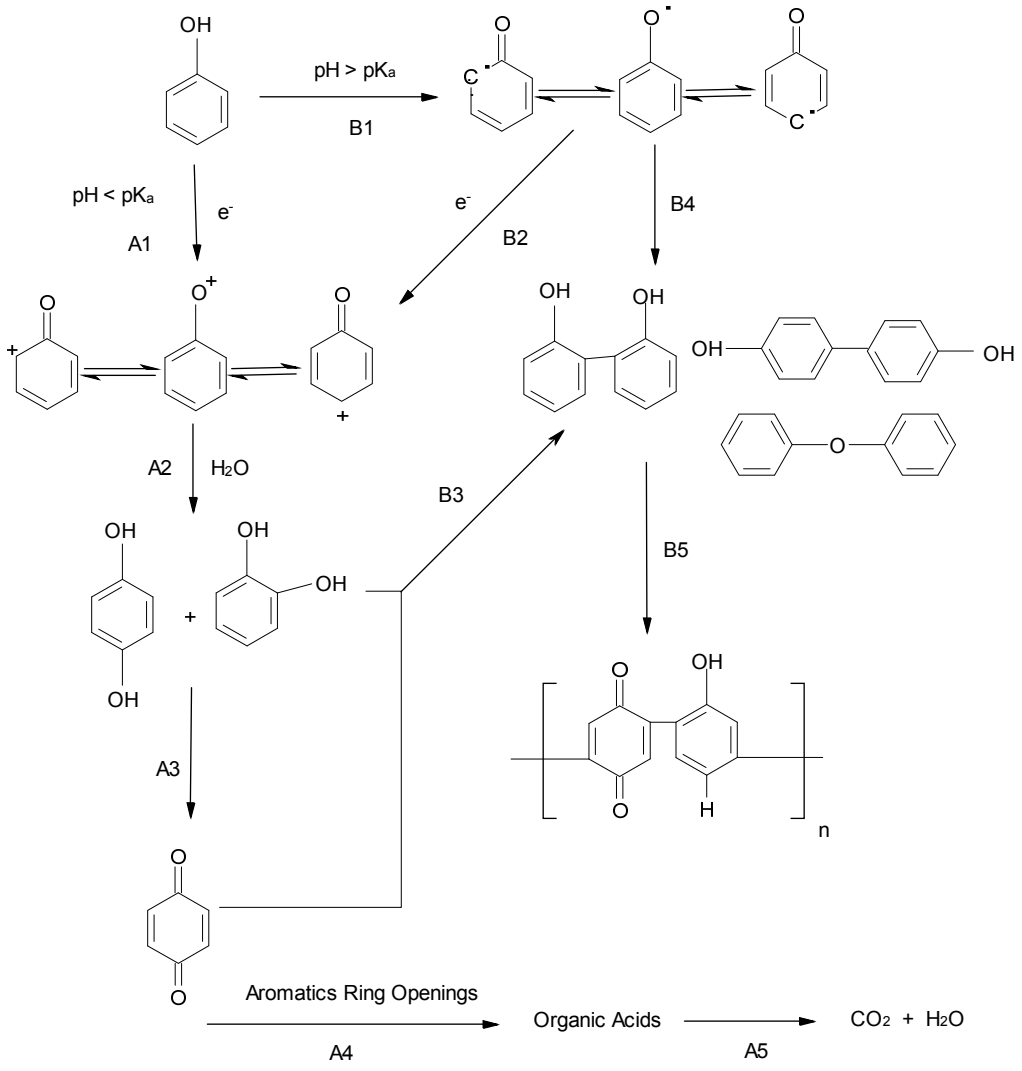

Figure 6.60: Proposed Pathways for Phenol Oxidation

In addition, it was experimentally proven by other authors (Canizares et al., 2005c; Murugananthan et al., 2008), that aliphatic acids are formed in the final step prior to CO_2 conversion when phenolic compounds undergo electrochemical oxidation process. Based on the GC-MS recovery data with the support of the HPLC analysis, it was concluded that the inability to identify all the expected aliphatic acids could be attributed to the presence of the inorganic species and/or their oxidation intermediaries that perhaps hindered their effective extraction. The opening of the aromatic ring and succeeding aliphatic compound generation was generally considered to be the limiting step for the successful completion of mineralization process of phenol to CO_2. Hence, the final step in the pathway involved destruction of the short chain aliphatic acids to CO_2 (→A5) thereby resulting in a complete oxidation of phenol which was evidently suggested by the several profiles of phenol removal vis-à-vis TOC, COD and percent composition of generated byproducts presented earlier. Moreover, there was no substantial information based on the presented data herein suggesting that the different compositions of the inorganic species in the different mix matrixes would have severely altered this proposed phenol oxidation pathway in anyway.

However, for initial pH greater than phenol pK_a, two possible initial phenol concentration dependent pathways were postulated with both routes mediated by phenoxy radical formation (→B1) as phenate anion (produced by speciation of phenol) loses an electron. At higher initial concentrations, the phenoxy radical undergoes a second electron transfer leading to the formation of phenoxonium cation which also predominantly continues the kinetically control pathway B2→A2→A3→A4→A5 with minor possibility of following neither A2→B3→B4→A5 nor A2→A3→B3→B5; the possible polymerization routes. However, at lower initial phenol concentration, substantial data presented earlier substantiate the

hypothesis that the pathway followed inherently support polymerization rather than oxidation of phenol. Consequently, in this case, the phenoxy radical capable of reacting with either the parent phenol molecule or another generated radical by C–C and/or C–O coupling mediated the generation of dimmers (→B4) which eventually lead to formation of more complex polymers (→B5) by further coupling reactions as reported by other authors (Noureddine et al., 2009; Noureddine and André, 2009; Wang et al., 1998). Therefore, the prevailing proposed oxidation reaction pathway in this case follows that route B1→B4→B5, thereby leading to total hindrance of phenol oxidation.

6.8 Kinetics of Inorganic Species Removal in the Different Mix Matrixes

Analyses for cohabiting inorganic species residual concentrations in samples during the different mix matrixes experiments revealed good removal efficiencies for cyanide and sulfide ions. However, for ammonium ions, ISE readings consistently showed that the ammonium was either degraded below the ISE detection limit (i.e., 0.000001 ppm) in very short period of time (less than 30 minutes) or else there were severe interferences due to the presence of SO_4^{2-} in solution that hindered its effective measurements. However, as standard procedure for removing sulfate ions inference were strictly adhered in order to avert negative effects of interference, it appeared that the removal of ammonia was very fast. The fact that Krishnan et al (Krishnan et al., 2006) completely removed 60 ppm NH_3-N in simulated wastewater within 20 minutes of electrolysis using graphite anode and stainless steel cathode while operating at 75 $mAcm^{-2}$ could support the idea that the ammonium ions were all removed below ISE detectable limit in less than 30 minutes (with the more active BDD used in this study). Therefore, the results obtained here could imply that the degradation rate of ammonium ions

to be much higher compared to results reported by other authors using Ti/IrO_2 anode (Liu et al., 2009b) despite NH_3-N was cohabited by other competing ions in solution.

In light of the NH_4^+ speciation chemistry, aqueous NH_4^+ dissociates to give two species according to Equation 6.6:

$$NH_4^+ + H_2O \rightarrow NH_3 + H_3O^+ \quad pK_a(NH_4^+) = 9.246 \qquad 6.6$$

Hence, the concentration of ammonia in molecular form (NH_3) and that of ammonia in ionic form (NH_4^+) are approximately equal at pH 9.3 while at pH 7.0, NH_4^+ was the predominant component (99.5%) in the solution. Therefore, the amount of ammonia in molecular form rises rapidly once the solution becomes basic. Ammonia removal by hydroxyl radical was found to be accelerated with increase in pH suggesting that molecular ammonia compared to NH_4^+ was more easily oxidized by $OH^\bullet$ (Li Huang, 2008). Consequently, as all experiments were ran at initial pH 5 and the pH kept decaying with time, NH_4^+ was continuously the predominant species; suggesting that the good removal of the NH_4^+ could be due to the conversion of NH_4^+ to other byproducts rather than its complete oxidation to N_2. NH_4^+ can be completely oxidized to nitrate via formation of intermediary oxidation to nitrite according to Equations 6.7 to 6.11. The attack by $OH^\bullet$ radicals were expected to oxidize ammonia to amine radical ($^\bullet NH_2$), further oxidation of this radical would generate amine compounds $^\bullet NHOH$ and NH_2O_2 in sequence and afterward, the unstable $NH_2O_2^-$ splits to nitrite (NO_2^-) which could be oxidized to nitrate (NO_3^-) before eventually oxidizing to the final byproduct, N_2 (Li Huang, 2008).

$$NH_4^+ + 2OH^\bullet \rightarrow {}^\bullet NH_2 + 2H_2O \quad 6.7$$

$${}^\bullet NH_2 + H_2O_2 \rightarrow {}^\bullet NHOH + H_2O \quad 6.8$$

$${}^\bullet NH_2 + {}^\bullet OH \rightarrow NH_2OH \text{ (Hydroxylamine)} \quad 6.9$$

$$NH_4^+ + 1.5O_2 \rightarrow NO_2^- + 2H^+ + H_2O \quad 6.10$$

$$NO_2^- + 0.5O_2 \rightarrow NO_3 \quad 6.11$$

For BDD1, the various removal trends for cyanide in different mix matrixes presented in Figure 6.61B reveal that high removals of 99.9, 99.99, 99.97 and 97.58% were achieved for CN^-, respectively. While for BDD2 (Figure 6.61A), 88.6%, 93.4%, 83.46% and 84.21% CN^- removal were obtained for the final effluent in the binary, two ternaries and the quaternary mix matrixes, respectively. The highest removal of 93.4% was observed in the ternary mixture with NH_4^+ which improved slightly over the binary mixture of CN^- and phenol.

The reaction mechanism for cyanide oxidation was believed to depend on the concentration of hydroxyl ions (the key mediator) as indicated by other authors and was effectively achievable at alkaline pH (Ogtveren et al., 1999). They found that the oxidation of cyanide to follow direct oxidation via cyanate formation, which subsequently underwent combustion to produce CO_2 and N_2 as final products according to Equations 6.12 and 6.13, respectively.

$$CN^- + 2OH^- \rightarrow CNO^- + H_2O + 2\bar{e} \quad 6.12$$

$$CNO^- + 2OH^- \rightarrow CO_2 + 1/2N_2 + H_2O + 3\bar{e} \quad 6.13$$

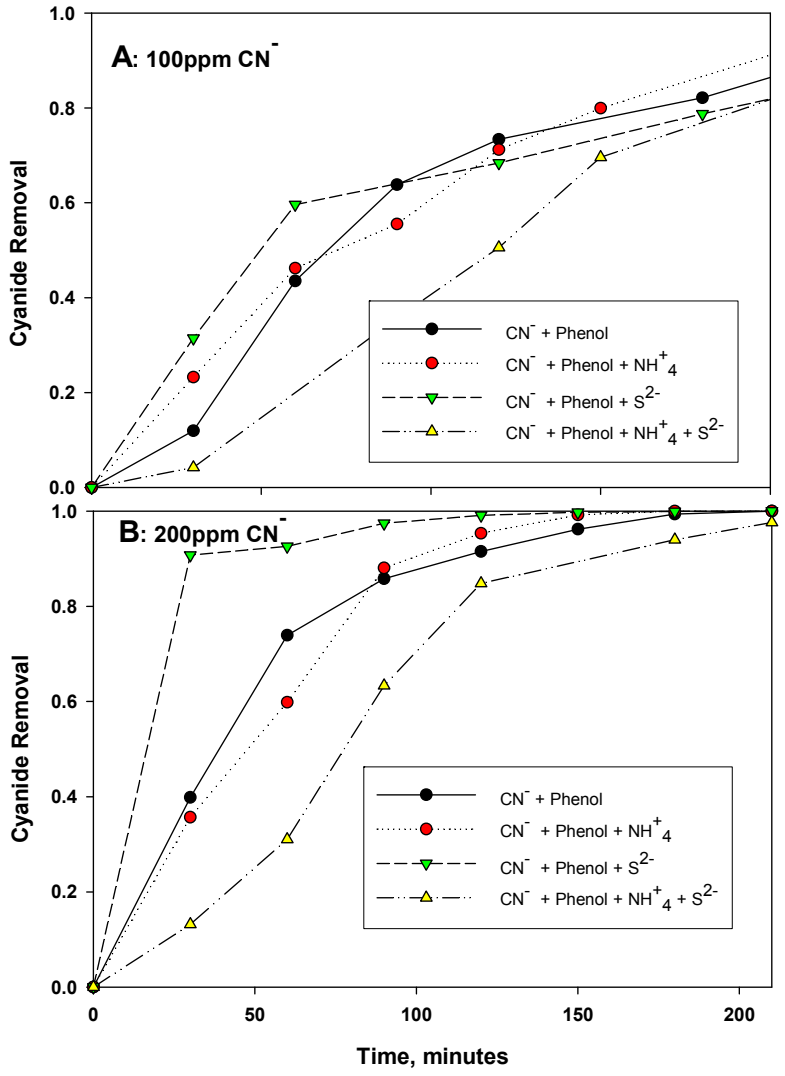

Figure 6.61: Cyanide Removal Profiles for Different Mix Matrixes

Similarly, the fact that the initial pH during all electrolysis in the different mix matrixes was set at 5 and that the constant pH decay experienced revealed that most of the free cyanide were in the molecular form i.e., HCN (pK_a = 9.2). Nonetheless, the removal of the total CN^- was comparable with results reported by Canizares et al. (2005a). However, within the designed retention time of 3.5 hours, the overall trends in the COD elimination suggest that complete simultaneous oxidations of CN^- and the other inorganic species were not feasible for all the different mix matrixes.

Sulfide ions removal efficiencies were much better than that of CN^- with 100% removal for all the different mix matrixes for both BDD1 and BDD2 (Figures 6.62B and 6.62A, respectively). In fact, in all the different circumstances, reduction below threshold limit was achievable in less than 120 and 60 minutes for the two different BDD2 and BDD1, respectively. The S^{-2} removal data presented here go in line with the data presented by Katie and co-researchers (Katie et al., 2007) that used also BDD anode with graphite cathode (as the case of this study). They also reported very excellent removal of higher concentration S^{-2} within 15 minutes of electrolysis. Moreover, the good removal of S^{2-} may provide an explanation for the leading negative consequences the presence of the S^{2-} was observed to have on phenol removal. It was speculated that the S^{2-} has more affinity towards the electro-generated oxidants responsible for the oxidation than phenol and the other inorganic species, thereby; the sulfide ion competitively consumed more of the oxidants (once in solution). This could have let to the lowering of the phenol removal. In addition to that, for the NH_4^+, as the results here revealed the possibility of comparatively faster removal rate than that of CN^- and S^{2-}, it may be assumed that NH_4^+ has lesser negative impact on competing with phenol in reacting with the electro generated oxidants, and hence the reason for the best removal efficiencies observed in mix matrixes containing NH_4^+.

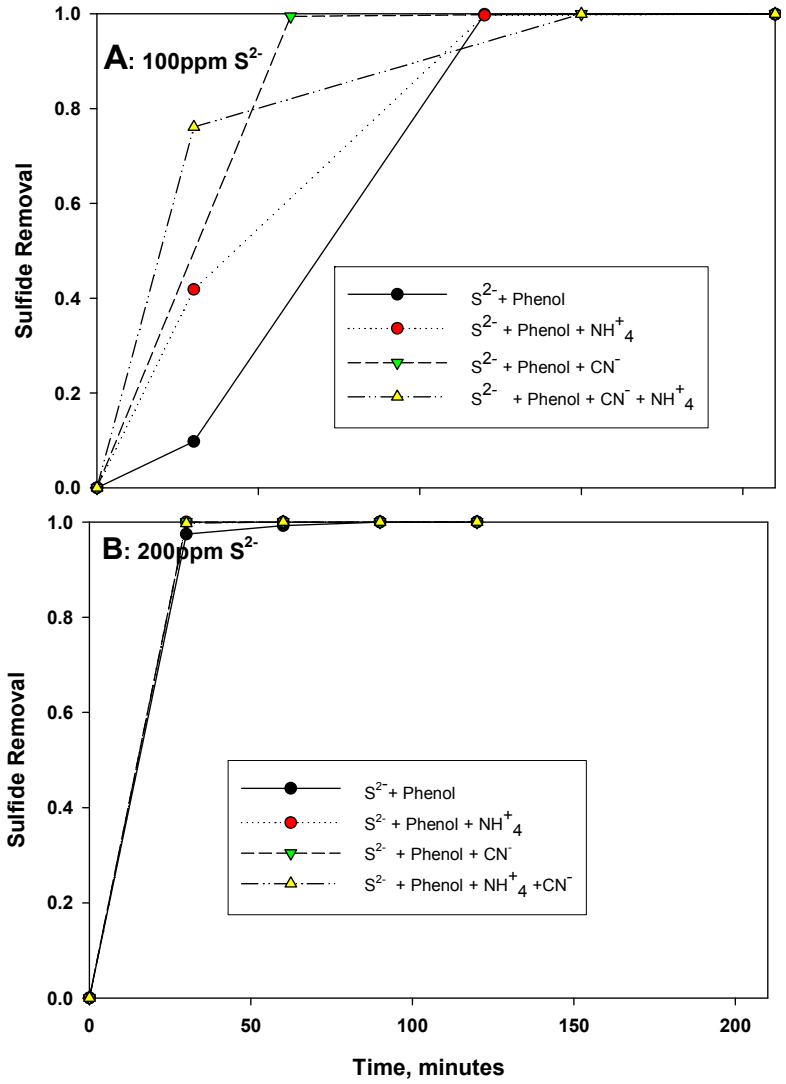

Figure 6.62: Sulfide Removal Profiles for Different Mix Matrixes

Since both phenol and the inorganic species exert oxygen demand, the COD removal profile is capable of providing the relevant and sufficient information to evaluate the extent of the electrochemical oxidation of all the species in solution collectively. It can be inferred from the reduction in COD already observed earlier that both phenol and the inorganic species (including NH_4^+) were partially oxidized during the treatment process. However, the lower COD removal encountered that increases with COD_0 is an indicative that inorganic ions were partially oxidized to other species that exert lesser oxygen demand.

Degradation kinetics of the cohabiting inorganic species was studied using SIGMAPLOT regression tool from which the best fitted models were identified. Similarly, as in the case of phenol, the best fitted models for cyanide and sulfide showed that there exists good linearity between $\ln(C/C_0)$ and the treatment time; i.e., a pseudo-first-order reaction kinetic also as the was case for phenol, TOC and COD. Hence, initial concentration of the species in solution influenced the decay patterns; the higher the initial concentration, the faster the rate of oxidation and/or disappearance of the species was expected. For ammonia, though a specific model a number of researchers such as Liu and co-investigators (Li and Liu, 2009; Liu et al., 2009b) corroborated that the degradation of ammonia follows zero-order kinetics. However, due to fast disappearances of NH_4^+ encountered in this study, specific model couldn't be ascribed to the removal of ammonia in the presence of phenol and the other inorganic species.

Despite the presence of phenol and the reduced activity of the BDD2, the decay constant for degradation of 100 ppm cyanide (k = 10 x 10^{-3} min^{-1}) obtained here was in close agreement with that reported by Canizares et al (2005a). In the case of BDD1, the remarkable increase in the k–value to 37 x 10^{-3} min^{-1} could be jointly attributed to increase in concentration to 200 ppm and better activity of the BDD1 compared to BDD2. For the higher mix matrixes, as high

as *k*-value of 46 x 10^{-3} min^{-1} was estimated due to significant improvement in the CN^- removal rates. On the other hand, sulfide degradation *k*-values ranges between 37-59 x 10^3 min^{-1} for the lower initial concentration despite the nature of the BDD2, while the decay constants were not estimable for the higher concentrations due to the swift disappearance of sulfide ion as observed earlier. For cyanide and sulfide, the binary decay rates also decreased to a lesser degree in the presence of other species in the higher mix matrixes. Similarly, the half-life ($t_{1/2}$) which is inversely proportional to the decay rate underscored the fact that sulfide possessing the highest decay rates, could be removed completely within shorter duration compared to the longer period of time required for the removal of phenol and cyanide.

6.9 Current Efficiency and Energy Consumptions in the Different Mix Matrixes

The ACE and SEC for phenol and COD removal for the different mix matrixes experiments were also approximated using Equations 5.1, 5.15 and 5.16, respectively.

6.9.1 Average Current Efficiency

The decay of the ACE with specific charge passed is perceivable due to the exponential behavior of degradation COD with time of electrolysis, showing the undesirability of longer electrolysis in this regard. Under all the different mix matrixes, there exist tremendous ACE improvements as result of presence of the inorganic species. As previously established in the case of single phenol matrixes, this was attributed to the increase in the amount of COD removed which was directly proportional to the COD_0. This fact is very clear by comparing the percent increase in the ACE for BDD1 and BDD2 as well as the differences between the

ACEs for the binary and higher mix matrixes cases as illustrated in Figure 6.63. For the binary mix matrixes, the ACE ranges between 44.34 - 58.75% and 29.53 - 34.0% resulting in 132 - 207% and 54.6 -71.3% increase in the ACE for the BDD1 and BDD2, respectively. On the other hand, for the ternary and quaternary cases, the ACE considerably were in the range of 58.88 - 79.26% and 48.25 - 54.37% thereby resulting in percent increase of 208 – 314.9% and 78.52 –131.3% for the BDD1 and BDD2, respectively.

6.9.2 Phenol Removal Specific Energy Consumption

The profiles for variation of SEC for phenol removal with respect to specific charge passed for the binary and higher mix matrixes generally revealed a strict linear relationship. It can be seen from Figure 6.64 that the change in the SEC was greatly influenced by the degree of the mix matrix as well as the nature of the BDD anodes. While this figure reveals that higher energy was consumed in phenol removal for BDD2, in contrast, for BDD1, a different picture could be deduced. For the binary mix matrixes, the estimated SEC was ranging between 359.97 - 398.5 kWh/kg-phenol and 460.9 - 626.1 kWh/kg-phenol which correspond to 7 - 45% decrease and 0.209 - 50.245% increase for the BDD1 and BDD2, respectively. On the other hand, for the ternary and quaternary cases, the SEC was estimated to be in the range of 244.9–363.9 kWh/kg-phenol and 428.6- 607.2 kWh/kg-phenol corresponding to 7.2 - 16.25% decrease and 17.7 - 42.98 increase, respectively. The reason for the estimated values of SEC for the different mix matrixes to show consistent deviations from 429.5kWh/kg-phenol for the single matrix could be attributed to the trends of phenol removal as observed earlier in this chapter.

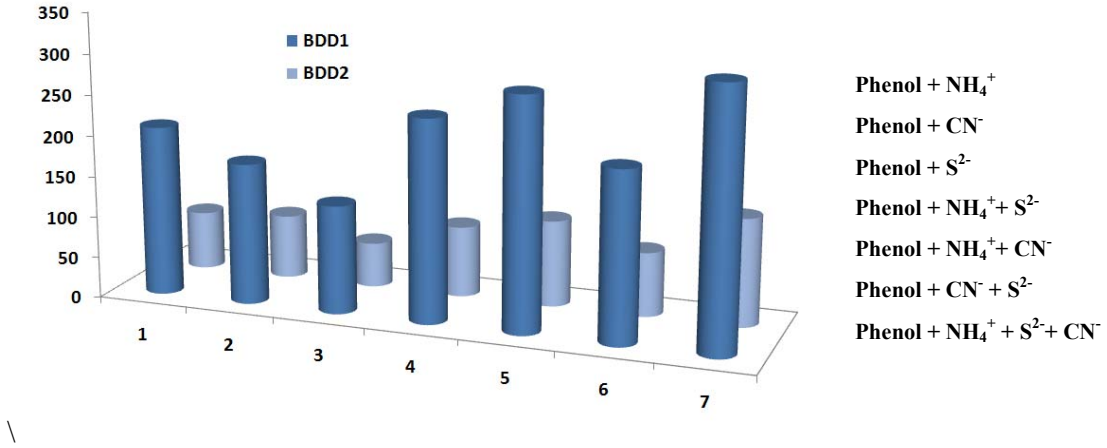

\

Figure 6.63: Percent Increase in Average Current Efficiency for the Different Mix Matrixes

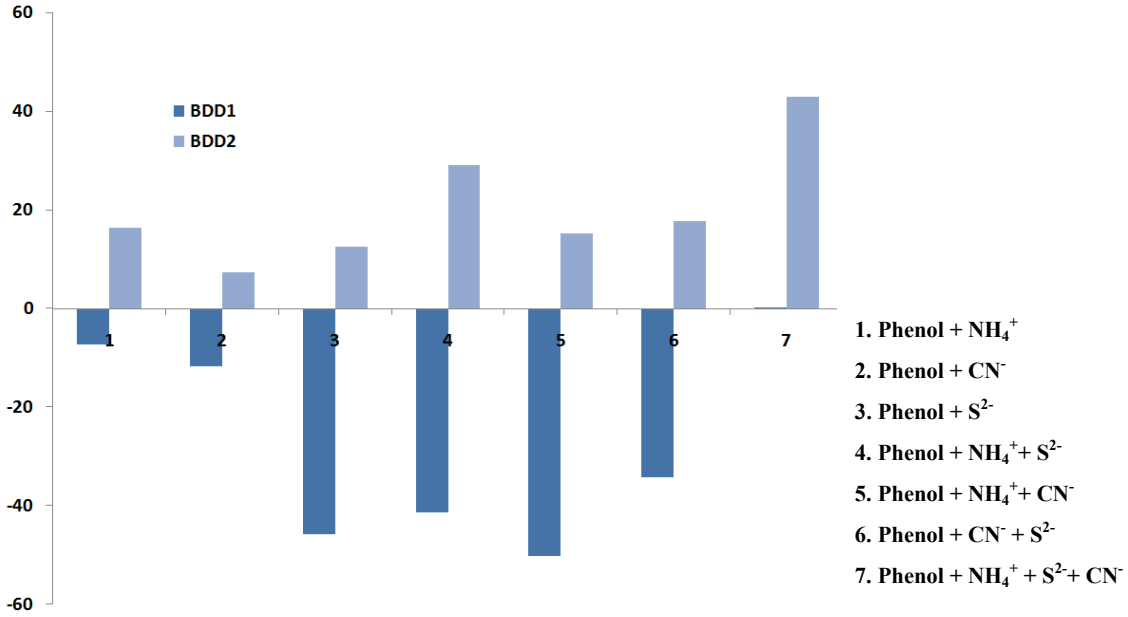

Figure 6.64: Percent Change in Phenol Removal Specific Energy Consumption for the Different Mix Matrixes

6.9.3 COD Removal Specific Energy Consumption

Similarly, SEC for COD removal increases with supplied electric charge during electrolysis. However, in this case, lower energy was consumed per gram of COD removed as compared with that dissipated in removing corresponding gram of phenol. Moreover, in this case, regardless of the nature of the species in the mix matrixes and the BDD anode used, the SEC generally dropped due to the presence of the inorganic species. The percent change (decrease in all the different mix cases) in SEC for the binary and higher mix matrixes are plotted in Figure 6.65. For the binary mix matrixes, the SEC dropped from 57.0 kWh/kg-COD to between 15.096 - 20.62 kWh/kg-COD and 31.84 - 40.23 kWh/kg-COD for BDD1 and BDD2, respectively. While for the ternary and quaternary cases, the SEC was estimated to range between 7.83-15.24 kWh/kg-COD and 21.59-33.10kWh/kg-COD, respectively. Hence, the corresponding percent decrease in SEC for COD removal could be estimated as 63.2 - 73.5% and 29.42 - 44.14% for the former case, while for the later cases was 73.26 - 86.3% and 41.9 - 62.12%, respectively. The reason for the estimated values of SEC for the different combinations of the species in solution to show consistent decrease from that of the single matrix could be attributed to the corresponding COD removal. This could be also explained by the earlier observation of increase in rate of COD removal with COD_0 under fixed experimental condition, and hence the much lower SEC when the inorganic ions cohabited phenol is solution. In view of that, the SEC decreases proportionally with increase in COD_0. Table provided in APPENDIX C summarizes the maximum attainable ACE and the specific energies required for the different simulated wastewaters at the end of the design retention time of 3.5 hours.

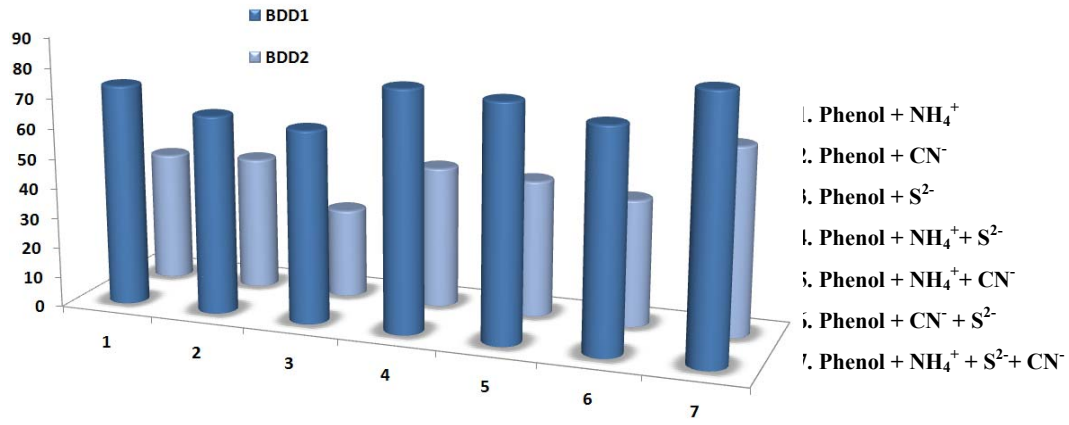

Figure 6.65: Percent Decrease in COD Removal Specific Energy Consumption for the Different Mix matrixes

Chapter 7

RSM Modeling and Optimization of Electrochemical Oxidation of Phenol on BDD Anode

Response Surface Methodology (RSM), a collection of statistical and mathematical techniques is popularly used for designing, developing, improving and optimizing processes. The most critical aspect of this approach is the selection of independent variables affecting a given system under study and delineating the experimental region of interest according to the objective of the study and the experience of the researcher. After defining and designating clearly the region of interest, the technique usually contains three stages: (i) the choice of the experimental design and carrying out the experiments according to the selected experimental matrix (ii) response surface modeling of the obtained experimental data through regression and (iii) optimization; obtaining the optimum location within the specified region of interest (Myers and Montgomery, 1995). The main advantage of RSM is the reduced number of costly experimental trials and data points needed to evaluate the effect of multiple parameters and their interaction effects on certain response of interest (Lee et al., 2000)

Application of RSM technique has recently became an attractive aproach for effective electrochemical processess for wastewater treatment scheme (Chatzisymeon et al., 2009; Deligiorgi et al., 2008; Güven et al., 2008, 2009; Rajkumar et al., 2005). Currently, available literature suggests that modeling elecrochemical oxidation of phenol on BDD anode using RSM technique was unprecedentent. Therefore, the aim of this section was to model and optimize the process for electrochemical oxidation of phenol on BDD anode via the RSM

design. This technique was adopted in order develope 3D-models that could provide better insight into the complex attractions of the experimental parameters. Also it was also employed in order to check the reproducibity of the data obtained at different experimental conditions in the previous sections (Chapter Three). Hence, a means to sustantiate the fact that the variation of the experimental data were not as result of experimental errors. For variations due to a given parameter, analysis of variance (ANOVA) was invoked from which the null hypothesis was tested againt the alternate hypothesis using *F*-value and *p*-value tests as detailed in sections to follow.

Thirty (30) extra experiments were conducted from which about sixty samples (some in duplicates) were drawn for the purpose of the RSM design. The independent variables considered to be affecting electrochemical treatment process as widely reported by number of authors are current density, initial pH, electrolyte concentration and treatment time (Chatzisymeon et al., 2009; Güven et al., 2008). The modeled response surfaces (i.e., the dependent variables) that can collectively indicate the degree of efficiency towards electrochemical oxidation of phenol considered for optimizing the process were classified into two categories. First, are the treatment indicators which include residual concentrations of phenol, TOC and COD. The second category comprises of the performance indicators, namely, percent byproducts generated, average current efficiency (ACE) and specific energy consumption (SEC).

7.1 Factorial Experimental Design and Models Fitting

7.1.1 Central Composite Design (CDD) for Second-Order Model Design

Face Centered Central Composite Design (FC-CCD) technique was used for the RSM design to thoroughly evaluate the effects of the independent variables on target responses and to

optimize the process. This experimental design technique, a second order factorial design, is suitable for (i) exploration of quadratic response surfaces (ii) construction of second order polynomial models (iii) catering for curvature (i.e. non-linear nature of response surface) in the response function which cannot be achieved in the first-order statistical design approaches (Myers and Montgomery, 1995). The design consists of replicated central points and a set of points lying at the each edge of the multidimensional cube that defines the region of interest. As the FC-CCD design is an orthogonal design, the factor levels are evenly spaced and coded (for statistical calculations conveniences) for the low, medium (central point) and high levels as −1, 0 and +1 respectively (Table 7.1). The coding was according to the relationship in Equation 7.1.

$$x_i = \frac{X_i - \left(X_{high} + X_{low}\right)/2}{\left(X_{high} - X_{low}\right)/2} \tag{7.1}$$

where x_i is the new coded value. X_i represents the value of a given parameter (low, medium or high), while X_{low} and X_{high} are the high and levels of the parameter.

The behavior of the mathematical response system was explained by the following general quadratic function given in Equation 7.2:

$$y = \beta_0 + \sum_{i=1}^{k} \beta_i x_i + \sum_{i=1}^{k} \beta_{ii} x_i^2 + \sum_{i=1}^{k-1} \sum_{j=2}^{k} \beta_{ij} x_i x_j + \varepsilon \tag{7.2}$$

where y is the predicted response, β_o the constant coefficient, β_i the linear coefficients, β_{ij} the interaction coefficients, β_{ii} the quadratic coefficients, x_i and x_j are the coded values of the independent variable variables (as detailed in Table 7.1) and ε is the statistical error term.

The 2^4 full factorial design experimental runs were supplemented with other necessary runs in order to acquire the required complete FC-CDD runs. The total calculated number of experiments runs for four factors design were thirty (30) runs i.e., from $2^k + 2k + 6$, where k is the number of factors. Hence, the runs composed of sixteen (16) detailed full factorial experimental runs at the cube edges augmented with eight (8) "nominal" axial (or star) runs and six (6) "nominal" replicated central runs making the required total runs for acquiring the data for the RSM modeling and optimization. The centre points are introduced and replicated to enable the model to statistically determine the experimental error (i.e., pure error) and the reproducibility of the data. The factorial runs and the nominal augmented runs were split into three (3) blocks in a randomized order (as required in many design procedures) to ensure blockage of any unnoticeable nuisance so as to minimize unavoidable errors in the data collection. For a three parameters experimental design, Figure 7.1 illustrated a cube for the FC-CDD. Details of the experimental design and data for the various response of interest are provided in Tables 7.1 and 7.2.

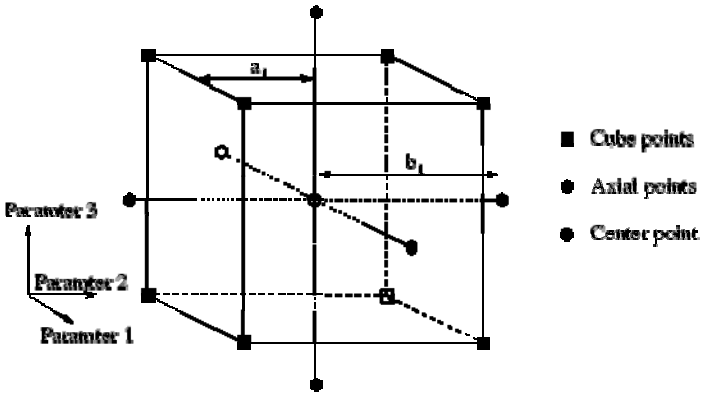

Figure 7.1: Faced Centered Central Composite Experimental Design

Table 7.1: Independent variables and their levels Used for the Central Composite Design

Independent variable	**Range and level**		
	-1	0	+1
x_1 (Current Density, $mAcm^{-2}$)	30	45	60
x_2 (Initial pH)	2	7	12
x_3 (Electrolyte Concentration, ppm)	1000	3000	5000
x_4 (Treatment time, minutes)	30	120	210

Table 7.2: Experimental Design and Data for 2^4 Central Composite Designs (CDD)

Standard Order	Run Order	Block	Coded Independent Variables				Residual Concentration, ppm		
			x_1	x_2	x_3	x_4	Phenol	TOC	COD
1	20	Block 2	-1	-1	-1	-1	71.3104	62.6117	199.3259
2	5	Block 1	1	-1	-1	-1	65.9866	57.4527	135.9873
3	2	Block 1	-1	1	-1	-1	58.633	75.6	224
4	17	Block 2	1	1	-1	-1	47.8529	75.6052	205.2692
5	8	Block 1	-1	-1	1	-1	76.5824	63.2305	216.6422
6	18	Block 2	1	-1	1	-1	66.916	58.876	214.2159
7	13	Block 2	-1	1	1	-1	75.494	79.467	225.9497
8	6	Block 1	1	1	1	-1	69.6453	81.36459	234
9	1	Block 1	-1	-1	-1	1	0.2703	14.3889	55.3824
10	16	Block 2	1	-1	-1	1	2.3082	16.5751	0
11	14	Block 2	-1	1	-1	1	2.5225	76.6	200
12	9	Block 1	1	1	-1	1	0.0856	84.0962	132
13	11	Block 2	-1	-1	1	1	9.929	15.7228	107.539
15	3	Block 1	-1	1	1	1	5.3222	9.3458	62.1944
16	12	Block 2	1	1	1	1	6.9438	76.62	199
17	7	Block 1	0	0	0	0	0	72.43229	200
18	10	Block 1	0	0	0	0	16.063	25.5575	69.0769
19	15	Block 2	0	0	0	0	0.5219	10.0756	43.1479
20	19	Block 2	0	0	0	0	20.4105	21.196	115.3993
21	23	Block 3	-1	0	0	0	16.3327	77.6289	148.5254
22	25	Block 3	1	0	0	0	6.1947	11.5485	52.2794
23	24	Block 3	0	-1	0	0	14.1559	20.4274	92.7104
24	26	Block 3	0	1	0	0	47.4225	56.1594	188.6047
25	28	Block 3	0	0	-1	0	0.8229	6.5178	37.5416
26	27	Block 3	0	0	1	0	7.5461	20.7959	96.7376
27	30	Block 3	0	0	0	-1	5.461	22.5	110
28	22	Block 3	0	0	0	1	10.6	14.87	77
29	29	Block 3	0	0	0	0	8.4	11.876	95.42
30	21	Block 3	0	0	0	0	11.45	26.86	65

7.1.2 Models' fitting and Statistical Analysis

Data obtained from the experimental runs were studied and interpreted by Design-Expert@ statistical software package version 7.0.b1.1 (STAT-EASE Inc., Minneapolis, USA 2004). The software uses the least square regression method for the estimation of coefficients in the approximating polynomial function (i.e., Equation 7.2) applying the coded values of the factor levels obtained from Equation 7.1 and also for evaluation of the statistical significance of the equations and the various parameters under study.

According to the sequential model sum of squares (SMSS), the response models were selected based on the highest-order polynomials where the additional terms were significant and the models were not aliased. Hence, as provided in Tables 7.3 and 7.4, for the various parameters of interest affecting the overall efficiency of the electrochemical oxidation of phenol, the quadratic model was the suggested model for all the parameters. However, the cubic model was aliased due to the fact that the CCD doesn't contains enough runs to support a cubic model (Montgomery, 1991; Myers and Montgomery, 1995). Therefore, based on the *p*-values < 0.05, the quadratic model was selected. As given in Equation 7.3, for each model, the robustness of the fits as well as the significance of a given effect (main, interaction or squared term) were assessed and evaluated based on either acceptance or rejection of the null hypothesis (H_o) against the alternate hypothesis (H_1) (also according to the criteria: *p*-value $\leq 0.05 = \alpha$). The model was reduced by dropping the parameters and/or their interactions that insignificantly affects the respective response.

Table 7.3: Statistic Summary for Phenol, TOC and COD Response Surface Models

Measured Parameter	Source	Std. Dev.	R^2	Adjusted R^2	Predicted R^2	PRESS	
	Linear	14.03953	0.779957	0.74475	0.688097	6984.85206	
Residual Phenol	2FI	15.86125	0.786553	0.674212	0.212616	17632.92735	
	Quadratic	4.766219	0.984784	0.970582	0.916985	1859.060077	Suggested
	Cubic	2.710285	0.997704	0.990488	0.952664	1060.047675	Aliased
	Linear	22.57969	0.467806	0.382655	0.225036	18560.41333	
Residual TOC	2FI	23.54786	0.560103	0.328579	-0.50087	35945.86008	
	Quadratic	7.026701	0.969077	0.940215	0.877091	2943.674819	Suggested
	Cubic	4.564538	0.99391	0.974772	0.980197	474.2942945	Aliased
	Linear	50.36692	0.542828	0.469681	0.322887	93931.77275	
Residual COD	2FI	51.57125	0.635735	0.444016	-0.26069	174887.6235	
	Quadratic	19.17389	0.960248	0.923146	0.847021	21221.90462	Suggested
	Cubic	19.61059	0.980594	0.919605	-0.73761	241047.7784	Aliased

Table 7.4: Statistic Summary for Percent Byproducts, Average Current Efficiency and Specific Energy Consumption Response Surface Models

Measured Parameter	Source	Std. Dev.	R^2	Adjusted R^2	Predicted R^2	PRESS	
% Byproducts	Linear	22.09202	0.700282	0.652327	0.581093	17053.58908	
	2FI	25.05903	0.706922	0.55267	0.013798	40148.03153	
	Quadratic	7.916548	0.976908	0.955355	0.906868	3791.38626	Suggested
	Cubic	5.908646	0.993997	0.97513	0.628561	15121.16881	Aliased
ACE	Linear	4.532739	0.574179	0.506048	0.379519	748.4507965	
	2FI	4.570299	0.67099	0.497828	0.02203	1179.668106	
	Quadratic	3.674061	0.832139	0.675469	0.295374	849.9491161	Suggested
	Cubic	3.590813	0.925175	0.690009	-1.80182	3379.667577	Aliased
SEC	Linear	249.3974	0.678721	0.627317	0.489039	2473031.488	
	2FI	208.3328	0.829617	0.739941	0.386149	2971013.214	
	Quadratic	168.911	0.911577	0.829049	0.467083	2579298.991	Suggested
	Cubic	137.9738	0.972467	0.885936	-1.44305	11824266.49	Aliased

$$H_o : \beta_1 = \beta_2 = \beta_3 = ...\beta_n = 0 \quad \text{For all n coefficients}$$

7.3

$$H_1 : \beta_i \neq 0 \quad \text{For at least one coefficient}$$

The respective reduced response surface empirical models in terms of coded factors are written in Equations 7.4 to 7.9 (i.e., y_1 to y_6) for phenol, TOC, COD, percent byproducts generated, ACE and SEC respectively. Positive and negative coefficients in the response functions indicate a synergistic and antagonistic effect between the corresponding independent variable and the response, respectively. The relative contribution of a given factor in the models could be directly evaluated according to the values of its respective coefficients. The qualities of the models developed were evaluated based on the correlation coefficients values provided in Tables 7.3 and 7.4. Detailed ANOVA for the phenol, TOC, COD, ACE, SEC and percent byproducts generated are presented in Tables 7.5 to 7.10, respectively.

The R^2 of 0.979 for the residual phenol response surface model (Table 7.3) was good, while the predicted-R^2 of 0.958 was in reasonable agreement with the adjusted- R^2 of 0.972 suggesting a high quality model. This means that 97.90% of the total variation in the residual phenol could be attributed to the experimental variables studied and that there was approximately 0.5% chance that the variation of the surface was due to noise, indicating that the prediction values for the response would be within 95% confidence limit. The standard deviation for the model was 4.64. As the closer the R^2 value to unity and the smaller the standard deviation, the better the model will be as it will give predicted values closer to the actual values for a given response. The lack of fit test (LOF) *F*-value of 2.69 implies that LOF is insignificance relative to the pure error (as desired) and that there is 5.12% chance that a LOF F-value this large could be due to noise. Also the adequate precision which measures the

signal to noise ratio was measured as 36.212 (> 4 is desirable) implies an adequate signal, thereby indicating predictions from the developed model was reasonable and hence can be used to navigate the design space (Ahmadi et al., 2005; Anderson and Whitcomb, 2005)

$$y_1 = 8.309 - 3.283x_1 - 2.306x_2 + 3.873x_3 - 30.646x_4 + 10.442x_2^2 + 16.193x_4^2 \quad 7.4$$

$$y_2 = +18.762 + 21.111x_2 - 13.23x_4 + 11.49x_2x_4 + 30.35x_2^2 + 12.28x_4^2 \quad 7.5$$

$$y_3 = +79.295 - 15.01x_1 + 36.78x_2 + 19.33x_3 - 47.24x_4 + 10.42x_1x_3 - 23.927x_2x_4 + 51.481x_2^2 + 32.591x_4^2 \quad 7.6$$

$$y_4 = +20.067 + 39.32x_2 - 5.85x_4 + 36.46x_2^2 + 10.43x_4^2 \quad 7.7$$

$$y_5 = +14.509 - 4.69x_2 - 2.68x_3 - 2.93x_4 - 5.56x_2^2 \quad 7.8$$

$$y_6 = +498.206 + 241.18x_1 + 167.03x_2 - 168.31x_3 + 260.97x_4 + 107.95x_1x_4 + 116.46x_2x_4 - 94.62x_3x_4 + 284.78x_3^2 \quad 7.9$$

Similarly, considering the quadratic response surface models, for TOC, COD, and percent byproducts generated, the R^2 values of 0.9691, 0.96025 and 0.97691 are good while their respective predicted-R^2 were also in reasonable agreement with the adjusted-R^2 values as provided in Tables 7.3 and 7.4, respectively. Moreover, all other statistical model adequacy evaluations were found to be sound in similar fashion to that of phenol. These indicate that the models are of high integrity and are adequate for navigating the design surfaces for drawing credible inferences. Similar explanations could also be extended for adequacies of the ACE and SEC response surface developed according to the correlation statistics summary provided in Table 7.4. However, it is noteworthy to state that the fits for these two former parameters

are slightly lower in quality compared to those for the later four responses. Although, the R^2 values of 0.8322 and 0.9116 were not quite as desired; nonetheless, considering the insignificance nature of LOF (Tables 7.9 and 7.10) coupled with the adequate precision ratio of 9.358 and 15.635 (> 4 is desirable) indicate an adequate signal, respectively. Hence, these suggest that such model can provide an insight -to a greater extent- into the behavior of the response due independent variables changes and can be used to navigate and explore the design space (Ahmadi et al., 2005; Anderson and Whitcomb, 2005).

The credibility of the developed response models were further evaluated statistically through analysis of variance (ANOVA) at the 5% significance level as provided in the respective tables of the responses (Tables 7.5 to 7.10). The models' *F*-values of 69.34 (p-value < 0.0001), 33.58 (*p*-value < 0.0001), and 25.88 (*p*-value < 0.0001), 5.31(*p*-value < 0.0014), 11.05 (*p*-value < 0.0001 and 45.33 (*p*-value < 0.0001) for residual phenol, TOC and COD and ACE, SCE and percent generated byproducts, respectively, imply that all the models are statistically significant in their predictions. In similar fashion (i.e., based on the statistically significant *p*-values), all the investigated factors were found to be significant models terms in one way and/or the other by considering the different sources of the each model's variations either as a single (main), quadratic interaction or squared term effects as detailed in the respective tables. For instance, from the residual phenol ANOVA given in Table 7.5, based on the *p*-values of the linear and the quadratic terms, it can be concluded that all the main effects x_1, x_2, x_3 and x_4 and the two squared terms x_2^2 and x_4^2 were only the major significant model terms whereas all the cross-product contribution (i.e., interaction) effects x_1x_2, x_1x_3, x_2x_3 and x_3x_4 and the remaining squared effects x_1^2 and x_3^2 were all insignificant to the response. As x_3^2 and x_3x_4 show mild effects (least comparative *p*-values), they were removed in the reduced model.

Table 7.5: ANOVA for Reduced Response Surface Model (Top) Residual Phenol and (Bottom) Residual TOC

ANOVA Table for Residual Phenol [Partial sum of squares - Type III]						
Source	Sum of Squares	df	Mean Square	F Value	*p*-value Prob > F	
Model	21898.61	6	3649.768	169.3424	< 0.0001	significant
x_1	194.1087	1	194.1087	9.00628	0.0064	
x_2	95.79956	1	95.79956	4.44492	0.0461	
x_3	270.8582	1	270.8582	12.56731	0.0017	
x_4	16905.84	1	16905.84	784.3993	< 0.0001	
x_2^2	375.6175	1	375.6175	17.42795	0.0004	
x_4^2	903.2697	1	903.2697	41.91002	< 0.0001	
Residual	495.7097	23	21.5526			
Lack of Fit	449.2924	18	24.96069	2.688724	0.1388	not significant

ANOVA Table for Residual TOC [Partial sum of squares - Type III]						
Source	Sum of Squares	df	Mean Square	F -Value	*p*-value Prob >F	
Model	23041.32	5	4608.264	121.7097	< 0.0001	significant
x_2	8022.842	1	8022.842	211.8928	< 0.0001	
x_4	3148.693	1	3148.693	83.16071	< 0.0001	
x_2x_4	2112.551	1	2112.551	55.79498	< 0.0001	
x_2^2	2805.08	1	2805.08	74.08548	< 0.0001	
x_4^2	377.1115	1	377.1115	9.959961	0.0043	
Residual	908.7059	24	37.86275			
Lack of Fit	764.1658	19	40.21926	1.391284	0.3827	not significant

Table 7.6: ANOVA for Reduced Response Surface Model for (Top) Residual COD and (Bottom) Percent Byproducts Generated

ANOVA Table for Residual COD [Partial sum of squares - Type III]						
Source	Sum of Squares	df	Mean Square	F -Value	*p*-value Prob >F	
Model	130380.9	8	16297.61	41.02246	< 0.0001	significant
x_1	4053.043	1	4053.043	10.20185	0.0044	
x_2	24351.15	1	24351.15	61.29387	< 0.0001	
x_3	6728.286	1	6728.286	16.93566	0.0005	
x_4	40170.77	1	40170.77	101.1132	< 0.0001	
x_1x_3	1737.456	1	1737.456	4.373322	0.0488	
x_2x_4	9160.241	1	9160.241	23.05709	< 0.0001	
x_2^2	9128.806	1	9128.806	22.97797	< 0.0001	
x_4^2	3658.788	1	3658.788	9.209474	0.0063	
Residual	8342.989	21	397.2852			
Lack of Fit	7080.931	16	442.5582	1.753319	0.2782	not significant

ANOVA Table for Percent Byproducts Generated[Partial sum of squares - Type III]						
Source	Sum of Squares	df	Mean Square	F -Value	*p*-value Prob >F	
Model	39306.95	4	9826.736	175.1276	< 0.0001	significant
x_2	27827.93	1	27827.93	495.9366	< 0.0001	
x_4	615.0304	1	615.0304	10.96079	0.0028	
x_2^2	3815.506	1	3815.506	67.99818	< 0.0001	
x_4^2	181.0918	1	181.0918	3.227335	0.0845	
Residual	1402.797	25	56.11188			
Lack of Fit	1274.252	20	63.71259	2.47822	0.1594	not significant

Table 7.7: ANOVA for Reduced Response Surface Model for (Top) ACE and (Bottom) SEC

ANOVA Table for ACE [Partial sum of squares - Type III]						
Source	Sum of Squares	df	Mean Square	F -Value	*p*-value Prob >F	
Model	840.5893	4	210.1473	14.36796	< 0.0001	significant
x_2	395.8644	1	395.8644	27.0656	< 0.0001	
x_3	128.8241	1	128.8241	8.807816	0.0065	
x_4	155.0283	1	155.0283	10.59942	0.0032	
x_2^2	160.8725	1	160.8725	10.999	0.0028	
Residual	365.6527	25	14.62611			
Lack of Fit	301.4618	20	15.07309	1.174082	0.4703	not significant

ANOVA Table for SEC [Partial sum of squares - Type III]						
Source	Sum of Squares	df	Mean Square	F -Value	*p*-value Prob >F	
Model	4200884	8	525110.4	17.25503	< 0.0001	significant
x_1	1047007	1	1047007	34.40446	< 0.0001	
x_2	502186.5	1	502186.5	16.50175	0.0006	
x_3	509907.7	1	509907.7	16.75547	0.0005	
x_4	1225884	1	1225884	40.28233	< 0.0001	
x_1x_4	186437.9	1	186437.9	6.126316	0.0219	
x_2x_4	217000.3	1	217000.3	7.130589	0.0143	
x_3x_4	143252.4	1	143252.4	4.707247	0.0417	
x_3^2	369207.5	1	369207.5	12.13209	0.0022	
Residual	639078.5	21	30432.31			
Lack of Fit	583193	16	36449.56	3.261095	0.0982	not significant

Although all the independent variables individually have significant effects on removal of phenol, yet their various interactive effects are insignificant. Similar explanations can be extended for the rest of the models in accordance with their respective estimated *p*-values and reduced models (detailed ANOVA are provided in Tables 7.6 to 7.10, respectively). The reduced regression models clearly indicated that pH (x_2) and treatment time (x_4) are the major sources of curvature, while relative contributions of the main effects on the curvature follows the order $x_4 > x_2 > x_3 > x_1$.

7.2 RSM Models' Validations

The forgoing statistical analysis showed that the developed RSM models are statistically adequate to predict their respective responses (with high degree of accuracy) within the defined region of interest under study. Hence, the accuracies of the models' predictions were further validated within 95% confidence limit. The predicted values obtained were found to be closed to the experimental values within such confidence interval, particularly for residual phenol, TOC and COD and percent generated byproducts as depicted in Figures 7.2, 7.4, 5.6 and 5.8, respectively. However, for ACE and SEC, less predictions accuracies were visible as shown in Figures 7.10 and 7.12, respectively, though acceptable within 95% confidence interval. It can be observed from these later figures that more of the experimental data show wider dispersions from the prediction line, which is not the case compared to that of residual phenol, TOC, COD and percent byproducts generated. Nonetheless, the forgone statistical analysis and inferences underscore the fact that all the models developed are capable to a considerable extent in capturing the correlation between the operation variables and the environmental and performance parameters of concern herein. Similarly, the normal probability plots provided in Figures 7.3, 7.5, 7.7, 7.9, 7.11 and 7.13 reaffirm the credibility of

the models due to meeting the criteria for adequacy of the assumption of normality which served as their bases.

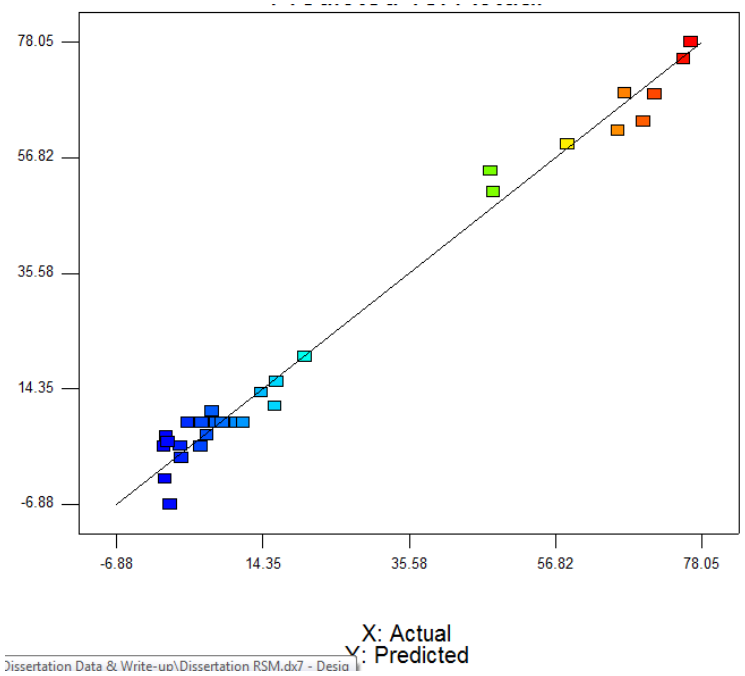

Figure 7.2: Residual Phenol Response Surface Model Validation; Actual vs Predicted

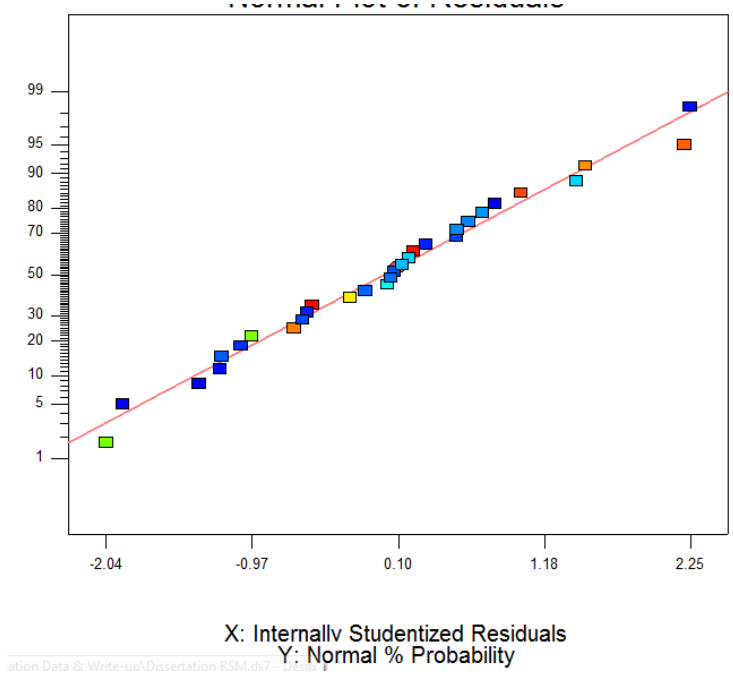

Figure 7.3: Residual Phenol Normal probability plot Diagnostics

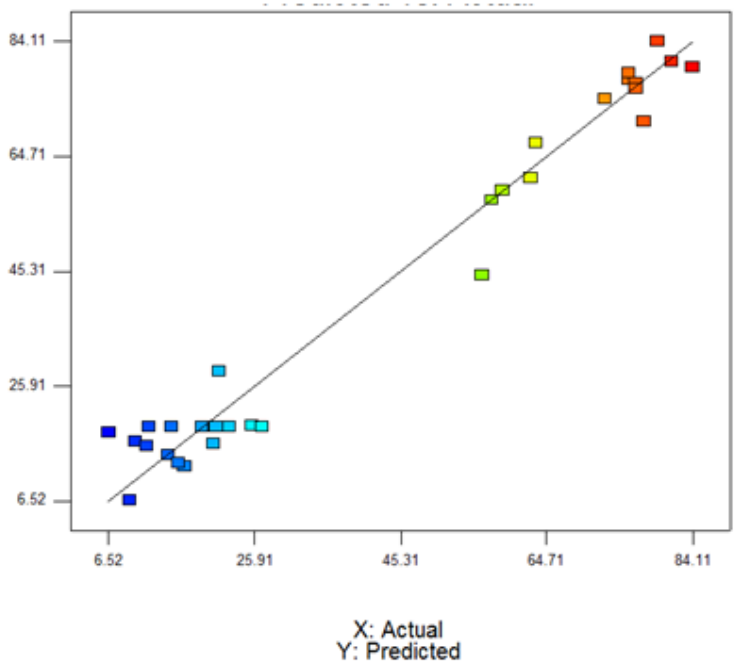

Figure 7.4: TOC Response Surface Model Validation; Actual vs Predicted

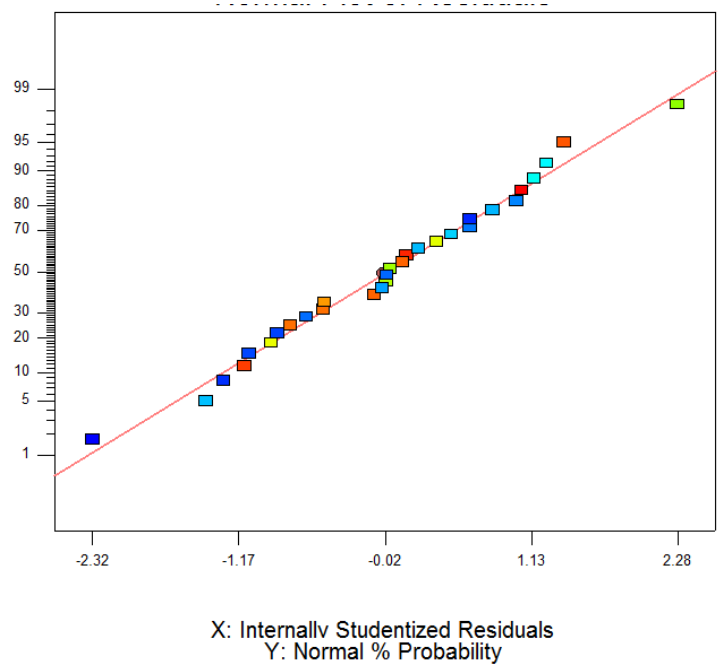

Figure 7.5: Residual TOC Normal probability plot Diagnostics

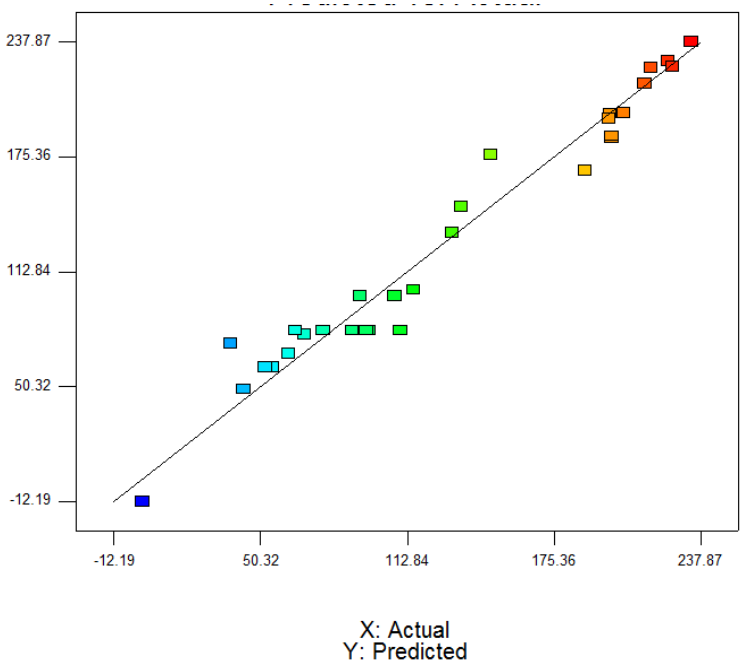

Figure 7.6: COD Response Surface Model Validation: Actual vs Predicted

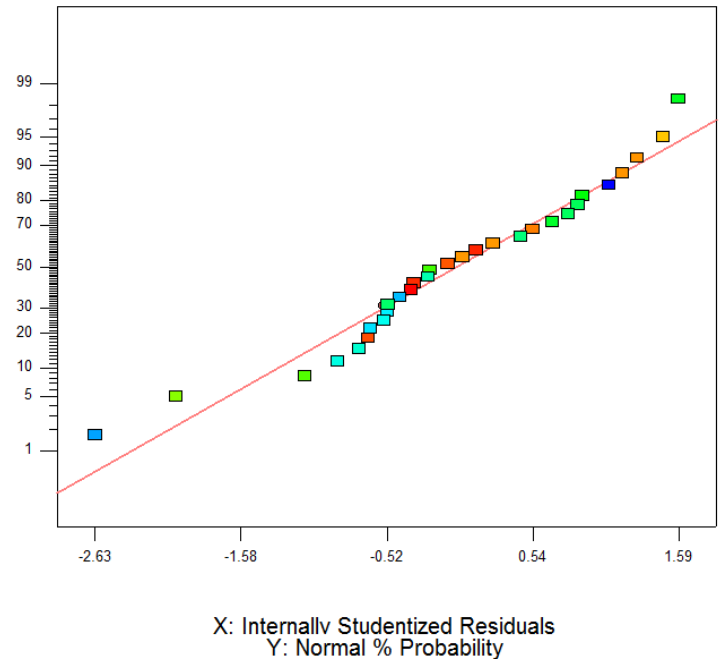

Figure 7.7: Residual COD Normal probability plot Diagnostics

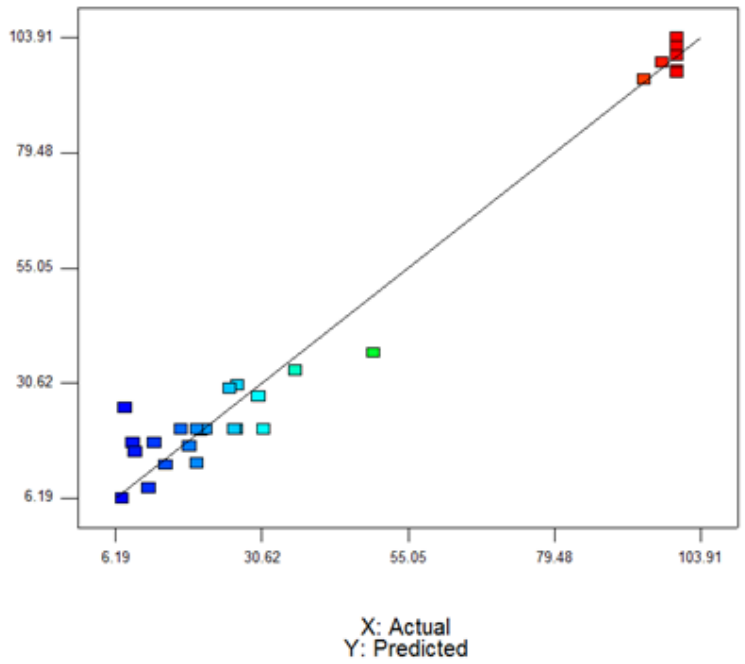

Figure 7.8 Byproducts Response Surface Model Validation: Actual vs Predicted

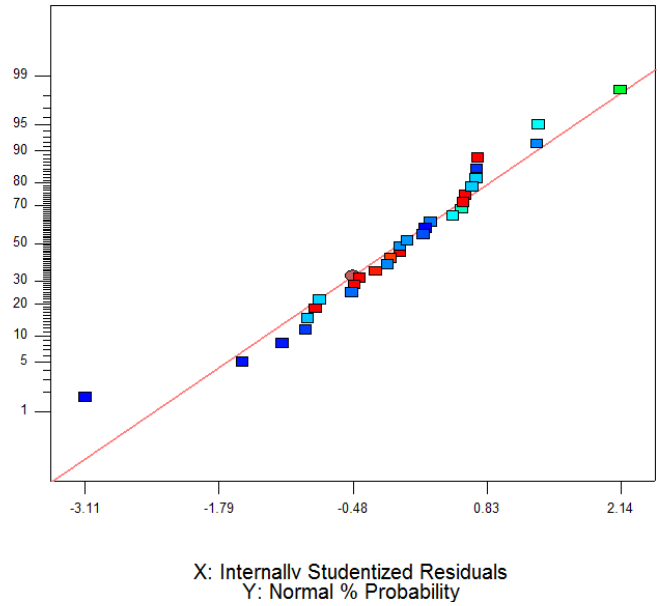

Figure 7.9 Byproducts Normal probability plot Diagnostics

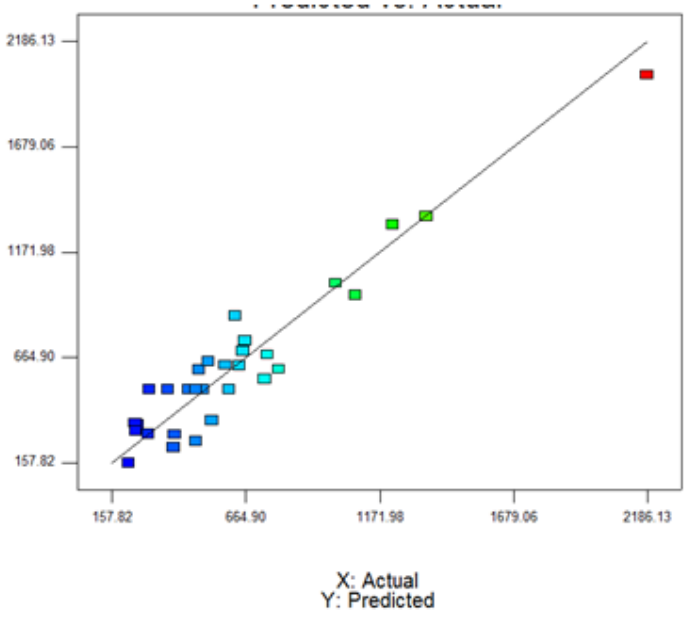

Figure 7.10: SEC Response Surface Model Validation: Actual vs Predicted

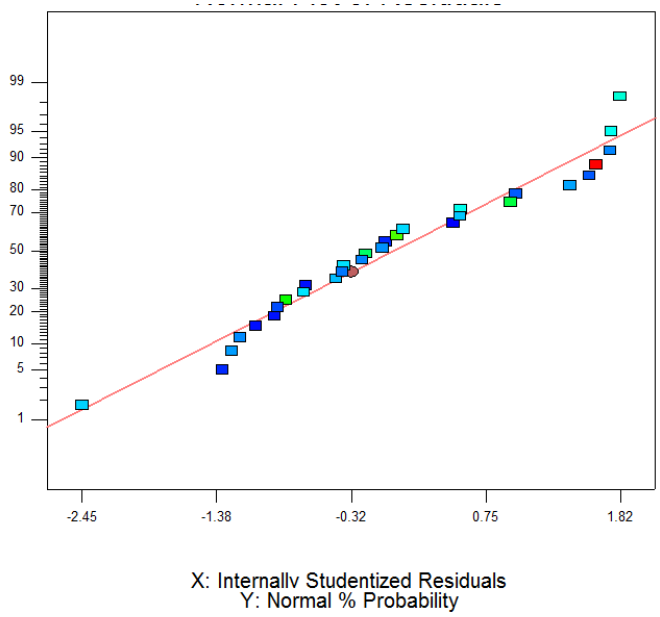

Figure 7.11: SEC Normal probability plot Diagnostics

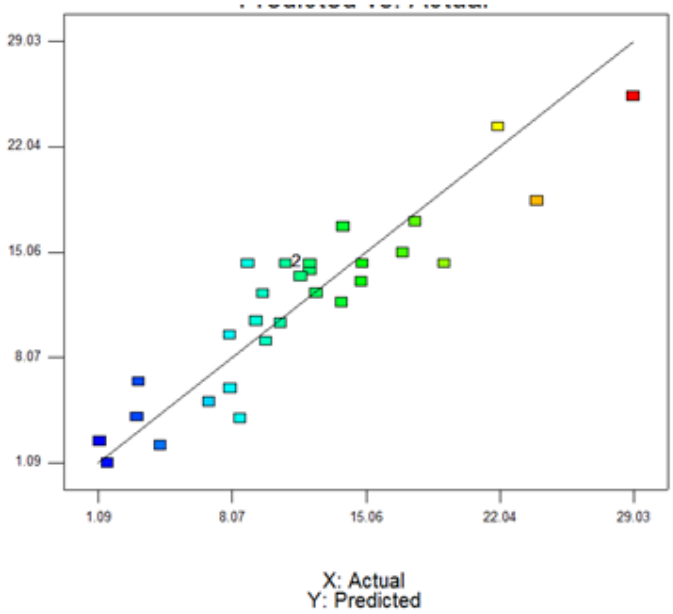

Figure 7.12: Average Current Efficiency Response Surface Model Validation: Actual vs Predicted

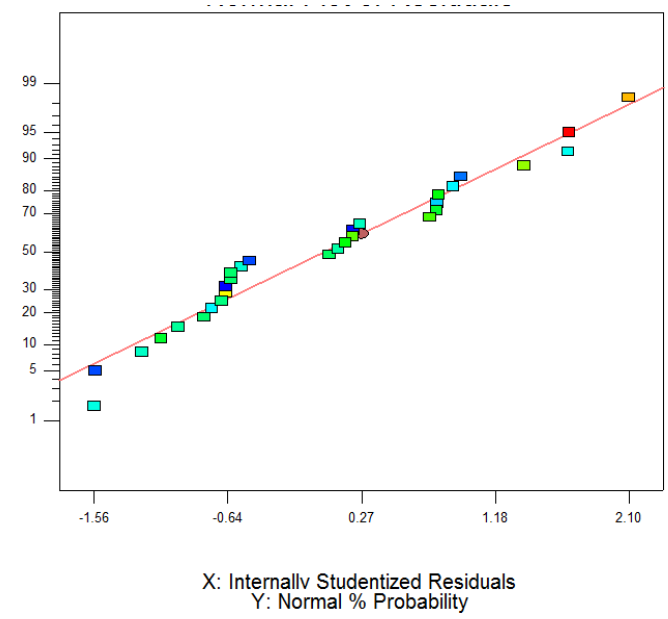

Figure 7.13: Average Current Efficiency COD Normal probability plot Diagnostics

7.3 Response Surface and Contour Plots for Second-order Models

Three-dimensional 3D-plots for the measured responses and their corresponding contour maps were constructed based on the response surface equations (Equations 7.4 to 7.9) to assess, visualize and further understand the change of the response surface with changes in the independent variables in a more detailed perspective. The two factor response plots and contour maps for phenol, TOC and COD are displayed in Figures 7.14 to 7.25. Because higher relative contributions of treatment time on all the various responses, time as an independent variable was excluded in the analysis. Taking into consideration that as current density was estimated to be significant parameter mainly influencing residual phenol, COD and SEC, extra plots were provided for these dependent variables showing the curvature as result of the applied current density's variation.

Evidently, navigating through the surface and contour plots corroborated the observations made earlier in Chapter Five regarding the influence of the various operating parameters on the removal efficiencies of the phenol, TOC, COD, percent byproducts generation, ACE and SEC. However, these generated 3D-plots expanded the scope of the previous analysis by widening the superficial and incomplete visualization of the 2D-relationships (between the dependent and the independent variables). Figures 7.14 to 7.16 show the dependency of y_1 (residual phenol) on variables x_1, x_2 and x_3. The plots show a strong degree of curvature of the 3D surface with variation in pH levels assuming a downward plateau shape. Phenol removal increases with increasing in pH reaching the least value in the region around the pH central point (i.e., pH 7). Thereafter, the removal continuously decreases at similar rate until the highest pH level (pH 12) was reached (Figure 5.14). Meanwhile, Figures 7.15 and 7.16 show that phenol removal increases linearly with decrease in electrolyte and slightly improves with

increasing in the current density. The reduced models' ANOVA analysis revealed that the dependency of TOC and byproduct generated was only significantly influence by initial pH to extend that the effects of other factors (x_1 and x_3) were notably dwarfed. Plots provided in Figure 7.17 reveal the pH variation with TOC and electrolyte concentration; a clear indication of observation deduced from the response model (y_2). In contrast to TOC, considering residual COD (y_3), all the independent variables were found to be significant with some interaction effects and initial pH being the major source of curvature (as depicted in Figures 7.18, 7.19 and 7.20). It can be seen that the residual COD decreases with both increases in pH and electrolyte concentration, while there was less appreciable increment due to decrease in current density (lesser value of coefficient in y_3) on the COD residuals. Meanwhile, Figures 7.21 and 7.22 clearly indicate that the percent byproducts generated is essentially pH defendant as the influence of current density and electrolyte concentration are rendered completely insignificant. The influence of the independent variables on the average current efficiency (ACE) was more or less similar to that of COD owing to the fact that the ACE mainly depends on the COD removal (Figures 7.23 and 7.24); the main difference been that the effect of current density has not much to do with the variation in ACE due to the higher influence by x_2 and x_3. By navigating the response surface for the SEC provided in Figure 7.25; noticeably the SEC increases with increase in both x_1 and x_2. It is interesting to observe that the model has also excellently captured the trends presented earlier for energy requirements for phenol removal.

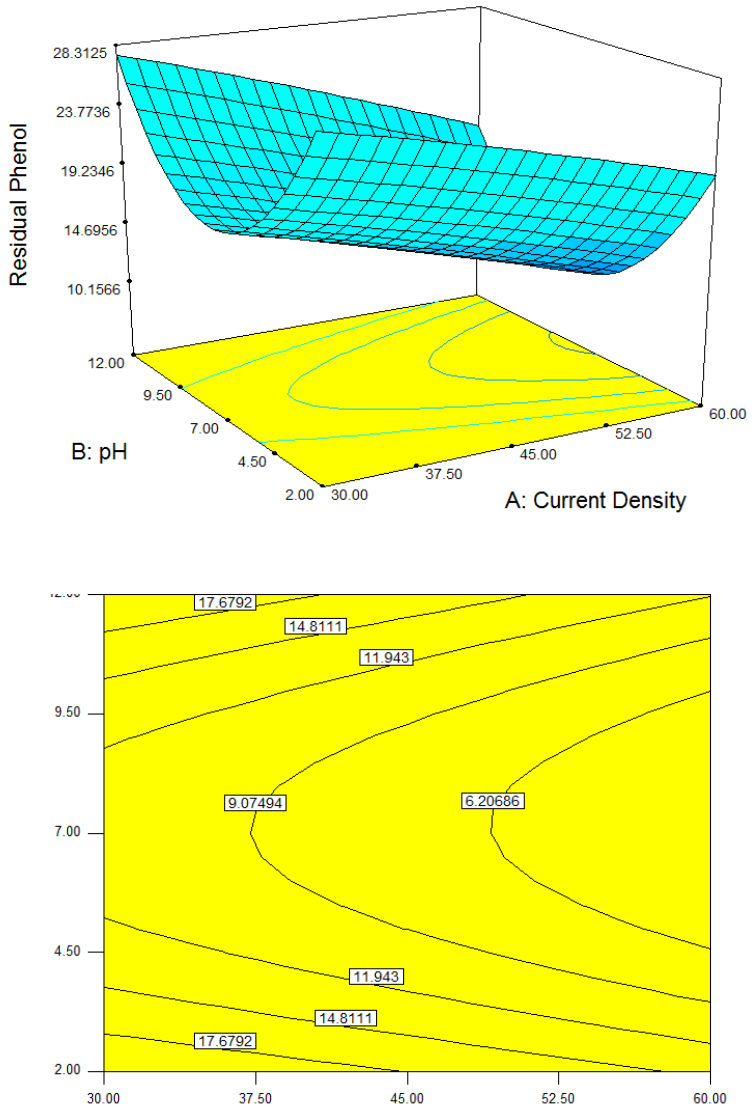

Figure 7.14: Response and Contour Plots for Residual Phenol: pH vs Current Density

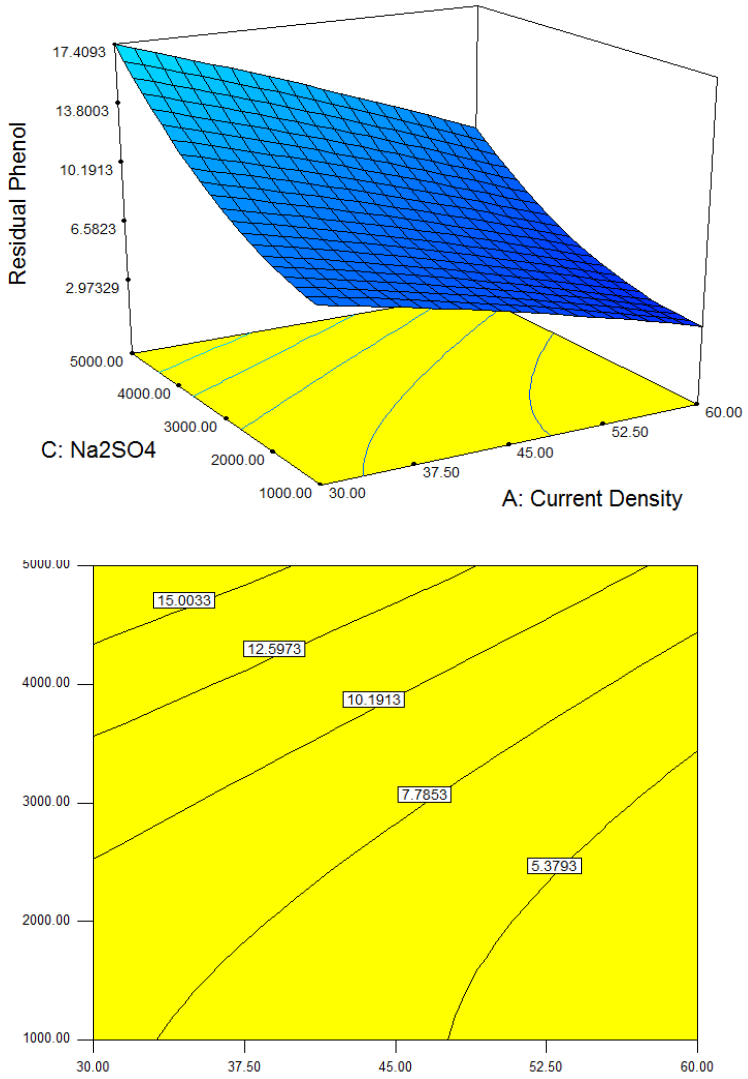

Figure 7.15: Response and Contour Plots for Residual Phenol: Electrolyte vs Current Density

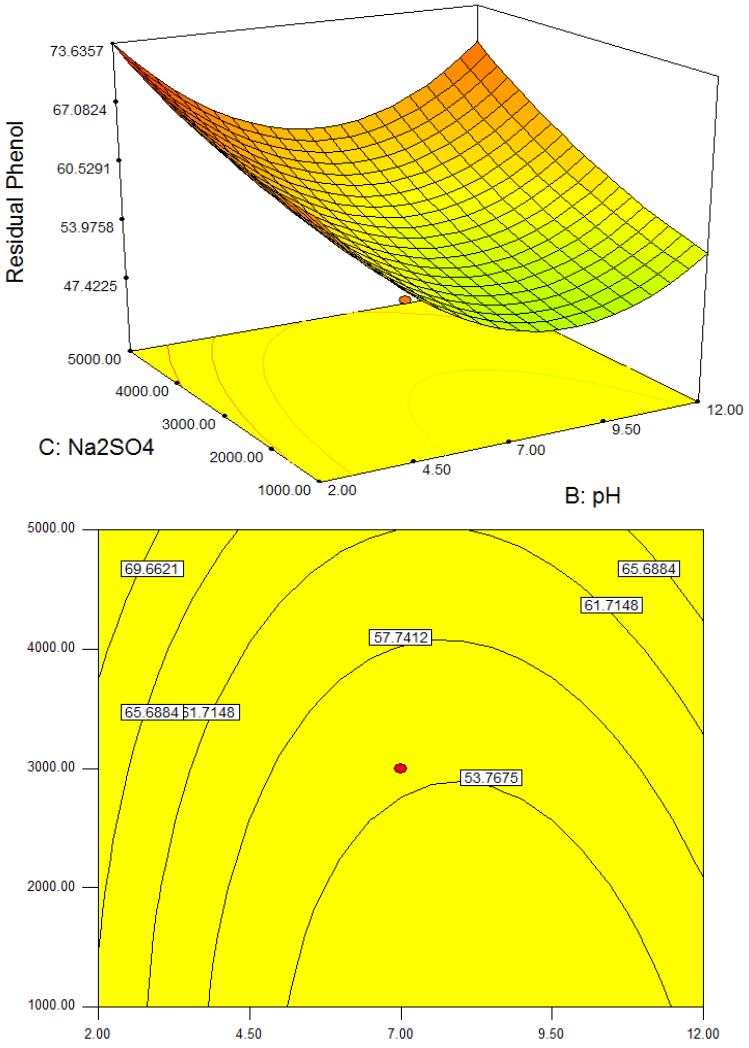

Figure 7.16: Response and Contour Plots for Residual Phenol: Electrolyte vs pH

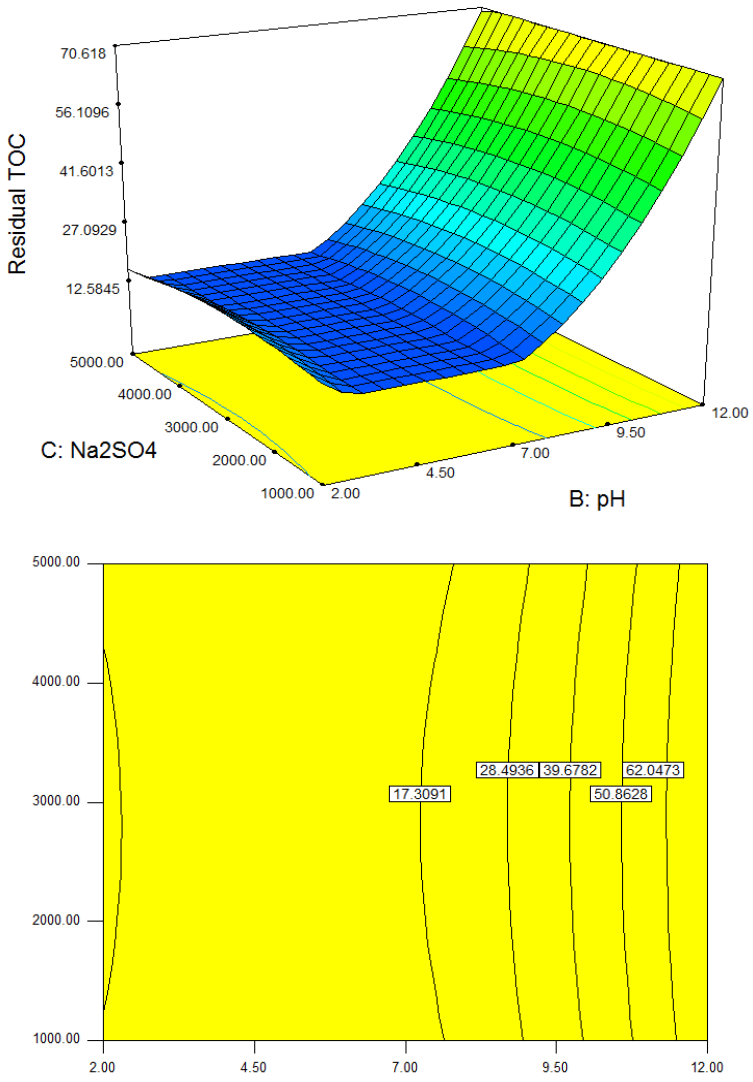

Figure 7.17: Response and Contour Plots for Residual TOC: Electrolyte vs pH

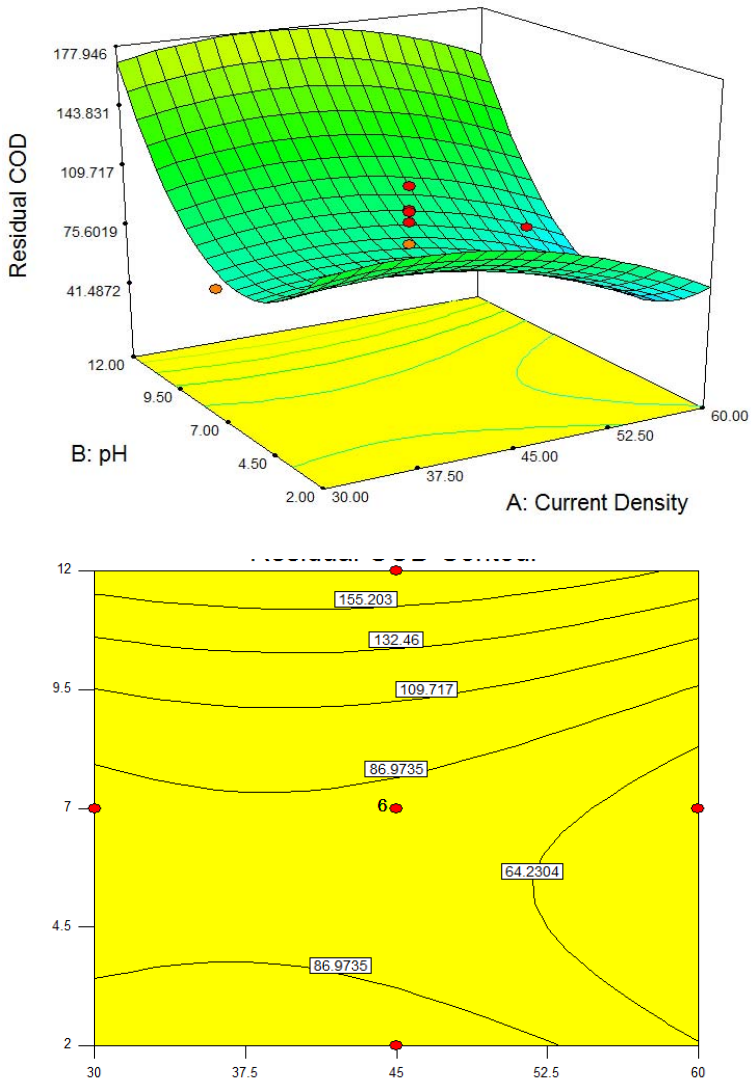

Figure 7.18: Response and Contour Plots for Residual COD: pH vs Current Density

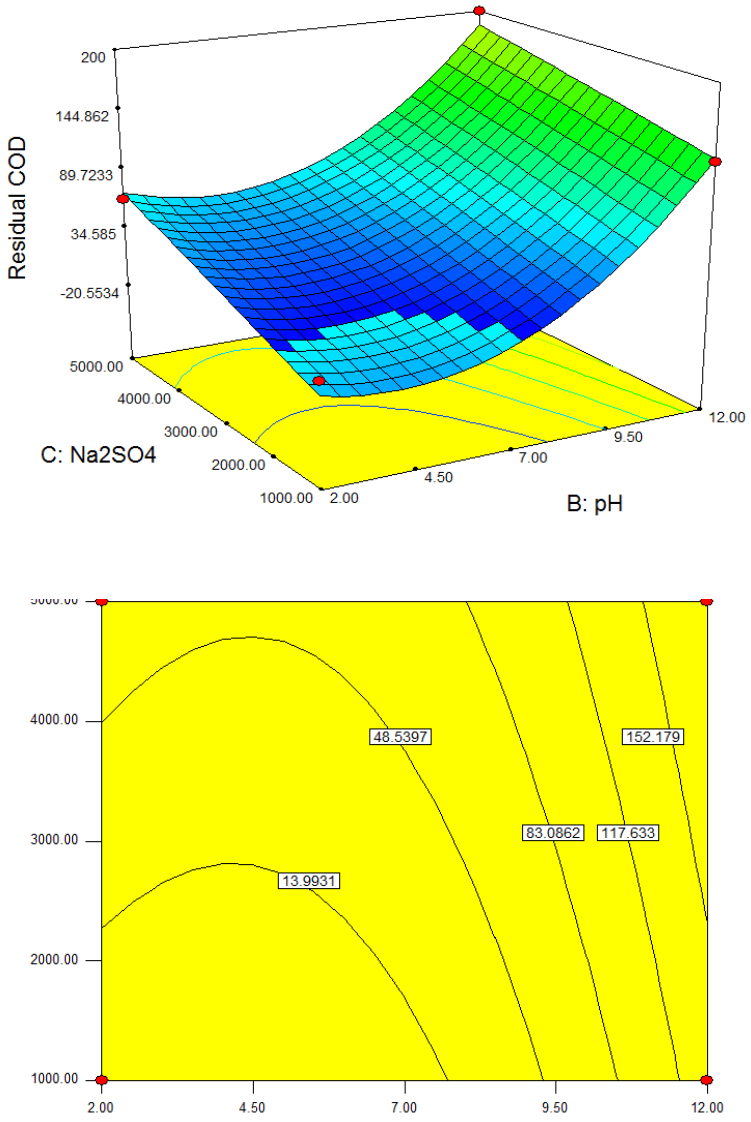

Figure 7.19: Response and Contour Plots for Residual COD: Electrolyte vs pH

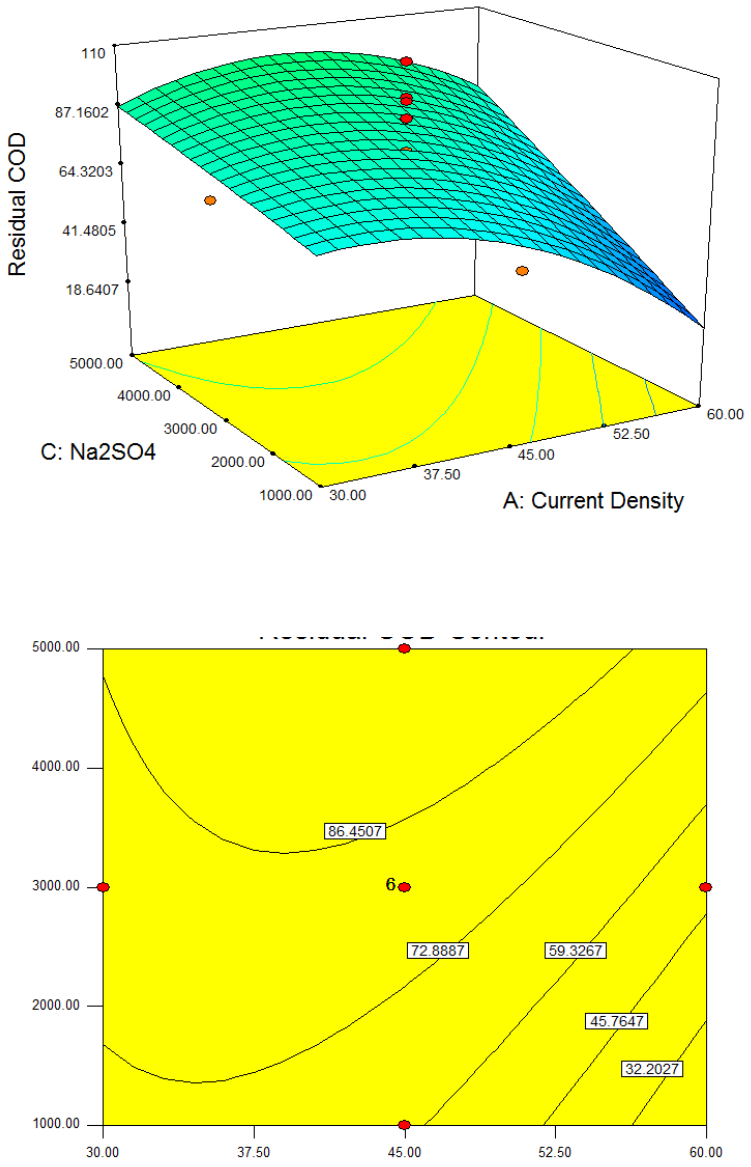

Figure 7.20: Response and Contour Plots for Residual COD: Electrolyte vs Current Density

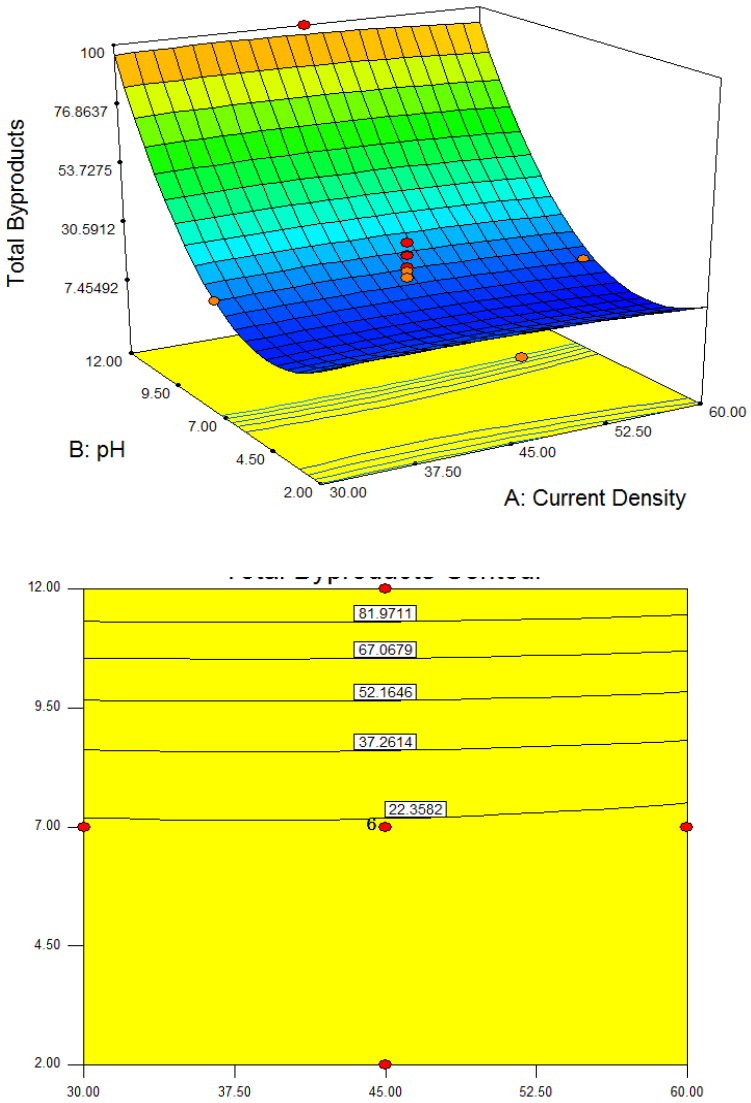

Figure 7.21: Response and Contour Plots for Byproducts Generated: pH vs Current Density

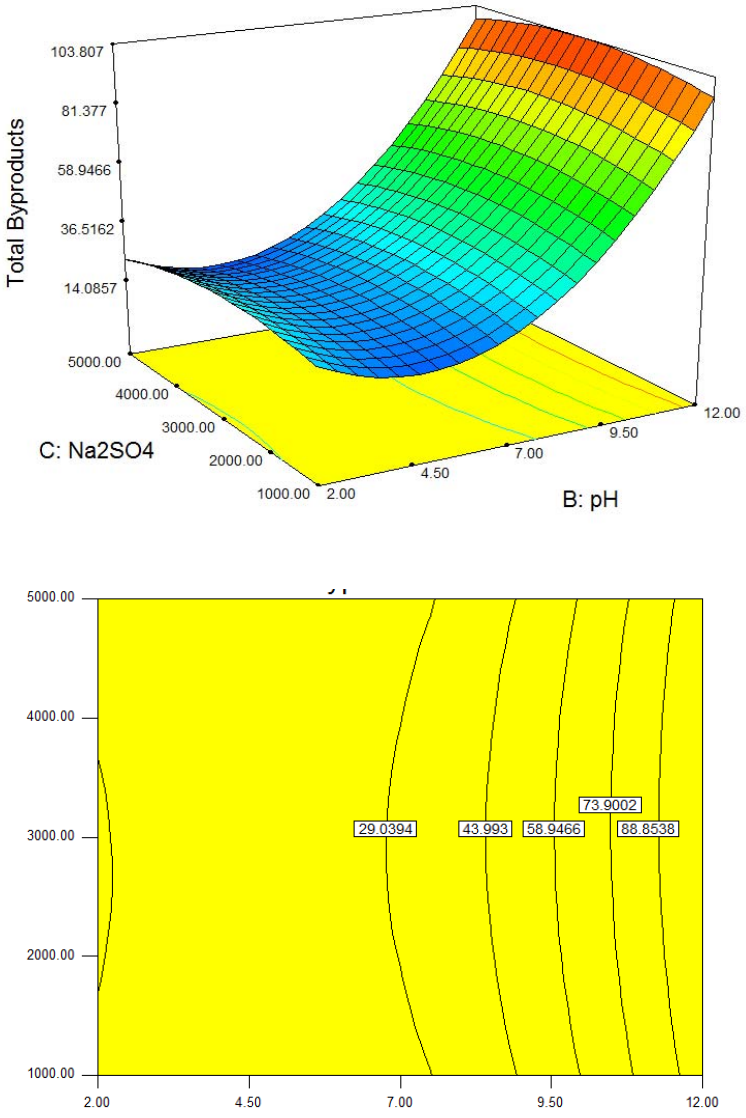

Figure 7.22: Response and Contour Plots for Byproducts Generated: Electrolyte vs pH

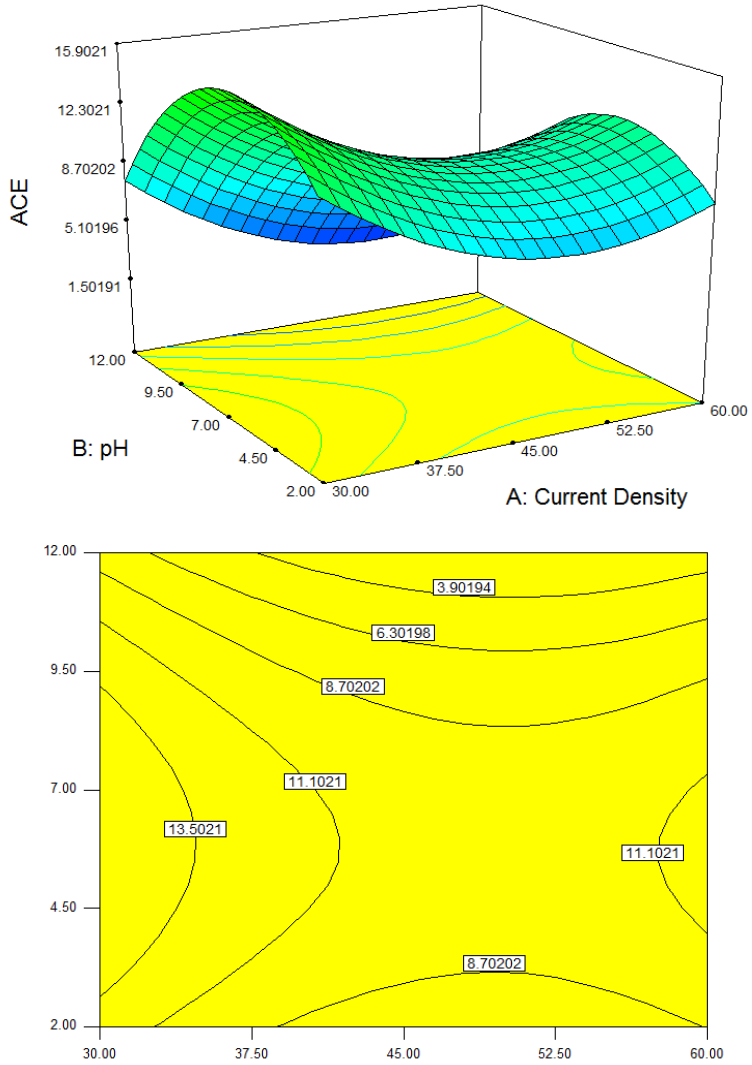

Figure 7.23: Response and Contour Plots for Average Current Efficiency: pH vs Current Density

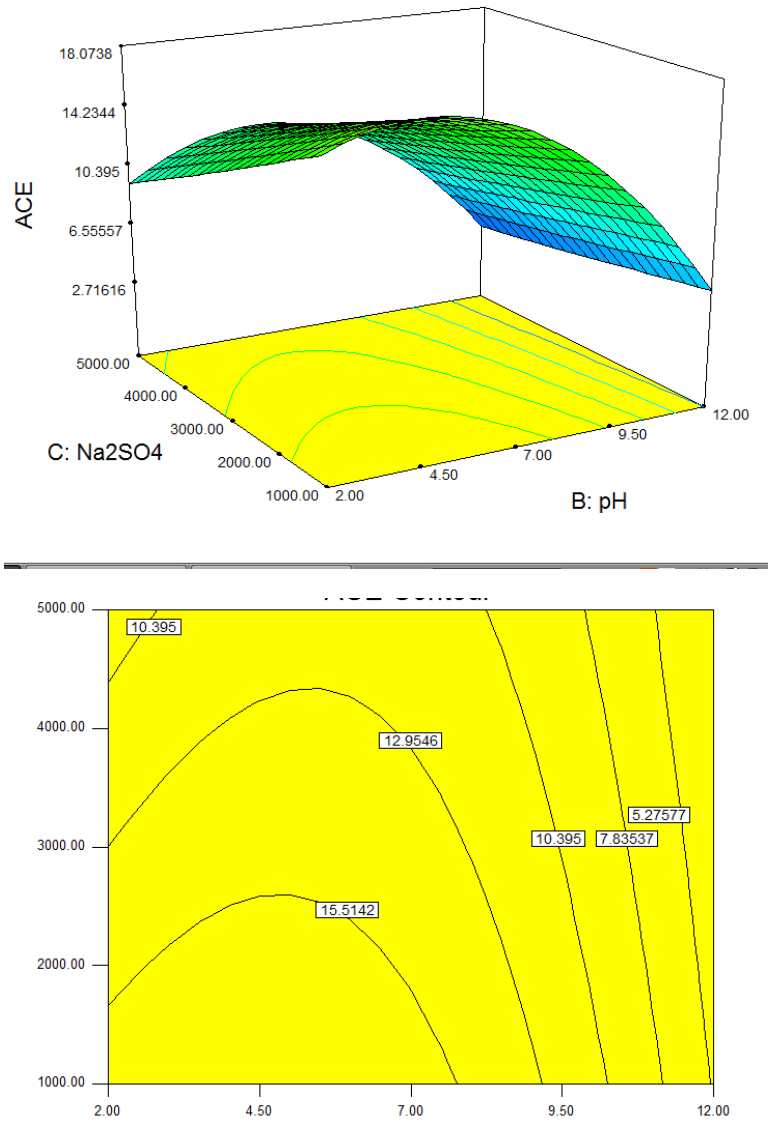

Figure 7.24: Response and Contour Plots for Byproducts Generated: Electrolyte vs pH

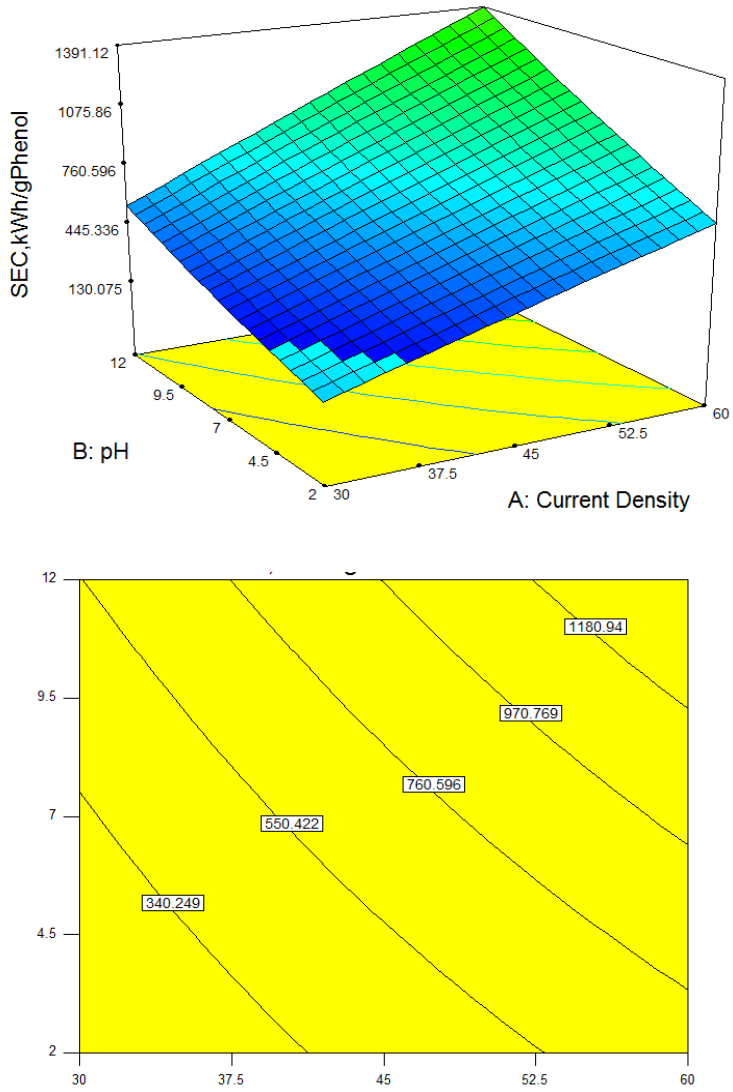

Figure 7.25: Response and Contour Plots for Specific Energy Consumption: pH vs Current Density

7.4 RSM Optimization of Electrochemical Oxidation of Phenol

7.4.1 RSM Parameters Optimization

Optimization of electrochemical process for oxidation of phenol is achievable at the best set of experimental conditions that lead to complete mineralization of phenol (carbon dioxide as the main byproducts) with the best performance in terms of energy consumption and current efficiency. In order to obtain the optimum conditions, optimization was formed based on the developed quadratic models. The coordinates of the critical points were calculated through equating the first derivatives of the mathematical response surface functions to zero. Thus Equation 7.2 yields Equation 7.10:

$$\frac{\partial y}{\partial x_i} = \beta_i + 2\beta_{ii}x_i + \sum_{j=2}^{k} \beta_{ij}x_j = 0 \qquad 7.10$$

For the four parameters under study, Equation 7.10 can be expanded to yield Equation 7.11:

$$\begin{aligned} &\frac{\partial y}{\partial x_1} = \beta_1 + 2\beta_{11}x_1 + \beta_{12}x_2 + \beta_{13}x_3 + \beta_{14}x_4 = 0 \\ &\vdots \\ &\vdots \\ &\vdots \\ &\frac{\partial y}{\partial x_4} = \beta_4 + 2\beta_{44}x_4 + \beta_{41}x_1 + \beta_{42}x_2 + \beta_{43}x_3 = 0 \end{aligned} \qquad 7.11$$

Thus, for getting the coordinate of the critical points in this case, it is necessary to solve the first grade system formed in Equations 7.11 to find the optimum values.

Numerical optimization of the treatment process adopted was performed with the help of the Design-Expert@ software. Stringent criteria that guarantee an efficient process was achievable were set. The criteria composed of set of goals based on desired constraints for the parameters of interest (combination of individual responses as well as the independent variables). Once collectively satisfied, an efficient electrochemical treatment process with high degree of certainty is expected to be achievable. The set of goals are provided in Table 7.11 with upper and lower level of the parameters given according to the experimental data supplied. Moreover, the individual parameters were weighed according to their relative priority and/or importance in contributing towards attaining the desired overall targeted goal.

As given in Table 7.12, twenty one (21) numerical solutions were obtained for optimality with desirability ranging from 0.940, the best, to 0.88 the worst. This short range of desirability suggests that, the region of interest for optimal solution is contracted. Consequently, this indicates a unanimous point of convergence due to existence of very slight variations of the parameters within the various numerical solutions. Therefore, by mere inspecting Table 7.12, the prevalent optimal solution was around initial pH 5, 1000 ppm Na_2SO_4, 30 $mAcm^{-2}$ applied current density within the defined region of interest. This implies that, with operating electrolysis at his optimal point, not only phenol was expected to be removed completely within 210 minutes of treatment, but even TOC and COD can be effectively brought down below their regulated thresholds level. In addition, this excellent phenol oxidation process can be achieved with the hypothetical highest ACE (see Chapter Five), moderate SEC and less byproducts generations 19.40%, 678.08 kWh/kg-phenol and 6.53% respectively.

Table 7.8: RSM Numerical Optimization Constraints

Constraints						
Name	Goal	Lower Limit	Upper Limit	Lower Weight	Upper Weight	Importance
Current Density	minimize	30	60	1	1	5
pH	is in range	2	12	1	1	4
Na_2SO_4	minimize	1000	5000	1	0.5	2
Time	is in range	30	210	1	1	1
Residual Phenol	minimize	0	76.5824	1	0.5	5
Residual TOC	minimize	6.5178	84.0962	1	0.5	5
Residual COD	minimize	0	234	1	0.5	5
ACE	maximize	1.13824	29.0287	0.5	1	5
Total byproducts	minimize	7.26012	100	1	0.5	5
SEC,kWh/gPhenol	minimize	217.893	2186.13	1	0.5	4

.

Table 7.9: RSM Numerical Optimization Results

Number No.	Current Density, $mAcm^{-2}$	pH	Na_2SO_4, ppm	Time, minutes	Residual Phenol, ppm	Residual TOC, ppm	Residual COD, ppm	ACE, %	Byproduct %	SEC, kWh/gPhenol	Desirability
1	30.00	5.09	1000.51	199.66	0.75	7.09	47.60	19.40	6.53	678.08	0.94
2	30.00	5.04	1000.04	197.16	0.76	7.04	47.46	19.37	6.43	677.63	0.94
3	30.00	5.09	1000.18	205.48	0.41	6.98	47.22	19.27	6.59	680.61	0.94
4	30.00	5.08	1000.51	201.54	0.04	6.87	46.82	19.12	6.67	683.09	0.94
5	30.00	4.96	1052.97	197.85	1.16	7.30	48.12	19.43	6.48	655.61	0.94
6	30.00	5.05	1077.35	209.37	0.70	7.28	47.97	19.29	6.81	651.39	0.94
7	30.00	5.08	1079.17	201.08	0.31	7.19	47.66	19.16	6.95	653.78	0.94
8	30.00	5.26	1000.19	202.68	1.61	7.58	49.23	19.77	6.82	673.89	0.94
9	30.00	4.99	1106.71	203.81	0.00	7.11	47.30	18.96	7.01	645.52	0.94
10	30.00	4.83	1000.32	197.21	3.76	8.09	50.90	20.20	5.83	655.11	0.94
11	30.00	5.44	1000.03	208.92	2.58	8.19	51.18	20.08	7.26	668.62	0.94
12	30.00	5.25	1000.87	205.95	-0.86	6.82	46.50	18.84	7.26	691.72	0.94
13	30.00	4.63	1000.18	190.62	-0.26	6.53	45.56	18.55	6.33	679.87	0.94
14	30.49	5.02	1001.66	198.49	0.86	7.15	47.72	19.20	6.43	687.14	0.94
15	30.00	5.04	1423.49	196.76	3.50	9.36	53.83	19.79	7.95	526.05	0.94
16	30.00	5.00	2024.96	194.33	0.22	9.26	53.78	18.19	9.73	395.31	0.93
17	30.00	4.59	2044.32	181.10	1.72	9.63	54.98	18.34	8.96	378.32	0.93
18	30.00	3.81	1193.68	196.69	-0.02	7.74	48.02	16.85	8.43	598.54	0.93
19	30.00	4.77	2549.15	188.15	0.49	9.68	57.14	17.53	9.80	300.86	0.93
20	30.00	5.17	2974.77	189.94	0.00	9.91	59.70	17.18	10.47	267.35	0.92
21	38.00	5.52	1000.01	181.85	-1.49	8.07	45.21	16.37	8.17	883.47	0.88

7.4.2 Results Experimental Validation of RSM Optimization Result

To experimentally verify the models' prediction adequacies, additional experiments were conducted in two replicates at the optimum operating point obtained from the RSM optimization (i.e., 30 $mAcm^{-2}$, initial pH 5 and 1000 ppm Na_2SO_4). The results from these experiments summarized in Tables 7.13 and 7.14 (for better comparison) show that all the developed response models appeared to have either underestimated or overestimated the experimental data. However, taken into consideration the high regression coefficients between the actual and the predicted values (above 95%), the models' predictions are excellent. Therefore, the results derived from this part of this study underscore the fact that the response surface methodology is a powerful reliable tool for optimizing electrochemical oxidation of phenol for an effective phenolic wastewaters treatment scheme.

Table 7.10: Predicted and Experimental Values for (Top) Residual Phenol, TOC and COD (Bottom) ACE, SEC and Percent Byproducts Generated at Optimum Conditions

Time, minutes	Residual Phenol, ppm		Residual TOC, ppm		Residual COD, ppm	
	Experimental	Predicted	Experimental	Predicted	Experimental	Predicted
30	62.13	46.9941	53.08221	54.04872	162.880	177.8215
120	10.02203	14.36707	15.597	13.699072	47.858	48.38345
210	0	0	0	0	2.555	4.6726
R^2	0.961		0.997		0.998	

Time, minutes	ACE, %		SEC, kWh/kg-phenol		% Byproducts	
	Experimental	Predicted	Experimental	Predicted	Experimental	Predicted
30	9.662	6.994	162.046	168.3	8.914	9.662
120	26.996	22.367	272.778	253.699	11.486	26.996
210	19.1	19.5	429.52	482.2	0	19.1
R^2	0.914		0.962		0.958	

Chapter 8

Conclusions and Recommendation

8.1 Conclusions

Based on the findings from this dissertation, it was concluded that:

- Within the range of experimental parameters investigated in the present study, pH and initial phenol concentration were the key influencers of the mechanisms of electrochemical oxidation of phenol using Boron Doped Diamond (BDD) anode.

- Oxidation of phenol was effectively achievable regardless of initial concentration of phenol at pH < pK_a of phenol. While at pH > pK_a of phenol and low phenol concentration, conversion of phenol to its aromatic and other intermediary byproducts prevailed over its oxidation to CO_2 thereby severely hindering phenol oxidation.

- Direct and fast electro-oxidation of phenol to CO_2 predominantly didn't occur, but rather phenol oxidation was through gradual and sequential generation of series of intermediary byproducts which were eventually converted to CO_2.

- Based on the comprehensive analyses of intermediary byproducts, it was speculated that the mechanism for the phenol oxidation in presence of the inorganic species was primarily initiated by speciation of phenol molecules followed by generation of aromatic intermediates via hydroxylation which were further oxidized and converted to ring cleavage small fragmented products that give up short chain aliphatic acids. The final step in the pathway involved the destruction of the short chain aliphatic acids to CO_2.

- Indirect oxidation in the bulk solution was mildly harnessed and it became ineffective as other expected in-situ generated oxidants (such as peroxodisulfate, $S_2O_8^{2-}$, and hydrogen peroxide, H_2O_2) beside $OH^{\bullet}$ radicals electro-generated on the BDD anode appeared not to be active enough to improve phenol oxidation.

- Direct oxidation process mediated by the electro-generated $OH^{\bullet}$ produced at the anode surface was the key phenol oxidation dominant process.

- The removal of phenol, TOC and COD were kinetically controlled processes dominated by heterogeneous and irreversible direct oxidation reactions on the BDD anode surface mainly mediated by the electro-generated $OH^{\bullet}$ with mass transport to the BDD anode surface as the rate limiting step.

- Presence of the inorganic species rendered kinetic modeling of electrochemical oxidation of phenol using COD evolution data to be inappropriate as predictions of operating regime using existing models based on the COD data were significantly erroneous which were corrected by modified models employing TOC data.

- Total amount of phenol, TOC and COD removal increases with phenol initial concentration, while the relative percent removal decreases with initial phenol concentration.

- The BDD anode was very efficient in simultaneous removal of phenol and the cohabiting inorganic species in the different mix matrix.

- In the presence of the inorganic species, total amount of COD removal, average current efficiency (ACE) and the specific energy consumed (SEC) for COD removal were proportional to the degree of mix matrix due to increase in the initial COD concentration. However, the relative percent COD removal decreases with increase in initial COD.

- The ACE achieved for the binary and higher mix matrixes ranged between 44.34 - 58.75% and 58.88 - 79.26% resulting in 132 - 207% and 208 - 314.9% increase in the ACE, respectively. Meanwhile, the SEC dropped from 57.0 kWh/kg-COD to between 15.096-20.62 and 7.83-15.24 kWh/kg-COD kg-COD which correspond to the percent decrease in SEC for COD removal estimated to be in the range of 63.2 - 73.5% and 73.26 - 86.3%, respectively.

- For the binary and higher mix matrixes, the SEC for phenol removal was in the range of 359.97 - 398.5 and 244.9 -363.9 kWh/kg-phenol which correspond to 7.3 - 45.77% and 7.2 – 50% decrease in the energy requirement

- With very active BDD anode and in presence of the inorganic species, the kinetics of phenol decay was observed to be negatively affected significantly due to decline in the BDD anode activity.

- Better removal kinetics for phenol in presence of some inorganic species may suggest some autocatalytic effects by the inorganic species or their associated byproducts generated during the treatment process

- Excellent simultaneous removal of phenol and the cohabiting inorganic species in the different mix matrixes were achievable with removal rates of the inorganic species following the order $NH_4^+ > S^{2-} > CN^-$.

- The presence of the inorganic species have varying degree of repercussions on electrochemical destruction of phenol and such scenarios didn't hamper the overall oxidation potentials of the BDD anode, though reaching steady state of complete decontamination was significantly delayed according to the added species in solution

- The degradation kinetics of phenol as well as the inorganic species in the different mix matrixes was consistently pseudo-first order in nature and that the presence of the inorganic species in the different mix systems was prone to reduce the phenol decay rate particularly due to drop in the activity of the BDD anode.

- Response surface methodology (RSM) was an adequate modeling tool for optimization and in-depth comprehending the operating parameters main and interaction effects during electrochemical oxidation process for effective wastewater treatment scheme

- Boron-doped diamond electrode (in conjunction with graphite cathode) is very robust electrode material for electrochemical oxidation of phenol that may not need further downstream treatment (such as filtration, sludge treatment etc); thereby rendering it a candidate cost-effective approach for mitigating wastewater pollution associated with petroleum refinery and petrochemical industries.

8.2 Recommendations

The following are recommended for further studies:

- Investigating phenol oxidation hindrance dependency on initial phenol concentration at pH $> pK_a$ of phenol and also effective means for oxidizing phenol at such operating condition.

- Response Surface Modeling (RSM) technique should be employed to model and optimize the phenol oxidation considering different mix matrixes separately. And in that regards, both lower and higher concentrations of the inorganic species should be considered

- Other optimization approaches should be also used to study means for effective phenol oxidation in presence of the inorganic species in order to check their suitability beside the RSM technique.

- Employing cyclic voltammetry and chronoamperometry measurements approaches for better understanding of oxidation of phenol and the inorganic species on the BDD in the different mix matrixes.

- Investigating the effect of sodium sulfate concentration, temperature, current density and other experimental variables on generation of active in-situ oxidants and strategy for optimization the generation of peroxodisulfate

- Investigating effects of different supporting electrolytes and anode materials under varying experimental conditions in order to identify the best combination that would

reduce the mass transfer dependency of the process and improve the overall process efficiency

- Designing different reactors and comparing their respective performances in enhancing indirect oxidation, reducing the mass transfer effects and improving the effectiveness of the phenol oxidation and the overall decontamination process.

- Optimizing electrochemical process using BDD electrodes for real industrial wastewater from petroleum refining or petrochemical industry containing phenol and the investigated inorganic species

References

1. Adelaida, C., Urtiaga, A., Rivero, M.-J., and Ortiz, I. (2007). Ammonium removal from landfill leachate by anodic oxidation. *Journal of Hazardous Materials* **144**, 715-719.
2. Agnieszka, K., Gyorgy, F., and Comninellis, C. (2008). Kinetic modelling of the electrochemical mineralization of organic pollutants for wastewater treatment. *J Appl Electrochem* **38**.
3. Ahmadi, M., Vahabzadeh, F., Bonakdarpour, B., Mofarrah, E., and Mehranian, M. (2005). Application of the central composite design and response surface methodology to the advanced treatment of olive oil processing wastewater using Fenton's peroxidation. *Journal of Hazardous Materials;* **B123**, 187-195.
4. Akira, F., Einaga, Y., Tata, N. R., and Donald, A. T. (2005). Diamond Electrochemistry. pp. 449-501. Elsevier, Tokyo.
5. Alaxender., K., Blaschke, M., Kreysig, D., Sandt, B., Schröder, F., and Rennau, J. (1999). Electrochemical water disinfection, Part II. Hypochlorite production from potable water, chlorine consumption, and the problem of calcareous deposits. *J. Appl. Electrochem* **29**, 895.
6. Alessandra, C., C, A. V., D, M., and G.L. Sant'Anna, J. (2006). Treatment of petroleum refinery sourwater by advanced oxidation processes. *Journal of Hazardous Materials* **137**, 178-184.
7. Alexander, K. (2007). Doped Diamond: A Compact Review on a New, Versatile Electrode Material. *International J. Electrochem. Sci.* **2**, 355 - 385.
8. Alexander, K., Stadelmann, M., and Blaschke, M. (2003). Anodic oxidation with doped diamond electrodes a new advanced oxidation process. *Journal of Hazardous Materials* **B103**, 247-261.
9. Al-Maznai, H., and Conway, B. (2001). *J Serb Chem Soc* **66**, 765.
10. Anderson, M. J., and Whitcomb, P. J. (2005). "RSM simplified: Optimizing Processes Using Response Surface Methods for Design of Experiments," Productivity Press, New York.

11. Andreozzi, R., Caprio, V., Insola, A., and Marotta, R. (1999). Advanced oxidation processes (AOP) for water purification and recovery. *Catal. Today* **53**, 51.
12. Awad, Y. M., and Abuzaid, N. S. (1997). Electrochemical Treatment of Phenolic Wastewater: Efficiency, Designed Considerations an Economic Evaluation. *Journal of Environmnetal Science Health* **A32**, 1393-1414.
13. Awad, Y. M., and Abuzaid, N. S. (1999). Electrochemical oxidation of phenol using graphite anodes. *Separation Science Technology* **34**, 699-708.
14. Azzam, M. O., Tahboub, Y., and Al-Tarazi, M. (1999). Effect of Counter Electrode Material on the Anodic destruction of 4-Cl Phenol Solution. *Process Safety and Environmental Protection* **77**, 219-226.
15. Bagarinao, T. (1992). Sulfide as Environmental Factor and Toxicant: Tolerance and Adaptations in Aquatic Organisms. *Aquatic Toxicology* **24**, 21-62.
16. Beck, F., Krohn, H., Kaiser, W., Fryda, M., Klages, C. P., and Schafer, L. (1998). *Electrochim. Acta* **44**, 525.
17. Belaid, C., Kallel, M., Khadhraou, M., Gerard Lalleve, Elleuch, B., and Fauvarque, J.-F. (2006). Electrochemical treatment of olive mill wastewaters: Removal of phenolic compounds and decolourization. *Journal of Applied Electrochemistry:* **36**, 1175–1182.
18. Bergmann, P. M. E. H., and Rollin, J. (2007). product and by-product formation in laboratory studies on disinfection electrolysis of water using boron-doped diamond anodes. *Catalysis Today* **xxxxxxx**.
19. Berne., F., and Cordonnier, J. (1995). "Refining, petrochemical and gas processing techniques industrial water treatment," 1995/Ed. Gulf Publishing Company, Houston, Texas, USA.
20. Bonfatti, F., Ferro, S., Lavezzo, F., Malacarne, M., Lodi, G., and Battisti, A. D. (1999). Electrochemical incineration of glucose as a model organic substrate. I. Role of the electrode material,. *J. Electrochem. Soc.* **146**, 2175.
21. Boudenne, J. L., Cerclier, O., Galea, J., and Vlist, E. V. (1996). Electrochemical Oxidation of Aqueous Phenol at a Carbon Black Slurry Electrode. *Appl. Catal.* **143**, 185.
22. Boye, B., Michaud, P. A., Marselli, B., Dieng, M. M., Brillas, E., and Comninellis, C. (2002). *New Diamond Frontier Carbon Technol.* **12**, 63.

23. Brillas, E., Boyea, B., Sirésa, I., Garridoa, J. A., Rodrígueza, R. M., Ariasa, C., Cabota, P., and Comninellis, C. (2004). Electrochemical destruction of chlorophenoxy herbicides by anodic oxidation and electro-Fenton using a boron-doped diamond electrode. *Electrochimica Acta* **49**.
24. Bruno, F., Pham, M. C., and Dubois, J. E. (1977). *Electrochim Acta* **22**, 451.
25. Busca, G., Berardinelli, S., Resini, C., and Arrighi, L. (2008). Technologies for the removal of phenol from fluid streams: A short review of recent developments. *Journal of Hazardous Materials* **160**, 265-288.
26. Canizare, P., Saez, C., Lobato, J., and Rodrigo, M. A. (2006). Detoxification of synthetic industrial wastewaters using electrochemical oxidation with boron-doped diamond anodes. *J Chem Technol Biotechnol* **81**, 352-358.
27. Canizares, P., Diaz, M., Dominguez, J. A., Lobato, J., and Rodrigo, M. A. (2005a). Electrochemical treatment of diluted cyanide aqueous wastes. *J Chem Technol Biotechnol* **80**, 565-573.
28. Canizares, P., Dominguez, J. A., Rodrigo, M. A., Villasen, J., and Rodriguez, J. (1999). Effect of the Current Intensity in the Electrochemical Oxidation of Aqueous Phenol Wastes at an Activated Carbon and Steel Anode. *Ind. Eng. Chem. Res* **39**, 3779-3785.
29. Canizares, P., Hernandez, M., Rodrigo, M. A., Saez, C., Barrera, C. E., and Roa, G. (2009). Electrooxidation of Brown-Colored Molasses Wastewater. Effect of the Electrolyte Salt on the Process Efficiency. *Ind. Eng. Chem. Res.* **48**, 1298–1301.
30. Canizares, P., Larrondo, F., Lobato, J., Rodrigo, M. A., and Saez, C. (2005b). *Journal of the Electrochemical Society* **152**, D191-D196.
31. Canizares, P., Lobato, J., Garcia-Gomez, J., and Rodrigoz, M. A. (2004). Combined adsorption and electrochemical processes for the treatment of acidic aqueous phenol wastes. *Journal of Applied Electrochemistry 34* **34**, 111–117.
32. Canizares, P., Lobato, J., Paz, R., Rodrigo, M. A., and Saez, C. (2005c). Electrochemical oxidation of phenolic wastes with boron-doped diamond anodes. *Water Research* **39**, 2687-2703.

33. Canizares, P., Lobato, J., Paz, R., Saez, C., and Rodrigo, M. A. (2003). Electrochemical oxidation of several chlorophenols on diamond electrodes Part I. Reaction mechanismq. *Journal of Applied Electrochemistry* **33**, 917–927.
34. Canizares, P., M. Diaz, J., Dominguez, A., Garcia-Gomez, J., and Rodrigo, M. A. (2002a). Electrochemical Oxidation of Aqueous Phenol Wastes on Synthetic Diamond Thin-Film Electrodes. *Ind. Eng. Chem. Res* **41**, 4187-4194.
35. Canizares, P., Martinez, F., Diaz, M., Garcia-Gomez, J., and Rodrigo, M. A. (2002b). Electrochemical Oxidation of Aqueous Phenol Wastes Using Active and Nonactive Electrodes. *Journal of The Electrochemical Society* **149**, D118-D124.
36. Canizares, P., Saez, C., Lobato, J., Paz, R., and Rodrigoz, M. A. (2007). Effect of the Operating Conditions on the Oxidation Mechanisms in Conductive-Diamond Electrolyses. *Journal of The Electrochemical Society* **154**, E37-E44.
37. Cestarollia, D. T., and Andrade, A. R. d. (2007). Electrochemical Oxidation of Phenol at Ti/Ru0.3Pb,,0.7-x…TixOy Electrodes in Aqueous Media. *Journal of The Electrochemical Society* **154**, E25-E30.
38. Chatzisymeon, E., Xekoukoulotakis, N. P., Diamadopoulos, E., Katsaounis, A., and Mantzavinos, D. (2009). Boron-doped diamond anodic treatment of olive mill wastewaters: Statistical analysis, kinetic modeling and biodegradability. *Water Research* **In Press, Corrected Proof**.
39. Chen, X., Chen, G., Gao, F., and Yue, P. L. (2003a). High performance Ti/BDD electrodes for pollutant oxidation. *J. Environ. Sci. Technol* **37**, 5021–5026.
40. Chen, X., Chen, G., and Yue, P. L. (2003b). Anodic oxidation of dyes at novel Ti/B-diamond electrode. *Chem. Eng. Sci.* **58**, 995-1001.
41. Comninellis, C. (1994). *Electrochim Acta* **39**, 1857.
42. Comninellis, C., and Nerini, A. (1995). Anodic oxidation of phenol in the presence of NaCl for waste water treatment. *J. Appl. Electrochem* **25**, 23-28.
43. Comninellis, C., and Plattner., E. (1988). *CHIMIA* **42**, 250-252.
44. Comninellis, C., and Pulgarin, C. (1991). Anodic oxidation of phenol for waste water treatment. *Appl. Electrochem* **21**, 703-708.

45. Comninellis, C., and Pulgarin, C. (1993). Electrochemical oxidation of phenol for waste water treatment using SnO2 anodes. *J. Appl. Electrochem* **23**, 108-112.
46. Conway, B., Ayranci, E., and Al-Maznai, H. (2001). Electrochim Acta. **47**, 705.
47. Correa-Lozano, B., Comninellis, C., A.D. Battisti, and (1996). Preparation of SnO2–Sb2O5 films by the spray pyrolysis technique. *J. Appl. Electrochem* **26**, 83–89.
48. Correa-Lozano, B., Comninellis, C., and Battisti, A. D. (1997). *J Appl Electrochem* **27**, 970.
49. Cui, Y.-h., Li, X.-y., and Chen, G. (2009). Electrochemical degradation of bisphenol A on different anodes. *Water Research* **43**, 1968-1976.
50. Dasha, R. R., Gaur, A., and Balomajumder, C. (2009). Cyanide in industrial wastewaters and its removal: A review on biotreatment. *Journal of Hazardous Materials* **163**, 1-11.
51. Deligiorgi, A., Xekoukoulotaki, N. P., Diamadopoulos, E., and Mantzavinos, D. (2008). Electrochemical oxidation of table olive processing wastewater over boron-doped diamond electrodes: Treatment optimization by factorial design. *WATER RESEARCH* **42**, 1229-1237.
52. Diniz, A. V., Ferreira, N. G., Corat, E. J., and Tarava-Airoldi, V. J. (2003). Efficiency study of perforated diamond electrodes for organic compounds oxidation process. *Diamond and Related Materials* **12**, 577–582.
53. Duo, I., Fujishima, A., and Comninellis, C. (2003). *Electrochem. Commun* **5**, 695.
54. Feng, J., and Johnson, D. C. (1991). Electrocatalysis of anodic oxygentransfer reaction: titanium substrates for pure and doped lead dioxide films. *J. Electrochem. Soc.* **138**, 3329–3337.
55. Feng, Y. J., and Li, X. Y. (2003). *Water Res* **37**, 2399.
56. Fisher, V., Gandini, D., Laufer, S., Blank, E., and Comninellis, C. (1998). *Electrochim. Acta* **44**, 521.
57. Foti, G., Gandini, D., and Comninellis, C. (1997). *Curr. Top. Electrochem* **5**, 71.
58. Foti, G., Gandini, D., Comninellis, C., Perret, A., and Haenni, W. (1999). Oxidation of Organics by Intermediates of Water Discharge on IrO2 and Synthetic Diamond Anodes. *Electrochem. Solid-State Lett.* **2**, 228.

59. Fryda, M., Herrmann, D., Schafer, L., Klages, C. P., A. Perret, Haenn, W., Comninellis, C., and Gandini, D. Wastewater Treatment With Diamond Electrodes. *Electrochemical Society Proceedings* **99**.
60. Fryda, M., Herrmann, D., Schafer, L., Klages, C. P., A. Perret, Haenn, W., Comninellis, C., and Gandini, D. (1999). Properties of diamond electrodes for wastewater treatment. *New Diam.Front. C. Technol* **9**, 229–240.
61. Galil, N., Rebhun, M., and -, Y. B.-. (1988). Disturbance & Inhibition compounds in biological treatment of wastewater from an integrated oil refinery. *Water Science & Technology,* **20**, 21-29.
62. Gandini, D., E, M., P.A, M., W, H., A, P., and Ch, C. (2000). *J. Appl. Electrochem.* **30**, 1345.
63. Gattrell, M., and Kirk., D. W. (1990). *Can. J. Chem. Eng* **68**, 673.
64. Gattrell, M., and W, K. D. (1993). A Study of the Oxidation of Phenol at Platinum and Preoxidized Platinum Surfaces. *J. Electrochem. Soc* **6**, 153.
65. Gherardini, L., A, M. P., M, P., Ch, C., and N, V. (2001). Electrochemical Oxidation of 4-Chlorophenol for Wastewater Treatment Definition of Normalized Current Efficiency. *Journal of The Electrochemical Society* **148**, D78-D82.
66. Glarum, S. H., and Marshall, J. H. (1985). *J Electrochem Soc* **132**, 2939.
67. Glarum, S. H., Mashall, J. H., Hellman, M. Y., and Taylor, G. N. (1987). *J Electrochem Soc* **134**, 81.
68. Güven, G., Perendeci, A., and Tanyolaç, A. (2008). Electrochemical treatment of deproteinated whey wastewater and optimization of treatment conditions with response surface methodology. *Journal of Hazardous Materials* **157**, 69-78.
69. Güven, G., Perendeci, A., and Tanyolaç, A. (2009). Electrochemical treatment of simulated beet sugar factory wastewater. *Chemical Engineering Journal* **151**, 149-159.
70. Guohua, C. (2004). Electrochemical technologies in wastewater treatment. *Separation and Purification Technology* **38**, 11-41.
71. Hagans, P. L., Natishan, P. M., Stoner, B. R., and O'Grady, W. E. (2001). Electrochemical Oxidation of Phenol Using Boron-Doped Diamond Electrodes. *J Electrochem Soc* **148**, E298-E301.

72. Hamoda, M. R., and Al-Haddad, A. A. (1987). Investigation of Petroleum Refinery Effluent Treatment in an Aerobic Fixed-Film Biological System. *J. Inst. Water Environ. Manage* **2**, 239-246.
73. Hayashi, K., Yamanaka, S., Okushi, H., and Kajimura, K. (1996). *Appl. Phys. Lett* **68**, 376.
74. Hegea, K. V., Verhaegeb, M., and Verstraete, W. (2004). Electro-oxidative abatement of low-salinity reverse osmosis membrane concentrates. *Water Research* **38**, 1550–1558.
75. Herrmann, J. M. (1999). Heterogeneous photocatalysis: fundamentals and applications to the removal of various types of aqueous pollutants. *Catal. Today* **53**, 115.
76. Iniesta, J., E., E., Gonzalez-Garc, Montiel, V., and Aldaz, A. (2002). *J Electrochem Soc* **149**, D57.
77. Iniesta, J., Michaud, A., Panizza, M., and Comninellis, C. (2001a). *Electrochemistry Communications* **3**, 346-351.
78. Iniesta, J., Michaud, P. A., Panizza, M., Cerisola, G., Aldaz, A., and Comninellis, C. (2001b). Electrochemical oxidation of phenol on boron-doped diamond electrode. *Electrochim Acta* **46**, 3573-3578.
79. Jedral, W., Merica, S. G., and Bunce, N. J. (1999). *Electrochemical Communication* **1**, 108.
80. Jin-Fang, Z., Hai-Bin, W., Nakashima, T., Tata, N. R., and Fujishima, A. (2003). Electrochemical Incineration of Organic Pollutants on Boron-Doped Diamond Electrode. Evidence for Direct Electrochemical Oxidation Pathway. *J. Phys. Chem* **107**, 13389-13395.
81. Jirka, A. M., and Carter, M. J. (1975). Micro Semi-Automated Analysis of Surface and Wastewaters for Chemical Oxygen Demand. *ANALYTICALCHEMISTRY* **47**, 137-1402.
82. Juttner, K., Galla, U., and Schmieder, H. (2000). Electrochemical approaches to environmental problems in the process industry. *Electrochimica Acta* **45**, 2575-2594.
83. Katie, W., Bejan, D., and Bunce, N. J. (2007). Electrochemical oxidation of sulfide ion at a boron-doped diamond anode. *Journal of Applied Electrochemistry* **37**, 367-373.

84. Katsuki, N., Takahashi, E., Toyoda, M., Kurosa, T., Iida, M., Wakita, S., Nishiki, Y., and Shinamune, T. (1998). Water electrolysis using diamond thin-film electrodes. *J. Electrochem. Soc.* **145**, 2358.
85. Kondo, T., Einaga, Y., Sarada, B. V., Rao, T. N., Tryk, D. A., and Fujishima., A. (2002). *J. Electrochem. Soc.* **149**, E179.
86. Koparal, A. S., and Ogutveren, U. B. (2002). Removal of the nitrate from water by electroreduction and electrocoagulation. *Hazard. Mater.* **B 89**, 84-94.
87. Koparal, A. S., Yavuz, Y., and Ogutveren, U. B. (2002). Electro-adsorption of Acilan blue dye from textile effluents by using activated carbon-perlite mixtures, . . *Water Environ. Res* **6**, 521-525.
88. Kotz, R., Stucki, S., and Carcer, B. (1991). Electrochemical waste water treatment using high overvoltage anodes. Part I. Physical and electrochemical properties of SnO2 anodes. *J. Appl. Electrochem* **21**, 14.
89. Krishnan, V., Desa, A., and Renny, L. (2006). Electrolytic Treatment of Beer Brewery Wastewater. *Ind. Eng. Chem. Res* **45**, 6854-6859.
90. Lanonette, K. H. (1977). Treatment of Phenolic Wastes. *Chem. Eng* **84**, 99.
91. Lapuente, R., Cases, F., Garces, P., Marallon, E., and Vazquez, J. L. (1998). *J. Electroanalytical Chemistry* **451**, 163.
92. Lee, J., Ye, L., Landen, W. O., and Eitenmiller, R. R. (2000). Optimization of an extraction procedure for the quantification of vitamin E in tomato and broccoli using response surface methodology. *J. Food Composition Analysis* **13**, 45-57.
93. Li Huang, L. L., Wenbo Dong, Yan Liu, and Huiqi Hou (2008). Removal of Ammonia by OH Radical in Aqueous Phase. *Environ. Sci. Technol* **42**.
94. Li, L., and Liu, Y. (2009). Ammonia removal in electrochemical oxidation: Mechanism and pseudo-kinetics. *Journal of Hazardous Materials* **161**, 1010-1016.
95. Liu, L., Zhao, G., Wu, M., Lei, Y., and Geng, R. (2009a). Electrochemical degradation of chlorobenzene on boron-doped diamond and platinum electrodes. *Journal of Hazardous Materials* **168**, 179-186.

96. Liu, Y., Li, L., and Goel, R. (2009b). Kinetic study of electrolytic ammonia removal using Ti/IrO2 as anode under different experimental conditions. *Journal of Hazardous Materials* **In Press, Corrected Proof**.

97. Lotov, P. I., and Kalcheva, S. V. (1998). Mechanistic Approach to the Oxidation of Phenol at a Platinum/Gold Electrode in an Acid Medium. J. Electroanal. Chem. *J Electroanal Chem* **442**, 19.

98. Marco, A. Q. A., FerroII, S., Martinez-Huitle, C. A., and Vong, Y. M. (2006). Boron doped diamond electrode for the wastewater treatment. *Journal of the Brazilian Chemical Society* **17**, 227-236.

99. Marselli, B., and Comninellis, C. (2004). *In* "Proceedings of the 7th Workshop on Diamond Electrodes". Interlaken, Switzerland.

100. Marselli, B., Garcia-Gomez, J., Michaud, P. A., Rodrigo, M. A., and Comninellis, C. (2003). Electrogeneration of hydroxyl radicals on boron-doped diamond electrodes. *J. Electrochem. Soc.* **150**, D79-D83.

101. Martin, H. B., Argoitia, A., Angus, J. C., and Landau, U. (1999). *J. Electrochem. Soc* **146**, 2959.

102. Martin, H. B., Argoitia, A., Landau, U., Anderson, A. B., and Angus, J. C. (1996). Hydrogen and oxygen evolution on boron-doped diamond electrodes. *J. Electrochem. Soc.* **143**, L133–L13.

103. Michaud, P. A., Mahe, E., Haenni, W., Perret, A., and Comninellis, C. (2000). Preparation of Peroxodisulfuric Acid Using Boron-Doped Diamond Thin Film Electrodes. *Electrochemical and Solid-State Letters* **3**, 77-79.

104. Montgomery, D. C. (1991). "Design and Analysis of Experiments," 3rd/Ed. John Wiley& Sons Inc, New York.

105. Morao, A., Lopes, A., Amorim, M. T. P. d., and Goncalves, I. C. (2004). Degradation of mixtures of phenols using boron doped diamond electrodes for wastewater treatment. *Electrochimica Acta* **49**, 1587-1595.

106. Mraz, R., and Krysa, J. (1994). Long service life IrO2/Ta2O5 electrodes for electroflotation. *J. Appl. Electrochem.* **24**, 1262–

107. 1266.

108. Murugananthan, M., Yoshihara, S., Rakuma, T., and Shirakashi, T. (2008). Mineralization of bisphenol A (BPA) by anodic oxidation with boron-doped diamond (BDD) electrode. *Journal of Hazardous Materials* **154**, 213-220.

109. Myers, R. H., and Montgomery, D. C. (1995). "Response Surface Methodology: Process and Product Optimization Using Designed Experiments," 1st/Ed. John Wiley& Sons Inc, New York.

110. Nasr, B., Abdellatif, G., Canizares, P., Cristina, S., Lobato, J., and Rodrigo, M. (2005). Electrochemical Oxidation of Hydroquinone, Resorcinol, and Catechol on Boron-Doped Diamond Anodes. *Environ. Sci. Technol* **39**, 7234-7239.

111. Nasr, B., Hsen, T., and Abdellatif, G. (2009). Electrochemical treatment of aqueous wastes containing pyrogallol by BDD-anodic oxidation. *Journal of Environmental Management* **90**, 523-530.

112. Neyens, E., and J. Baeyens , J. (2003). A review of classic Fenton's peroxidation as an advanced oxidation technique. *Hazard. Mater.* **98**, 33.

113. Nishiki, N., Uno, M., and Furuta, T. (2004). *In* "Proceedings of the 7th Workshop on Diamond Electrodes". Interlaken, Switzerland.

114. Noureddine, B. T., Abdelhe´di, R., and André, S. (2009). Electrochemical polymerisation of phenol in aqueous solution on a Ta/PbO2 anode. *J Appl Electrochem (2009)* **39**, 663–669.

115. Noureddine, B. T., and André, S. (1998). Mechanistic Aspects of Phenol Electrochemical Degradation by Oxidation on a Ta/Pb02 Anode. *J. Electrochem. Soc* **145**, 3427.

116. Noureddine, B. T., and André, S. (2009). Electrochemical removal of phenol in alkaline solution. Contribution of the anodic polymerization on different electrode materials. *Electrochimica Acta* **54**, 4809-4816.

117. Ogtveren, U. B., Toru, E., and Koparal, S. (1999). REMOVAL OF CYANIDE BY ANODIC OXIDATION FOR WASTEWATER TREATMENT. *Water Res* **33**, 1851-1856.

118. Pacheco, M. J., Morao, A., Lopes, A., and Ciriaco, L. (2007). Degradation of phenols using boron doped diamond electrodes: a method for quantifying the extent of combustion. *Electrochimica Acta xxxxxxx*.

119. Panic, V. V., Dekansk, A. B., Vidakovic, T. R., -Stankovic, V. B. M., Javanovic, B. Z., and Nikolic, B. Z. (2005). Oxidation of phenol on RuO2-TiO2/Ti anodes Solid State. *Electrochem Comm* **9**, 43-54.

120. Panizza, M., and Cerisola, G. (2004). Electrochemical Oxidation as a Final Treatment of Synthetic Tannery Wastewater. *Environmental Science & Technology* **38**, 5470-5475.

121. Panizza, M., and Cerisola, G. (2005). Application of diamond electrodes to electrochemical processes. *Electrochimica Acta* **51**, 191-199.

122. Panizza, M., and Cerisola, G. (2008). Removal of colour and COD from wastewater containing acid blue 22 by electrochemical oxidation. *Journal of Hazardous Materials* **153**, 83-88.

123. Panizza, M., Michaud, P. A., Cerisola, G., and Comninellis, C. (2001). Electrochemical treatment of wastewaters containing organic pollutants on boron-doped diamond electrodes: Prediction of specific energy consumption and required electrode area. *Electrochemistry Communications* **3**, 336-339.

124. Pearl, J., J., C., and X., D. (1988). Competitive processes in photocatalysis. Phenol-Sulfide and Phenol-Cyanide competitive photooxidation over ZnO. *Electrochemica acta* **34**, 1335- 1338.

125. Perret, A., Haenni, W., Skinner, N., M.Tang, X., Gandini, D., Comninellis, C., Correa, B., and Foti, G. (1999). Electrochemicalbehavior of synthetic diamond thin film electrodes. *Diamond Relat. Mater* **8**, 820.

126. Pleskov, Y. V. (1999). *Russ. J. Electrochem.* **68**, 381.

127. Pleskov, Y. V. (2002). *Russ. J. Electrochem.* **38**, 1275.

128. PME (2001). General Environmental Regulations And Rules for Implementation. Kingdom of Saudi Arabia Presidency of Meteorology and Environment.

129. Polcaro, A. M., Mascia, M., Palmas, S., and Vacca, A. (2002). *Ind. Eng. Chem. Res* **41**, 2874.

130. Polcaro, A. M., Palmas, S., Renoldi, F., and Mascia, M. (2000). *Electrochim. Acta* **46**.

131. Polcaro, A. M., Vacca, A., Palmas, S., and Mascia, M. (2003). Electrochemical treatment of wastewater containing phenolic compounds: oxidation at boron-doped diamond electrodes. *Journal of Applied Electrochemistry* **33**.

132. Rajeshwar, K., and Ibanez, J. G. (1997). "Environmental Electrochemistry: Fundamentals and Applications in Pollution Abatement," Academic Press, San Diego, CA.

133. Rajkumar, D., Kim, J. G., and Palanivelu, K. (2005). Indirect Electrochemical Oxidation of Phenol in the Presence of Chloride for Wastewater Treatment. *Chemical Engineering Technology* **28**, 98-105.

134. Ricardo, B.-C., Texier, A.-C., Sierra-Alvarez, R., Razo-Flores, E., Field, J. A., and Gomez, J. (2009). Effect of initial sulfide concentration on sulfide and phenol oxidation under denitrifying conditions. *Chemosphere* **74**, 200-205.

135. Rodrigo, M. A., P.A, M., Duo, I., M;, P., G, C., and Ch, C. (2001). *J. Electrochem. Soc* **148**, D60.

136. Scialdone, O., Randazzo, S., Galia, A., and Silvestri, G. (2009). Electrochemical oxidation of organics in water: Role of operative parameters in the absence and in the presence of NaCl. *Water Research* **43**, 2260-2272.

137. Serrano, K., Michaud, P. A., Comninellis, C., and Savall, A. (2002). Electrochemical preparation of peroxodisulfuric acid using boron doped diamond thin film electrodes. *Electrochimica Acta 48* **48**, 431-436.

138. Sharifian, H., and Kirk, D. W. (1986a). Electrochemical Oxidation of Phenol. *J. Electrochem. Soc.* **133**, 921-924.

139. Sharifian, H., and Kirk, D. W. (1986b). Electrochemical Oxidation of Phenol. *J. Electrochem. Soc* **Vol. 133**, 921-924.

140. Simond, O., Schaller, V., and Comninellis, C. (1997). *Electrochim. Acta* **42**, 2009.

141. Sistiaga, M., Pierna, A. R., Marzo, F. F., Altube, A., and Lorenzo, A. (1998). *Applied Surf Science* **133**, 124.

142. Smith, J. R., and Walsh, F. C. (1998). Electrodes based on magneli phase titanium oxides: the properties and applications of Ebonex® materials. *J. Appl. Electrochem* **28**, 1021–1033.

143. Stucki, S., Kotz, R., Carcer, B., and Suter, W. (1991). Electrochemical waste water treatment using high overvoltage anodes. Part II: anode performance and applications . *Journal of Applied Electrochemistry* **21**, 99-104.

144. Swain, G. M., Anderson, B. A. B., and Angus, J. C. (1998). Applications of diamond thin films in electrochemistry. *MRS Bull.*, 56–60.

145. Tahar, N. B., and Savall, A. (1999). Electrochemical degradation of phenol in aqueous solution on bismuth doped lead dioxide: a comparison of the activities of various electrode formulations. *J. Appl. Electrochem.* **29**, 277–283.

146. Thiem, L. T., and Alkhatib, E. A. (1988). In situ Adapation of Activated Sludge by Shock Loading to Enhance Treatment of High Ammonia Content Petrochemical Wastewater. *Journal of Water Pollution Control Federation* **60**, 1245-1252.

147. Tian, Y., Chen, X., Shang, C., and Chenz, G. (2006). Active and Stable Ti/Si/BDD Anodes for Electro-oxidation. *Journal of The Electrochemical Society* **153**, J80-J85.

148. Troster, I., Fryda, M., Herrmann, D., Schafer, L., Haenni, W., Perret, A., Blaschke, M., Kraft, A., and Stadelmann, M. (2002a). Electrochemical advanced oxidation process for water treatment using DiaChem® electrodes. *Diamond Relat. Mater* **11**, 640.

149. Troster, I., Schafer, L., and Fryda, M. (2002b). Recent developments in production and application of DiaChem® electrodes for wastewater treatment. *New Diamond Front. Carbon Technol* **12**, 89.

150. Tyagi, R. D., T, T. F., and Chowdhury A. K. M. M (1993). A pilot study of biodegradation of petroleum refinery wastewater in a polyurethane-attached RBC. *Process biochemistry* **28**, 75-82.

151. Ureta-Zanatu, M. S., Bustos, P., Berros, C., Diez, M. C., Mora, M. L., and Gutierez, C. (2002). *Electrochim Acta* **47**, 2399.

152. Ureta-Zanatu, M. S., Bustos, P., Diez, M. C., Mora, M. L., and Berros, C. (2001). *Electrochim Acta* **46**, 2545.

153. Urtiaga, A., Rueda, A., Anglada, Á., and Ortiz, I. (2009). Integrated treatment of landfill leachates including electrooxidation at pilot plant scale. *Journal of Hazardous Materials* **166**, 1530-1534.

154. USEPA (2006). "Edition of the Drinking Water Standards and Health Advisories," Rep. No. EPA 822-R-06-013, Washington, DC.

155. Vatistas, N., Comninellis, C., Serikawa, R. M., and Prosperi, G. (2005). Oxidant Production on BDD Anodes and Advanced Oxidation Processes. *In* "Diamond Electrochemistry", pp. 477-501. Elsevier, BKC Tokyo.

156. Vazquez, I., Rodríguez, J., Maranon, E., Castrillon, L., and Fernández, Y. (2006). Simultaneous removal of phenol, ammonium and thiocyanate from coke wastewater by aerobic biodegradation. *Journal of Hazardous Materials* **137**, 1773-1780.

157. Vercesi, G. P., J, R., and Ch, C. (1991). Characterization of DSA type Oxygen Evolving Electrodes. Choice of Base Metal. *Thermochim. Acta* **176**, 31.

158. Vermillion, F. J., and Pearl, I. A. (1964). *J Electrochem Soc* **111**, 1392.

159. Wang, J., .Jiang, M., and Lu, F. (1998). *J Electroanal Chem*, 444:127.

160. Xiao-yan, L., Cuib, Y.-h., Fengb, Y.-j., Xiea, Z.-m., and Gu, J.-D. (2005). Reaction pathways and mechanisms of the electrochemical degradation of phenol on different electrodes. *Water Research* **39**, 1972-1981.

161. Yao, P., Chen, X., Wu, H., and Wang, D. (2008). Active Ti/SnO2 anodes for pollutants oxidation prepared using chemical vapor deposition. *Surface and Coatings Technology* **202**, 3850-3855.

162. Yu, H., , C. M., Quan, X., Chen, S., and Zhao, H. (2009). Flow Injection Analysis of Chemical Oxygen Demand (COD) by Using a Boron-Doped Diamond (BDD) Electrode. *Environmental Science & Technology* **43**, 1935-1939.

163. Yusuf, Y., and Koparal, A. S. (2006). Electrochemical oxidation of phenol in a parallel plate reactor using ruthenium mixed metal oxide electrode. *Journal of Hazardous Materials* **B136**, 296-302.

164. Zhang, R. J., Lee, S. T., and Lam, Y. W. (1996). *Diamond Relat. Mater* **5**, 1288.

165. Zhao, G., Shen, S., Li, M., Wu, M., Cao, T., and Li, D. (2008). The mechanism and kinetics of ultrasound-enhanced electrochemical oxidation of phenol on boron-doped diamond and Pt electrodes. *Chemosphere* **73**, 1407-1413.

166. Zhu, X., Tong, M., Shi, S., Zhao, H., and Ni, J. (2008). Essential Explanation of the Strong Mineralization Performance of Boron-Doped Diamond Electrodes. *Environmental Science & Technology* **42**, 4914-4920.

167. Zwiener, C., and Frimmel, F. H. (2004). Oxidative treatment of pharmaceuticals in water. *Water Res.* **34**, 188.

APPENDIX

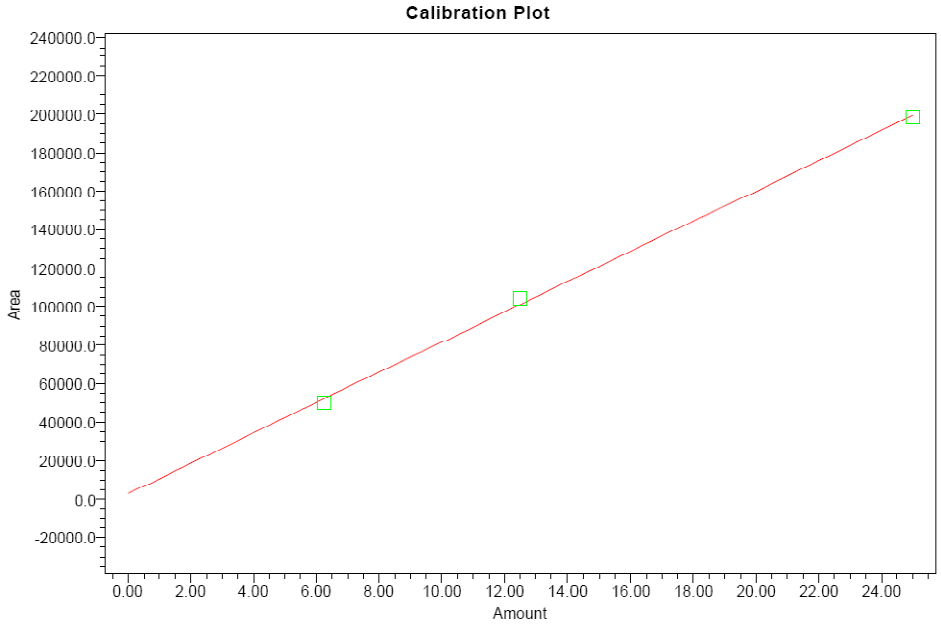

Typical HPLC Calibration Curve for Phenol Measurements (R^2 0.999)

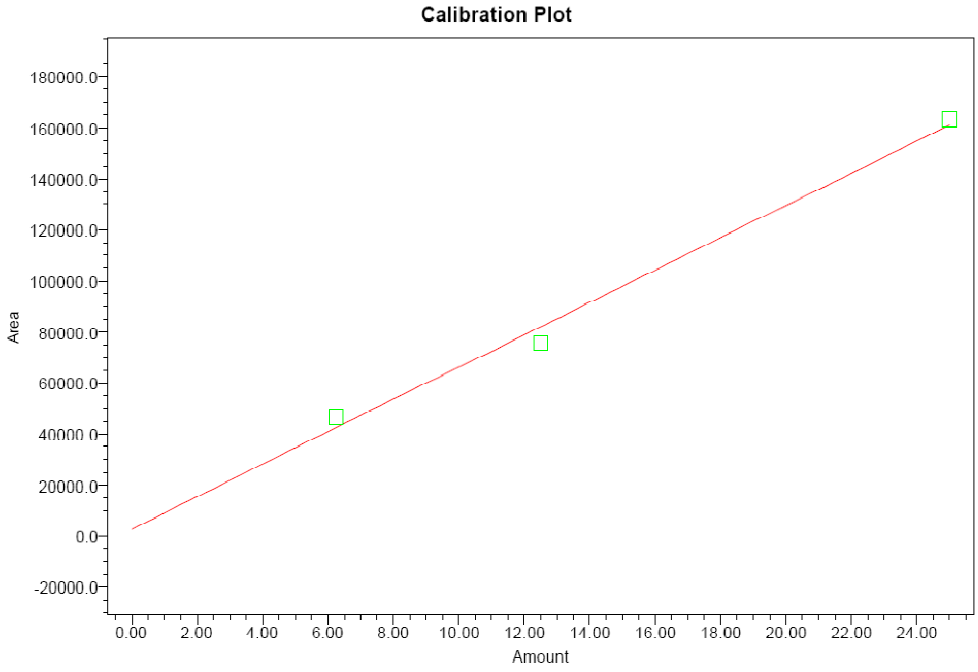

Typical HPLC Calibration Curve for Benzoquinone Measurements (R^2= 0.946)

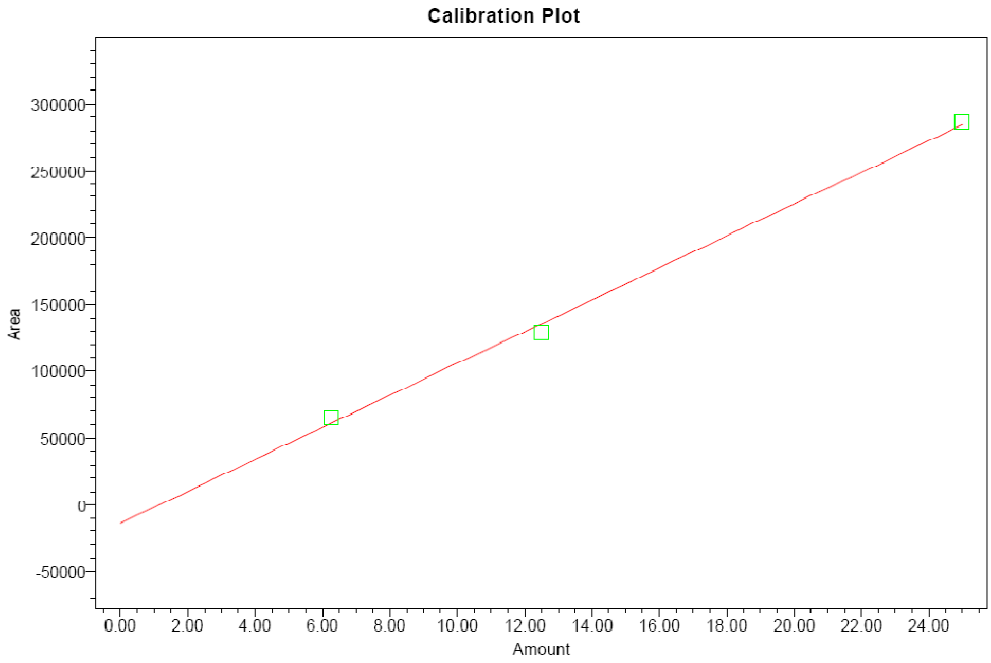

Typical HPLC Calibration Curve for Hydroquinone Measurements (R^2= 0.9918)

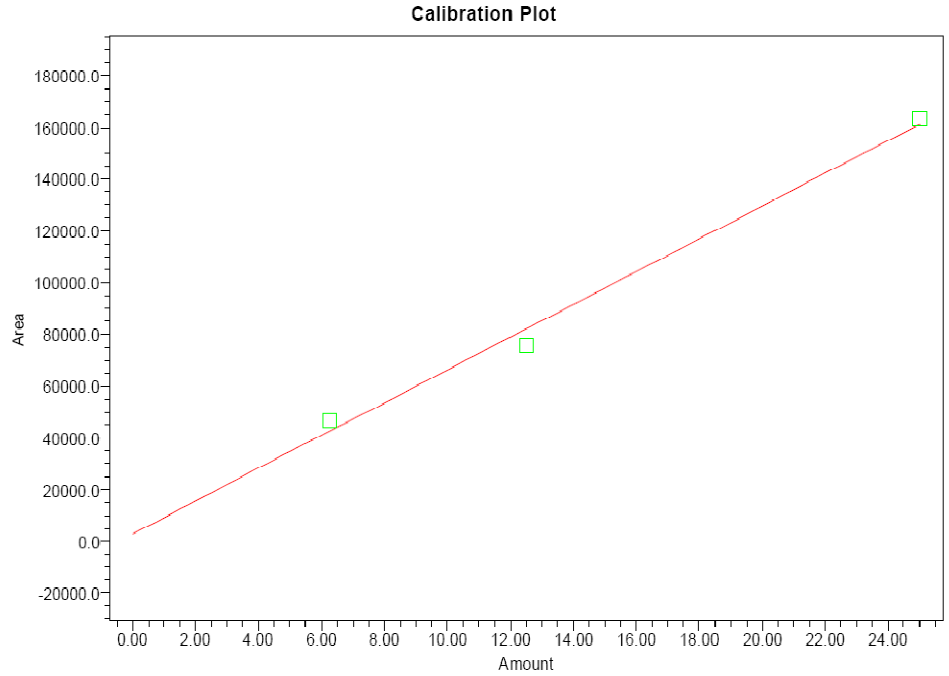

Typical HPLC Calibration Curve for Catechol Measurements (R^2=0.9975)

APPENDIX A: Removal Efficiencies for Phenol, TOC and COD at 3.5 hours Retention Time for the different Mix Matrixes for BDD1

Matrix Nature	Component (s)	Initial Phenol , ppm	Effluent Phenol, ppm	Removal %	Initial TOC, ppm	Effluent TOC, ppm	Removal %	Initial COD ppm	Effluent COD ppm	Removal %
Single	Phenol	100	0	100	76.6	0	100	238	2.56	98.92
Binary	Phenol, NH_4^+	100	2.74	97.26	76.6	9.582	87.49	949	224.76	76.32
	Phenol, CN^-	100	0	100	76.6	7.042	90.8	818	117.2	78.36
	Phenol , S^{2-}	100	4.19	95.81	76.6	13.52	82.35	638	91.52	85.66
Ternary	Phenol, NH_4^+, S^{2-}	100	0	100	76.6	19.73	78.16	1349	532	60.52
	Phenol, NH_4^+,CN^-	100	0	100	76.6	0	100	1529	625	59.12
	Phenol, CN^-, S^{2-}	100	0	100	76.6	1.89	97.53	1218	493	59.52
Quaternary	Phenol, NH_4, S^{2-}, CN^-	100	0	100	76.6	4.33	95.67	1929	952	50.65

APPENDIX B: Removal Efficiencies for Phenol, TOC and COD at 3.5 hours Retention Time for the Different Mix Matrixes for BDD2

Matrix Nature	Component (s)	Initial Phenol, ppm	Effluent Phenol, ppm	Removal %	Initial TOC, ppm	Effluent TOC, ppm	Removal %	Initial COD ppm	Effluent COD ppm	Removal %
Single	Phenol	100	0	100	76.6	0	100	238	2.56	98.92
Binary	Phenol, NH_4^+	100	4.9289	95.07	76.6	10.24	86.6	638.5	235	63.32
	Phenol, CN^-	100	10.175	89.82	76.6	27.68	63.39	573	154	73.12
	Phenol , S^{2-}	100	24.205	75.79	76.6	32.3	57.83	483	119	75.36
Ternary	Phenol, NH_4^+, S^{2-}	100	27.973	72.03	76.6	29.43	61.58	838.5	399.17	52.40
	Phenol, NH_4^+,CN^-	100	22.514	77.49	76.6	29.67	61.27	928.5	444.55	51.22
	Phenol, CN^-, S^{2-}	100	17.693	82.31	76.6	30.012	60.82	773	352.72	54.37
Quaternary	Phenol, NH_4, S^{2-}, CN^-	100	12.128	87.87	76.6	28.35	62.99	1210.4	584	48.25

APPENDIX C: Average Current Efficiencies and Specific Energy Consumptions at the 3.5 hours Retention Time in the Different Mix Matrixes

Matrix Nature	Component (s)	BDD1			BDD2		
		ACE %	SEC, kwh/kg Phenol	SEC, kwh/kg COD	ACE %	SEC, kwh/kg Phenol	SEC, kwh/kg COD
Single	Phenol	19.1	429.5	57.0	19.1	429.5	57.0
Binary	Phenol, NH_4^+	58.75	359.7	15.096	32.72	460.9	32.491
	Phenol, CN^-	52.00	398.5	19.43	33.993	479.6	31.84
	Phenol , S^{2-}	44.34	376.1	20.62	29.53	626.1	40.23
Ternary	Phenol, NH_4^+, S^{2-}	66.28	304.4	11.64	35.64	607.2	30.4
	Phenol, NH_4^+,CN^-	73.34	363.9	12.58	39.26	644.9	31.25
	Phenol, CN^-, S^{2-}	58.88	353.5	15.24	34.097	576.6	33.10
Quaternary	Phenol, NH_4, S^{2-}, CN^-	79.26	244.9	7.83	44.18	428.6	21.59

Vitae

Name: Nuhu Mu'azu Dalhat

Nationality: Nigerian

Permanent Address: No. 54 Albarkawa Zaria City, Kaduna State Nigeria

Present Address: Gezan Street Cross 12th Thoqba, Eastern Province Saudi Arabia

E-mail: nmdalhat@yahoo.com dalhat@gmail.com

- Graduated with Bachelor Degree in Civil Engineering from Ahmadu Bello University, Zaria Nigeria in 2000.
- Served Osun State Environmental Protection Agency, Osogbo Nigeria as Civil Engineer during NYSC program from April 2001 to May 2002.
- Joined Civil Engineering Department Ahmadu Bello University, Zaria Nigeria as Assistant Lecturer in August 2002.
- Joined Civil Engineering Department, KFUPM, Dhahran Saudi Arabia as Research Assistant in September 2002.
- Earned Master of Science Degree in Civil Engineering (Water Resources and Environmental Engineering Option) from KFUPM in May 2005.
- Joined Civil Engineering Department, KFUPM, Dhahran Saudi Arabia as a Lecturer-B in September 2005.
- Earned Doctorate Degree in Civil Engineering (Environmental Engineering Option) from KFUPM in January 2010.